Development of a High Throughput 3D Perfused Liver Tissue Bioreactor

by

Samuel Walker Inman

Bachelor of Science in Mechanical Engineering
Georgia Institute of Technology, 2004

Submitted to the Department of Mechanical Engineering in Partial Fulfillment of the Requirements for the Degree of

MASTER OF SCIENCE IN MECHANICAL ENGINEERING
at the
MASSACHUSETTS INSTITUTE OF TECHNOLOGY

February 2006

Signature of Author: _____
Department of Mechanical Engineering
January 15, 2006

Certified by: _____
Dr. Linda G. Griffith
Professor Biological Engineering and Mechanical Engineering
Thesis Supervisor

Accepted By: _____
Dr. Lallit Anand
Professor of Mechanical Engineering
Chairman, Committee for Graduate Students

This page intentionally left blank

Development of a High Throughput 3D Perfused Liver Tissue Bioreactor

by

Samuel Walker Inman

Submitted to the Department of Mechanical Engineering
on January 15, 2006 in Partial Fulfillment of the
Requirements for the Degree of Master of Science in
Mechanical Engineering

ABSTRACT

This thesis describes the development of a device designed for culturing liver tissue in a 3D perfused environment. Cells form tissue inside miniature channels of a scaffold, and the tissue is perfused with culture medium to create a culture microenvironment that has previously been described by the Griffith lab. In order to support this microenvironment, the reactor needs a pumping system, reservoirs and a controller. Previously, these have all been stand-alone components.

This work focuses on the development of a new, integrated culture system. This system integrates 12 reactor microenvironments, reservoirs and pumping systems onto a single plate with a configuration modeled after standard multi-well plates. Each of the 12 bioreactor units utilize pneumatic pumps driven by a single external controller. This design offers substantial advantages over previous systems as it is far more user-friendly and can be used in a higher throughput capacity.

The thesis describes the design and fabrication of the reactor and controller, including several models that were used during the development process. It also offers mechanical and biological characterizations of the device.

Thesis Supervisor: Linda G. Griffith
Title: Professor of Biological Engineering and Mechanical Engineering

This page intentionally left blank

ACKNOWLEDGEMENTS

First I would like to thank Linda Griffith, my advisor, for brining me into the lab and for letting me work on this project. Thank you for support throughout my MIT experience.

I would like to thank Karel Domansky and Jim Serdy for their work throughout the project with the design and development of the bioreactor. The original idea of a multi-well system came from Karel, and Karel developed the first prototype multi-well bioreactor. Karel, with the help of several others, also developed all of the initial, component based bioreactor systems. Jim was responsible for some of the biggest breakthroughs in the development process. Both the idea for fluidic capacitors, and the breakthroughs that made the valves work properly came from Jim. Jim, with the help of Fred Cote, also taught me how to use the CNC milling machine where all the bioreactors were manufactured.

Thank you Megan Whittemore and Laura Vineyard for performing biological experiments. I realize that they are hugely time consuming and there is no way I could have finished this without your help. I would also like to thank Megan for the PCR and Laura for the perfusions.

Bryan Owens and Nadeem Mazen, who shared their time as UROP students, were very helpful with mechanical characterization tests. Bryan also helped developed the 3D CAD model and Nadeem helped develop the controller.

Thanks go to the entirety of the BPEC lab and Pfizer, including Nate Tedford, Anand Sivaraman, Ben Cosgrove, Keith Hoffmaster and Susan Glynn for advice on requirements for the system and for helping teach me biology.

Thank you Peter Morely, Andy Gallant and the MIT Central Machine Shop for advice and help manufacturing the bioreactor and its components.

I would like to thank Dave Trumper for advice with the system design, specifically the scaffolds and the capacitor.

Thank you MITERS for helping developing the controller.

Finally, and most importantly, I would like to thank DuPont and Pfizer for funding the project.

This page intentionally left blank

TABLE OF CONTENTS

LIST OF FIGURES

---

* Photograph was taken by Dr. Karel Domansky

LIST OF TABLES

This page intentionally left blank

1. INTRODUCTION

1.1 Background

The liver is the primary site where drugs are metabolized in vivo [1]. As such, an accurate model for the liver is a requirement for predictive data about a candidate drug.

Immense amounts of money, $800 MM, and time, 10 to 15 years are invested in bringing a new drug to market [2]. Even still, only an estimated 1 of 5,000 candidates pass clinical trials [2,3]. Of the lead candidates that are accepted for initial tests on humans, a significant number fail due to liver toxicity [4,5]. It is clear that there is an unmet need for in vitro culture systems that more accurately model biological pathways in the liver.

Drug metabolism is mediated by a set of enzymes that are difficult to maintain in culture. Metabolism that occurs through these enzymes can alter the toxic and therapeutic profile of a drug, and therefore, their in vitro maintenance in a model system is very important. Many methods exist for culturing hepatocytes [6-9], and the benefits and drawbacks to each of these methods are well documented [6-12]. In general, the most relevant assays are more complex and are less ethically acceptable.

This thesis describes the development of a high throughput bioreactor for culturing liver tissue in a three-dimensional, perfused environment. This type of environment has been shown to improve the maintenance of liver specific functions, including the activity of important enzymes involved in drug metabolism [13]. The main focus of this project is to adapt a system previously developed in this lab into a format that is suitable for usage in a high throughput capacity suitable for industrial applications, or research where multiple treatment points are needed.

This chapter provides a background on the liver and its drug metabolizing functions. Bioreactor systems that were previously developed in this lab are also presented.

1.2 The Liver

The liver is the largest organ in the abdomen and is one of the most important organs in the body. One of the primary functions of liver is the metabolism of food after it is processed by the small intestine. Proteins, fats and carbohydrates are broken down by the liver, converted to useable sources of energy and either secreted into the blood or stored as glycogen or fatty acids depending upon the body's demand. The liver is also responsible for manufacturing and secreting bile, which aids in the with digestion of fats in the intestine. The liver is the primary source of albumin, which carries hormones, fatty acids and many drugs in the blood. Another essential function of liver is to filter and process ingested drugs and toxins, including ammonia, which it secretes as urea.

Liver is fed by the hepatic artery, providing a rich supply of oxygen, and by the portal vein which carries digested food directly from the small intestines. The micro-architecture of the liver, shown in Figure 1.1, is composed of parallel, one cell thick, plates of interconnected hepatocytes perfused on either side by blood. Hepatocytes, which comprise over 60% of liver mass [14], are highly polarized cells. Tight junctions between adjacent hepatocytes close off a canalicular space that transports bile in the opposite direction of blood flow. Hepatocytes are lined on either side by extracellular matrix (ECM) and by nonparenchymal cells including stellate cells, Kupffer cells and endothelial cells. The ECM, a basement membrane-like matrix, is composed of types IV, V and VI collagen, fibronectin, laminin, heparan sulfate proteoglycan and other matrix proteins [15, 16]. Hepatocytes express many adhesion proteins including the integrins $\alpha_1\beta_1$ and $\alpha_5\beta_1$, asialoglycoprotein receptors, and cell adhesion molecules. These proteins mediate cell-cell and cell matrix attachment and are involved in signaling pathways.

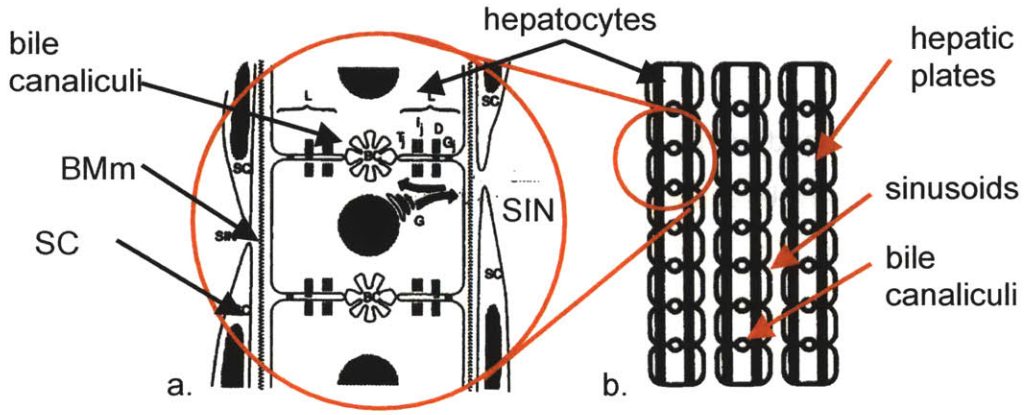

Figure 1.1: (a) A section of the liver micro-environment showing hepatocytes, lined on either side with basement membrane-like matrix (BMm), and sinusoidal endothelial cells (SC). Blood flows through the sinusoids (SIN) on either side of the hepatocytes and bile travels through the bile canaliculi located between adjacent hepatocytes. (b) Alignment of hepatocytes to form plate like structures. Figures were taken from Stamatoglou [15]

The liver is primarily responsible for the metabolism of xenobiotics in vivo. Xenobiotics, or chemicals that are foreign to the body, can be either man made or natural and can include pollutants, drugs, products in food, and many other substances. Because these substances are lipophilic, they are readily absorbed by the body. In order for them to be secreted, they must be converted into water-soluble chemicals. This process, known as biotransformation, is mediated by a set of enzymes that are generally categorized as either Phase I or Phase II. Among the most difficult to maintain in vitro are a subset of the Phases I enzymes know as cytochrome P450's. These enzymes are also some of the most important, as they are involved in a very large number of biotransformation reactions [17, 18]. A more detailed description of the liver and the drug development process is provided by Sivaraman [19].

1.3 Previous Bioreactors and the Team Involved in this Work

The microenvironment where cells are cultured in the bioreactor consists of a scaffold containing an array of channels [20-22]. Each of these channels holds one unit of tissue that is perfused with culture medium at a constant rate. The total number of channels in the system is scaleable and thus reactors containing differing numbers of cells were developed. The first reactors were designed for optical interrogation of cells and thus only 40 channels were used [20, 22]. As some experiments require large numbers of cells, the initial system was scaled up and a system containing 1,000 channels was developed [23].

The high throughput aspect of the bioreactor was next assessed. A prototype system, Figure 1.2, was developed in the multi-well format that integrated 5 pneumatic pumps and scaffold systems onto the same plate [23]. A PC based controller drove the pumps in series by actuating 3 three-way pneumatic valves in sequence.

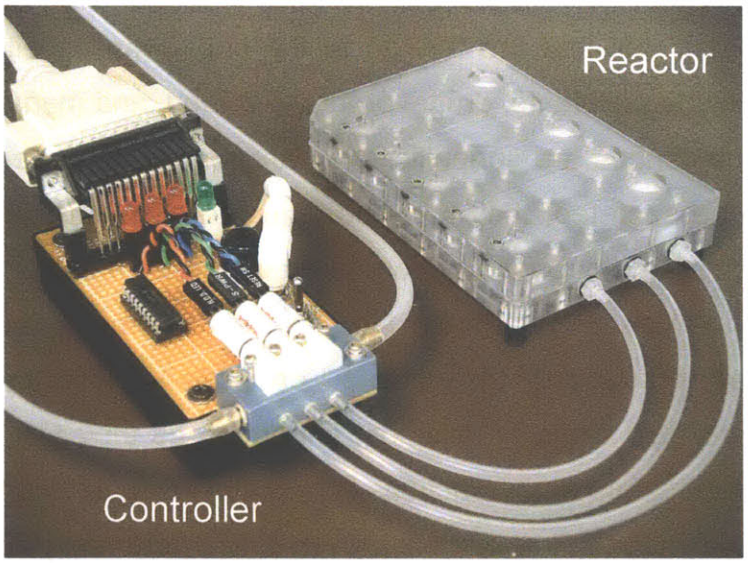

Figure 1.2: The initial prototype bioreactor system

The work described in this thesis is the result of a collaborative project between a large group of people. Dr. Karel Domansky and Jim Serdy were actively involved in all of the decisions that shaped the design of the bioreactor. Dr. Domansky developed the

prototype multi-well system as well as the initial component based bioreactor systems and thus offered a substantial amount of experience in regards to reactor design. Mr. Serdy is experienced in manufacturing and was generous with his expertise in development. Megan Whittemore was tremendously helpful with biological characterization and is responsible for all of the RT-PCR assays. Laura Vineyard was also very helpful with experiments and was responsible for all of the liver isolations. Bryan Owens helped with mechanical characterization and developed a 3D CAD model for the bioreactor. Mr. Owens also did all of the final dimensioning for the component drawings. Nadeem Mazen and the MITERs group helped develop the electronic controller.

2. DEVICE DESIGN

2.1 General

The multiwell bioreactor is a device that allows culture of cells in a perfused, three-dimensional environment. The bioreactor system, shown in Figure 2.1, consists of a bioreactor plate that is connected by three pneumatic lines to a controller. One bioreactor plate contains 12 reactor units where tissue can be cultured. Each of these reactor units are capable of holding ~ 850 thousand cells. This chapter describes the design of the individual reactor unit, the bioreactor plate used to integrate reactor systems, and the controller.

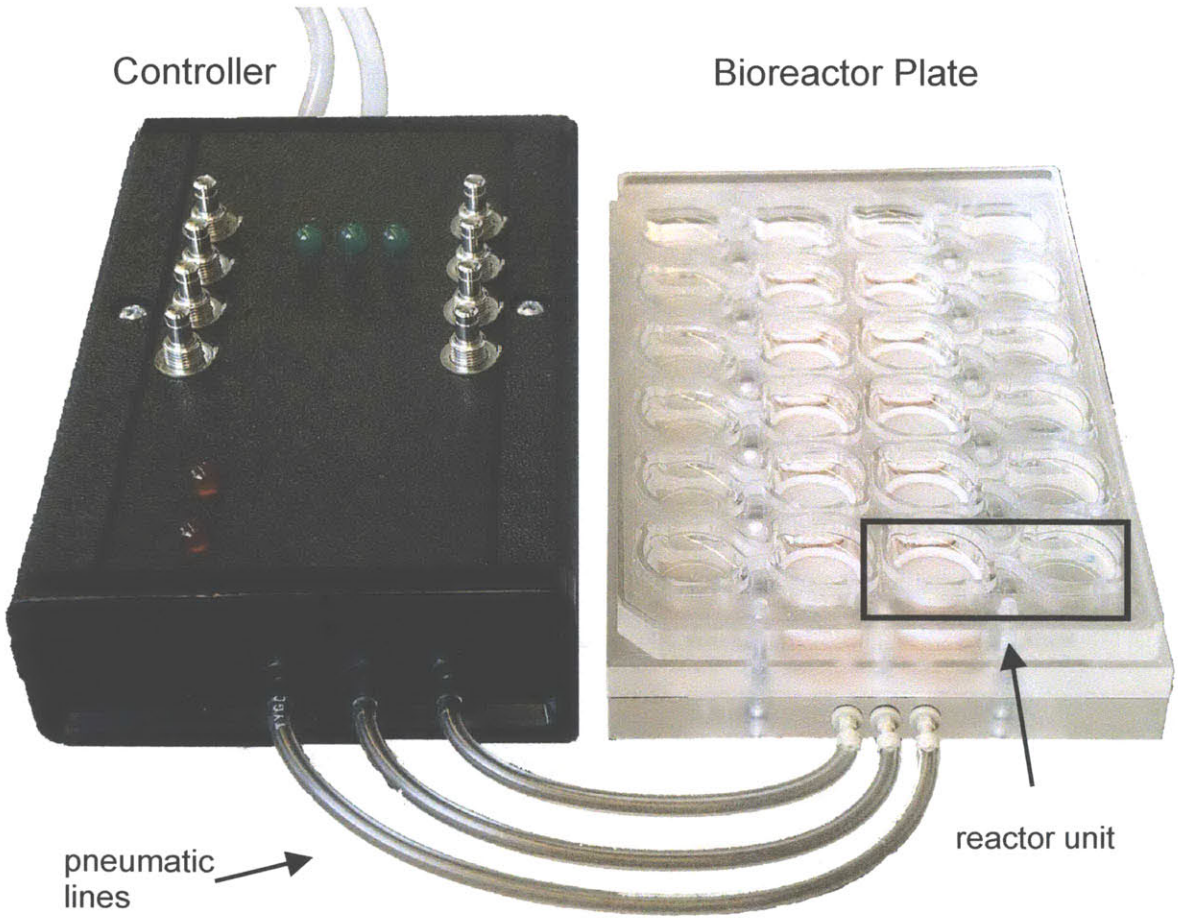

Figure 2.1: The bioreactor system

Each of the reactor units, shown in Figure 2.2, include a scaffold assembly where cells are cultured, and a reservoir that holds culture medium. Medium is perfused through the scaffold using a pneumatic pump and re-circulates across a surface channel back to the reservoir. Each of the 12 reactor units are fluidically isolated and all pumps are driven pneumatically by pressure pulses sent from the controller. The frequency of the controller sets the rate of perfusion in the device. Fluidic capacitors are used to damp pulses of fluid created by the pumps.

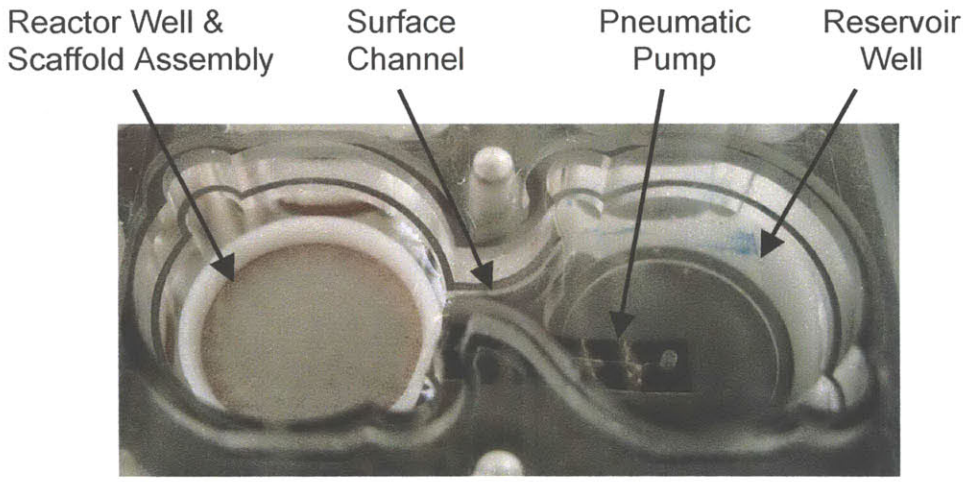

Figure 2.2: The reactor unit includes a scaffold, a reservoir and pumping system

The assembled bioreactor consists of a fluidic plate, a pneumatic plate, and a membrane sandwiched between the two, Figure 2.3. The plates are held together with 14 screws and sandwich the membrane to create a fluidic seal at each reactor unit. The exterior dimensions of the bioreactor conform with the 96 well plate standard set forth by the Society for Biomolecular Screening [25]. A lid covers the bioreactor in order to prevent contamination.

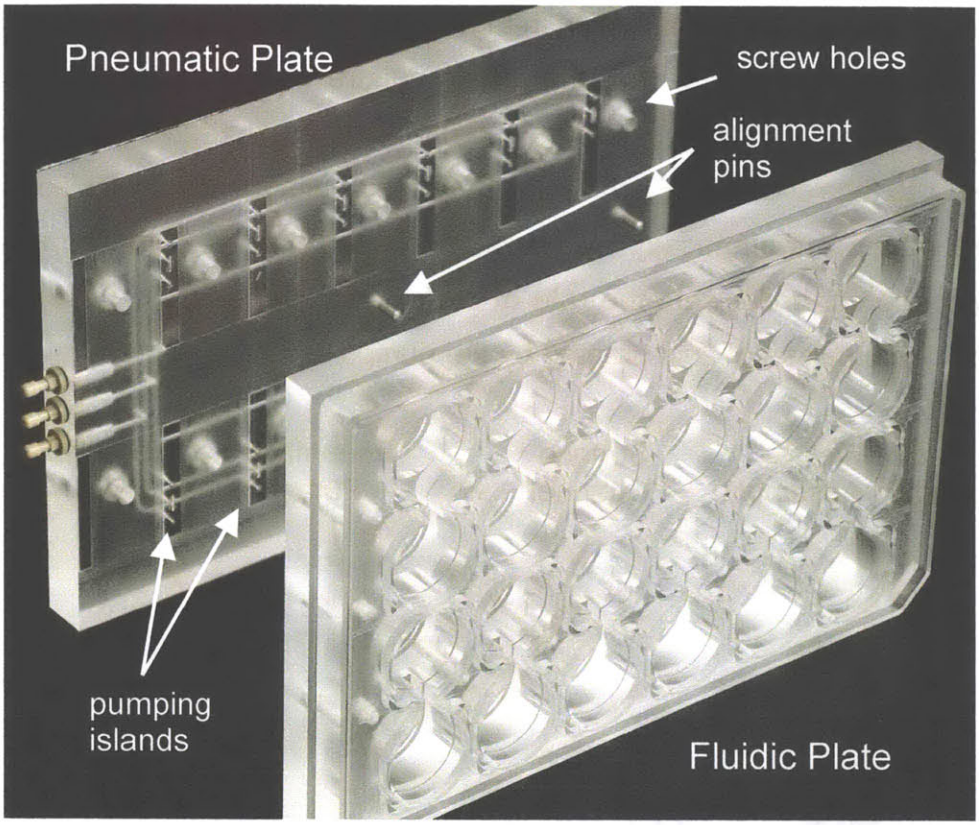

Figure 2.3: The fluidic and pneumatic plates are screwed together to make the bioreactor. Each bioreactor contains 12 reactor units.

2.2 Reactor Unit

2.2.1 Scaffold Assembly

The scaffold assembly is the microenvironment where cells reside in the reactor unit. Shown in Figure 2.4, the scaffold assembly consists of a scaffold, a filter, a filter support, a retaining ring, and gasket. Dimensioned drawings are provided in Appendix A1.

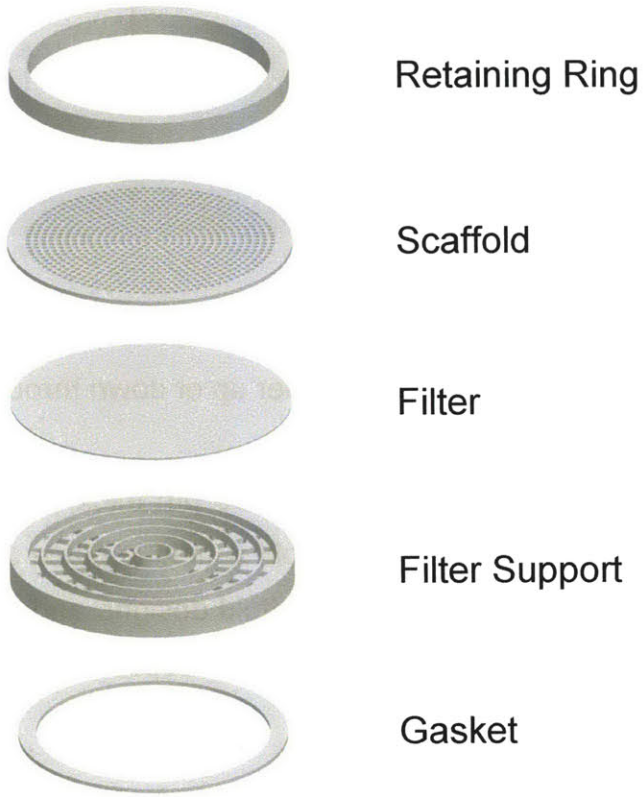

Figure 2.4: The scaffold assembly consists of a scaffold, a filter, a filter support, a retaining ring and a gasket

A scaffold is a thin disk containing channels that hold ~ 1,000 cells; these cells comprise one unit of tissue. Cells form 3D structures by adhering to the channel walls. Each channel is perfused with culture medium that can be pumped either up or down through the scaffold. An operational diagram that highlights the geometry of the scaffold assembly and localization of cells is shown in Figure 2.5.

Upon initial seeding, a 5 μm microporous filter keeps cells from falling through the scaffold. The number of channels, and thus the number of cells, can vary from scaffold to scaffold, giving the user freedom to define a scaffold design to meet specific experimental needs.

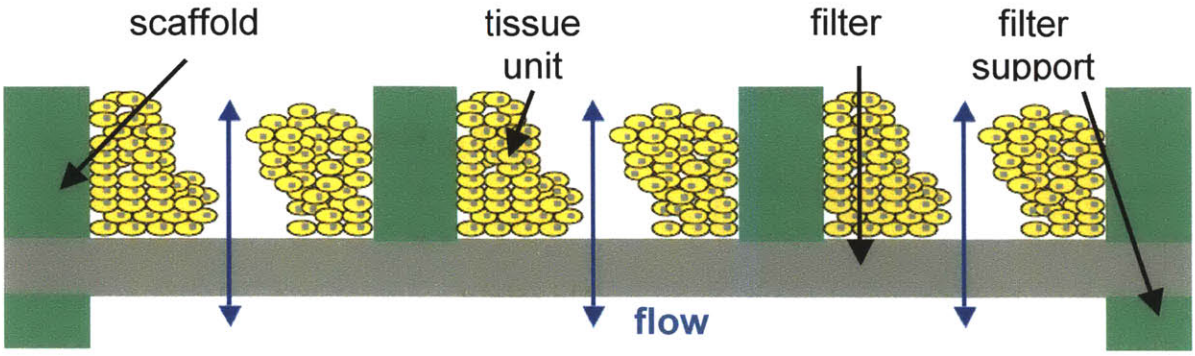

Figure 2.5: Schematic of a channel cross-section. Cells adhere to the channel walls and are perfused with medium that is pumped either up or down through the scaffold.

A typical scaffold, shown in Figure 2.6, is a 230 μm thick, 14.95 mm diameter disk with a defined pattern of channels. The scaffold is held in place along a 1 mm rim around the outer edge. A multitude of different scaffold designs and scaffold materials are possible. The channel, a 0.09 mm^2 through hole corresponding to a 300 x 300 μm square, is the defining feature of the scaffold.

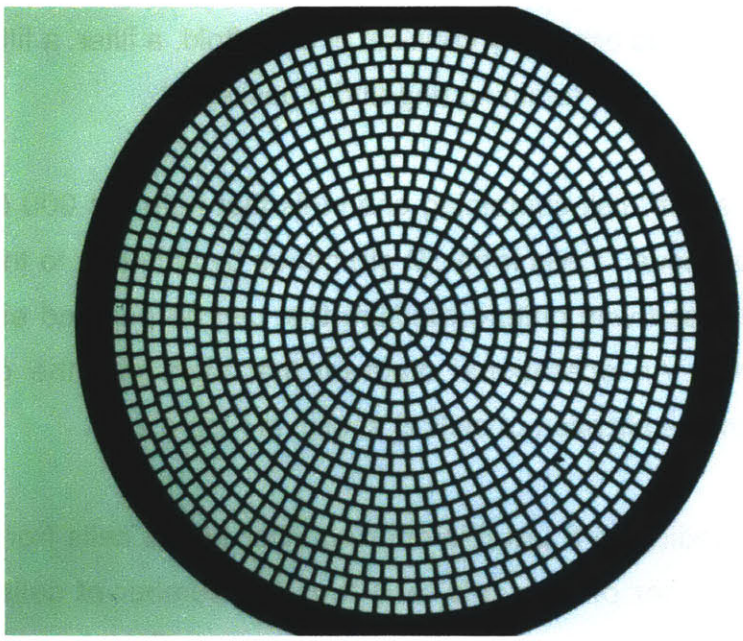

Figure 2.6: A 230 μm thick silicon scaffold with 861 0.09 mm^2 channels arranged in a circular pattern

The scaffold shown in Figure 2.6 has 861 channels arranged in a circular pattern. There are 100 μm walls between each of the channels to provide structural support. This scaffold represents the maximum number of channels that can be placed on a scaffold of this diameter. Figure 2.7, shows a variety of other scaffold designs and materials.

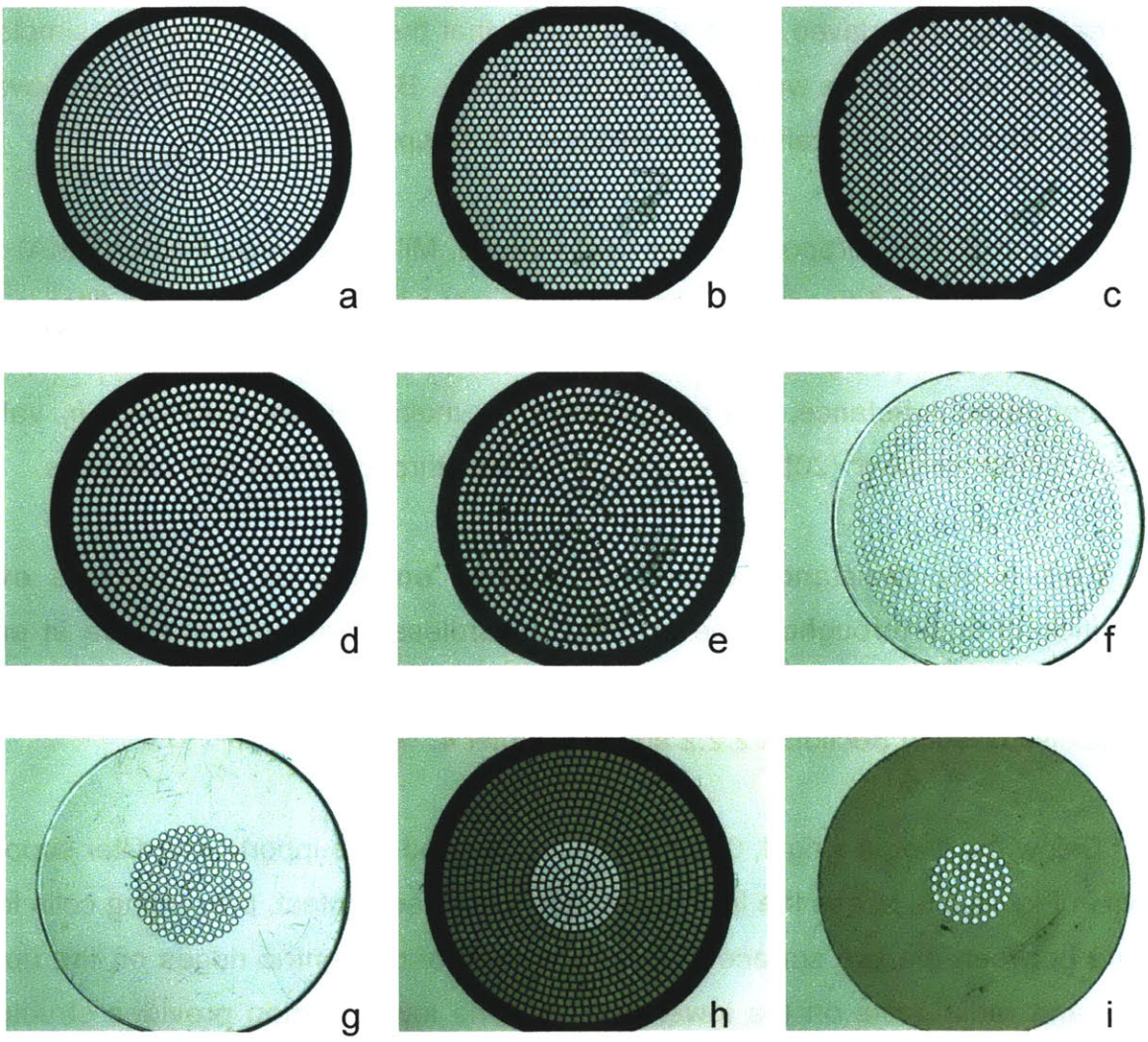

Figure 2.7: An assortment of scaffold designs and materials: a) silicon with 861 trapezoid channels; b) silicon with 859 hexagon channels; c) silicon with 837 square channels; d) silicon with 631 circular channels; e) Teflon with 631 drilled channels; f) polycarbonate with 631 channels; g) polycarbonate with 127 channels; h) silicon with 97 channels, other channels are blocked with a PEEK insert; i) PEEK with 61 channels.

Regardless of channel geometry, each channel has a cross sectional area of ~0.09 mm^2. Some of these scaffolds are etched silicon, which allows for endless possibilities of channel geometries. These scaffolds are very chemically resistant and can be sterilized by autoclaving. Unfortunately, they are expensive, brittle, and are not readily adaptable to manufacturing on a large scale. The other scaffolds are polymer disks with micro-drilled channels. These scaffolds are less resistant to chemicals and some cannot be autoclaved. The advantage is that they do not break, are simple to manufacture, and thus are well suited for prototyping. Biological comparisons between cells cultured in different scaffolds are discussed in Chapter 6.

A 5 μm SVPP Durapore ® filter (SVLP09050, Millipore Corp., Bedford, MA) sits below the scaffold and keeps cells held in place upon initial seeding. The filter is the primary source of fluidic resistance in the scaffold assembly. Hydraulic permeability, the inverse of fluidic resistance, can be calculated by multiplying the published h_p value, 73.5 $(mL/s)/(N/mm^2)/cm^2$ [20], by the area of the filter through which flow can pass.

This fluidic resistance below the scaffold ensures an approximate even distribution of flow throughout the scaffold, regardless of amount of tissue in each channel [20]. The fluidic resistance is also integral to the function of the capacitor, which is discussed in Section 2.2.2.2 and in Chapter 4.

Below the filter is a rigid, 0.75 mm thick disk used for support. The filter support, shown in Figure 2.8, keeps the filter and scaffold in close contact, preventing cells from slipping between the two surfaces. It is comprised of concentric ridges on the upper portion and radial slots on the lower portion. The lower portion provides structural support to the ridges. The ridges keep the filter in place, yet do not restrict flow through any regions of the filter. In order to minimize occlusion of channels in the scaffold, the surface area of the ridges, 18 mm^2, is minimal in comparison with the area of the filter, 135 mm^2. Spacing between adjacent ridges is maximized while still providing ample support to the filter between ridges. Also, the ridges line up directly with the solid rings between channels on the scaffold in Figure 2.6.

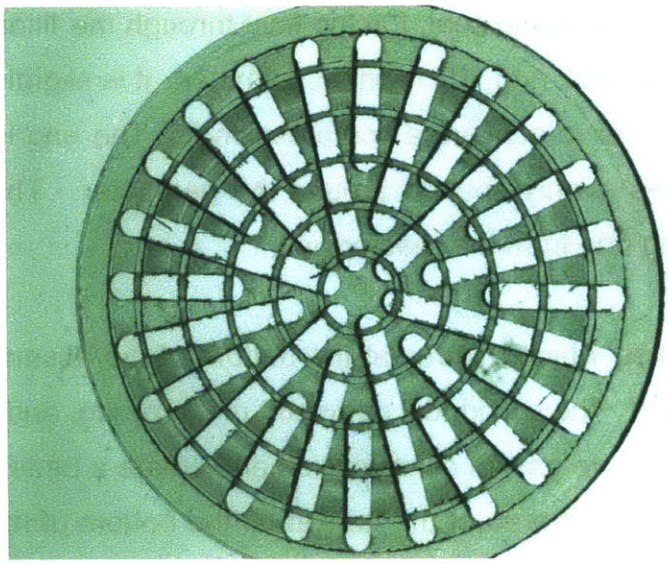

Figure 2.8: The filter support keeps the filter in close contact with the scaffold and allows flow to pass through unobstructed

A modified filter support can be used in combination with scaffolds containing fewer channels. These modified supports, shown in Figure 2.9, prevent medium from passing through the outer edges of the filter where there are no channels.

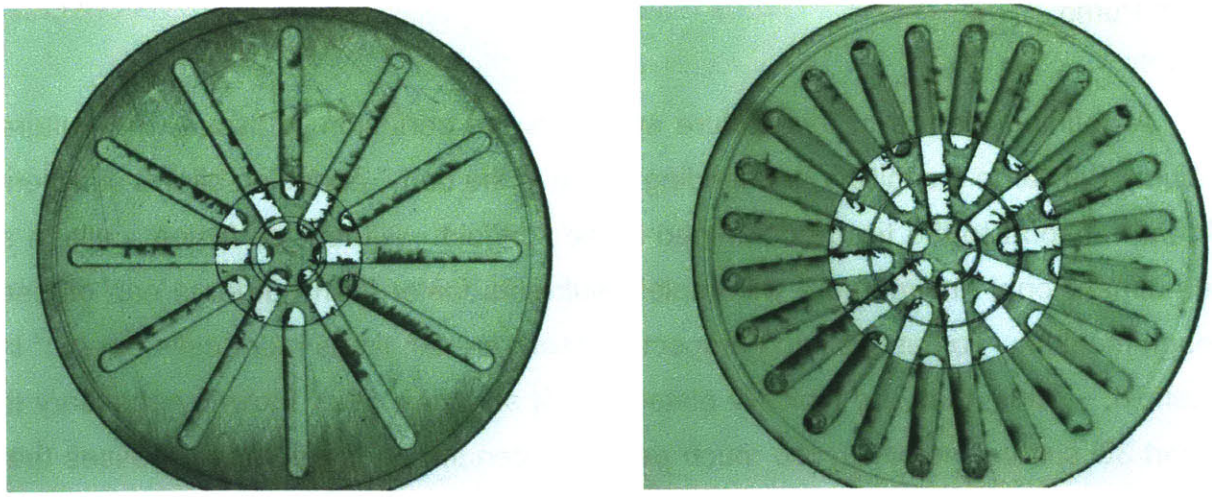

Figure 2.9: Filter supports that prevent flow through the outer edges of scaffolds containing fewer channels

A retaining ring is used to hold the scaffold assembly in place. It compresses the gasket in order to create a fluidic seal, forcing fluid through the filter and scaffold. The retaining ring is a 1 mm thick ring, 15.1 mm in diameter. It is slightly larger than the 15 mm diameter well in order to achieve a compression fit. The ring is 2 mm tall with six 0.8 mm diameter holes evenly spaced around the perimeter. These holes facilitate removal of the retaining ring from the reactor well.

The o-ring gasket, which resides at the bottom of the assembly, is made using very soft silicone rubber. The cylindrical geometry of the o-ring, and the low durometer, 30A, of the material improve gasket compression and create a better seal. A cylindrical shape decreases the contact area of the gasket on the bottom of the well; thus, higher compression and a better seal are achieved with a lower holding force. This seal is crucial to reactor operation because without it, flow would bypass the scaffold and there would be no tissue perfusion.

2.2.2 Pumping System

2.2.2.1 Pump

A defining feature of this culture system is the perfusion of tissue with culture medium. Similar to a capillary bed feeding tissue in the body, perfusion allows sufficient nutrient transport to the tissue contained in the scaffold. Without perfusion, cells in a three-dimensional environment will deplete nutrients faster than nutrients can diffuse through medium. To put this into perspective, there are ten times more cells per cm^2 in a scaffold, ~ 500k, than are typically plated on flat surfaces, 50k. Flow is necessary to support 3D culture; however, too much perfusion can impart large shear stresses that can be detrimental to cells [25, 26]. For these reasons, flow through the tissue must be precisely controlled.

Oxygen is poorly soluble in cell culture medium and is quickly metabolized by active hepatocytes [20]. As such, oxygen is the limiting factor when supplying nutrients to the tissue. A flow rate of 1 μL/channel/minute was chosen because it provides enough oxygen to the cells in a channel while keeping shear stresses below physiological values [20].

The bioreactor utilizes a pneumatic pumping system. This type of system offers several key advantages. Since the pump only requires a flexible membrane for actuation, there is no need for moving parts or electrical components within the bioreactor. Thus, the bioreactor plate is easy to assemble, inexpensive to fabricate on a large scale and could potentially be disposed of after use. Another benefit of this system is the partitioning of sterile and non-sterile surfaces. The more complicated parts, like the controller and the pneumatic pumping plate, do not come into contact with the cell culture medium and thus do not need to be sterile.

A detailed schematic of the pumping system is shown in Figure 2.10. This system consists of two pneumatic valves, a pumping chamber, and a capacitor to damp fluid pulses. Each reactor unit has its own pumping system that is fluidically isolated from all of the other pumps on the device.

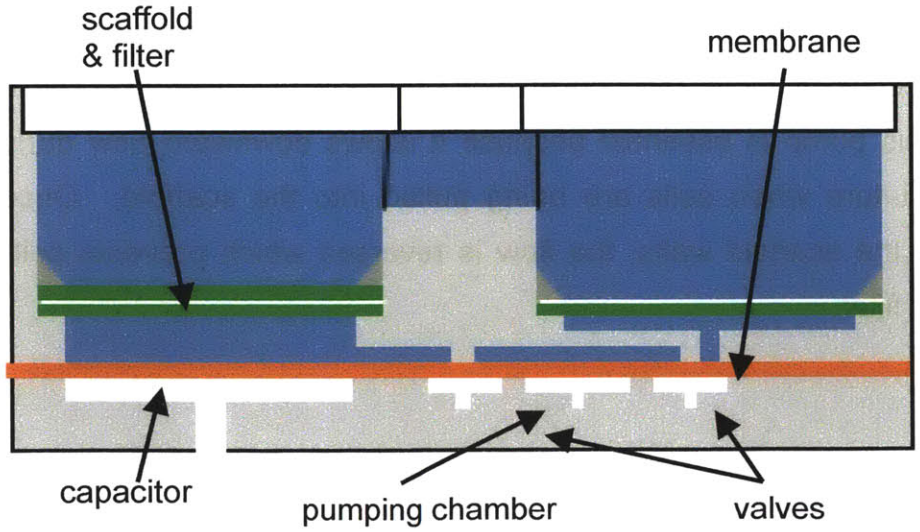

Figure 2.10: Cross section of the reactor pumping system

Fluid is moved through the pump by actuating the valves and pumping chamber in sequence. A valve, shown in Figure 2.11, is opened or closed when positive or negative air pressure is applied to it. Negative pressure below the valve pulls the membrane down to the surface of the pneumatic plate, filling the valve with fluid, and opening it. Fluid is pumped by opening the valve on one side, filling the pumping chamber, switching the valves and draining the pumping chamber out the other side.

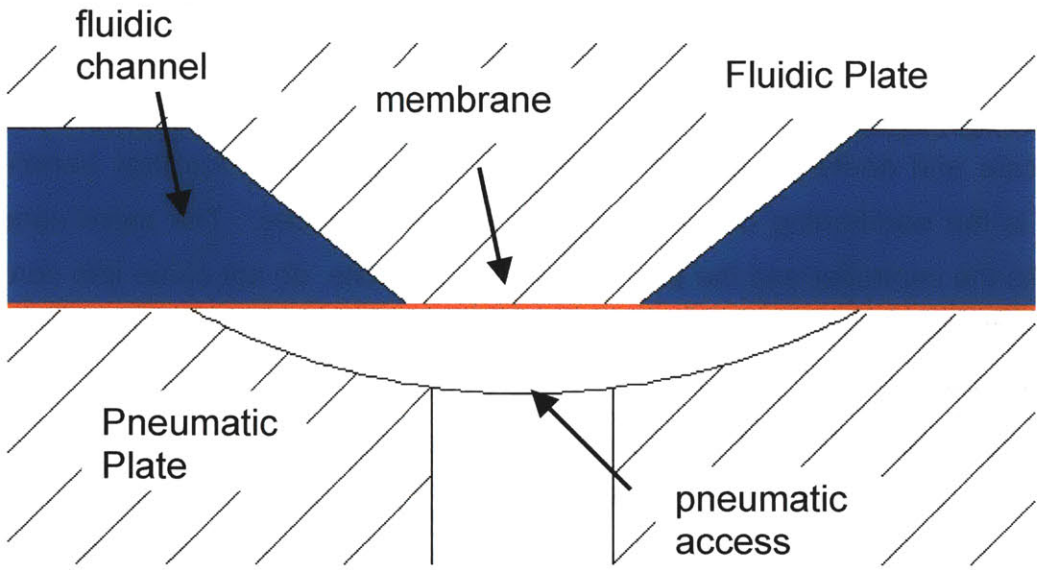

Figure 2.11: Cross-section of a valve

The pumping sequence, shown in Figure 2.12, can be run in the forward or reverse direction to move fluid up or down through the scaffold. The bi-directional nature of this pump is essential because it allows downward flow during the initial stages of culture when cells are being pulled into the scaffold. Once cells have attached to the scaffold walls, the flow is reversed which prevents cell debris from clogging the filter.

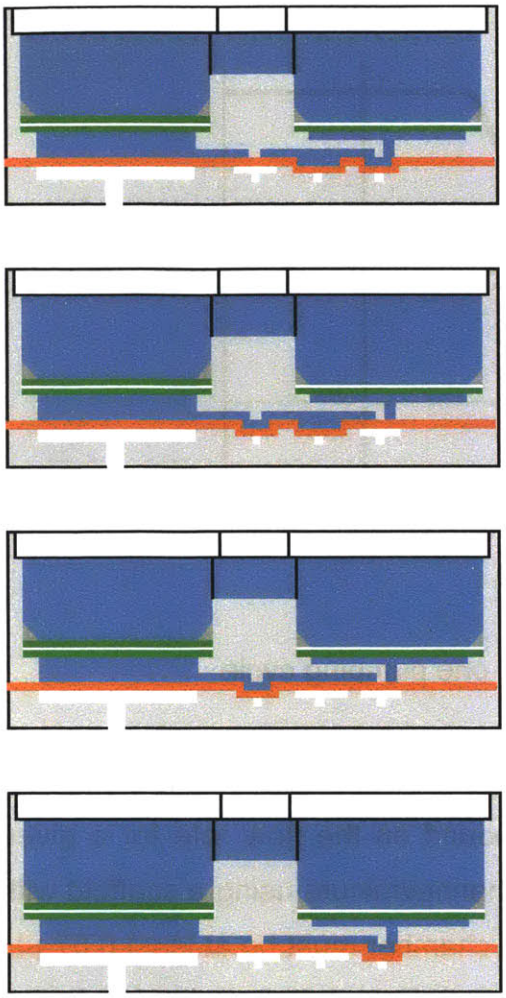

1. Fill Pumping Chamber

2. Switch Valves

3. Drain Pumping Chamber

4. Switch Valves

Figure 2.12: The pumping sequence can be run in both directions

The volume pumped per cycle and cycle frequency determine the flow rate. Figure 2.13 shows the volume output of the pump through one cycle. During the first step of the cycle, there is no output from the pump. In step two, when the final valve opens, fluid is pulled into the pump and the instantaneous flow is temporarily negative. In step three, the volume of fluid in the pumping chamber is ejected from the pump. In step four, the final valve closes and the volume it drew in during step two is sent out. The volume of the pumping chamber sets the volume pumped per cycle.

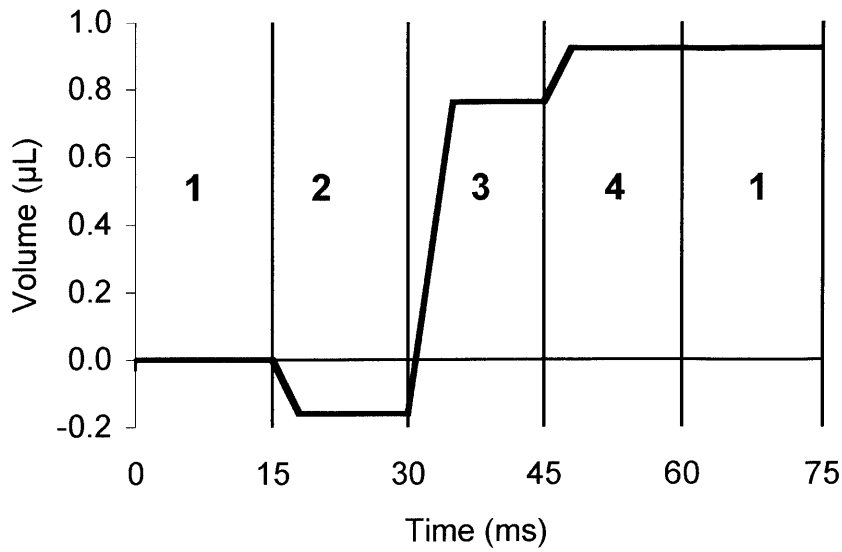

Figure 2.13: Flow from the pump over one pumping cycle

The pump can be run up to frequencies of ~ 25 Hz before the consistency of flow begins to suffer (Chapter 5). This sets an upper bound on the flow rate for a given pumping chamber volume. In order to flow at 1 µL/channel/minute using a scaffold with the maximum number of channels, 861, the pumping chamber must be at least 0.67 µL. As will be discussed in Chapter 4, the volume of the pumping chamber should be kept at a minimum in order to mitigate the effects of fluid pulses. For this reason, a pumping chamber volume of 0.92 µL was chosen, allowing dependable flows up to 1.6 µL/channel/minute in a system with 861 channels.

Since the volume of the pumping chamber determines the flow rate, it is important that this volume is very well-defined. The surfaces in the pumping chamber set a deterministic limit on the deflection of the membrane and the membrane must be able to completely conform to these surfaces.

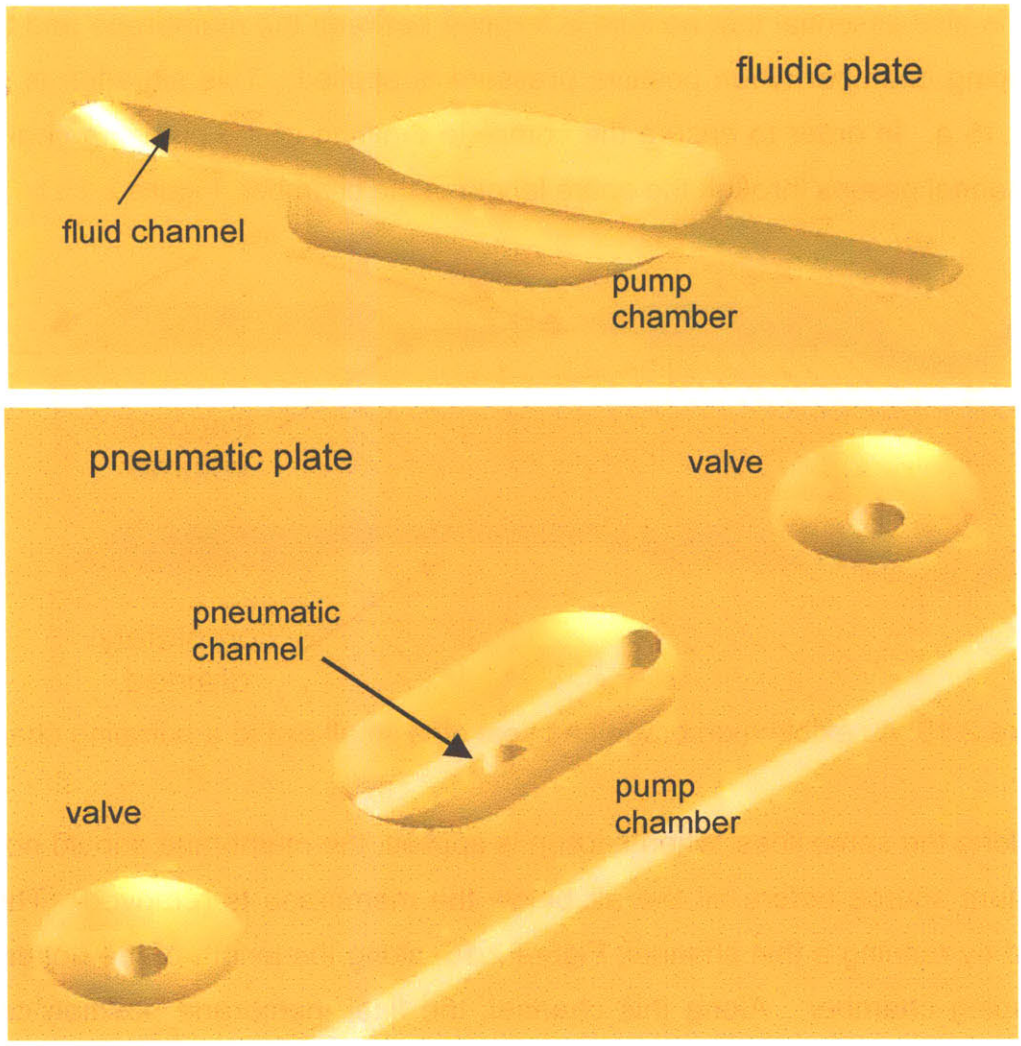

Figure 2.14: The pumping chamber

The pumping chamber, shown in Figure 2.14, is created by identical, shallow, radiused dimples on either side of the membrane. This radius, 1.575 mm, was set such that the membrane only needs to strain 4.2% in order to contact the top or bottom surface, requiring 12 kPa pressure difference across the membrane. These calculations are further discussed in Chapter 4 and are shown in Appendix A2. This pressure is well below the operating pressure of 35 kPa, which is set in Chapter 5. At 35 kPa, membrane stiffness will have a negligible effect on the pumping volume as the rigid body of the reactor sets membrane deflection limits.

It is also essential that no fluid is trapped between the membrane and the top of the pumping chamber when positive pressure is applied. This situation is shown in Figure 2.15 a. In order to ensure the complete draining of the pumping chamber, the fluidic channel passes through the entire length of the chamber, Figure 2.15 b.

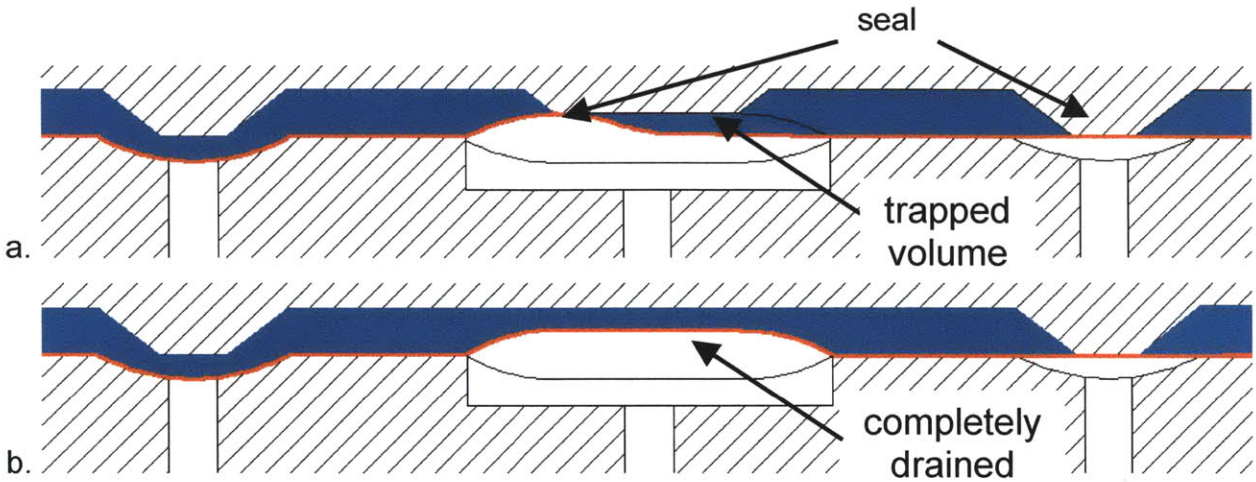

Figure 2.15: A flexible membrane can seal off a small exit to a pumping chamber

Along the same lines, when suction is applied, the membrane should not seal off the vacuum source before all the air below the membrane is removed. This risk is mitigated by running a thin channel, Figure 2.16, along the length of the bottom side of the pumping chamber. Along this channel, the final membrane position cannot be deterministically set. Therefore, width of the channel, 0.4 mm, is minimized such that volume doesn't noticeably change with different operating pressures.

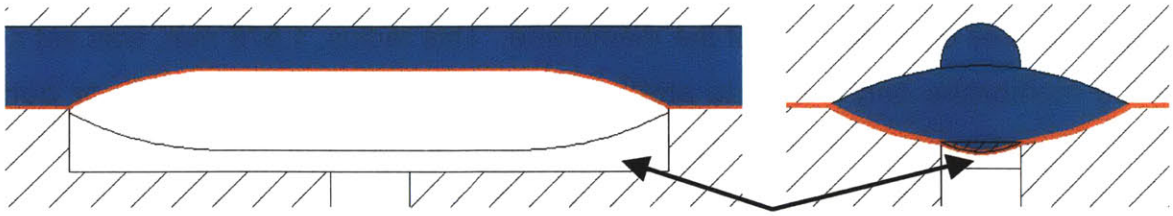

Figure 2.16: A small pneumatic channel spanning the pumping chamber ensures the complete filling of the pumping chamber with fluid when vacuum is applied

When the bioreactor is assembled, a fluidic seal is created by squeezing the membrane between the fluidic and pneumatic plates. If the membrane is too thick, it will

compress between the plates, but not in the pumping chamber. When this occurs, Figure 2.17, it is possible the membrane will partially or completely fill the pumping chamber. For this reason, a very thin, 25 μm, membrane was chosen.

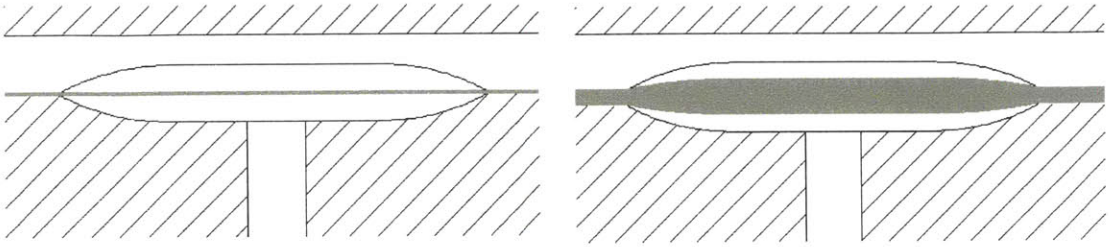

Figure 2.17: Comparison of thick and thin membranes. Thick membranes can fill the pumping chamber, changing the volume pumped per cycle and thus the flow rate.

The valves have a different set of design characteristics. It is imperative that the valves open and close reliably, and that they completely seal when closed. The volume of the valve does not influence the pumping cycle volume; however, minimizing valve volume is important because it eliminates the negative flow patterns shown in Figure 2.13.

Valves close by creating a seal across a break in the fluidic channels. When pressure is applied below a valve, the membrane is pushed flat against the bottom of the fluidic plate. When the valve is open, both segments of the fluidic channels are connected.

The fluidic channels, shown in Figure 2.18, are rounded troughs in the bottom of the reactor plate. This trough is sealed at the bottom by the membrane. Channels break at each of the valves for 0.5 mm by sloping down into the valve area. This slope is used to eliminate dead volumes where bubbles can be trapped.

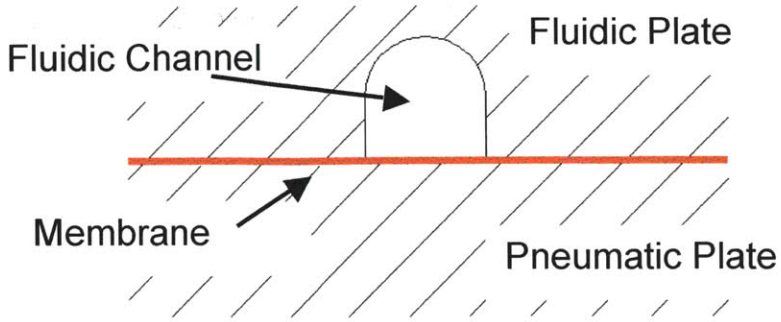

Figure 2.18: The fluidic channel

2.2.2.2 Fluidic Capacitor

When the pumping system operates, Figure 2.13, it creates fluid pulses. Due to the nature of the pump, these pulses, although kept at a minimum, are unavoidable and may be very detrimental to the cells cultured in the bioreactor. When cells are placed in the reactor these pulses cause the cells to visibly shake in the scaffold preventing cell adhesion. A fluidic capacitor is used in order to damp out the flow pulses created by the pump.

A capacitor effectively converts a volume-driven flow to a pressure-driven flow. The requirements for an effective capacitor are shown in Figure 2.19, and include a fluidic resistance and a closed fluid volume that can increase and decrease depending on fluid pressure. The fluidic resistance is set such that when a pulse of fluid enters the capacitor region it is more likely to fill the capacitor than pass immediately through the resistor. As the capacitor fills, the pressure increases. Over time, fluid bleeds through the resistor and drains the capacitor, lowering the pressure and making it again ready to absorb flow pulses.

In the reactor unit, the filter in the scaffold assembly supplies fluidic resistance. The capacitor, shown in Figure 2.20, is made by allowing the membrane to bulge up and down in response to positive and negative fluid pressures. The capacitor is located between the pump and the scaffold assembly and damps flow pulses both when the

pump sends fluid up through the scaffold and when fluid is pulled down through the scaffold to the pump. There is no capacitor on the far side of the pump.

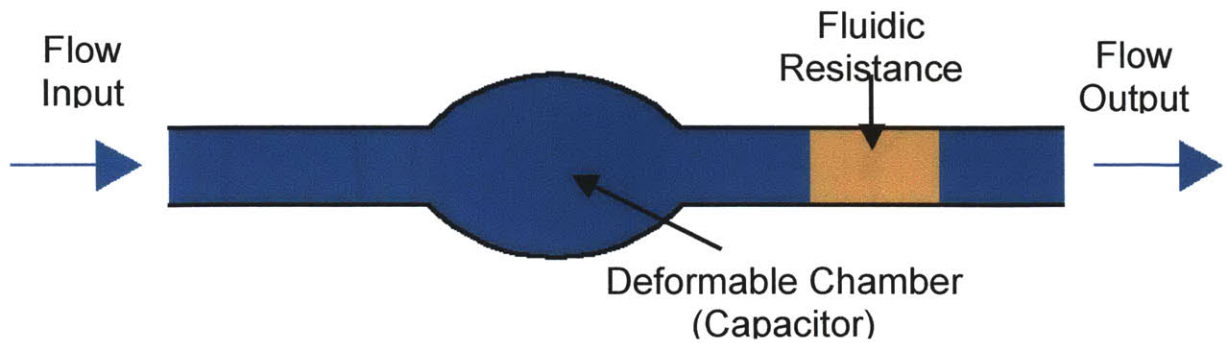

Figure 2.19: Capacitor components include a flow source, a capacitor and a resistor

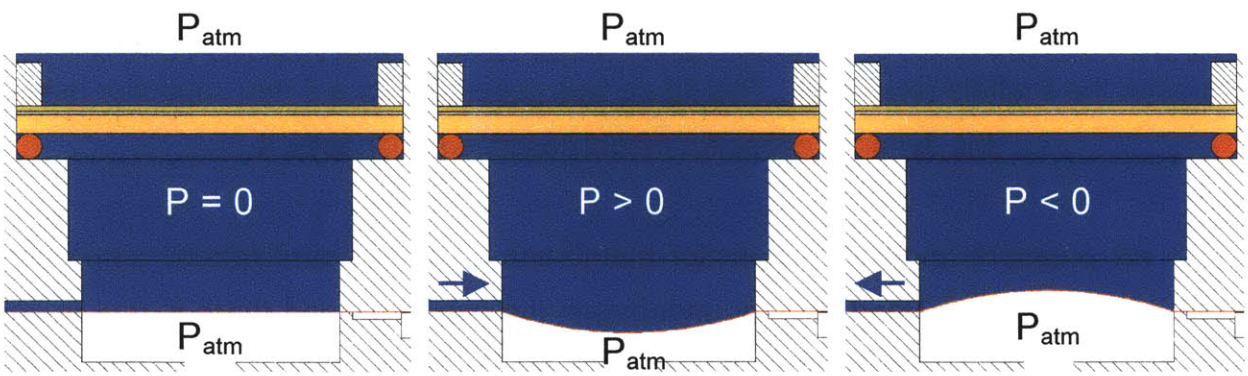

Figure 2.20: The fluidic capacitor in a) no flow, b) flow up through scaffold, and c) flow down through scaffold

When a pulse of fluid is sent from the pump into the capacitor the increased capacitor volume deflects the capacitor membrane and causes pressure to rise under the scaffold. Flow volume has been converted to a fluidic pressure. As a result of increased pressure, fluid flows through the scaffold and the capacitor deflates. When fluid flows in the reverse direction, from the scaffold into the pump, pressure below the scaffold is less than atmospheric and the capacitor membrane deflects upwards.

Figure 2.21 compares flow through the scaffold when a capacitor is used, to flow without a capacitor. Without a capacitor, all of the flow through the scaffold occurs during only one of the four cycles of the pump, Figure 2.14. With a properly balanced

capacitor, flow continuously occurs throughout the duration of the pumping cycle. This removes sharp pulses in the flow and brings the maximum flow rate and shear stress closer to the average flow. Chapter 4 goes into more detail on capacitor operation.

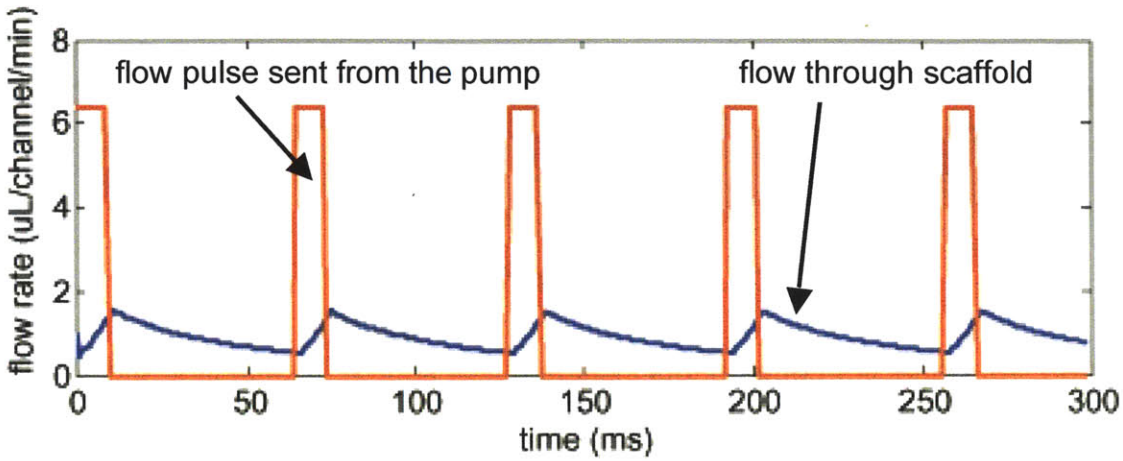

Figure 2.21: Flow into the capacitor from the pump (red line) compared with flow through the scaffold (blue line). This figure was generated for a 5 mm capacitor using the dynamic capacitor model described in Chapter 4.

Air pressure under the capacitor membrane is kept at atmospheric using vent ports. There is a vent port directly underneath the capacitor, and there is one in line with the channel. The second vent port helps bleed of any pressure leak that arises from the pumping system pneumatics. Since the bottom of the pneumatic plate is covered in order to seal the pneumatic lines, the openings to atmosphere are routed to the interface between plates.

2.2.3 Reactor Well

One reactor unit, shown in Figure 2.22, consists of two wells connected at the top by a surface channel and at the bottom by the pump. Medium circulates between these two wells and is perfused through tissue in the scaffold. Both wells are 12 mm deep and the total volume of medium held in the reactor unit can range between 1.75 and 3.5 mL with an optimal operating volume of 3 mL. Since some of that medium resides

below the scaffold, 1 mL, typically only 2 mL are accessible. The fluid surface of the reactor is open to atmosphere allowing oxygen exchange.

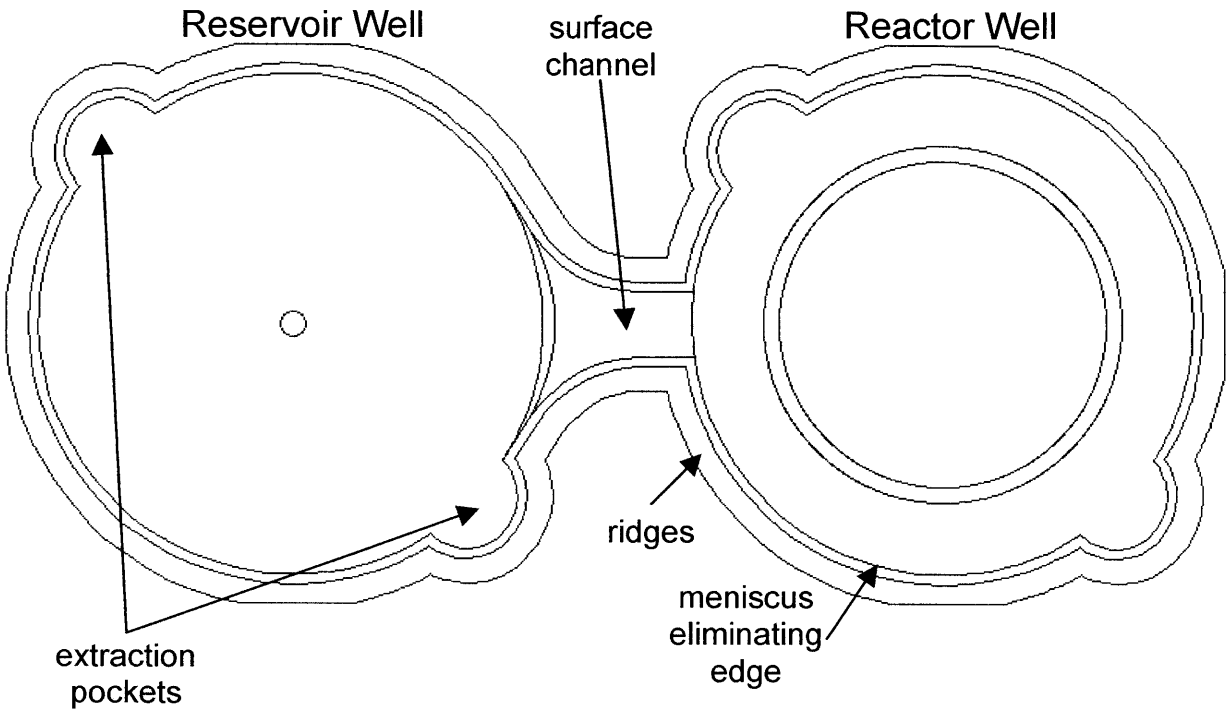

Figure 2.22: The reactor unit

The scaffold assembly sits in the 15 mm diameter reactor well and is accessible from above. A filter is used in the reservoir well. Unlike the filter under the scaffold, this filter can be replaced during the culture without disrupting the cells. This filter collects cell debris before it can get trapped on the filter under the scaffold. The reservoir well also contains a filter support, retaining ring and gasket.

Extraction pockets on either side of both wells are used to access the components in the reactor. These components can be inserted or removed from one reactor without disturbing the other reactor units on a plate.

The surface channel, shown in Figure 2.22, curves smoothly from the reservoir into the reactor well. This curve facilitates priming of the channel. The narrow entrance

on the reactor side helps prevent the scaffold assembly from hanging up on the ledge created at the bottom of the channel.

There are 2 mm tall ridges that line each reactor and the outside of the device. These ridges, shown in Figure 2.23, prevent spillage of fluid from one reactor to an adjacent reactor and help maintain fluidic isolation of reactors across the device.

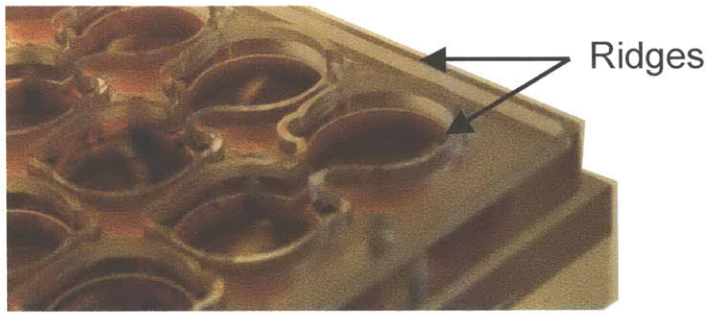

Figure 2.23: Ridges on the reactor surface help maintain fluidic isolation of reactor units

3.5 mm below the top of the ridges there is a ledge that can be used as target mark for the fluid level. It can also be used to level the fluid above the scaffold assembly, eliminating the meniscus. Without a meniscus there is no optical distortion and the cells are much easier to view. When fluid is filled to the proper height, the contact angle, α, will travel around the corner of the ledge until it becomes horizontal. This phenomenon is shown in Figure 2.24.

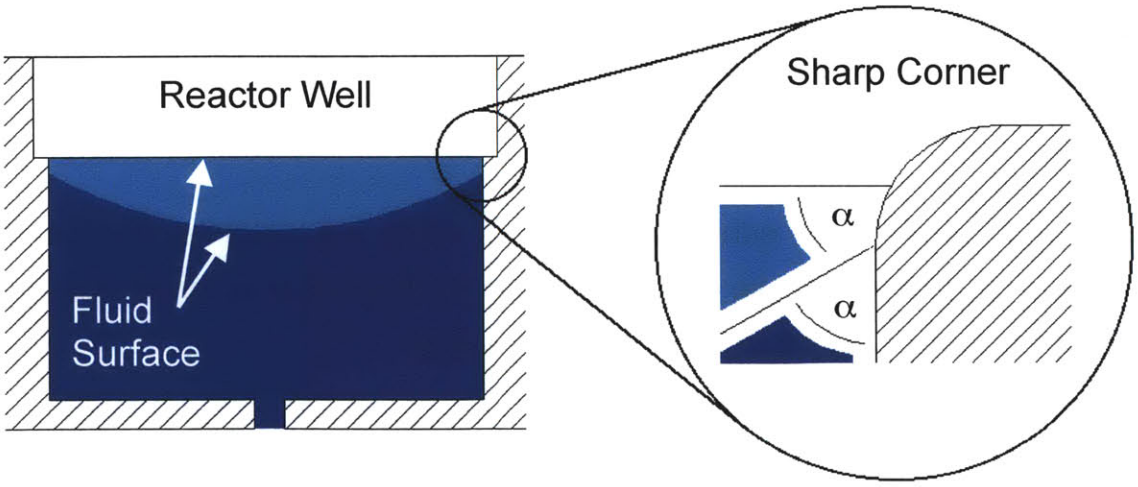

Figure 2.24: Contact angle of a fluid turns flat around a corner

Each reactor well is tapered at the top in order to facilitate loading of the scaffold assembly into the reactor. There is also a taper on the ledge created by the surface channel that serves the same purpose. Both of these tapers are shown in Figure 2.25.

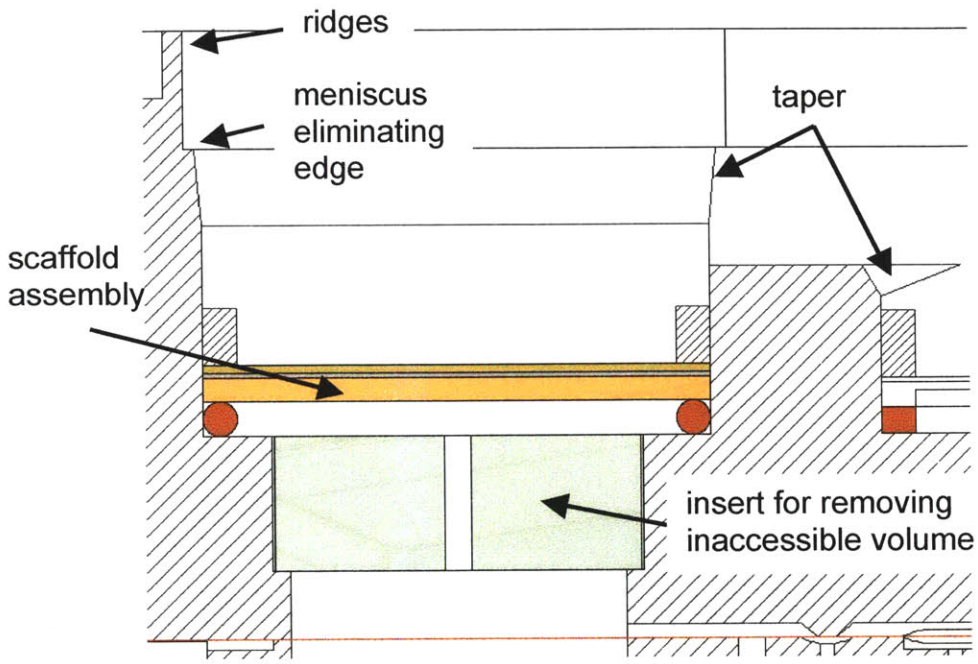

Figure 2.25: Cross section of a reactor well

An insert, seen in Figure 2.26, can be used to reduce the amount of inaccessible medium in the system. This insert is a solid piece of material with slots around the edge that facilitate removal of the piece from the reactor well. Medium flows through a hole in the middle of the part.

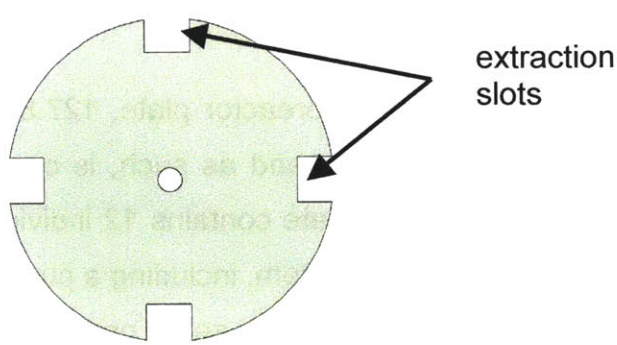

Figure 2.26: An insert used to remove inaccessible medium from the system

2.3 Bioreactor Plate

2.3.1 Plate Design

The bioreactor, seen in Figure 2.27, consists of a bottom 'pneumatic plate,' a top 'fluidic plate' and a membrane sandwiched between the two. Fully dimensioned drawings are shown in Appendix A1. The device is covered with a lid that minimizes the possibility of contamination. Three pneumatic lines connect the controller to the bioreactor and are used to drive the pumps.

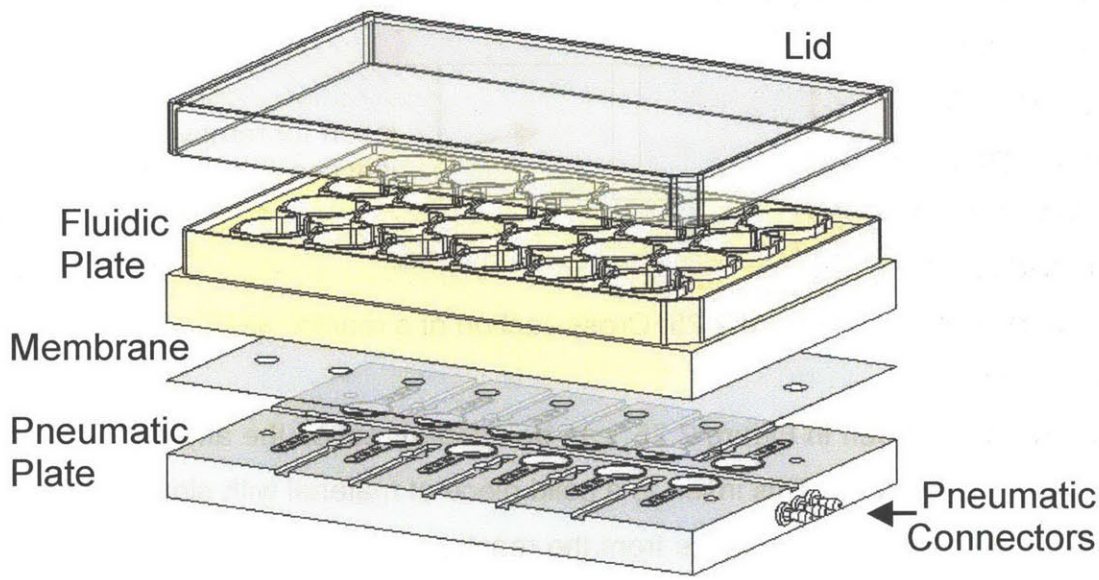

Figure 2.27: The bioreactor assembly consists of a reactor plate, a pumping plate, a flexible membrane and a lid

The footprint of the bioreactor plate, 127.8 x 85.5 mm, is identical to that of a standard tissue culture plate and as such, is compatible with existing fluid handling systems. Each bioreactor plate contains 12 individual reactor units. All of the reactor units have their own fluidic system, including a pump, capacitor and reservoir, and all 12 pumps are driven in parallel by one set of pneumatic inputs. Adjacent reactor wells are separated by 18 mm, double the spacing between wells in a 96 well plate. This spacing

was chosen so that a multi-channel pipette can be used with the reactor, and again, so the system is compatible with existing automation technology.

Each of the reactor units are fluidically isolated and in order to maintain that isolation, a complete fluidic seal must be made at the pumping interface of each reactor unit. The reactor and pumping plate are screwed together using 14 screws and must compress the membrane in order to create the seal.

Several important features improve this fluidic seal. First, the top of the pumping plate is recessed so that the membrane is compressed only at islands surrounding each reactor unit. Shown in Figure 2.28, each pumping system is isolated on an island where the fluidic seal is made. The use of islands reduces the area where the membrane is compressed from ~ 10,000 mm^2 to ~ 700 mm^2, and thus reduces the holding force between plates by more than ten fold. Since the membrane is thin, surface roughness and the flatness of the plate are also important. Achievement of these qualities is discussed in Chapter 3. Placement of the screws that hold the reactor together is also an important consideration. The screws are located along the center of the load created by compression of the membrane under a row of reactor units. Finally, the bioreactor plates are relatively thick, 18 mm and 9.5 mm, which minimizes bowing at the edges.

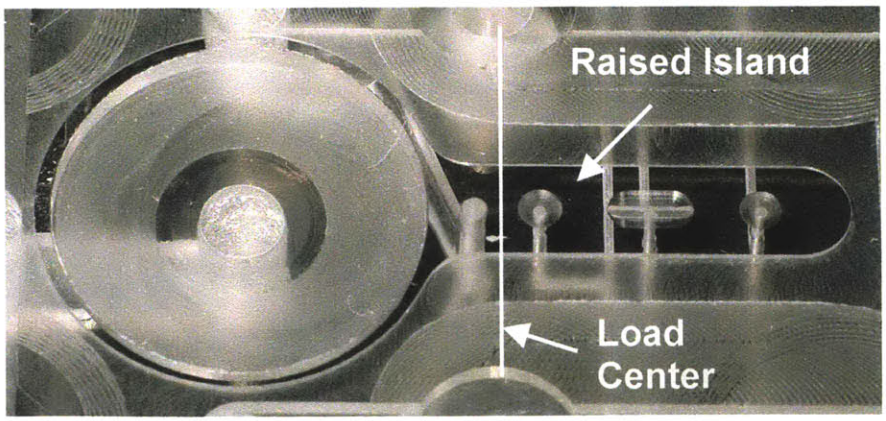

Figure 2.28: Islands are used to isolate pumping systems of adjacent reactor units. This figure shows the pumping system for one reactor unit on the pneumatic plate.

The pumps on each of the 12 reactors are driven in parallel by pressure pulses sent from the controller. Pressure is supplied through one of three pneumatic lines that connect to either all of the pumping chambers, or all of one of the two fluidic valves. These lines, shown in Figure 2.29, run along the bottom of the pumping plate. They are connected to valves on the top side of the pumping plate using through holes. Tape is used to create a seal along these lines.

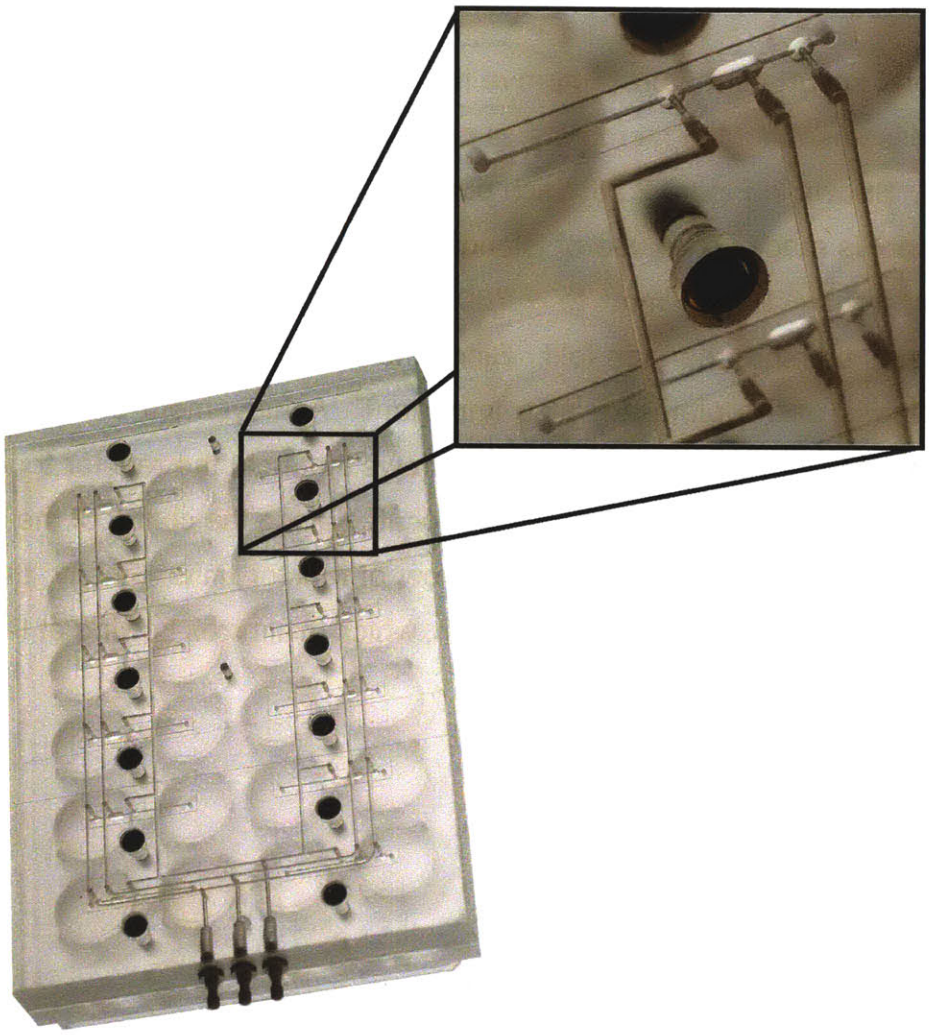

Figure 2.29: Pneumatic lines route pressure and suction to valves and pumping chamber

In typical reactor operation, the flow in all reactor units is the same. For this reason, there are only three connectors for pneumatic lines corresponding to the

pumping chamber and the two valves. Some experiments, however, call for different flows across the reactors. For these cases, a pumping plate has been made with two sets of pneumatic inputs, Figure 2.30.

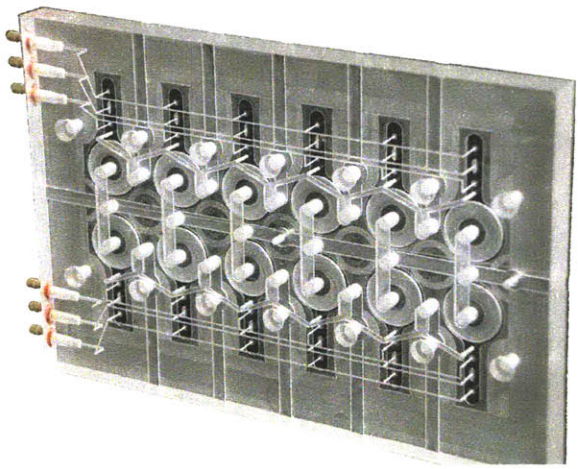

Figure 2.30: Two sets of pneumatic inputs allow different flows across the bioreactor

There is a secondary channel that runs along the fluidic lines. This channel, shown in Figure 2.31, causes a slight leak of pressure in the pneumatic system.

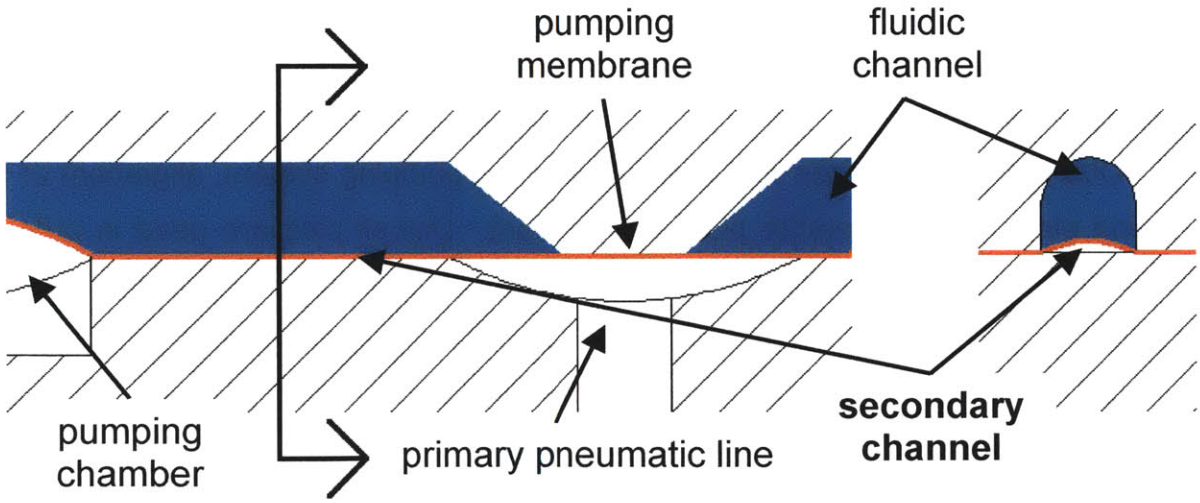

Figure 2.31: A secondary channel runs along the fluidic lines underneath the pumping membrane.

Since the resistance along this secondary channel is very high in comparison with the resistance through primary pneumatic lines the pressure set at the controller is

almost identical to the pressure at the valves. This is visually depicted in Figure 2.32 and is confirmed in Chapter 5. Also, because operating pressures are well above those required to move the membrane, this slight leak will not hinder the performance of the bioreactor.

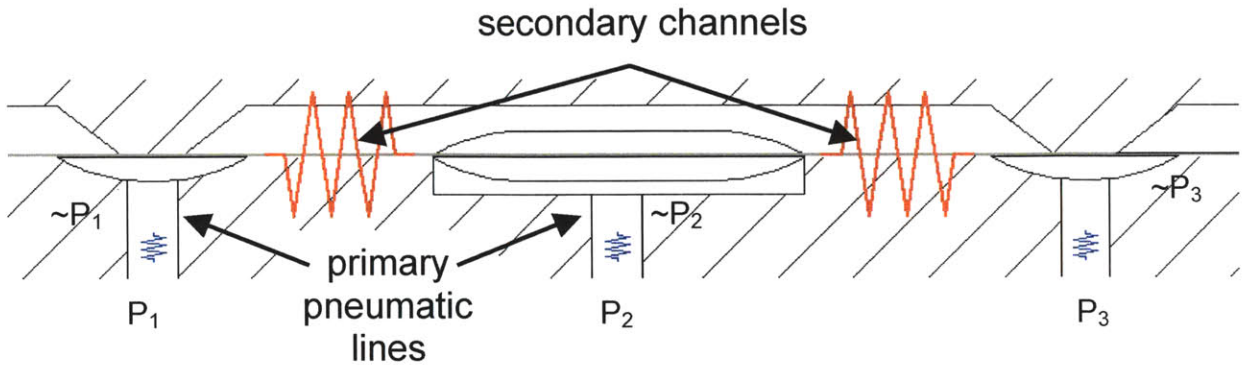

Figure 2.32: Circuits comparison of pneumatic leak. The larger resistance between valves prevents a significant drop in pressure at the valve

Pneumatic lines are run along the bottom of the pneumatic plate to ensure fluidic isolation of reactors. The use of a separate plane eliminates the need to create a seal at the pumping interface. If the pneumatic lines were run along this interface, a secondary channel would connect the fluidic systems of adjacent reactors.

Due to the small sizes and tolerances in the pumping system, alignment of the pumping plate with the reactor plate is important. Dowell pins are used in order to ensure proper alignment of the pumping features. A pin in the center of the pumping plate fits into a cylindrical hole in the reactor plate and is used as a position constraint. A pin on the edge of the pumping plate fits into a slot in the reactor plate and is used to constrain rotation.

2.3.2 Materials

Proper material selection is essential for maintaining viable cultures. All reactor components and the materials used to manufacture them are presented in Figure 2.33.

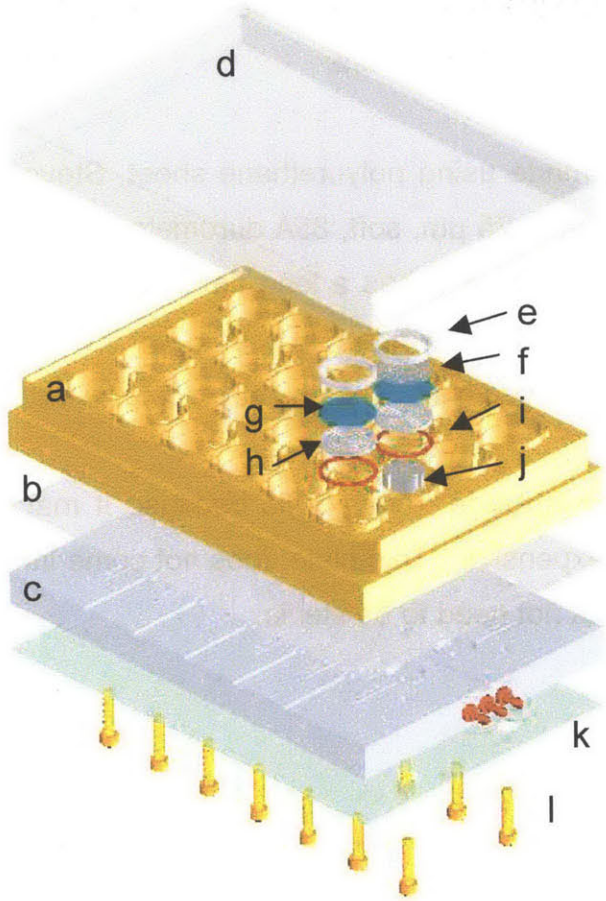

Figure 2.33: Exploded view of the bioreactor showing all bioreactor materials, manufacturing methods and quantities: a) machined polysulfone fluidic plate; b) punched polyurethane membrane; c) machined acrylic pneumatic plate; d) injection molded polystyrene lid; e) machined PEEK (polyetheretherketone) retaining ring (24); f) scaffolds are either etched silicon or micro-drilled PEEK or polycarbonate (12); g) punched PVDF filter (24); h) machined polysulfone filter support (24); i) silicone o-ring gasket (24); j) machined polysulfone filler (12); k) tape; l) stainless steel screws (14)

Polysuflone is used for a large number of reactor parts. Polysulfone is a translucent material with an amber tint. This material has good dimensional stability and chemical resistance. It is machineable and can be injection molded. Since most reactor parts come into contact with medium, they must be sterilized before each experiment. The maximum operating temperature for polysulfone is 140 °C making it suitable for autoclave sterilization. When viewing the cells under a microscope, light is

shined through the reactor from below. In order to see the cells, all reactor parts underneath the scaffold must be translucent.

The membrane is made using polyurethane sheet, Stevens Urethane ST-625. This polyurethane is very thin, 25 μm, soft, 85A durometer, and flexible. Polyurethane is a very tear resistant material and has a long flex-life. It is made with a minimum number of additives, only 7% by weight. There is an FDA approved food grade antioxidant and an FDA approved clay. There is also some wax.

The pumping plate is made from acrylic because it machines very well, it is optically clear and it is inexpensive. This plate does not come into contact with culture medium and therefore does not need to be sterile.

2.4 Auxiliary Systems

2.4.1 Controller

The controller, shown in Figure 2.34, is used to set the rate and direction of flow in the reactor units. The controller sends pneumatic pulses to the bioreactor plate and runs the valves and pumping chamber in sequence.

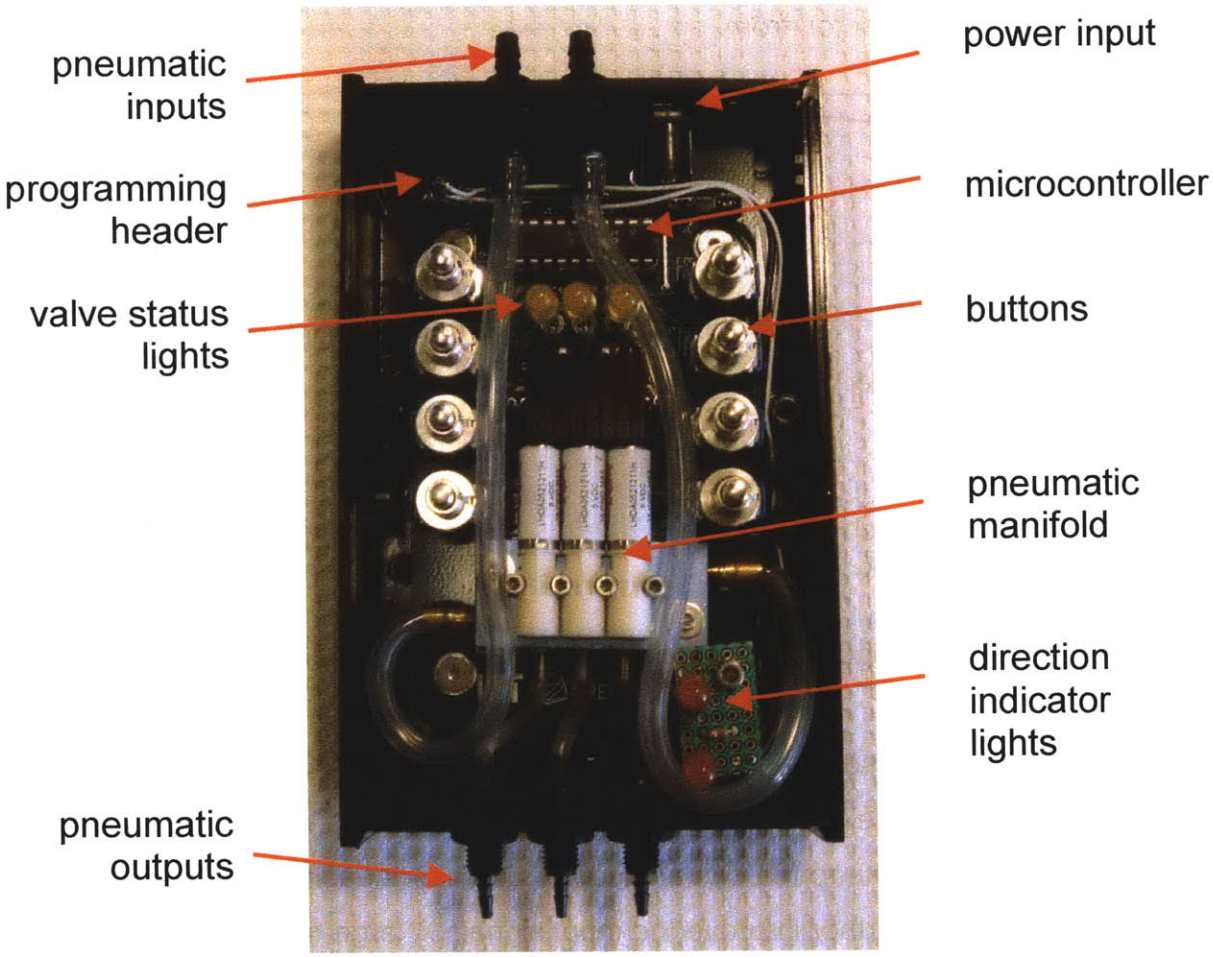

Figure 2.34: The controller with lid removed to show all components

2.4.1.1 Electronic System

A circuit diagram of the controller is presented in Figure 2.35. The controller is run using an Atmel ATtiny26L. This microcontroller is powered with 5 V, has 16 I/O ports and has a built in clock set to run at 1 MHz. Eight of the ports take input from switches. Three ports output to the pneumatic valves and four are used for in circuit programming. One port is unused.

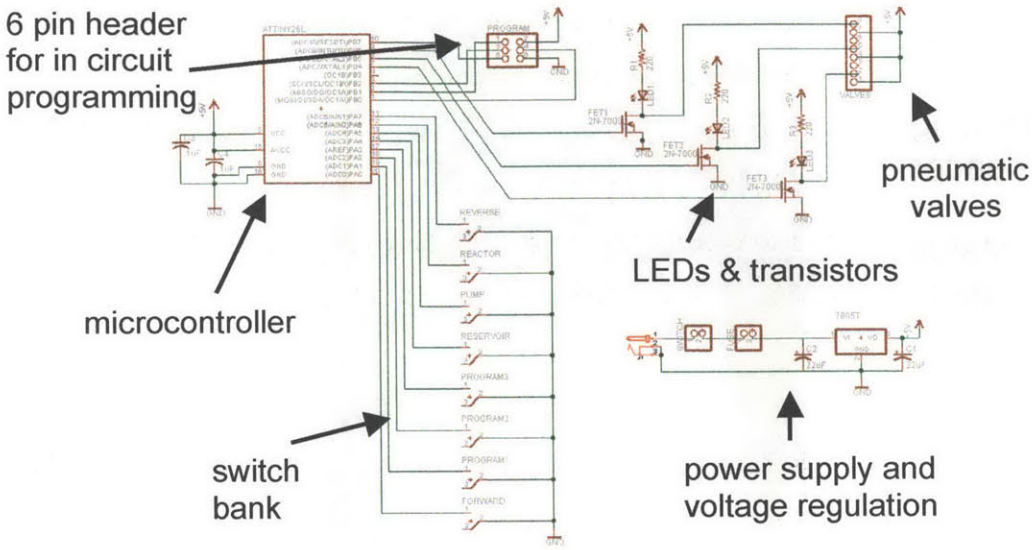

Figure 2.35: Circuit diagram of the controller

The controller is supplied with 12 V, which is regulated down to 5 V using a 1.5 A voltage regulator. The output from the voltage regulator is oscillatory so 22 μF capacitors are used to keep the signal steady. Smaller capacitors, 0.1 μF, are used at the microcontroller to further improve the input signal. A large metal pad is used to help dissipate heat from the voltage regulator. A CAD layout of the printed circuit board is shown in Figure 2.36.

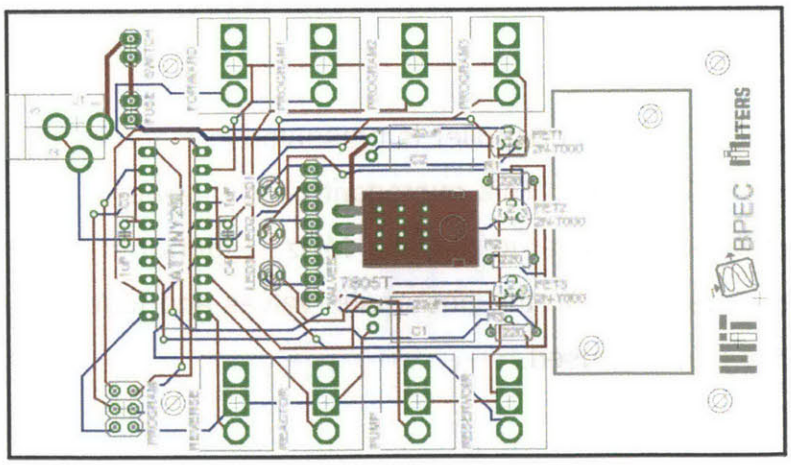

Figure 2.36: A CAD drawing of the controller printed circuit board. Red lines run along the top of the board and blue lines run underneath the board.

The switches, APEM 8432 AB, are momentary pushbutton switches. They are connected to pull-up resistors built into the microcontroller.

A 6-pin header is included on the circuit board and allows for in circuit programming. This means the microcontroller can be reprogrammed without removing it from the board. Since this controller was designed for development of the bioreactor, this feature is of huge importance.

The pneumatic valves are actuated by 5 V and draw a 110 mA current. Transistors, STMicroelectronics 350 mA, provide the necessary power to the valves. LEDs are also connected to the transistors and are used to indicate the state of the valve.

When the controller was designed, typical pumping frequencies were around 1 Hz. At a low frequency it is easy to determine the direction of flow by watching the status lights on the valves. At higher frequencies, the flow direction isn't readily seen in these lights. Two more LEDs, indicating flow direction, were connected to the 6-pin header used for programming.

2.4.1.2 Pneumatic System

A diagram of the pneumatic manifold is shown in Figure 2.37. The manifold receives positive and negative pressure inputs. Three, three-way solenoid valves, The Lee Company LHDA0521111H, are used to switch between pressures. The solenoid valves receive a signal from the microcontroller that sets them to output pressure or suction to the bioreactor pumping chamber and valves.

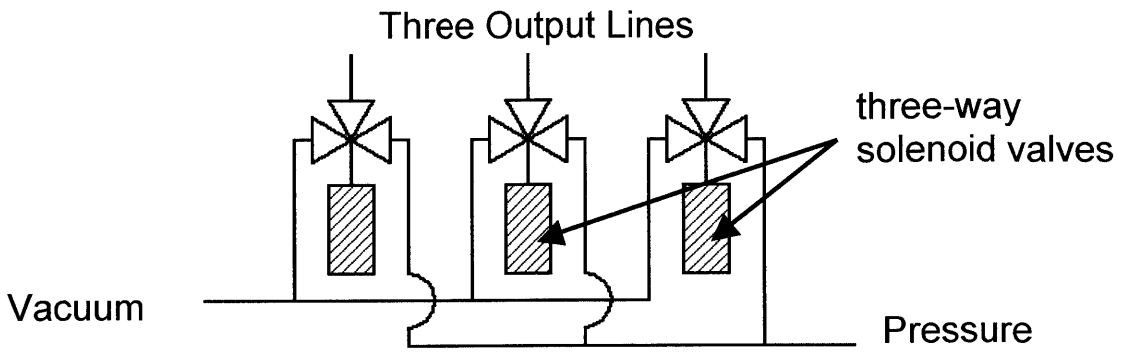

Figure 2.37: The pneumatic manifold takes input from pressure and vacuum lines and outputs to three separate lines

These valves have a rated life of 250 million cycles and can be used with inlet pressures up to ~ 350 kPa and differential pressures up to ~ 100 kPa. They have a response time of 3 ms.

2.4.1.3 Programming

The current bioreactor program, shown in Appendix A3, has five operating modes: flow can be sent up or down through the scaffold at a desired rate; the pump can operate in either direction for a set volume before stopping; and the pump can be controlled manually.

The rate of flow can be manipulated by changing the pumping frequency. Frequency is set by programming a delay between steps in the pumping cycle. This delay burns off clock cycles in the microcontroller and checks for input from the switches.

Input from the switches sets a variable that is used to determine which subroutine to run. When the pump is set to run indefinitely, it checks for a new input

after each pumping cycle. If the pump is set to run for a predetermined number of cycles, the pump will complete the cycles before re-checking for a new input.

The pump can also be run manually. Pressing the button corresponding to one of the valves or the pumping chamber will switch the pump over to the manual mode. In this mode, the valves and pumping chamber can be opened or closed by pressing the correct button on the controller. Manual pump operation was helpful during the development of the device. A schematic of the bioreactor control buttons is shown in Figure 2.38.

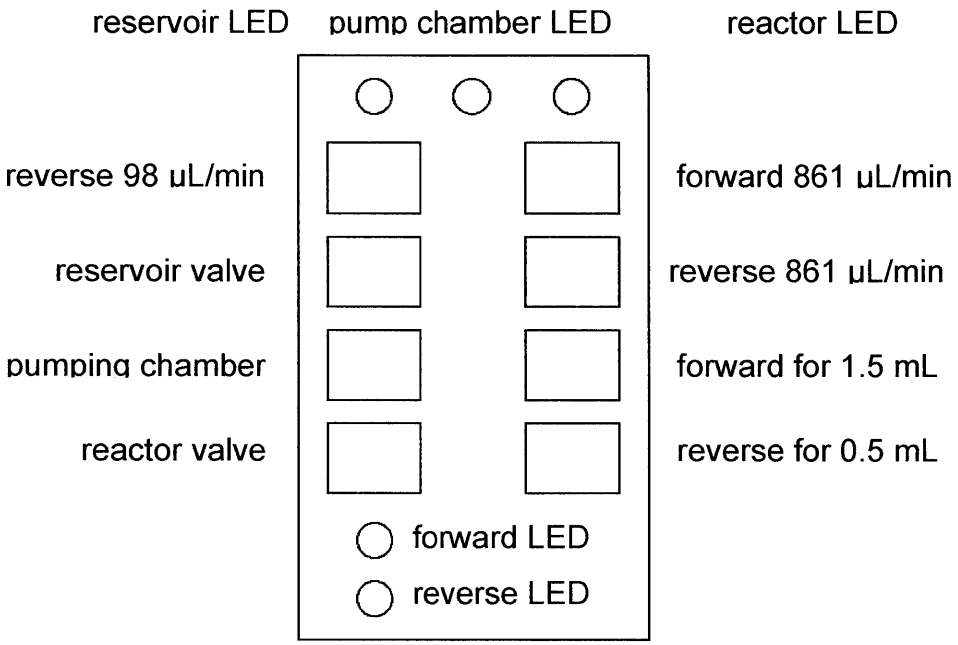

Figure 2.38: Bioreactor controls diagrammed for the current controller configuration

2.4.2 Pneumatic Regulation

Positive pressure and vacuum are available in most labs through hookups at the benches. These hookups can be used to run the bioreactor. Pressure that comes directly from theses lines can be ~ ±70 kPa. Since the reactor is typically run using ± 35

kPa, these inputs are regulated down to the desired pressures. The pneumatic manifold that regulates pressure is shown in Figure 2.39.

As suggested by The Lee Company, a 5 μm filter is used in order to keep unwanted particles from entering the pneumatic valves. Since the vacuum lines are sometimes used for medium aspiration, it is possible to contaminate these lines. Filters prevent this contamination from entering the system.

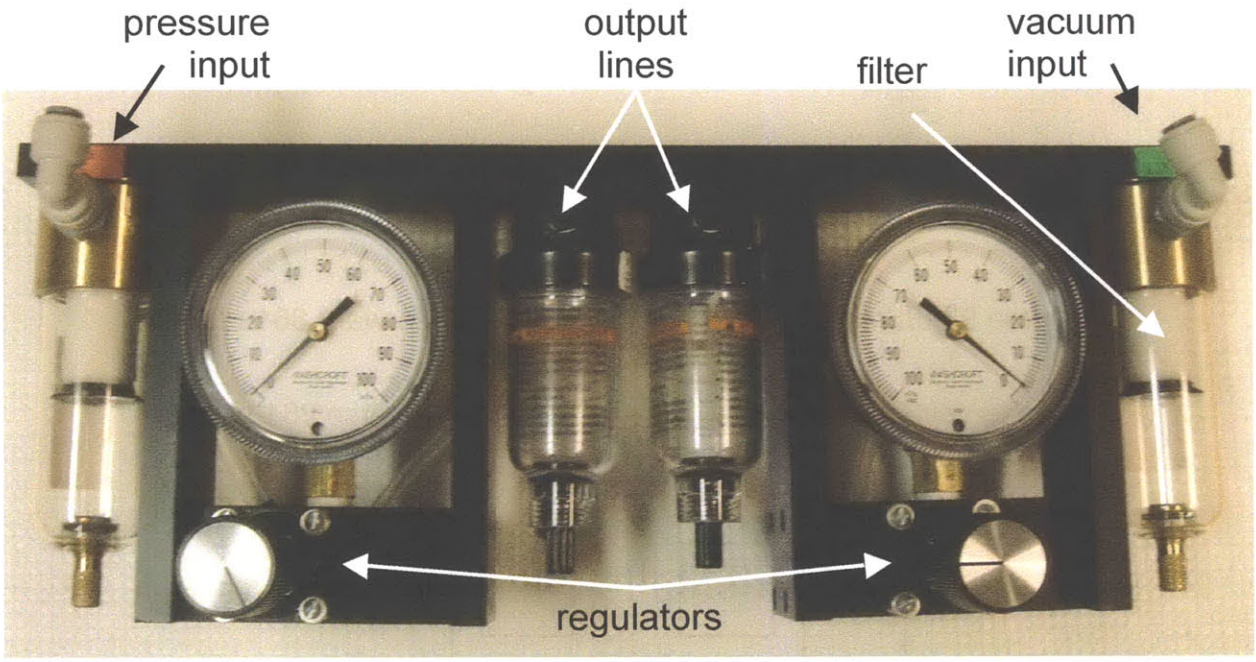

Figure 2.39: Pneumatic regulators and filters

3. FABRICATION

Most of the components in this system were made using a Bridgeport EZ-Track CNC milling machine. The milling machine offers a high level of precision and is a very good tool for prototyping. Because the bioreactor, scaffold, and pumping system utilize features with very tight tolerances, this precision is essential for reliable performance. For example, adjacent holes on a scaffold are separated by only 100 μm. The pumping system relies on the alignment of features located on separated plates and utilizes cuts that are as shallow as 190 μm. This chapter describes techniques utilized in bioreactor fabrication, including the steps taken while machining that allow for such precise features. The manufacture method for each component is presented in Figure 2.23, and a complete set of machining code is provided in Appendix A4.

3.1 Bioreactor

Achieving a good fluidic seal between the fluidic plate and the pneumatic plate is critical to the performance of the device. Since the membrane is only 25 μm thick, it does not conform around curved surfaces, thus the sealing surfaces must be perfectly flat and smooth. These surfaces also need to be level. If the surface is not level when cutting the pumping chambers, which are 190 μm deep, some chambers will be deeper than others. The volumes in deeper chambers will be greater and the flow rate for a given frequency will vary across the device.

The reactor plate comes from a rough stock and both surfaces must be fly cut. Fly cutting flattens a part, but leaves a rough surface. In addition to fly cutting, a small, 5.5 mm, tool is run around the sealing surface of the plate. This tool has slightly rounded edges, which leave a smoother finish. Using a smaller tool decreases the roughness of the cut and it keeps the cutting surface perfectly level. During this cut, the tool is programmed not to lift off of the surface of the part. This is to prevent any ridges

that would result if the tool were to lift then come back down to a slightly different height. Once this cut is made, the reactor surface is smooth, flat, and level. The pumping chamber and fluidic channels are machined before the part is removed from the vise.

The pumping plate is made using stock with polished surfaces. Although surfaces are smooth, they are generally wavy and are not level in the vise. Similar to the reactor plate, the top side of this plate is fly cut and a small tool is run around the pumping surface. The bottom side contains no features that are sensitive to tool depth and therefore it does not need to flattened.

The depth of the pumping chamber is one of the most critical machine operations when manufacturing the bioreactor. A ball end mill, shown in Figure 3.1, is used to machine the pumping chamber. Seen in this figure, the depth of this cut also sets the pumping chamber width and length and thus will have a dramatic influence on the pumping chamber volume.

The desired cutting depth, h, is found using the equation,

$$h = r - \sqrt{r^2 - (w/2)^2}, \tag{3.1}$$

where r is the radius of the tool used and w is the desired width of the chamber. Using a Bridgeport CNC machine, this depth can be controlled up to 5 μm. Since the depth is a critical feature, this machine tolerance influenced the design of the pumping chamber, detailed in Chapter 2 & 4.

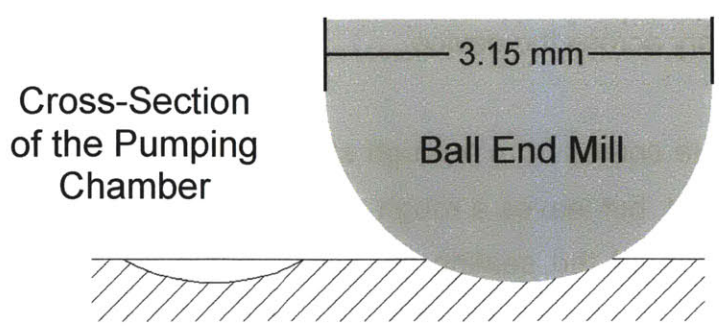

Figure 3.1: A schematic showing the tool used to create pumping chambers and valves and the to-scale depth of a pumping chamber. This figure gives perspective to the sensitivity of depth when cutting the pumping chamber.

A second feature that is sensitive to tool depth is the fluidic channel. This channel, shown in Figure 3.2, slopes at an angle down into the 1.5 mm diameter valves. If the cuts are made too deep, the channel will connect all the way through the valve, permanently opening the valve. When the cuts are too shallow, the channels will not extend far enough into the valves and flow will be restricted.

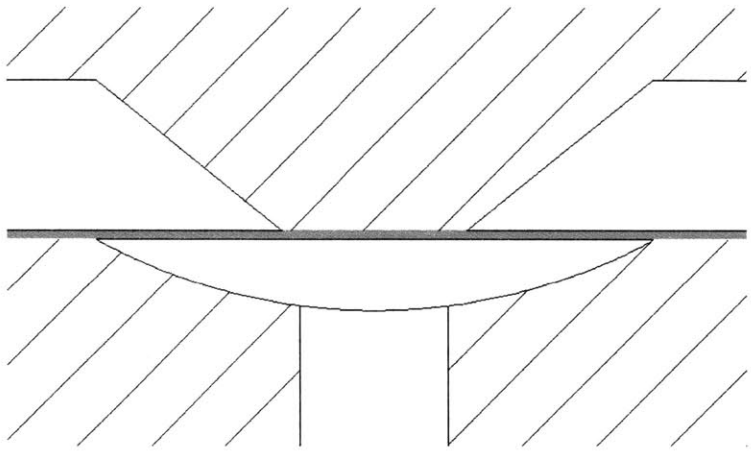

Figure 3.2: Cross-section of a valve and the fluidic channels above it

Alignment of the reactor plate with the pumping plate is important for the proper function of the pumping system. This alignment is achieved using dowel pins. Cuts for the alignment pins are made at the same time as the pumping chambers, valves and fluidic channels are made. Because of this, alignment of all features in the x-y plane is relative to the dowel pin and the placement of the part in the vise is less important.

Several of the features in the bioreactor require tapered cuts. Special tool paths and tool modifications necessary for creating these features are presented in Appendix A5.

3.2 Scaffolds

Polymer scaffolds were manufactured with the milling machine. A jig was used to hold the scaffold in place while a #80 drill bit (0.34 mm) cuts a circular arrangement of

holes. There is a minimum of 100 μm between adjacent holes, whose placements are shown in Appendix A6.

Since scaffolds are made using a thin, relatively flexible sheet of plastic that is held in place only by the 1 mm outer rim, it is important to have the scaffold well supported. A second plastic blank is placed under the scaffold in order provide this support and to keep the drill from cutting into the jig. Only the top scaffold can be used because the holes do not clear through the bottom blank. One scaffold is machined per run to prevent chips from accumulating between scaffold surfaces and bowing the outer most scaffolds. High spindle speeds, ~ 4,000 RPM, and traverse rates, 200 mm/min are used to achieve cleaner cuts.

Silicon scaffolds were fabricated from 6", 230 μm thick wafers using deep reactive ion etching [20]. A glass mask, Appendix A7, was used to manufacture 62 scaffolds per run.

3.3 Controller

The controller consists of a mechanical (pneumatic) system and an electronic system. Electronic components were soldered onto a printed circuit board and the pneumatic manifold is bolted to the board. The entire controller is enclosed inside a box. LEDs indicating pneumatic valve position are soldered to the board with 25 mm leads so they are level with the controller lid. LEDs used to indicate direction of flow plug into the 6-pin header used for programming. An STK-500 interfaces between the chip and a PC and is used to send programs to the microcontroller. The makefile used to send programs is shown in Appendix A3.

4. MODELS

Mechanical models were used during the development of this bioreactor to optimize design parameters and to assess validity of design options. The first model is used for the pneumatic pump. The second two models were created to better understand the effectiveness of various capacitor designs. Designs for the pneumatic pump and capacitor are detailed in Chapter 2.

4.1 Pump Model

A central feature of the bioreactor is the pumping system. It is essential that the pump can consistently achieve the flow rates necessary to sustain cell culture. Since these flow rates can vary from scaffold to scaffold or between experiments, there should be some flexibility in the flow rate. It is also desirable to minimize pulses of fluid sent through the scaffold.

The volume of the pumping chamber is a pivotal parameter in the design of the bioreactor fluidic system. A target volume was determined based on the desired flow rate through one channel in the scaffold. Since each channel comprises one functional unit of the bioreactor, overall flow rate should scale with the number of channels. There are a maximum of 861 channels in a scaffold and the bioreactor is run at 1 μL/channel/minute. This gives an overall flow rate near 1 mL/minute. The pump can be operated up to frequencies ~ 25 Hz, at which point flow consistency is affected. These parameters impose a lower limit to the pumping chamber volume. Frequency relates to pumping chamber volume, V_p, using the equation,

$$f = \frac{Q \times \#\text{ of channels}}{V_p \cdot 60}, \tag{4.1}$$

where Q is the desired flow rate in μL/channel/minute.

It will be seen in the capacitor section that the volume of the pumping chamber affects the size of flow pulses sent through the scaffold. Since it is desirable to keep this volume as small as possible, a value near the lower limit was used. The pumping chamber volume of 0.92 μL requires an operating frequency of 15 Hz to run 1 μL/channel/minute through a scaffold with 861 channels.

The volume of a round, dish shaped pumping chamber can be found using the equation,

$$V = \frac{\pi}{24}\left[16r^3 - \left(8r^2 + w^2\right)\sqrt{4r^2 - w^2}\right], \tag{4.2}$$

where r is the radius of curvature of the chamber and w is the chamber width. If the pumping chamber is oblong, an additional term,

$$V_{oblong} = V + (l - w)\left[r^2 \sin^{-1}\left(\frac{w}{2r}\right) - \frac{w}{4}\sqrt{4r^2 - w^2}\right], \tag{4.3}$$

must be added to the volume of a round chamber. Here, l is the overall length of the chamber.

In order to achieve a consistent flow rate, the membrane must deflect fully to the top and to the bottom of the pumping chamber. The pressure required for complete actuation can be calculated from the radius of curvature of the surface of the valve. This relationship between pressure and radius will also be important for modeling the capacitor, which requires a relationship between pressure and capacitor volume. For a circular valve, the pressure relates to strain like,

$$P \cdot \left(\pi (w/2)^2\right) = \sigma_n \cdot (\pi \cdot w), \tag{4.4}$$

where w is the width of the valve and σ_n is the stress in the membrane acting normal to the membrane. This equation is a balance of forces between pressure and stress and is visually depicted in Figure 4.1.

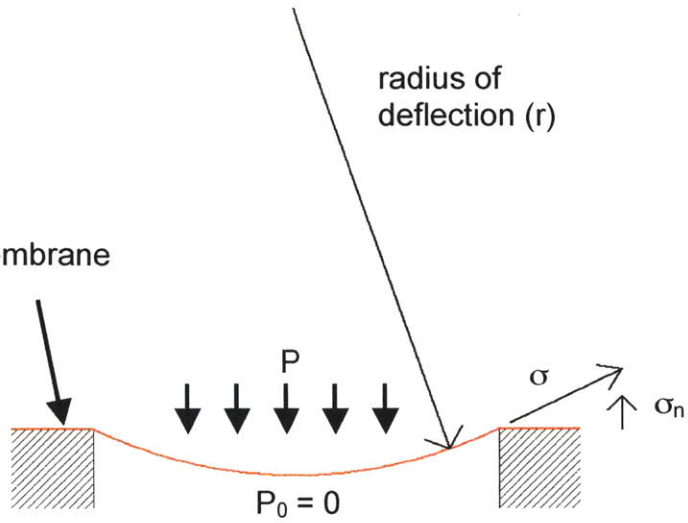

Figure 4.1: Pressure across a membrane is used to determine radius of deflection

The stress acting normal to membrane can be found from the radius of curvature of the membrane, *r*.

$$\sigma_n = \sigma \cdot \sin\theta = \frac{\sigma \cdot w}{2 \cdot r}, \tag{4.5}$$

This leads to,

$$P = \frac{2\sigma}{r}, \tag{4.6}$$

the formula for pressure across a thin membrane. Now, strain in the membrane must be found.

Strain is calculated by comparing the length across the valve to the arc that defines the valve surface. Equation 4.7 shows this calculation,

$$\varepsilon = \frac{l_f - l_i}{l_i} = \frac{2r}{w} \cdot \sin^{-1}\left(\frac{w}{2r}\right) - 1, \tag{4.7}$$

where *r* is half the diameter of the tool used to create the chamber. From this equation, one can find the ΔP required to fully deflect a membrane. Equation 4.8,

$$P = \frac{4E}{w}\left(\sin^{-1}\left(\frac{w}{2r}\right) - \frac{w}{2r}\right), \tag{4.8}$$

shows the difference between the pneumatic pressure and the pressure in the pumping fluid. In this equation *E* is the elastic constant of the membrane normalized to the

membrane thickness. This parameter is found in Chapter 5. As curvature of the valve increases, the depth increases, and the ΔP required for actuation also increases. For an oblong chamber, this equation becomes slightly more complicated.

In this situation, the pressure acts on a different area, and the strain is not uniform throughout the valve. The strain acting normal to the edge of the valve must be found. In the central region of the valve, shown in Figure 4.2, the strain is identical to that seen in a circular valve, Equation 4.7. The strain acting across the lateral axis of the valve can also be found directly,

$$\varepsilon_l = \frac{l_f - l_i}{l_i} = \frac{2r}{l} \cdot \sin^{-1}\left(\frac{w}{2r}\right) - \frac{w}{l}, \tag{4.9}$$

where l is the length of the valve. This strain will be less than strain across a circular valve and is equivalent to $\varepsilon \cdot w/l$. The calculation for pressure requires the integral of strain multiplied by the edge length, shown in Figure 4.2. An estimation,

$$\int \varepsilon \cdot \vec{n}\, ds \approx \bar{\varepsilon} \int ds = \pi w \cdot \left(\frac{\varepsilon + \varepsilon\, w/l}{2}\right) \tag{4.10}$$

uses the average between the horizontal and vertical values because strain will always be between these values.

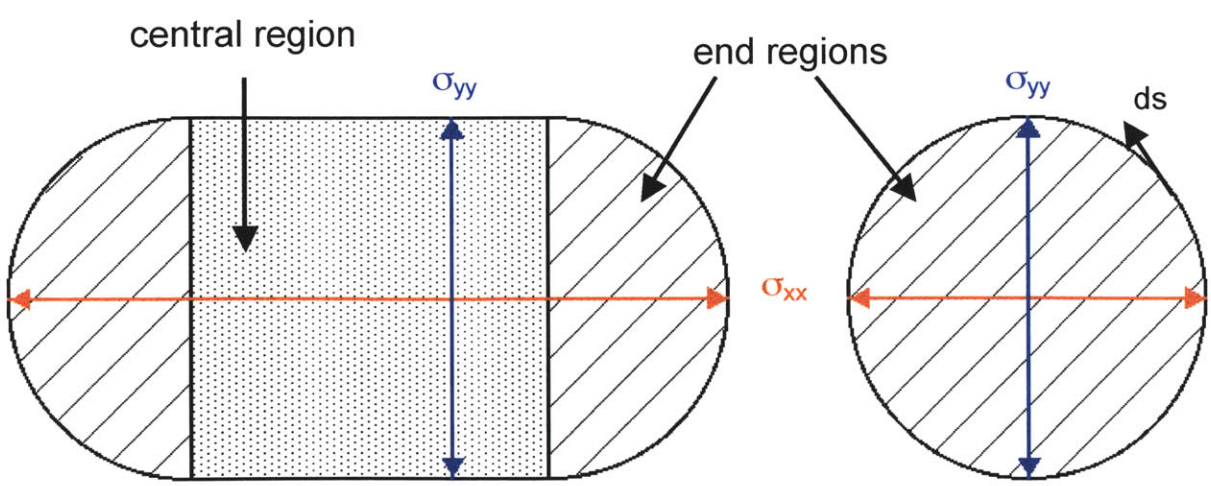

Figure 4.2: An oblong chamber is divided into regions when calculating average strain

From here we can equate a pressure difference to membrane strain using the equation,

$$P\left(lw - w^2 + \frac{\pi w^2}{4}\right) = \frac{\varepsilon E w}{2r}\left(2(l-w) + \frac{\pi w}{2}\left(1 + \frac{w}{l}\right)\right), \tag{4.11}$$

which reduces to,

$$P = \frac{2E}{w}\left(1 + \frac{\pi w^2}{4l^2 - 4wl + \pi wl}\right)\left(\sin^{-1}\left(\frac{w}{2r}\right) - \frac{w}{2r}\right), \tag{4.12}$$

the same as Equation 4.8 when $w = l$. When $l \rightarrow \infty$, this equation matches the equation for pressure across a membrane with two different radii of curvature.

The pressure required to actuate the pumping chamber is ± 12 kPa, well below the driving pressure of ±35 kPa.

Keeping the valve relatively flat will reduce the pressure required for actuation, but it can cause other problems. When using a flexible membrane it is possible for the membrane itself to seal off the fluid exit to the pumping chamber. This scenario is similar to the case shown in Figure 2.15. Also, a shallow cut requires a large tool. With a large tool, the volume of the pumping chamber will fluctuate more as a result of differences in manufacturing.

4.2 Static Capacitor Model

A capacitor can be used to convert discrete pulses of flow to a smooth continuous flow stream. The basic operation of a capacitor is detailed in Chapter 2. In order to achieve smooth flow, several features of the capacitor must be in balance. The capacitor must be large enough that it can accommodate the pulse of fluid sent from the pump. When the capacitor expands, the pressure in the fluid increases. This pressure drives flow through the scaffold. Fluidic resistance at the scaffold must be high enough that this increase in pressure does not result in excessive flows.

The system can also be thought of in terms of electronic components. The pump supplies an amount of charge in a discrete amount of time, or a current. Charge is allowed to build up in the capacitor and thus the voltage, or pressure, rises. This high capacitor voltage is discharged through the resistor, which models the filter. Essentially a capacitor converts a current source to a voltage source. A map of this system is shown in Figure 4.3.

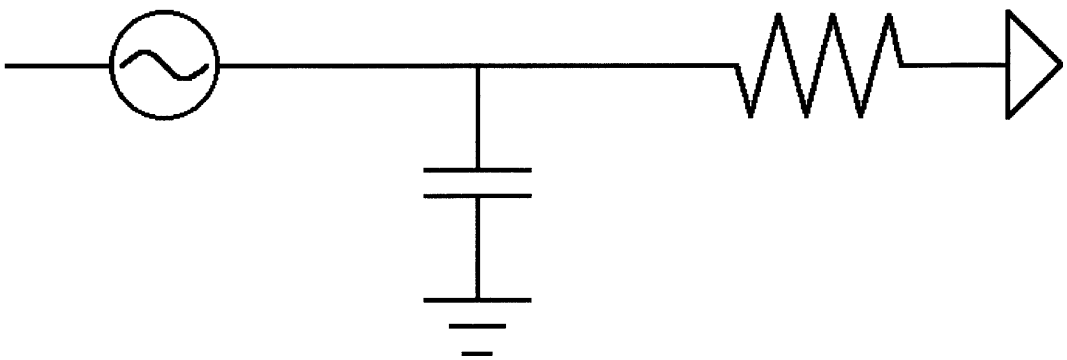

Figure 4.3: A model of the pumping system using electronic components

The capacitor is used to damp flow pulses sent from the pump before they pass through the filter. In order for the capacitor to function properly, several features must be in balance. Some of these features can be tuned for capacitor operation and others are predetermined. The volume of fluid from the pump, the elastic properties of the membrane, and the hydraulic permeability of the filter are all set for proper operation of other systems. This leaves the geometric shape of the capacitor.

When modeling the capacitor, there are some key terms that must be understood. Physically, the capacitance is the willingness of the capacitor to accept volume at the cost of increased pressure. In terms of electricity, the capacitance is the willingness of a capacitor to accept charge, at the cost of increasing the capacitor voltage. The volume contained in the capacitor is considered the volume of fluid inside a deflected membrane and is shown in Figure 4.4. The pressure is the pressure across the membrane. The equation for describing a fluidic capacitor is,

$$C = \frac{dV}{dP} = \frac{\Delta V}{\Delta P}, \tag{4.13}$$

where V and P for a circular capacitor can be found in Equations 4.2 and 4.8 respectively. When this equation is rearranged to the form,

$$\Delta P = \frac{\Delta V}{C}, \tag{4.14}$$

the influence of pumping chamber volume on capacitor operation becomes more apparent. When a larger pulse of fluid is sent to the capacitor, the pressure inside the capacitor increases more than it would in response to a smaller pulse. This increased pressure will drive fluid movement through the scaffold at a higher rate and will impart more shear stress on the cells.

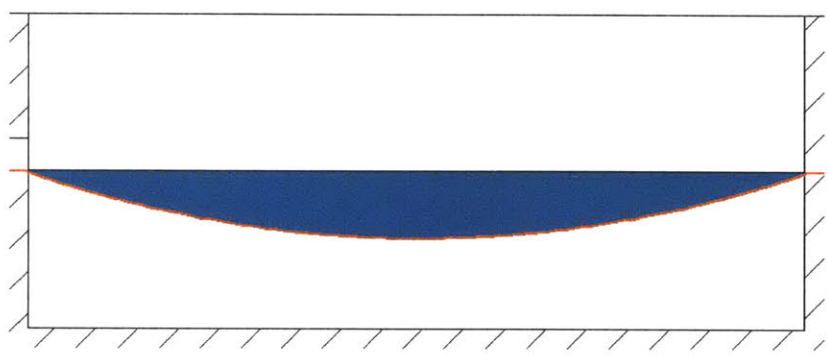

Figure 4.4: Volume of fluid 'in' the capacitor

The equations for both pressure and volume are nonlinear and thus the capacitance is not a constant value; it depends both on the geometry of the capacitor and the current state of the capacitor. Both equations

$$V = \frac{\pi}{24}\left[16r^3 - \left(8r^2 + w^2\right)\sqrt{4r^2 - w^2}\right], \tag{4.2}$$

$$P = \frac{4E}{w}\left(\sin^{-1}\left(\frac{w}{2r}\right) - \frac{w}{2r}\right), \tag{4.8}$$

depend on the radius by which the capacitor is deflected. To find capacitance, an arbitrary radius was used to find both pressure and corresponding volume. A second radius, $r + dr$, was used to again find pressure and volume. Capacitance is the difference in volumes divided by the difference in pressures. A sample calculation is

shown in Appendix A8. Capacitance values across a range of pressures are calculated for various capacitor diameters. Seen in Figure 4.5, when the capacitor is loaded with a high pressure, it is less willing to accept increased volume.

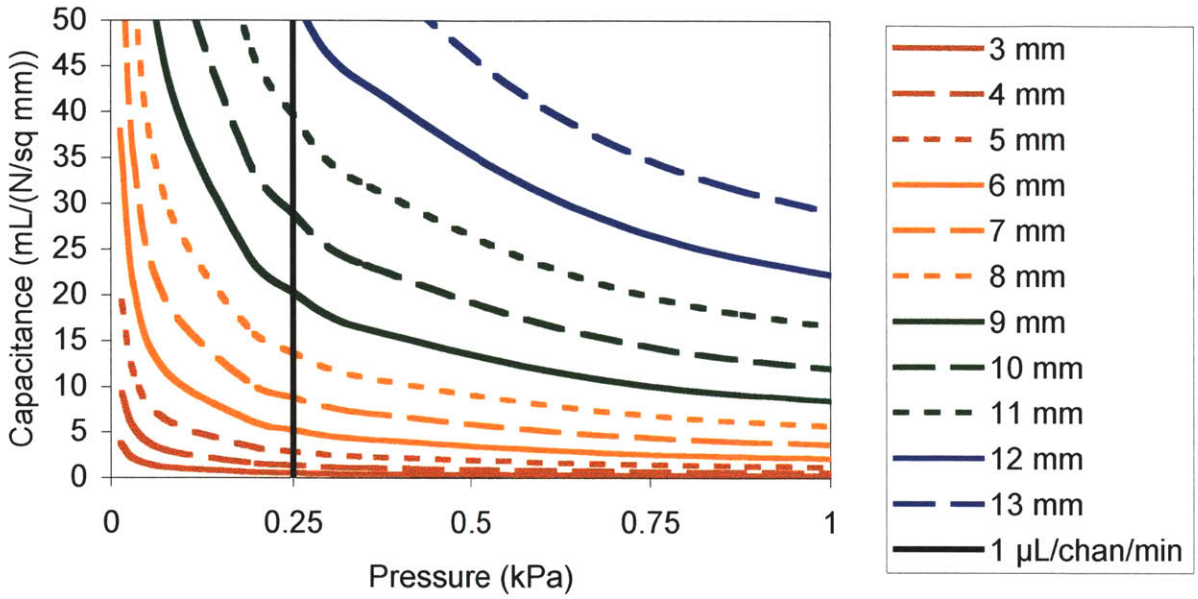

Figure 4.5: Capacitance vs. pressure for capacitors with a variety of different diameters. The pressure required for flow at 1 µL/channel/minute is 0.25 kPa.

Figure 4.6 shows two states of the capacitor and two identical ΔV's. In the first state, the capacitor is preloaded with 0.25 kPa and it requires an additional 0.21 kPa to deflect the membrane enough to accommodate 5 µL. In the second state, the capacitor is initially unloaded and the pressure required to change the volume by 5 µL is only 0.0033 kPa. The first condition requires a pressure increase that is 64 times greater in order to accommodate the same amount of volume. It is apparent in Figure 4.5 and Figure 4.6 that as the capacitor is loaded, the capacitance decreases.

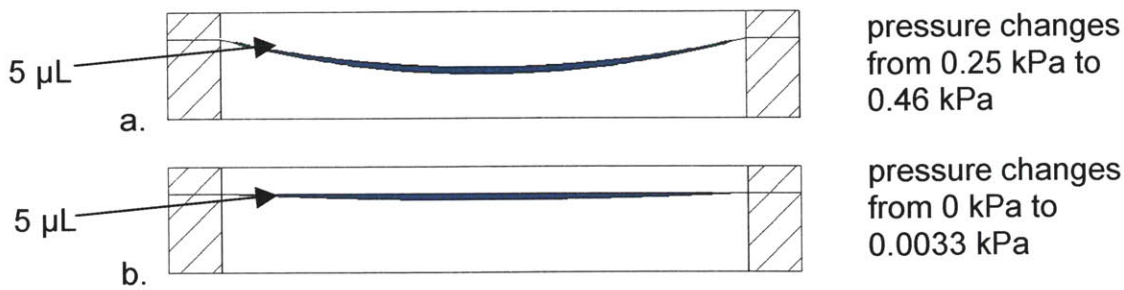

Figure 4.6: A 10 mm diameter capacitor a) is loaded with an initial pressure and is therefore less able to accept additional volume than capacitor b) that is initially unloaded. This figure is to scale.

In Figure 4.5 it can also be seen that capacitance decreases as the physical width of the capacitor decreases. This situation is shown in Figure 4.7 with a 5 mm diameter capacitor. Similar to Figure 4.6a, the pressure across this capacitor is initially 0.25 kPa. A 5 μL pulse of fluid deflects the capacitor membrane to a second position, increasing the pressure to 8.2 kPa. This pressure is substantially higher than the 0.46 kPa required to deflect a 10 mm capacitor the same volume; thus, capacitance increases with the diameter of the capacitor.

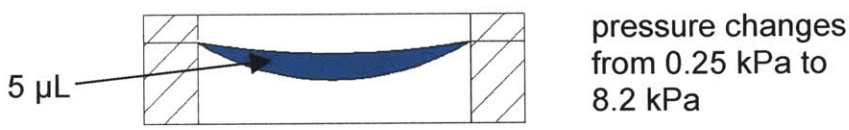

Figure 4.7: Capacitance increases with capacitor diameter because a larger diameter capacitor can accept more volume with a smaller change in pressure. This figure is to scale.

Now that the capacitance of various capacitors can be found, this information must be related back to the pumping system. Since capacitance depends on pressure, the optimal driving pressure for flow through the scaffold must be found. Typically the pump operates at a flow, q, of 1 μL/channel/minute. The total flow, Q, will scale with the number of channels and can be found using the equation,

$$Q_{total} = q \cdot \text{ \# of channels} = \frac{P}{R}, \tag{4.15}$$

where the fluidic resistance is supplied by the filter. This resistance is found from the hydraulic permeability of the filter, h_p. In order to convert to a resistance,

$$R = \frac{1}{A_{filter} h_p} = \frac{1}{A_{channel} \cdot \# \text{ of channels} \cdot h_p}, \tag{4.16}$$

the area of the filter exposed to flow, or the total area of the channels, is multiplied by the hydraulic permeability then inverted. Since total flow is normalized to the number of channels, and the resistance is dependant on the number of channels, the pressure required to drive flow,

$$P = \frac{q_{channel}}{A_{channel} \cdot h_p}, \tag{4.17}$$

at a desired rate does not change as the number of channels is scaled. This drastically simplifies analysis when considering new scaffolds, but it does assume that fluid does not flow through the portion filter that is occluded by the solid scaffold.

The reported hydraulic permeability of the filter is 73.5 (mL/s)/(N/mm^2)/cm^2 and the cross section of a channel is 0.09 mm^2. Therefore, the pressure required to drive flow at 1 μL/channel/minute is close to 0.25 kPa. Capacitances for various capacitor geometries evaluated at 0.25 kPa are shown in Table 4.1. As with any model, the predictions are made as a guide and are not meant to represent exact values. If operating conditions change, the actual capacitance values and flow patterns will change slightly, but the average flows will remain constant.

Table 4.1: Capacitances for several capacitor geometries evaluated at 0.25 kPa

Diameter	Capacitance mL/(N/mm^2)	RC (ms)	RC/Cycle Time
3 mm	0.5	9	0.14
5 mm	2.8	50	0.76
7 mm	8.8	153	2.35
10 mm	29.0	504	7.78
13 mm	69.8	1214	18.74

Now the time constant, *RC*, for each capacitor can be found. The time constant is a measure of how fast a system will react to some input; specifically, the time it takes a system to reach 63.2% of steady state. In the case of the bioreactor, input is flow from the pump. With a very small capacitance the time constant will be very short. The system will react to the quick pulse of fluid sent from the pump, or the slightly longer period of zero flow between pulses. As the capacitance increases so does the time constant. With a very large time constant the system will not react to the periodic input from the pump and pulses coming from the pump will not be seen at the scaffold. Instead, a steady, average flow will pass through the scaffold. With a long time constant, steady state is not achieved as quickly (on the order of seconds), but this is irrelevant as the pump is run continuously for days.

A capacitor should have a time constant that is longer than the period of the lowest frequency in the signal it is meant to damp. In this case that period is the pumping cycle time. Consider a scenario where the pump sends small pulses at a very high frequency. In this case the pump cycle time is short and the time constant can be very small. With a pump that sends infrequent, large pulses, the time constant, and thus the capacitor, will need to be very large. Because of this relationship between the time constant and the nature of the input signal to the capacitor, it is helpful to normalize the time constant to the cycle time of the pump.

Seen in Equation 4.15 and Equation 4.16, both resistance and total flow scale with the number of channels in the scaffold. When a scaffold with fewer channels is used, the total flow, *Q*, will need to decrease and the pump is run at lower frequencies. In order to maintain steady flow the time constant must increase with the increased cycle time. Since the resistance scales with the number of channels, this is exactly what occurs. The normalized time constant,

$$\tau_n = \frac{\tau}{t_{pump}} = \frac{Q \cdot RC}{V_{pump}} = \frac{q \cdot C}{V_{pump} \cdot A_{channel} \cdot h_p}, \tag{4.18}$$

does not change when different scaffolds are used. Since the capacitance does not depend on the number of channels (Equation 4.14), neither does the normalized time

constant. Again, this result is based upon the assumption that flow through the filter does not occur in areas that are occluded by the scaffold.

4.3 Dynamic Capacitor Model

Capacitor operation is very dynamic and there are many parameters that can't be seen in the static model. A simulation of capacitor operation was used to model time-dependant flow. In this model, the capacitor takes an input signal from the pump and outputs a flow through the scaffold. The full set of MATLAB code is shown in Appendix A9. The model first finds optimal starting conditions, then sets up a time vector and a representative input from the pump. Finally, capacitor output through the scaffold is calculated and some final values are found. This section provides an overview of how the capacitor model works.

When fluid begins to flow into an unloaded capacitor, most of that fluid goes into the capacitor and little goes through the scaffold. Flow through the scaffold during this initial startup phase is not representative of flow through the scaffold once the capacitor is fully loaded. For this reason, and because each data point requires ~ 20 ms to calculate, it is undesirable to begin modeling the system when the capacitor is unloaded. Instead, an average capacitor load is found and the system begins modeling a loaded capacitor.

To find this initial loading condition, the pressure required for flow at the desired rate is calculated using Equation 4.17. This pressure and the size of the capacitor can be used in Equation 4.8 to find the radius at which the capacitor is deflected. Using this radius, the average capacitor volume, or load, is found using equation 4.2.

Since the actual load on the capacitor varies throughout time, it is very difficult to find an initial loading condition exactly. An approximate value is found and flow

throughout five pumping cycles is measured. By the end of these five cycles, any error in the initial loading estimate has dissipated.

A time vector is created for running five pump cycles. In order to keep computation times low, the total number of points is limited to 500. The Δt between time points is kept much smaller than any of the steps in the pumping cycle.

Next, a flow pattern from the pump is created. This pattern is based on the operation of the pump, shown in Figure 2.13. The user sets the size of the pumping chamber and the desired average flow and the code sets a frequency and develops a pattern accordingly. The time required for a pulse of fluid to leave the pump, the pumping time, is ~ 10 ms and was found experimentally, Chapter 5. The flow rate of the pulse of fluid sent to the capacitor is found by dividing the pumping chamber volume by this time. When flow occurs from the pump it occurs at this flow rate for each of the time points contained within the pumping time. The short Δt keeps the total volume of fluid ejected from the pump consistent with the desired average flow.

Finally, flow through the scaffold is found. The radius of curvature of the membrane is found from the volume of fluid contained inside the capacitor, Equation 4.2. From this radius, the pressure of fluid in the capacitor is determined using Equation 4.8. This pressure will drive flow through the scaffold. Once flow out through the scaffold and flow into the capacitor are known, a new volume of fluid inside the capacitor can be found. From this volume, a new radius can be found and the process repeats.

Flows are converted to the proper units and are plotted. The total volume of fluid that enters the capacitor and the volume that flows through the scaffold can be found by integrating flow over time. These plots give another perspective on the same data. Figure 4.8 shows the result of this model for the 10 mm diameter capacitor used in the bioreactor. In this model, a volume pumped per cycle of 0.92 μL was used to pump fluid through a scaffold with 861 channels at 1 μL/channel/minute.

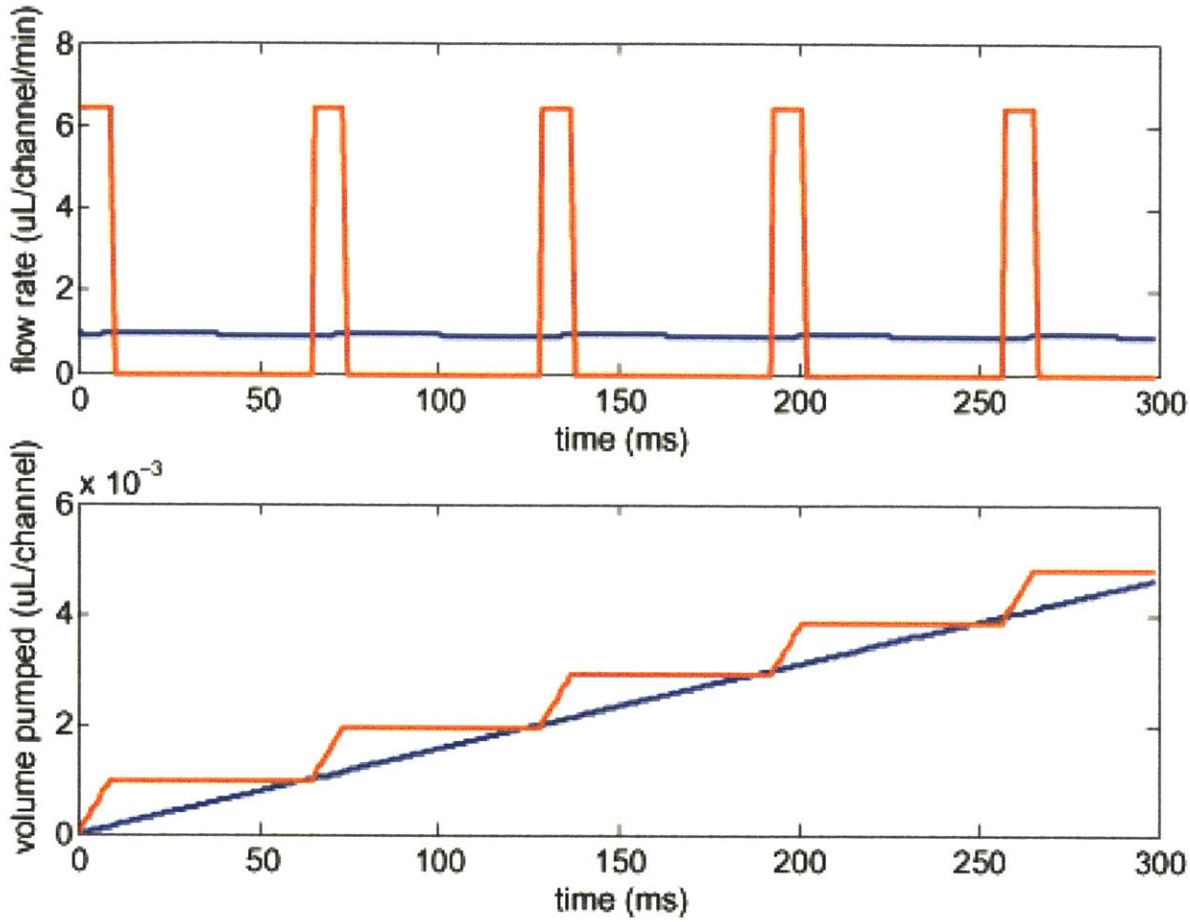

Figure 4.8: Flow through the scaffold as modeled by the dynamic capacitor model. The red line shows the flow pulses from the pump and the blue is flow through the scaffold.

The dynamic model offers far more insight into the actual performance of the capacitor. From this model, the maximum flow rate through the scaffold and the variation of flow in time can both be found. The deflection of the membrane from its unstrained position can be found from the radius of curvature and is useful when designing the capacitor chamber. This chamber should be deeper than the maximum deflection of the membrane.

A model for an oblong capacitor was made using Equations 4.3 and 4.12. These equations model deflection of a membrane to a rigid surface and are not exact representations for the deflection of a free membrane. A free membrane would deflect with a curve across the middle section and would not strain quite as much as these

equations suggest. Like any model, this model is only an estimation of actual performance, but since it overestimates strain, the actual capacitor should function better than predicted by the model. The code for this model is shown in Appendix A10.

5. MECHANICAL CHARACTERIZATION

In order to validate the performance of the reactor, the pumping system was tested experimentally. Models for the pumping volume were validated and operating ranges for frequencies and pressures were found. Consistency of the device across reactor units and throughout time was assessed. This chapter describes the characterization of the pumping system and the controller.

5.1 Characterizing the Controller

The controller sets the pumping frequency by running a delay subroutine, Appendix A3, between pumping cycles. When the subroutine is called, it delays for a set amount of time. The subroutine can be called anywhere from 1 to 255 times for each delay. This number is limited to 8 bits, so for delays over 255, the routine must be called twice, for example:

```
delay(250);
delay(250);
```

will run the delay subroutine 500 times. The actual time taken to run a delay subroutine was determined experimentally. The reactor was set to run for 250 pumping cycles and the delay between each of the 4 pumping operations was set to one of the four values shown in Table 5.1. A delay of 50 will be run four times during each of the 250 cycles, which adds to a total of 50,000 delays. The time required for each of these runs was recorded. The time required to run each delay subroutine averages to 0.202 ms; therefore, delay(82) will pause for 16.7 ms between each of the pumping operations and will result in a total pumping cycle time of 67 ms or 15 Hz.

Table 5.1: Measuring the time per delay cycle

Delay Value	Measured Time (s)	Time per Delay (ms)
50	10	0.2
100	20	0.2
250	51	0.204
500	102	0.204
Average		**0.202**

5.2 Experimental Setup for Flow Tests

In order to measure flow in the reactor, several reactor plates were made without surface channels. The pumping system on these plates is identical to the pumping system on finished reactor plates; however, no flow can cross back across the reactor once it has been sent through the pump. This allows an accurate measurement of flow through the pump.

Reactors were assembled according to the protocol described in Appendix A11. Small holes were cut in a reactor lid above each of the wells in the reactor plate. The modified lid and system are shown in Figure 5.1. The tip of a 1 mL syringe fits through a hole in the lid and is used to level the fluid in a reactor well. Flow is now sent through the pump and an empty syringe is again used to level the fluid in the well. The volume of fluid now in the syringe is the amount of fluid that has passed through the pump. This process is detailed in Figure 5.2.

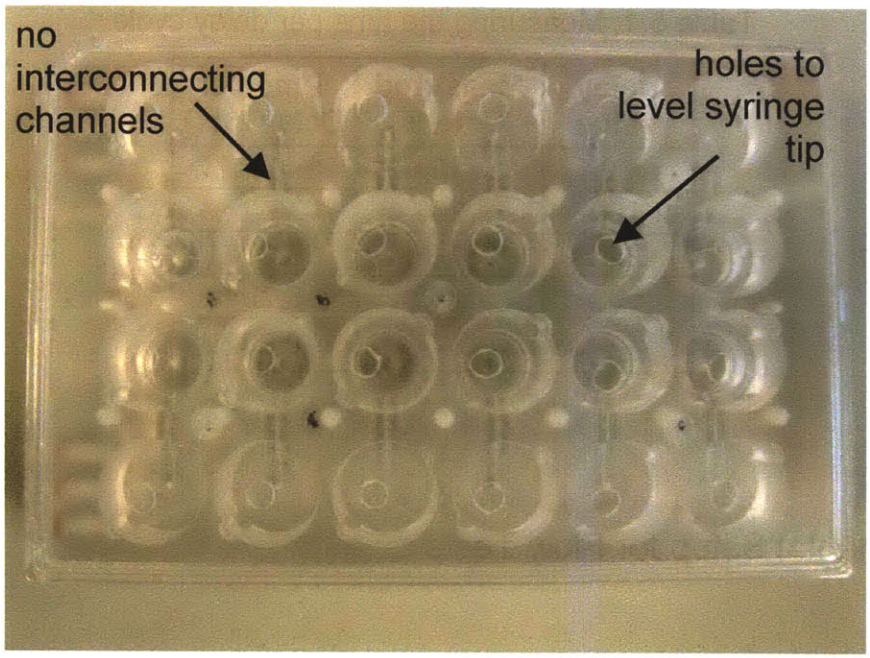

Figure 5.1: The bioreactor system developed for flow tests

The controller is set to run for a certain number of cycles before stopping. For most flow conditions, 500 cycles are sufficient to get an accurate flow measurement. More cycles are needed when flow through the pump drops below the volume of the pumping chamber.

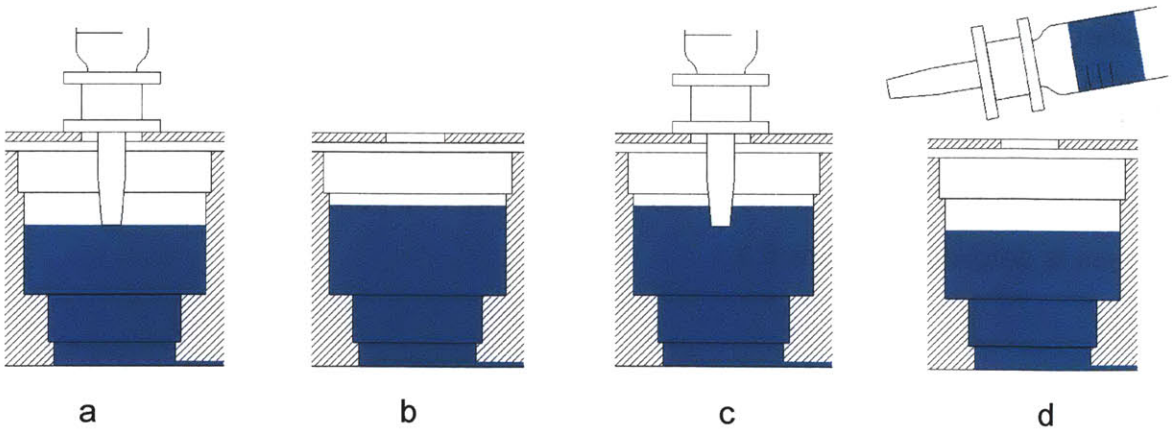

Figure 5.2: Method for measuring flow through the pump: a) a syringe is used to level fluid in the reactor well; b) the pump is run for a set number of cycles; c) the syringe is again used to level fluid in the well; d) fluid in the syringe is recorded.

5.3 Pumping Chamber Volume

The volume of the pumping chamber can be found experimentally. The experimental setup detailed above is used and the controller is set to run for 500 cycles. The frequencies and pressures are set to 15 Hz and ± 35 kPa, that, as will be shown later in this section, produce consistent flows. The total flow through 500 cycles is measured ten times in each of the reactors on the device. The average volume measured is divided by the number of cycles to find the volume pumped per cycle. This volume, shown in Table 5.2, should correspond directly with the volume of the pumping chamber, 0.92 μL.

Table 5.2: Volume of the pumping chamber measured at each reactor unit

Reactor Unit	A1	A2	A3	A4	A5	A6
Volume	0.92	0.89	0.96	0.95	0.94	0.91
Reactor Unit	B1	B2	B3	B4	B5	B6
Volume	0.96	0.96	0.89	0.95	0.93	0.91
	Average Volume		**0.93 μL**	**Variation**		**2.7%**

The average volume pumped, 0.93 μL, is only slightly larger than the volume set in the design. This difference can be accounted for in the manufacturing process if the tool used to cut the pumping chambers is set too deep. If the volume pumped per cycle were lower than expected, this could suggest that the membrane is not fully deflecting to the chamber surface, or it could suggest a leak in the valves. The variation between reactor units, 2.7%, is calculated by dividing the standard deviation by the average.

5.4 Flow Consistency

Flow through the reactor is set by the frequency of the pumping cycle. However, when operating parameters are out of tune they can also influence the flow rate. It is crucial for the consistency of reactor operation that these parameters are kept within

operational limits and thus these limits should be known. When pressures are too low, they may not be sufficient to fully actuate the membrane. When frequencies are too high, or pressures are too high, there may not be sufficient time to change from positive to negative pressure under the valves. This section characterizes the dependency of flow on frequency and pneumatic pressure and suction.

5.4.1 Flow Cycle Timing

There are four steps involved in each cycle of the pump, Figure 2.12. Each of these steps takes a certain amount of time and that time can be measured. The controller is set to allow ample time for three of the four steps, and the time for the final step is varied.

For example, the pump is allowed to completely fill with fluid and the valves have ample time to switch. Only a short amount of time is allowed for the pumping chamber to eject fluid before the valves switch and flow from the pump is stopped.

The modified pumping cycle for these tests allows ample time for the pumping chamber to fill with fluid from the reservoir. The valves switch so that the pump is open to eject fluid into the capacitor. A pressure pulse is sent to the pump and fluid begins to eject into the capacitor. After a set amount of time, the valves switch and fluid leaving the pump can no longer enter the capacitor. The remaining fluid in the pumping chamber is ejected back into the reservoir. The next step in the cycle again fills the pumping chamber from the reservoir and the process repeats. The only fluid that has passed through the pump during this cycle is the small amount that left the pump before the valves were programmed to switch.

This cycle repeats until a measurable amount of volume has been pumped. The volume of fluid ejected from the pump during a short time interval can be found by

dividing the total volume measured by the number of cycles. If enough time intervals are measured, the actual instantaneous flow from the pump can be found.

For these measurements, a test unit was assembled with scaffolds and filters and the pneumatics were set to ±35 kPa.

Figure 5.3 shows this curve for draining the pumping chamber. As more time is allowed for the chamber to drain, more fluid is ejected. After around 10 ms, the total volume of the pumping chamber has been ejected. Since the reactor is bidirectional, this test was performed with flow moving down through the scaffold, through the pump and into the reservoir, and from the reservoir, through the pump and up through the scaffold. Since this curve is an amount of volume that is sent from the pump over a certain time interval, the slope represents the actual flow rate from the pump.

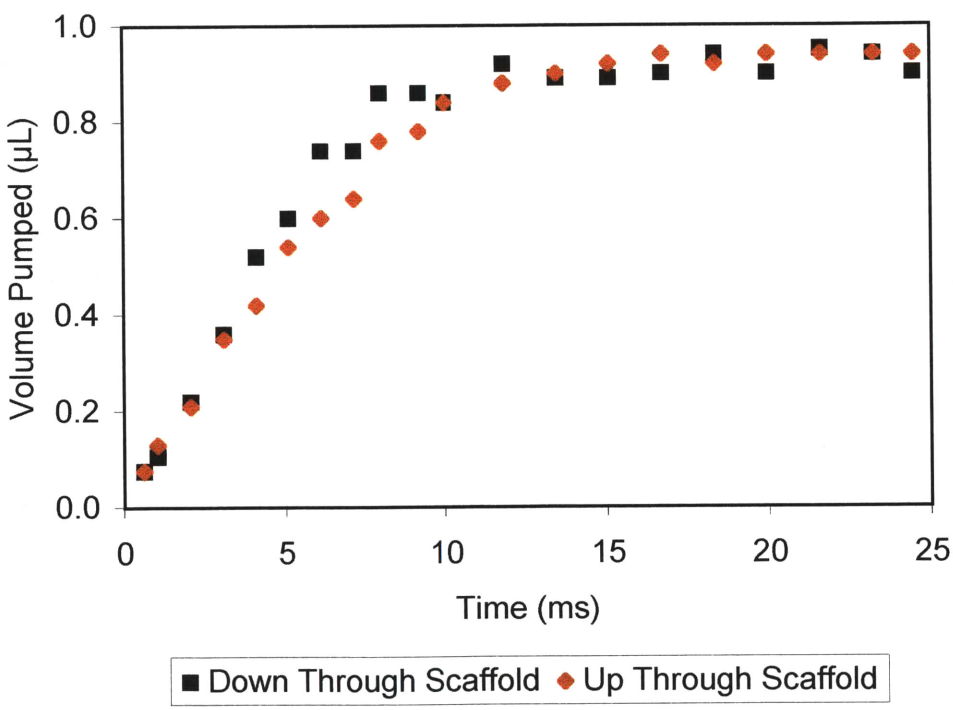

Figure 5.3: Volume of fluid ejected from the pumping chamber during a pumping cycle. The slope of this curve represents the actual rate of flow from the pump. Flow measurements were taken for both directions of the pump.

A similar curve is found for the time required to fill the pumping chamber, Figure 5.4. In this case ample time is allowed for the pumping chamber to drain and flow is cut short when filling the chamber. The amount of fluid that passes through the pump during each cycle represents the volume of fluid that travels into the pumping chamber before the valves switch.

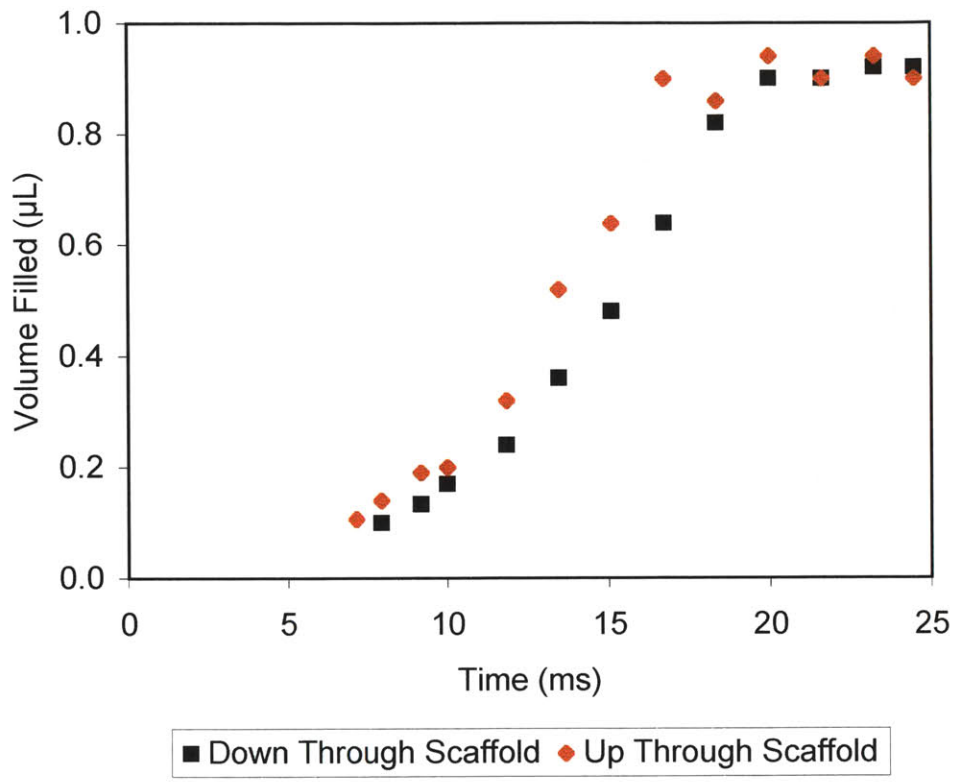

Figure 5.4: Volume of fluid that is pulled into the pumping chamber during a cycle of the pump. Flow is measured in both directions.

This curve is shifted because no fluid is pulled into the pumping chamber during the first 5 ms. The reason for this is because it only takes a small amount of pressure to move the membrane to the top of the pumping chamber. The actual pressures used are well above this pressure so, when vacuum is applied at the controller, the pressure below the membrane begins to fall. After a certain amount of time has elapsed, that pressure is no longer enough to keep the membrane fully deflected against the top of the pumping chamber. At this point, ~ 5 ms, fluid begins moving into the pumping

chamber. The pressure under the membrane continues to drop and the membrane is pulled to the bottom surface of the pumping chamber, ~ 20 ms.

When lower positive pressures are used in combination with 35 kPa vacuum, fluid begins to enter the pumping chamber immediately after vacuum is applied. This happens because the time required for the pressure under the membrane to fall below what it takes to keep the membrane deflected to the top of the chamber is shortened. This phenomenon is shown in Figure 5.5a and 5.5b.

There are some interesting things to note about these figures. These three curves have basically the same slope, only they are shifted by ~ 5 ms for each 10 kPa the positive pressure drops. This means that it takes around 10 ms for pressure under the valve to drop from 35 to 15 kPa. Once the pressure has dropped to 15 kPa, the movement of the membrane in the pumping chamber is consistent across pressures.

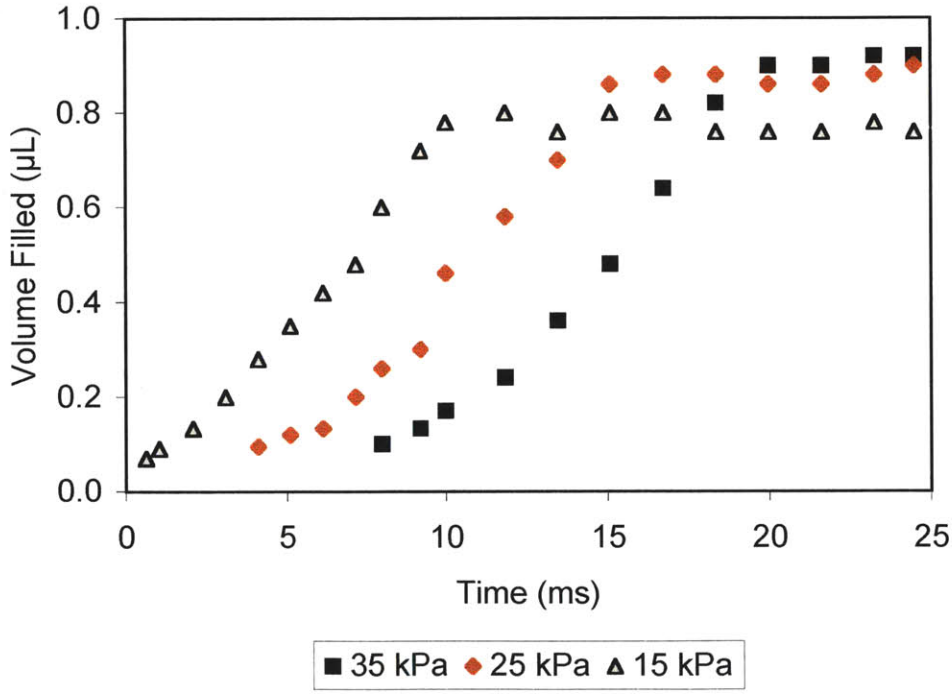

a.

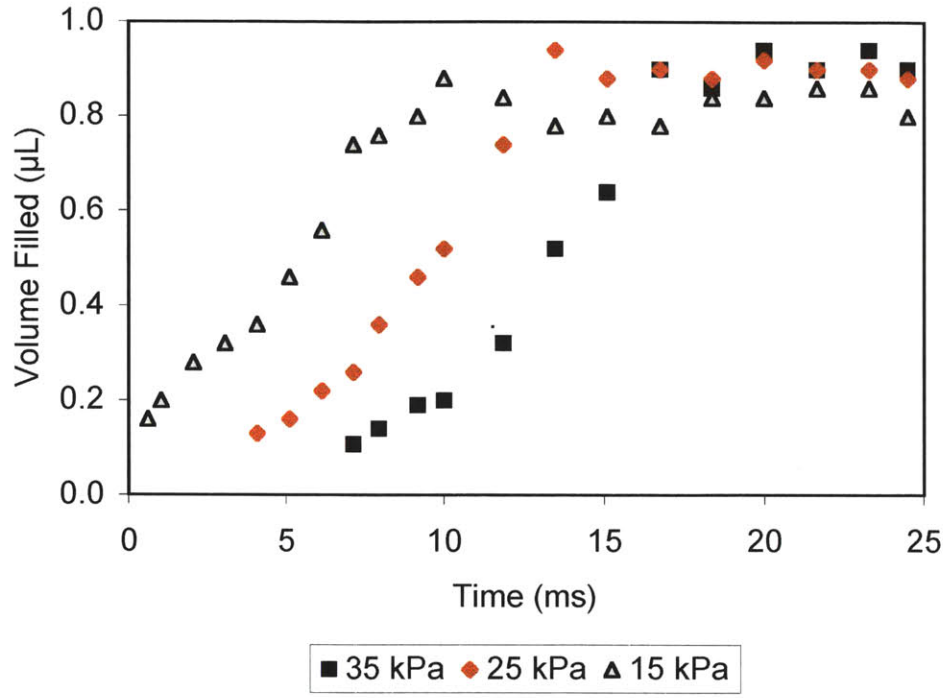

b.

Figure 5.5: Volume of fluid that is pulled into the pumping chamber during a cycle of the pump. As positive driving pressure decreases, the pumping chamber fills sooner after vacuum is applied. a) Direction of the pump moves fluid down through the capacitor, through the pump and into the reservoir. b) Fluid is moved from the reservoir, through the pump and into the capacitor.

Although this does not conclusively show, it is good evidence that after the positive pressure drops below 15 kPa the membrane in the pumping chamber begins to move. This suggests that 15 kPa is very close to the pressure required to deflect the membrane to the top of the pumping chamber, supporting the calculation made in Chapter 4 that 12 kPa is the required ΔP for complete membrane actuation.

Another thing to notice is that the maximum volume pumped per cycle decreases slightly when the positive pressure drops below 15 kPa. This also supports the calculation that 15 kPa is a borderline value for complete membrane actuation.

Using the same pressure combinations (15 kPa & -35 kPa, 25 kPa & -35 kPa, and 35 kPa & -35 kPa), the flow curve for fluid leaving the pumping chamber was found, Figure 5.6. Similar to the curves in Figure 5.5, the maximum volume pumped per cycle decreases when only 15 kPa is used.

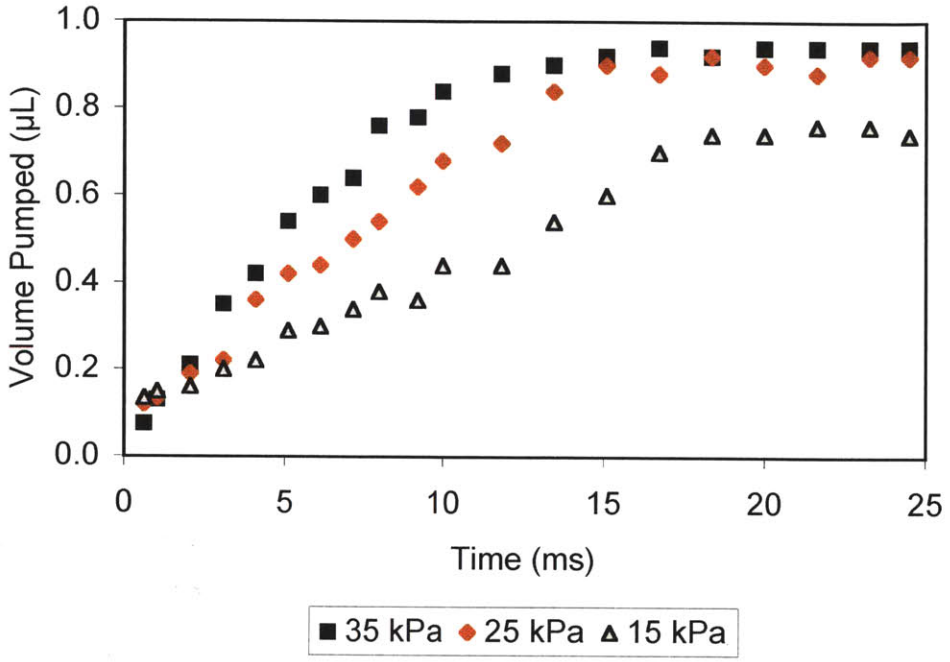

Figure 5.6: Volume of fluid ejected from the pumping chamber during a pumping cycle. Three positive pneumatic pressures are tested with vacuum set to 35 kPa. Measurements were taken with flow moving from the reservoir through the pump and into the capacitor.

These three curves begin, for the first ~ 3 ms, with roughly the same slope, then diverge with the highest positive pressure driving fluid at the fastest rate. The beginning of this curve represents the time period when pneumatic pressure is rising from –35 kPa to some intermediate value. Since the pneumatic pressures in all scenarios are roughly the same during this interval, it makes sense that all curves have the same slope. As time passes, the pneumatic pressure rises to different values for each of the three cases. During this time, the three curves are relatively liner, but all have different slopes, Figure 5.7. The linear slope suggests that a constant pressure is driving the fluid flow. This means that the driving pressure under the valve quickly reaches the

maximum value (15, 25, or 35 kPa), and that pressure drives flow across a resistance in the fluidic channels.

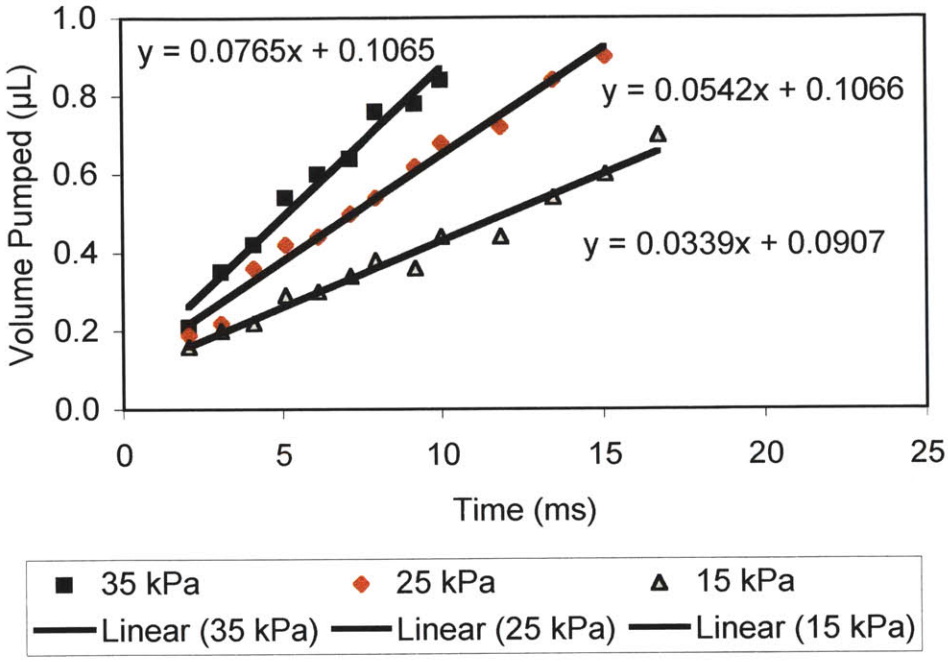

Figure 5.7: Slopes of curves for fluid exiting the pumping chamber in response to three different positive pneumatic pressures.

From the slopes of these curves, the flow rate for each scenario can be calculated. If the driving pressure is constant, the flow rate should scale with pressure by the fluidic resistance. Table 5.3 shows that the calculated fluidic resistance is constant across pressures, suggesting that indeed, flow is driven by a constant pressure. In order for flow to be driven by a constant pressure, pressure under the valve must change very rapidly. After the pressure has reached a maximum value (15, 25, or 35 kPa), the bulk of fluid drains from the pumping chamber.

Table 5.3: Flow driven by different pressures through a fluidic resistance

	35 kPa	25 kPa	15 kPa	
Slope	0.0765	0.0542	0.0339	µL/ms
Flow	4.6	3.3	2.0	mL/min
Resistance	0.46	0.46	0.44	$(N/mm^2)/(mL/s)$

The consistency of these resistance values also says something about the actual pressure at the valves. If the pressures driving flow were all 5 kPa lower, ie. if there was a loss of 5 kPa between the controller and the valves, the resistance values would change to 0.39, 0.37 and 0.29 $(N/mm^2)/(mL/s)$, and the flow would no longer be proportional to pressure. Since flow is proportional to the pneumatic driving pressures set at the controller, this suggests that pressure applied at the valves is very close to the pressure that can be read on the gages. This supports the model presented in Figure 2.32 that the secondary channels have minimal effects on the actual pressure under the valves.

As these curves do not change when filters are removed, the fluidic resistance calculated here resides in the pump itself (data not shown). This makes sense, as the resistance calculated for flow passing through a filter, h_p of 73.5 $(mL/s)/(N/mm^2)/cm^2$, where 861 channels are exposed is only 0.02 $(N/mm^2)/(mL/s)$. Since the resistance in the fluidic lines occurs before flow enters the capacitor, this resistance does not affect capacitor operation.

The time required to actuate the valves was also found experimentally. Similar tests were run where the valve timing was varied and flow through a large number of cycles was measured. Positive and negative 35 kPa were used as the pneumatic inputs. Figure 5.8 shows the results from this test for step four in the pumping cycle, Figure 2.12, where the valves are switched before filling the pumping chamber.

Seen in this figure, little time is required before the controller can begin to apply vacuum to the pumping chamber. Since the pumping chamber requires around 5 ms before it begins to fill with fluid, Figure 5.4, it makes sense that vacuum can be applied immediately after a signal is sent from the controller to switch the valves.

Figure 5.9 shows the volume pumped per cycle when the time allowed for step two, Figure 2.12, is varied. In this step, the valves switch positions before the pumping chamber is drained.

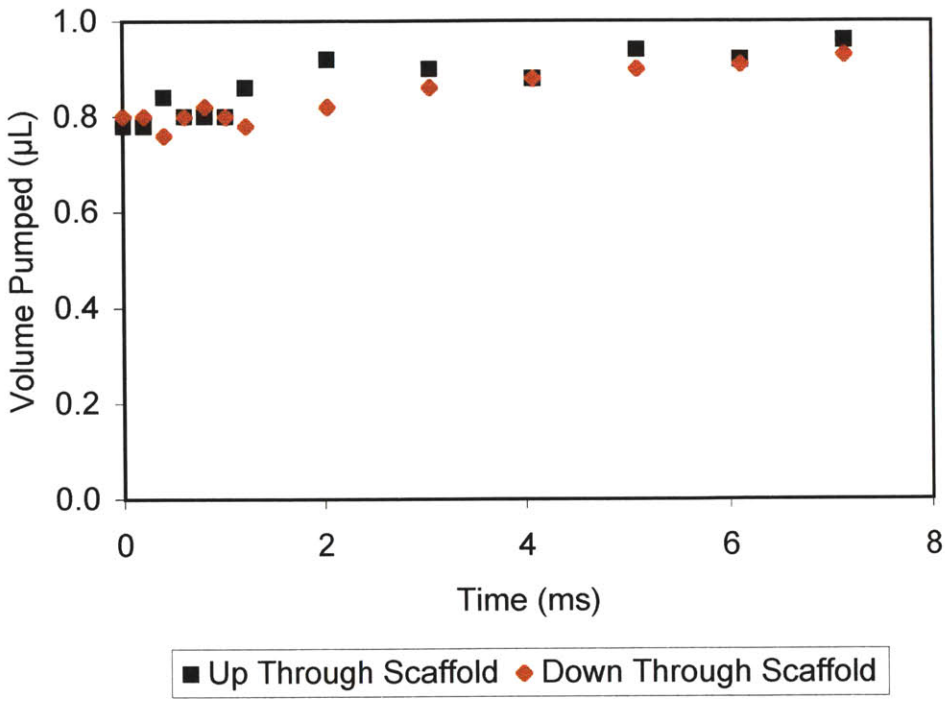

Figure 5.8: Time required to switch the valves in order to fill the pumping chamber.

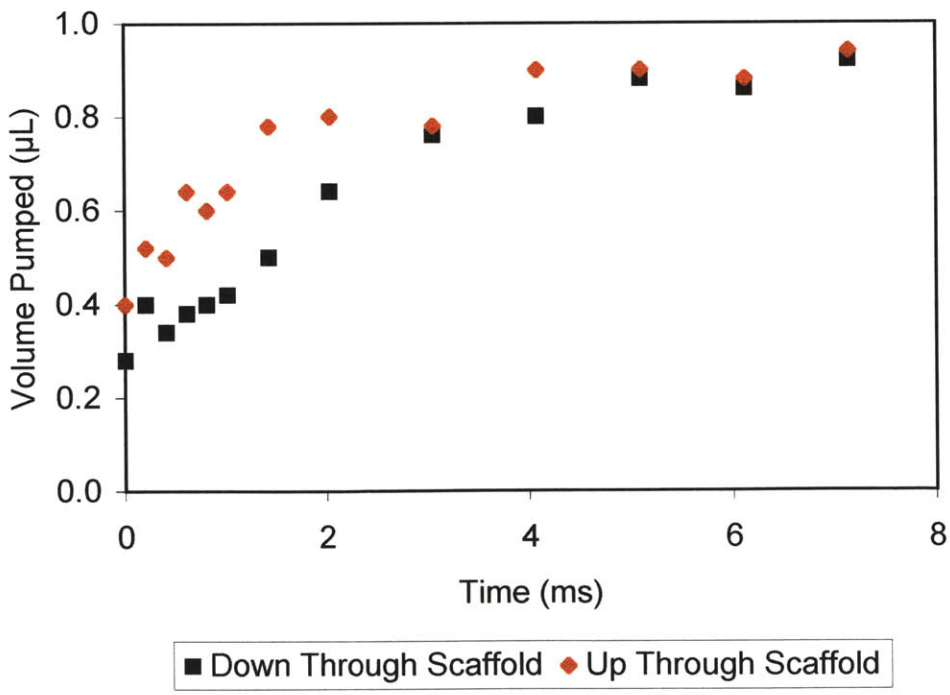

Figure 5.9: Time required to switch the valves in order to drain the pumping chamber. Flow was measured in both directions.

Looking back to Figure 5.3, the pumping chamber begins to drain immediately following actuation. This requires that ~ 5 ms is allowed for the valves to switch prior to sending a pressure pulse to the pumping chamber.

5.4.2 Frequency

Now that the required times for each of the steps in the pumping cycle have been found, Figures 5.3, 5.4, 5.8 & 5.9, operating frequencies can be set. The times required for each step in the pumping cycle, shown in Table 5.4, result in a minimum pumping cycle time of 40 ms, (25 Hz).

Table 5.4: Times required to complete each step of the pumping cycle, and delay values used to program the controller

		Time (ms)	Delay
Step 1:	Fill Pump Chamber	20	99
Step 2:	Switch Valve	5	25
Step 3:	Drain Pump Chamber	12	59
Step 4:	Switch Valve	3	15
	Total time	40 ms	
	Frequency	25 Hz	

For frequencies close to 25 Hz, it makes sense to use optimized cycle times. For much lower frequencies each of the steps in the cycle have ample time for actuation, and for higher frequencies the pump begins to break down. Other optimized frequencies, as well as the delay values used to program the controller, are shown in Table 5.5.

Using these optimized cycle times, flow as a function of frequency can be tested. Figure 5.10 shows this test for pneumatic pressures of ±35 kPa. Flow for cycles where each of the steps are allowed equal times for actuation, and flow when cycle times have been optimized have been tested.

Table 5.5: Cycle timing for 15 Hz, 20 Hz, 25 Hz & 30 Hz pumping cycles.

	Time	Delay	Time	Delay	Time	Delay	Time	Delay
Step 1: Fill P. Chamber	27	134	23	114	20	99	18	87
Step 2: Switch Valve	12	59	7	35	5	25	5	25
Step 3: Drain P. Chamber	18	89	15	74	12	59	8	40
Step 4: Switch Valve	10	50	5	25	3	15	3	15
Total time (ms)	67 ms		50 ms		40 ms		34 ms	
Frequency	15 Hz		20 Hz		25 Hz		30 Hz	

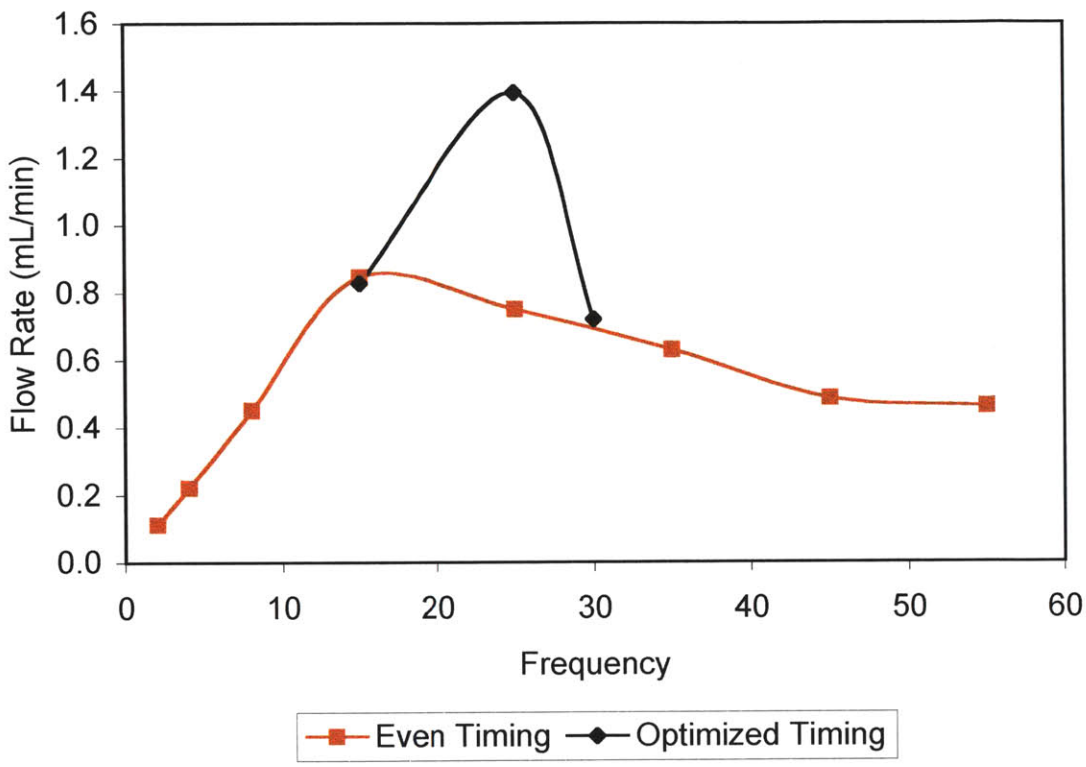

Figure 5.10: Flow rate as a function of frequency when pneumatic controls are set to ±35 kPa. Optimized cycle times are plotted in black and cycles allowing equal times for each step are plotted in red.

The initial linear slope of this figure signifies that an equal amount of volume is pumped during each cycle. As expected, after 25 Hz, the frequency becomes too fast and the entire volume of the pumping chamber is not pumped during each cycle. Clearly, the optimized cycle times have outperformed pump cycles utilizing equal delay times.

5.4.3 Pneumatic Pressures

Pressure can have a significant impact on pump cycle volume. If pressure values are set too low, the pressure will not sufficiently deflect the membrane to the surfaces of the pumping chamber. If pressure values are too high, there may not be ample time to switch from positive to negative pressure under the valves and pumping chamber.

First, the minimum operating pressures are determined. These are the pressures required to actuate the membrane from one position in the pumping chamber to another. Low frequencies, 2 to 4 Hz, were used for these tests to allow ample time for the pressure under the valves to equilibrate and for the membrane to actuate.

Equal positive and negative pressures were set on the regulator. Total flow measurements, normalized to the number of cycles measured, are plotted in Figure 5.3.

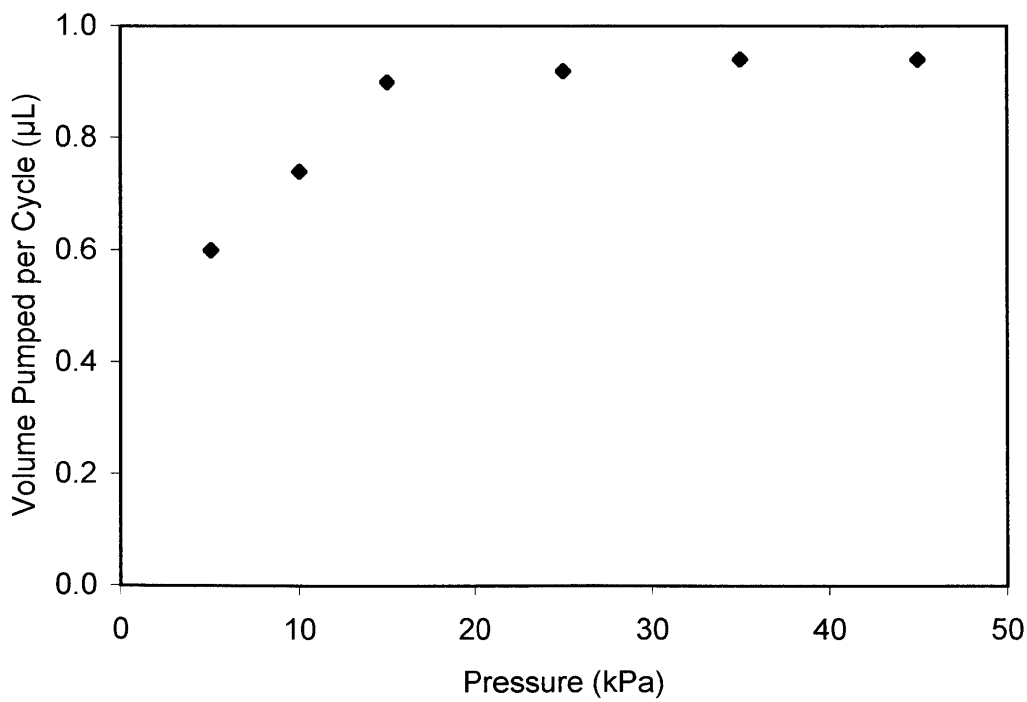

Figure 5.11: Pumping chamber volume in relation to actuation pressures, pumps were driven at low frequencies

Seen in this figure, the volume pumped per cycle begins to decline as pressures drop below 15 kPa. This value helps confirm the calculations made in Chapter 4 that ±12 kPa is required to fully deflect the membrane from one side of the pumping chamber to another.

Next, pressure dependencies across a range of frequencies were found, Figure 5.12. The entire scaffold assembly is used in order to most accurately represent culture conditions. Equal positive and negative pressures were set on the regulator.

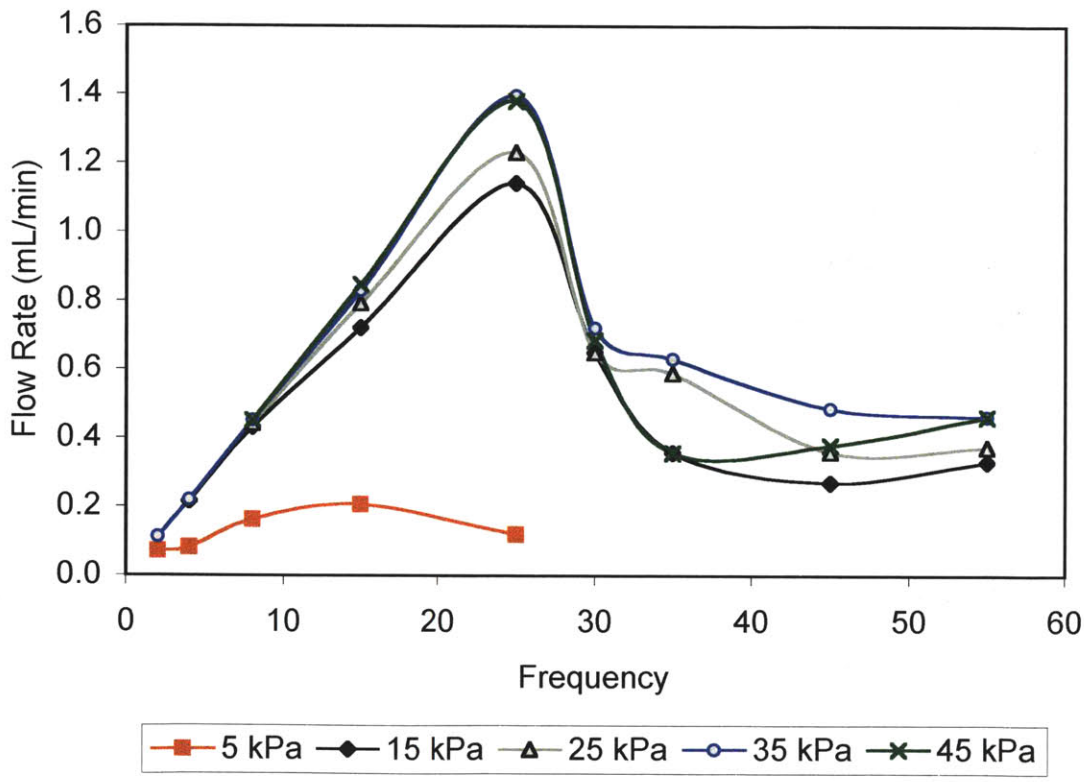

Figure 5.12: Flow rates in relation to actuation pressures, pumps were driven at 15 Hz

Seen in this figure, flow increases linearly with frequencies up to 25 Hz. When higher frequencies are used, both the consistency of flow, and the total flow rate suffer. At ± 35 kPa, flow increases linearly at a maximum slope up to 25 Hz. Above 25 Hz, 35 kPa maintains flow better than any other pressure setting. Also, ± 35 kPa is well below

the rated maximum differential pressure across the three-way pneumatic valves in the controller, 100 kPa (Chapter 2).

As higher frequencies are used (15 & 25 Hz), flow for pressure settings of 15 & 25 kPa begins to fall below the flow for 35 kPa. This is because these frequencies do not allow ample time for the pumping chamber to fully actuate. Seen in Figure 5.7, lower pressures drive flow from the pumping chamber at slower rates. These rates become limiting factors at higher frequencies.

A potential limit on the maximum operating frequency is the time required to send pressure and suction to the valves. If this time were reduced, the pumping chamber would fill sooner (curves in Figure 5.4 would shift to the left), and higher frequencies would be attainable. This could be achieved by using shorter connective tubing between the bioreactor and the controller. Also, the inner diameter of the tubing could be optimized. If the diameter is made smaller, less air will need to be evacuated in order for the pressure to change.

5.4.4 Head Pressures

The filter in the scaffold assembly presents a resistance to flow. This resistance will create a head pressure in the capacitor proportional to the flow rate through the scaffold. Resistance can be calculated from the hydraulic permeability of the filter, 73.5 $(mL/s)/(N/mm^2)/cm^2$, and the effective area of the filter. For a flow rate of 1 µL/channel/minute, and a filter where flow only passes through the open channels, the head pressure in the capacitor will be 0.25 kPa.

The relationship between flow and head pressure was measured experimentally. The test setup described in Section 5.2 was modified by connecting a long, 1.6 mm inner diameter tubing with one side of the pump, Figure 5.13. The pump is programmed to run for 250 cycles and the resulting height of fluid is measured. As more fluid is

pumped into the tube, the height of the fluid rises and so does the head pressure at the pump. The volume of fluid pumped per cycle can be found from the change in height over 250 cycles.

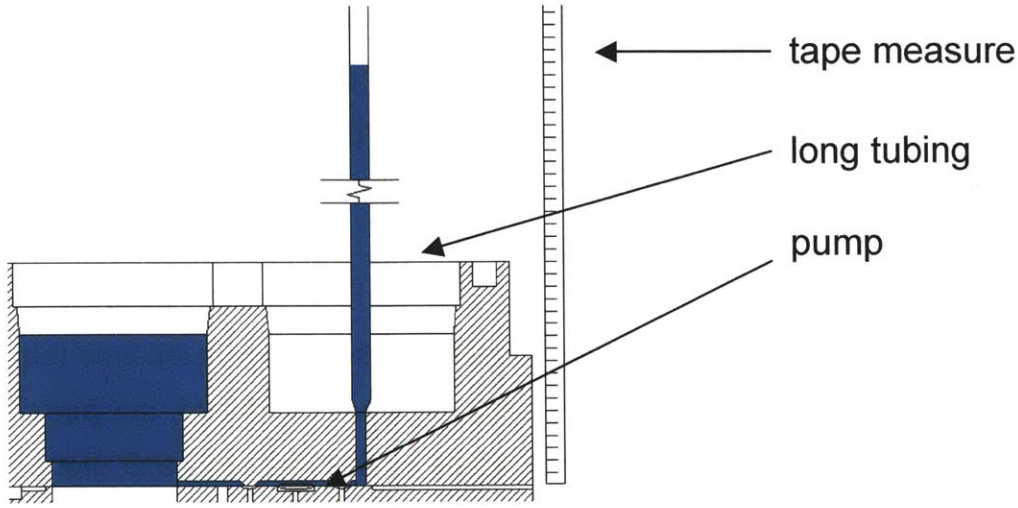

Figure 5.13: Test setup for measuring flow vs. head pressure.

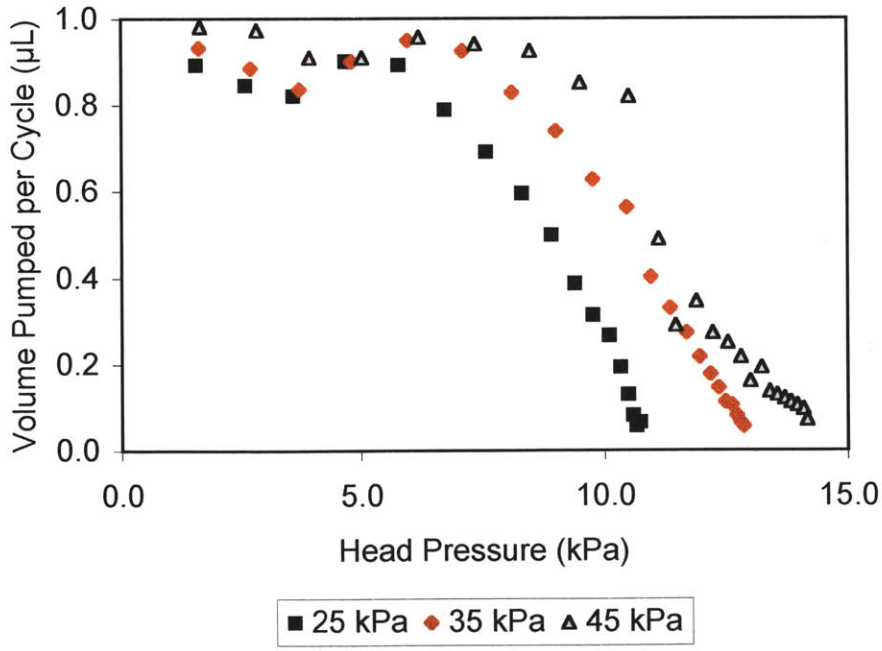

Figure 5.14: Head pressure curves for the pump when operated at 15 Hz with pneumatics set to ±25, ±35 & ± 45 kPa.

Figure 5.14 shows the relation between head pressure and the volume pumped per cycle. A constant volume of 0.93 µL per cycle means that the pump is functioning

properly and the expected flow rate for a given frequency will be realized. When this volume drops, so will the flow rate for a given frequency. As the pneumatic pressure increases, the pump is able to drive flow against higher head pressures. The maximum head pressure where the pump outputs the total volume of the pumping chamber is shown in Table 5.6.

Table 5.6: Maximum head pressures against which the pump can drive consistent flows

Pneumatic Pressure	Head Pressure
45 kPa	8.5 kPa
35 kPa	7.1 kPa
25 kPa	5.8 kPa

For all of the pneumatic input values tested, the pump works consistently for head pressure values well above the 0.25 kPa required to drive flow through a clean filter. Through the course of an experiment it is possible that the filter will begin to clog with cell debris. This will reduce the effective area of the filter and will cause an increase in resistance and pressure. Resistance would need to increase by nearly 30 fold before any effects could be seen in the pumping system. In order for the performance of the pump to begin to decline, an extremely high percentage, 98%, of the filter would need to be totally clogged with debris. To validate that this is not occurring, a flow test was performed at the end of an experiment, Section 5.4.5.

There are several reasons why the maximum attainable head pressures are below the pneumatic input pressures. If the pumping frequency is too high, there will not be sufficient time for the pressures under the valves and pumping chambers to reach maximum values. When frequencies are decreased, to 8 Hz, these head pressure curves reach higher values, Figure 5.15.

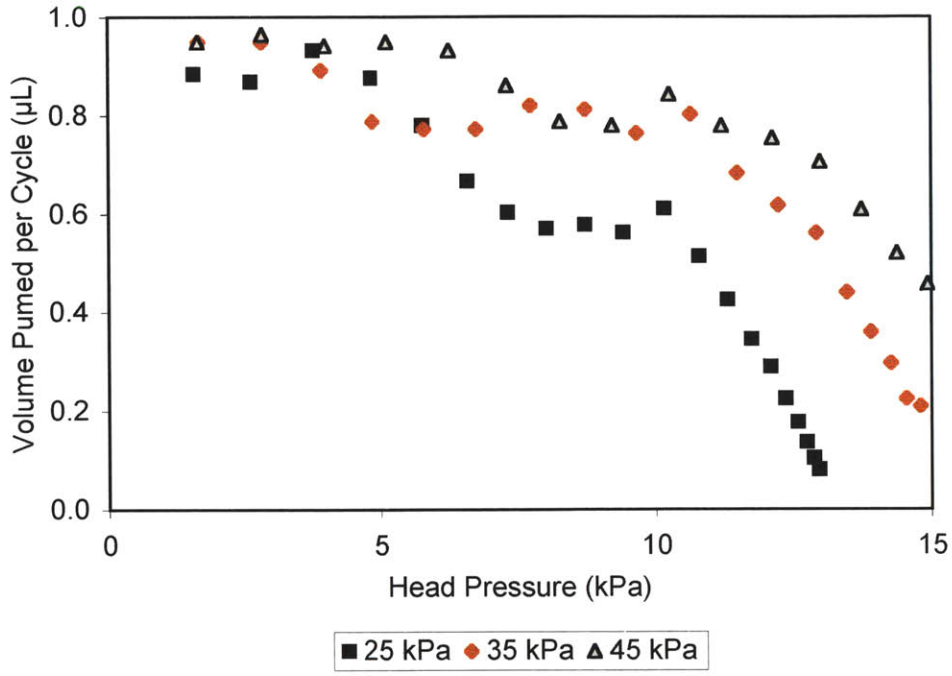

Figure 5.15: Head pressure curves for the pump when operated at 8 Hz with pneumatics set to ±25, ±35 & ± 45 kPa.

The maximum attainable head pressure for 25 kPa rises from around 11 to 13 kPa, and the maximum head pressures for 35 and 45 kPa are both higher than 15 kPa. In all three curves, pumping values for head pressures ranging from 5 to 10 kPa are below expected. This is most likely due to inconsistencies in the measurement system, such as the surface of the fluid not being exposed to atmospheric pressure.

Another reason for not obtaining head pressures equal to the pneumatic driving pressures is because of leakage of fluid back through the pump when valves are switched. During steps 2 and 4 of the pumping cycle, Figure 2.12, it is possible that while one valve is closing, the other is opening. During this time, fluid can fall backwards down through the pump. When these steps are divided into additional steps, so that at least one valve is closed at all times, the maximum head pressure increases. Seen in Figure 5.16, pneumatic pressures of 35 & 45 kPa will drive fluid against head pressures over 15 kPa without being affected. Clearly, an altered pumping cycle is ideal for pumping against high head pressures.

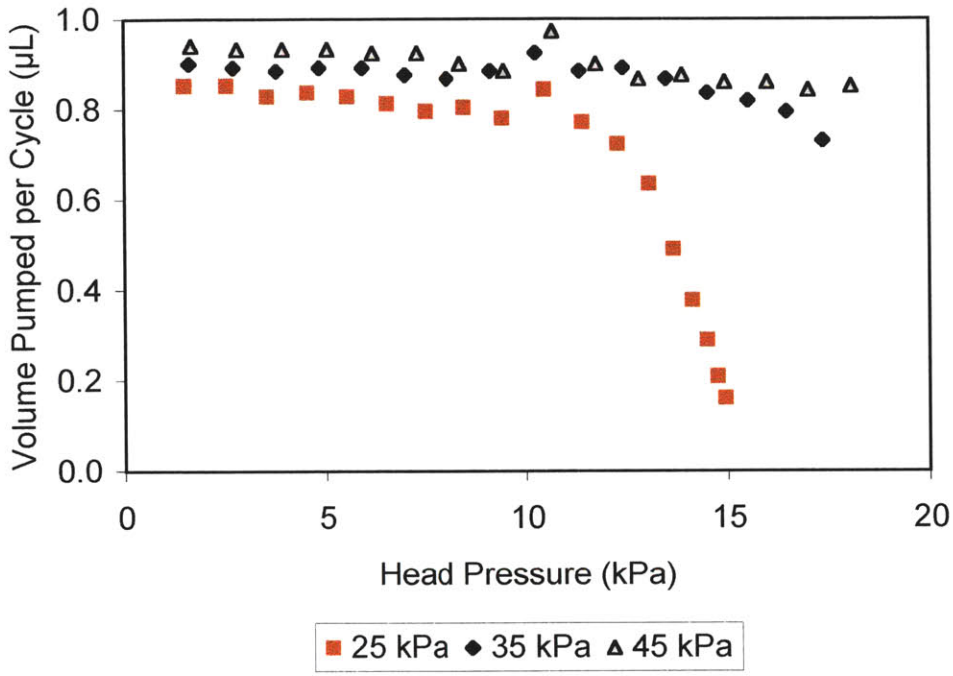

Figure 5.16: Head pressure curves for the pump when operated with an altered pumping cycle

5.4.5 Flow Test After Cell Culture

Flow was tested at the end of a 7 day experiment where cells were cultured in the reactor for 4 days. Since a surface channel connects adjacent wells in a functioning reactor, it is not possible to measure flow in the conventional manner. Instead, the test reactor was primed with warm medium and the scaffold assembly containing cells and filters from a reactor unit with 861 channels was transferred to the test system. Flow through 500 cycles at 15 Hz was measured 5 times in both pumping directions. The scaffolds were removed and flow was again measured 5 times for a control. In order to measure the medium consistently, a small amount of medium had to be used to prime the syringe. Because of this, the volume measured is not the volume pumped per cycle. Table 5.7 shows the average fluid volume measured for each condition.

Table 5.7: Average volume of medium measured at a pumping frequency of 15 Hz for a reactor unit with no scaffolds and a reactor unit with scaffolds, filters and cells

	Down Through Scaffold	Up Through Scaffold
With Cells	0.41	0.49
No Filters	0.40	0.49

The volume measured both with and without cells is very consistent; however, it appears that more flow occurred in one direction than the other. Due to the difficulties in measuring medium in a syringe, and the lack of repeated tests, no firm conclusions can be made from this difference. However, it is encouraging that a scaffold assembly filled with cells has no effect on the pumping system.

5.5 Membrane Characterization

Operation of the pumping system is heavily influenced by the physical properties of the membrane that separates the fluidic plate from the pneumatic plate. The Young's Modulus of the membrane was measured using the experimental setup shown in Figure 5.16. A 40 mm wide section of membrane was clamped between two parallel clamps separated by 42 mm. The lower clamp is attached to a stationary scale and the upper portion is connected to the moveable Z-axis of the CNC milling machine. Strain was measured on the milling machine and the corresponding force was measured on the scale. Force was normalized to width and the results are plotted in Figure 5.17.

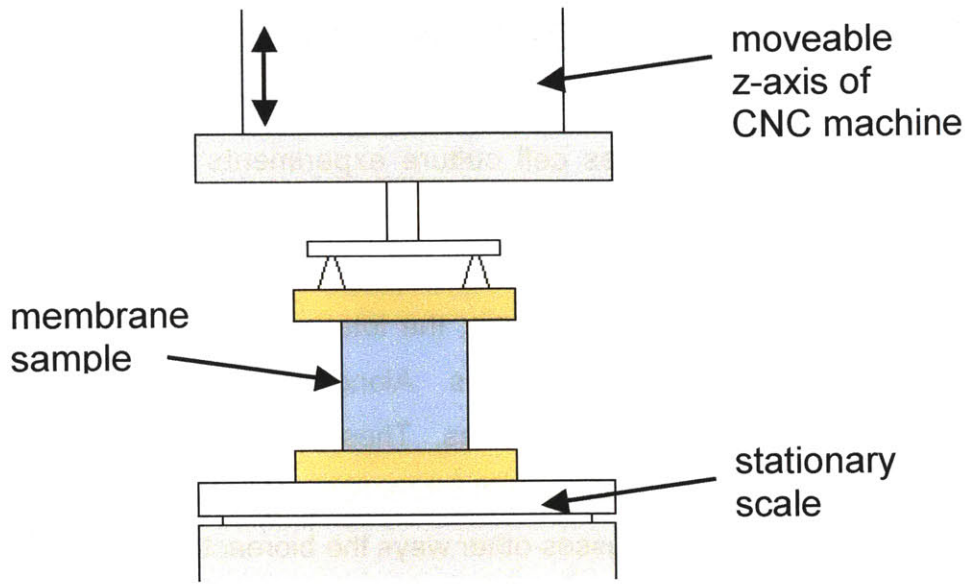

Figure 5.17: Experimental setup for measuring stress vs. strain in the membrane

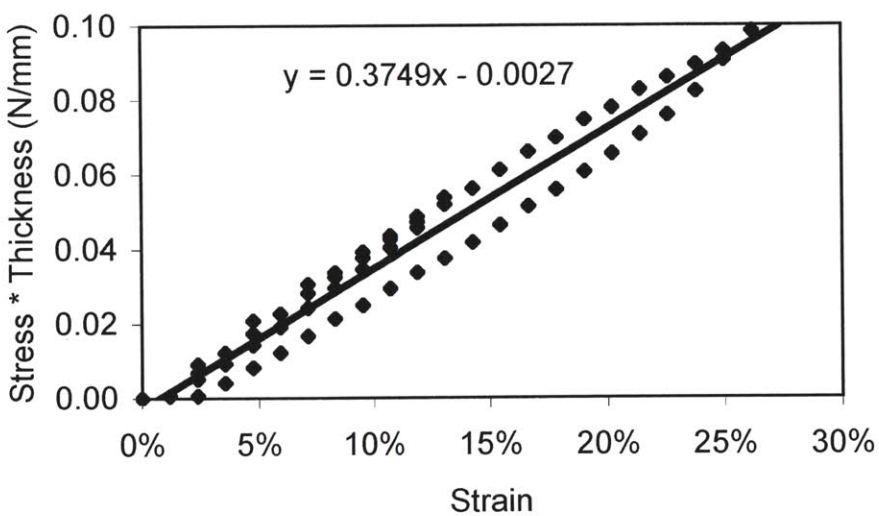

Figure 5.18: Stress-strain curve for the membrane. This curve is normalized to unit width and the actual thickness of the membrane.

The slope of this curve, 0.3749 N/mm, represents the Young's modulus for this particular membrane and is not normalized to the membrane thickness, 25 μm. This value can be used in models using a thin, flexible membrane of constant thickness. Membrane tension is the dominant force in these models and internal shear stresses are neglected.

6. BIOLOGICAL APPLICATIONS AND CHARACTERIZATION

This chapter describes cell culture experiments that were performed in the bioreactor and gives insight into the versatility of the system. A multitude of comparative studies are possible using a single bioreactor plate. These studies include varying the culture micro-environment, the total number of cells, and cell to medium ratios, and testing different compounds. Along the same lines, a broad spectrum of assays can be used to evaluate cultures. These include assays that require end point analysis, medium sampling, and visual inspection. This chapter begins by describing a typical experiment, then discusses other ways the bioreactor can be used.

6.1 Protocol for a Typical Experiment

6.1.1 Preparing the Cells

Liver cells are isolated from male Fischer rats using the protocol described by Sivaraman, [19]. 100 mL of hepatocyte suspension in HGM (Hepatocyte Growth Medum, [19]) is placed into a spinner flask (Bellco Glass, Vineland, NJ) at a concentration of 3×10^5 cells per mL. Spinner flasks rotate at 85 rpm for 3 days while cells aggregate into spheroids. After 3 days, cells are taken from the spinner flask and filtered to select for 50 to 300 μm spheroids (50 & 300 μm filters, Sefar America, Kansas City, MO). This size range is used to remove debris, marginally viable cells, and aggregates that are larger than the channels. Selected cells are centrifuged at 50 g for 3 min, then resuspended in ~ 15 mL cold HGM.

6.1.2 Preparing the Reactor

All of the reactor components that will contact the cell culture medium are cleaned and autoclaved in preparation for assembly. Scaffolds are coated by soaking in a 30 μg/mL Type I rat tail collagen (BD Biosciences, Bedford, MA). Silicon scaffolds are coated for 30 minutes at room temperature and polymer scaffolds are coated for 2 hours and are allowed to dry for 2 hours. The differences in times are the result of a functional difference in protein adsorption for the two materials. Filters are soaked for 30 minutes in a 1% w/w BSA (Fraction V, Sigma-Aldrich) in PBS solution (pH7.4, Invitrogen). Immediately prior to assembly, each reactor part is rinsed with PBS.

The reactor is assembled according to the protocol described in Appendix A11, and is primed with warm HGM (37 °C). The reactor is run for 5 minutes, then washed with fresh, warm, medium. Warm medium is used to prime the reactor in order to ensure that bubbles do not form below the scaffold when the reactor is placed in the incubator.

6.1.3 Seeding Cells

Downward flows of 1 to 2 μL/channel/minute are run through the reactors with medium levels just above the height of the surface channel. This reduced volume allows ~ 1.5 mL cell suspension to be added to each reactor unit without overfilling. A 0.5 mL volume of cell suspension is added to the first reactor unit using a pipette. The first 3 mm of the pipette tip is removed in order to increase the diameter of the pipette opening. Enlarging this opening minimizes exit velocities and shear stresses in the cell suspension during seeding.

After spheroids are seeded into the first reactor, the scaffold is examined under the microscope. If there are too many empty channels, an additional volume of cell suspension is added and the reactor is checked again. The remaining reactors are

seeded once the optimal volume of cell suspension is determined. After all reactor units are seeded, a final visual inspection is performed to assess uniformity of seeding across reactor units.

6.1.4 Cell Attachment

During the first 24 hours of culture, flow remains in the downward direction allowing time for cells to adhere to the walls of the scaffold. Time-lapse photos, shown in Figure 6.1, were taken during these initial stages of culture and show the rearrangement of cells to form tissue structures. Adherence of cells to the scaffold is critical for successful cultures and is a positive indicator for the performance of the bioreactor. The cells used in this experiment were previously cultured for 3 days in spinner flasks and have been filtered to select for spheroids between 100 and 300 μm in diameter.

Flow is reversed once cells have attached to the scaffold (usually ~ 24 hrs). This reversal prevents cell debris from clogging the filter underneath the scaffold.

6.1.5 Extended Culture

Each day, 1.5 mL of HGM is aspirated from the reservoir and is replaced with fresh HGM, refreshing ~ 50% of the total medium in the system. Medium samples can be analyzed for secretion of albumin, urea or bile and other medium components.

At the end of the experiment, scaffolds are removed from the reactor wells and can be placed into Trizol to lyse the cells (Trizol, Invitrogen). RT-PCR is performed on all of the samples using the protocol described by Sivaraman [19]. A typical set of gene expression data from day 7 (post isolation) cultures is shown in Figure 6.2. The genes measured transcribe Phase I and Phase II enzymes, transcription factors and surface

proteins. The bioreactor data is an average across 8 technical replicates and 2 biological replicates and the collagen gel sandwich data is from 2 biological replicates where samples were pooled from 6 wells on a tissue culture plate.

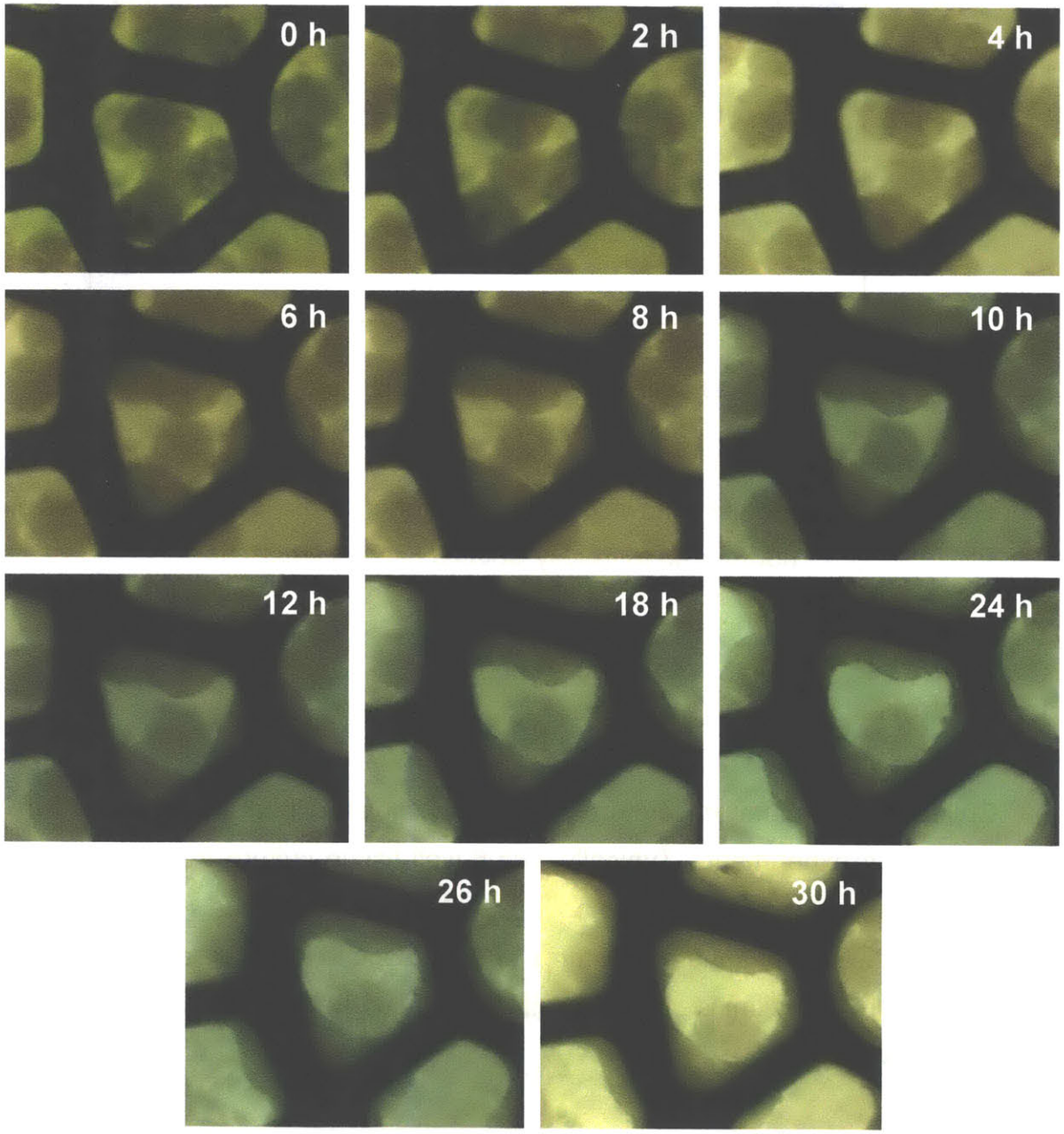

Figure 6.1: Time-lapse pictures of cells forming tissue in the silicon scaffold. Spheroids were allowed to aggregate for three days prior to seeding in the reactor.

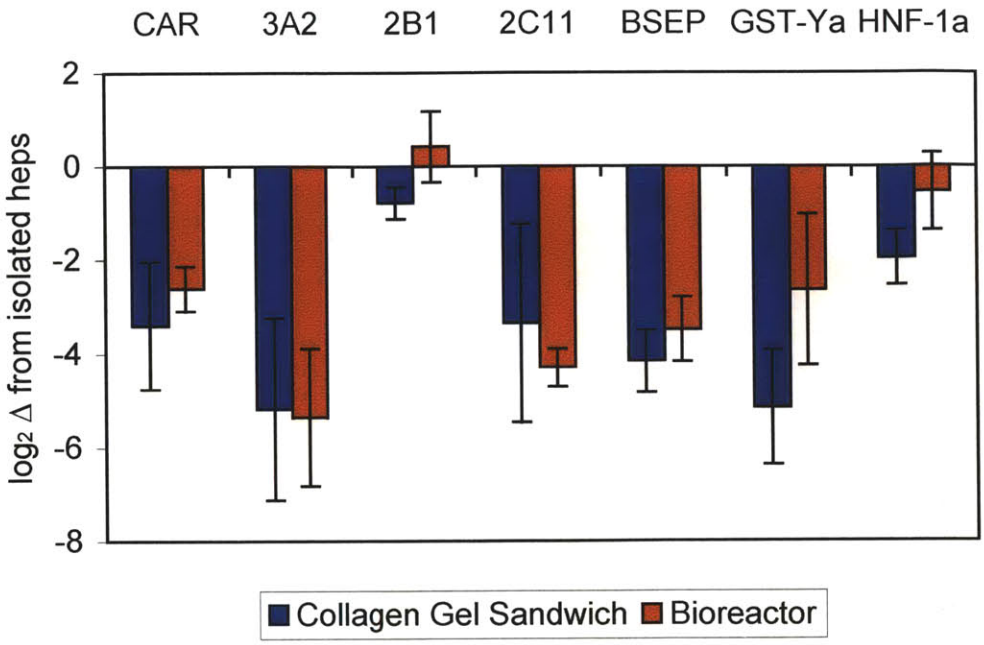

Figure 6.2: Gene expression data from a typical experiment, day 7 post isolation. This chart compares collagen gel sandwich and bioreactor cultures. Expression levels are normalized to freshly isolated hepatocytes.

6.1.6 Controls

Collagen gel sandwich cultures of freshly isolated hepatocytes are run as controls for each experiment. Typically, two 6-well tissue culture treated plates (BD Bioscience) are run, utilizing the protocol described by Sivaraman [19]. The first is taken down at the end of spheroid cultures and the second is cultured until the end of the reactor culture. Medium is changed daily throughout the duration of the culture with 1 mL fresh HGM.

At the beginning of each experiment, a sample of freshly isolated hepatocytes is lysed in Trizol for RT-PCR analysis. This sample is used to normalize gene expression data. Spheroid samples are also taken immediately prior to seeding cells into the reactor.

6.2 Other Experiments

6.2.1 Metabolism and Induction

The liver is primarily responsible for the in vivo metabolism of many drugs. This metabolism is mediated by a specific set of enzymes (including CYP450's), and the activity of these enzymes can be measured using a number of methods. A compound can be added to the culture medium and circulated through the system. After a set period of time has elapsed, a sample of medium is taken from the reactor unit and is analyzed for the formation of metabolites.

These experiments are typically done on cells once tissue has formed and stabilized in the bioreactor (4 to 7 days). In order to prepare the system for this type of experiment, the medium must be free of albumin. Since hepatocytes secrete albumin, culture medium must be exchanged with albumin free medium immediately prior to each experiment.

In each reactor unit there is a total of 3 mL of medium, 2 mL of which is accessible. In order to exchange all medium, two wash steps must be performed. For each step, the medium in the reservoir is aspirated, 2 mL of new medium is added, and the reactor is run for 5 minutes in order to completely mix the new medium.

After the wash, medium is again aspirated and 2 mL of new, drug containing medium is added. At the end of this step, 96 % of the medium is fresh and does not contain albumin. For a testosterone experiment, the desired testosterone concentration is 250 μM. As such, the dose concentration should be 375 μM, as it will be diluted by the additional medium in the reactor unit.

Testosterone is run through the reactor for 1 hour before the medium is sampled. A sample of medium can be analyzed with HPLC using the protocol discussed by Sivaraman [19]. If the culture will be maintained after this test, the testosterone should

be washed 3 times from the system. This will remove 96% of the testosterone containing medium.

This experiment has been performed, and metabolites have been seen, however, the data was not analyzed quantitatively.

For metabolism experiments it is important to check for adsorption of a compound to the surfaces of the reactor. Adsorption of testosterone was tested for partially and fully assembled reactors without cells. The reactor was run with medium containing 250 μM testosterone for 1 hour and the final concentration was measured using HPLC. The amount of adsorbed testosterone to each reactor setup is shown in Table 6.1. A control sample was analyzed using HPLC and each of the other samples are normalized to the control. Seen in this table, the maximum amount of absorbed testosterone was 29%.

Table 6.1: Amounts of testosterone absorbed to the reactor surfaces after 1 hour of exposure

	Control	Empty Reactor	Reactor no Filters	No BSA on Filters	Full Reactor
Concentration	250 μM	209 μM	194 μM	182 μM	178 μM
% Absorbed	0%	16%	22%	27%	29%

Induction of a specific p450 gene can be measured by similar dosing experiments. In these experiments, a drug is added to one set of reactor units and is not added to others. At the end of the experiment, gene expression levels can be compared across different dosing conditions in the bioreactor. Since each reactor unit is an isolated system, the cells from one set of reactors can be removed without altering the operation of other reactor units on the plate. This allows the user to take gene expression data at multiple time points after cells have been dosed with a drug.

In one study, midazolam was added to one reactor unit and was not added to others. Hoen has shown that midazolam induces the CYP2B1 gene, and that result is

reproduced in the bioreactor [27]. Figure 6.3 shows differences in 2B1 expression levels between treated and untreated cells. A 10 μM concentration of midazolam was added to cells on day 4 of culture and gene expression levels were assayed on day 7.

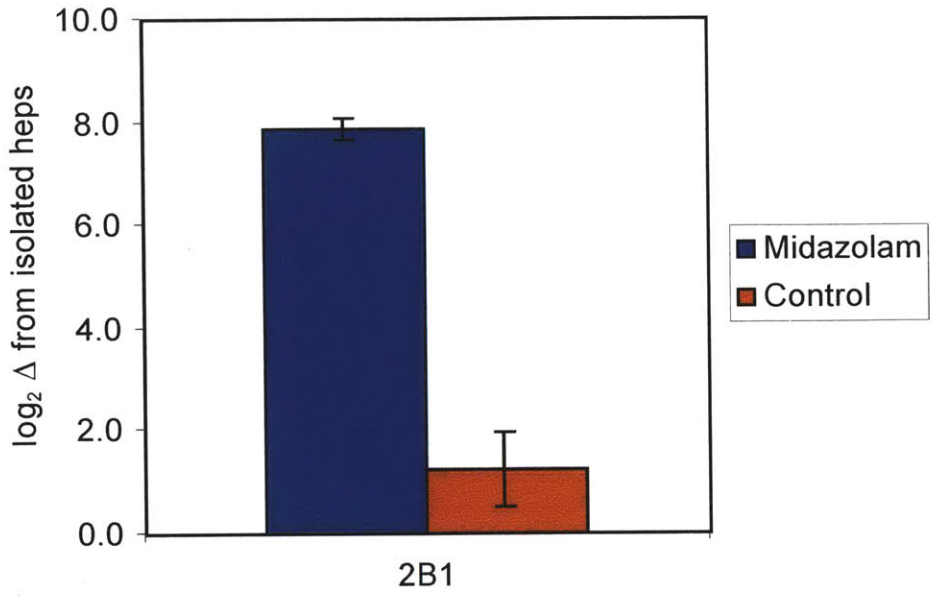

Figure 6.3: Expression of 2B1 mRNA for cultures dosed with midazolam

6.2.2 Variations in Culture Microenvironment

There are many ways in which the microenvironment of the cells can be modified. Flows through the scaffold can be changed, channel geometries can change, and so can the scaffold material. These changes are incredibly simple to make and a matrix of differing conditions can be tested on one bioreactor plate. A variety of culture conditions have been tested in search for an optimal culture microenvironment.

6.2.2.1 Flows

Flow through the scaffold can be modified in a number of ways. The rate of flow, as well as the timing of flow reversal can be changed. Similar to the pneumatic plate with two inputs, FIgure 2.30, a plate with four sets of inputs, Figure 6.4, allows for 4 different flow patterns.

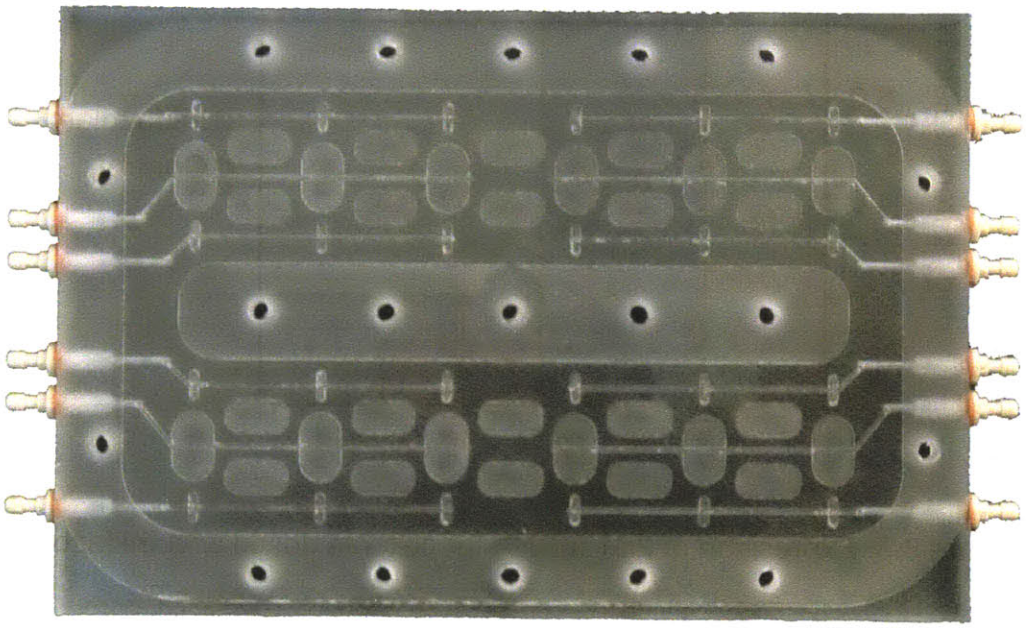

Figure 6.4: A pneumatic plate with 4 sets of inputs. The pumping system on this plate is from an earlier prototype.

An experiment has been done to test the differences between seeding single cell suspensions and cells that have been pre-aggregated into spheroids. Because single cells are seeded immediately after isolation and spheroids are seeded on day 3, this experiment requires differing flows on the reactor throughout the culture period. Achieving these flow patterns, shown in Table 6.2, requires the use of this special pneumatic plate.

Table 6.2: Required flow patterns through the scaffold when culturing cells seeded at different times

Day	Flow Direction	
	Single Cells	Spheroids
1	Down	--
2	Up	--
3	Up	--
4	Up	Down
5 - 7	Up	Up

Figure 6.5 shows pictures taken of freshly isolated cells directly after seeding. Each of the channels is well filled with cells, and there is an even dispersion of cells throughout the scaffold.

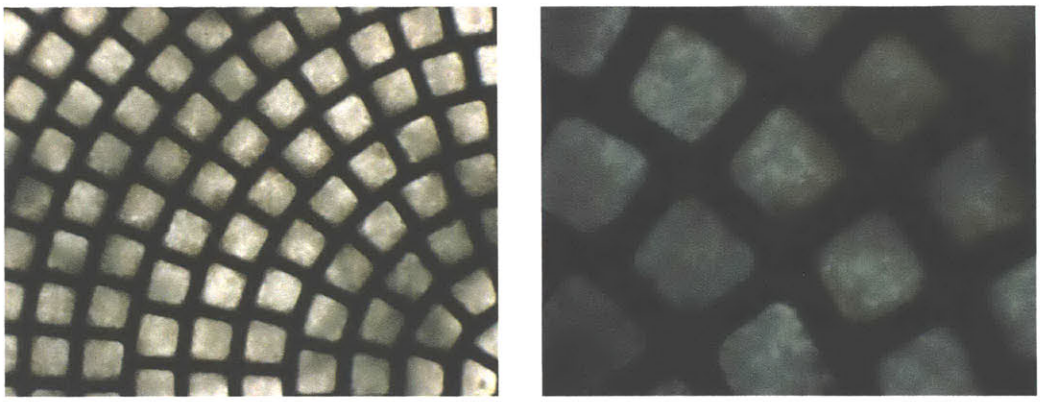

Figure 6.5: Cell isolates day 1 after being seeded into the reactor

Gene expression was measured on day 7 in spheroid reactors and in reactors seeded with single cells. This data, Figure 6.6, shows comparable gene expression levels across the majority of genes measured.

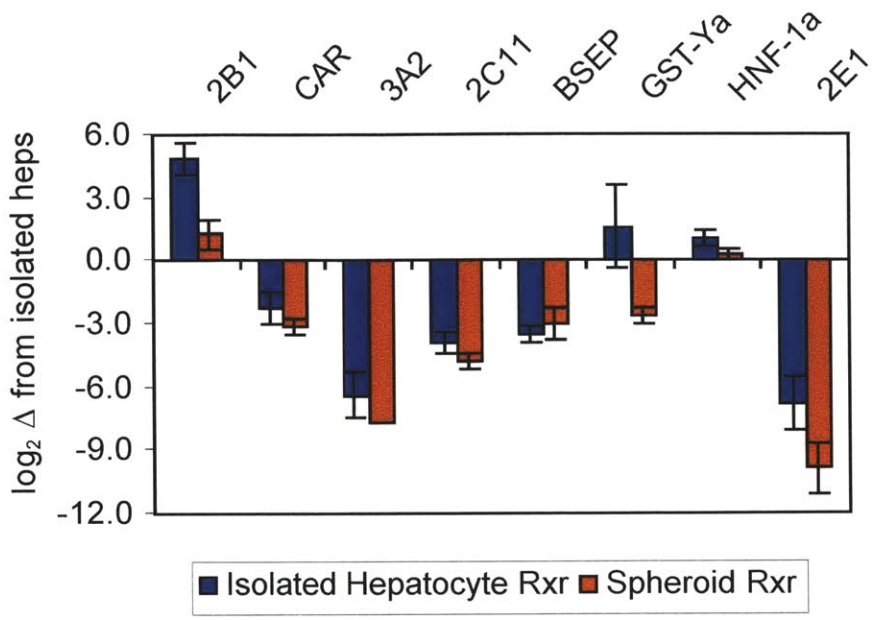

Figure 6.6: Gene expression levels for reactors seeded with cell isolates and reactors seeded with cells that have aggregated into spheroids

In addition to changing flow directions, the rate of flow can be varied across reactor units. Slight variations in flow have occurred when scaffolds with differing numbers of channels are used. These flows have varied by ~ 30% and no noticeable effects have been observed. An experiment could easily be performed where flow is varied drastically across reactor units. A pneumatic plate with four inputs, similar to the one shown in Figure 6.4 would be ideal for this type of experiment.

6.2.2.2 Scaffolds

Scaffolds are readily interchangeable in the bioreactor, thus many different types of scaffolds have been manufactured and tested. The properties of the material that cells adhere to can have dramatic effects on the culture [28, 29]. A variety of different materials, silicon and many polymers, have been tested and advantages to each material are described in this section.

Silicon scaffolds have been used in previous bioreactor systems developed in this lab. These scaffolds can be made with incredibly precise dimensional control and limitless channel geometries are possible. Cell adhesion to these scaffolds is very good, suggesting that collagen deposition to the scaffolds surfaces is very efficient. Silicon is also a very inert material. These scaffolds can be autoclaved numerous times, they can also be submerged in Trizol without adverse effects.

Along with these advantages, there are some limitations. Silicon is a very brittle material, especially when it is made into a thin scaffold. Even when these scaffold are handled very carefully, they are still prone to breaking. These scaffolds are also relatively difficult and expensive to manufacture.

Polycarbonate scaffolds have also been used previously in the lab. In contrast to silicon scaffolds, these scaffolds can be manufactured very easily and they are not brittle. Unfortunately, they cannot be autoclaved, or exposed to Trizol. More importantly, cells don't adhere as well to polycarbonate scaffolds. These scaffolds typically soak in collagen for two hours, then dry for two more hours before insertion into the bioreactor.

Because plastics are not brittle and can be easily machined, they offer advantages over silicon. For this reason, more plastic scaffolds were tested. PEEK (polyether ether ketone) and PVDF (polyvinylidene fluoride) were selected because both of these materials can be autoclaved and are more chemically resistant than polycarbonate.

PVDF is fairly hydrophobic, thus priming the channels with fluid is difficult. In general, these scaffolds are not user friendly. PEEK scaffolds, on the other hand, are relatively easy to use. Similar to silicon, they can be autoclaved and can be submerged in Trizol without noticeably altering the material. Experiments with these scaffolds have been run to assess collagen deposition and cell adhesion. PEEK scaffolds have been

coated with collagen using both the 30-minute silicon and the 2/2-hour polycarbonate method, and cells have been cultured.

Figure 6.7 shows some representative pictures from experiments comparing silicon, polycarbonate and PEEK scaffolds. Gene expression data from these cultures was measured by RT-PCR and is shown in Figure 6.8. From these figures, there doesn't appear to be much of a difference between scaffold materials.

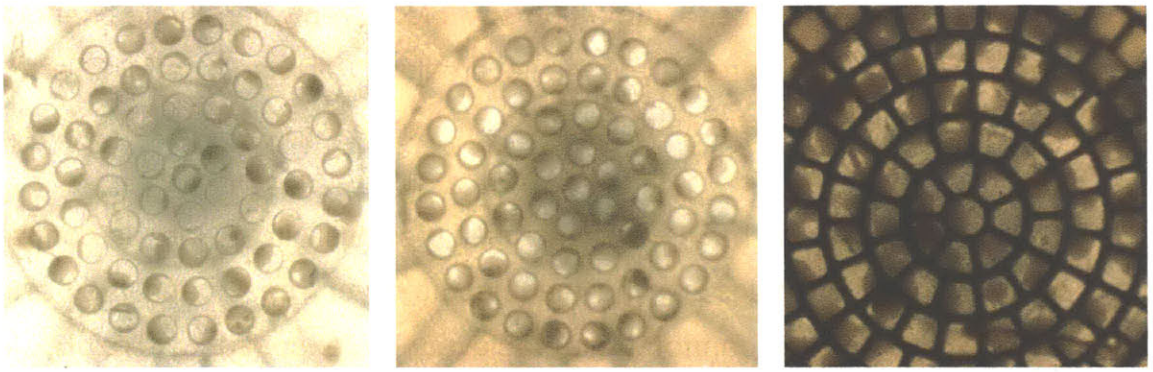

Polycarbonate PEEK Silicon

Figure 6.7: Pictures from cells cultured on different scaffolds

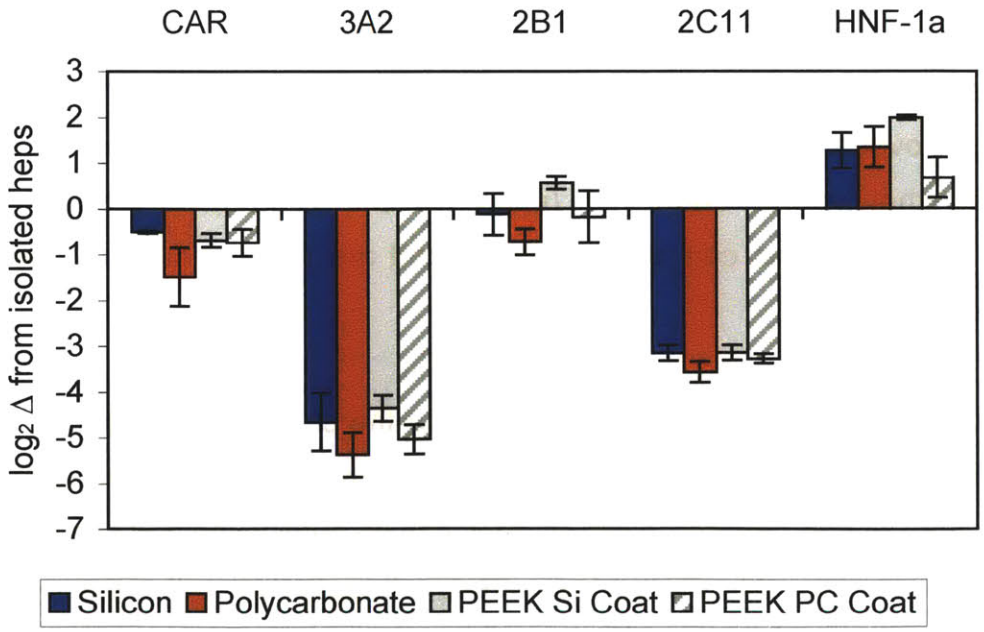

Figure 6.8: Gene expression for cells cultured on a variety of scaffold materials. PEEK scaffolds were coated with collagen for 30 minutes (Si Coat) and for 2 hours (PC Coat).

There are many other materials that can be used as scaffolds. Several of these materials have been previously tested in other bioreactor systems developed in this lab; however, there are still other materials that can be investigated for use in this bioreactor setup.

6.2.3 Variations in Numbers of Cells and Cell to Medium Ratios

Depending on the number of cells required for a given experiment, the number of channels in a scaffold can be modified. Scaffolds containing anywhere between 61 and 861 channels can be used, thus the number of cells in a culture can be varied by more than ten fold. Flow in the reactor can be tailored to suit the number of channels utilized. The use of inserts, similar to the one shown in Figure 2.26, allows some flexibility in volume; however, there are obvious limits to the maximum and minimum amounts of medium in a reactor unit (~1.75 mL to ~ 3.5 mL).

Experiments have been performed with silicon scaffolds where only 97 channels contain tissue. Gene expression data for these experiments is compared with data from previous experiments in Figure 6.9. The minimal differences in expression levels shows that the system performs similarly across a wide range of cell numbers.

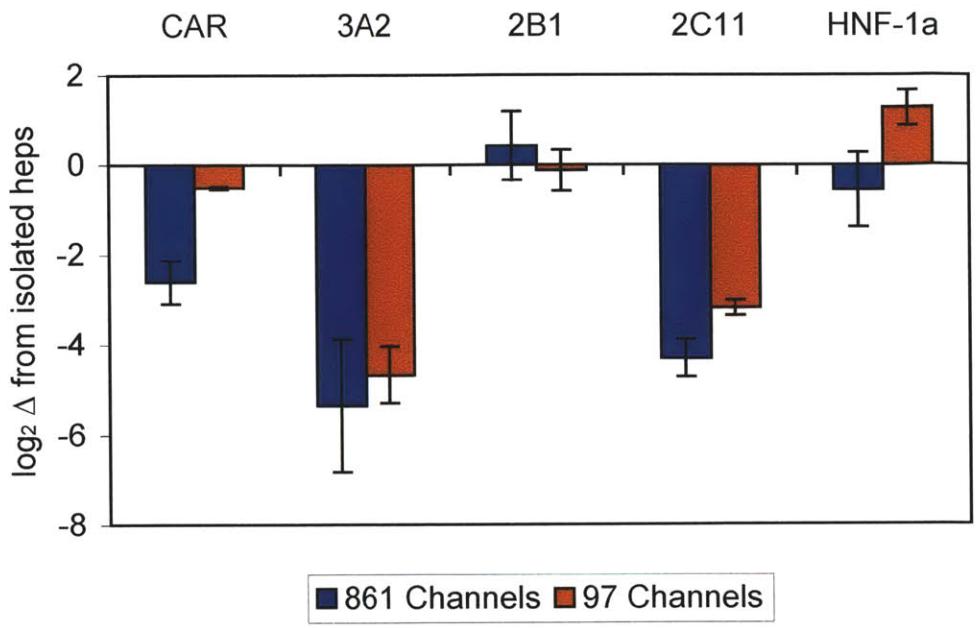

Figure 6.9: Gene expression levels for scaffolds with only 97 and 861 channels

Since the same volumes of medium were used for all of these experiments, cell to medium ratios were vastly different. One can compare cultures with different ratios, however, this has yet to be done with cells from a single isolation.

These cell to medium ratios are potentially very important. With many cells in a relatively small amount of medium, the metabolism of these cells can change the concentration of medium components. As the cell to medium ratios change, so do the rates of depletion of medium components.

Since the rates of formation of testosterone metabolites have been measured for previous bioreactor systems, Table 6.3 [19], testosterone is a good example. From these rates of formation, the total depletion of testosterone can be estimated for a one-hour exposure time. Assuming similar rates for the current bioreactor system, a calculation is made for the drop in testosterone concentration in a system containing 61k cells and a system containing 861k cells. In the 861k cell system, the final concentration drops by 31%, ~ 15 times more than in the system with fewer channels.

Table 6.3: Rates of metabolism of testosterone for previously reported systems [19] and estimated depletion of testosterone in the bioreactor plate.

Rates of formation of testosterone products	
16 alpha	609 p mol / 10^6 cells / min
16 beta	811 p mol / 10^6 cells / min
2 alpha	367 p mol / 10^6 cells / min
6 beta	2662 p mol / 10^6 cells / min

Total Depletion of testosterone	
	4449 p mol / 10^6 cells / min
	2.7E-07 μ mol / cell / hour

Initial Concentration	250 μM
Medium Volume	3.2 mL
Initial Ammount of Testosterone	0.8 μ mol

	# of cells	Cells to Medium (1k / mL)	Final Amt. Testos. (μ mol)	Final Concen. (μM)	Concen. Drop
61 Channels	61000	19	0.78	245	2%
861 Channels	861000	269	0.57	178	29%

It is important to keep this type of phenomenon in mind when determining dose concentrations for metabolism experiments. In addition, if components in the medium are being metabolized at significant rates, this could help to explain differences across systems with different cell to medium ratios.

7. RECCOMENDATIONS FOR FUTURE WORK

7.1 Capacitor

7.1.1 Capacitor Validation

The current capacitor should be mechanically characterized. In order to validate the performance of the capacitor, the reactor was seeded with cells and the movement of the cells was monitored under a microscope. Without a capacitor the cells shake at the frequency of the pump and with a capacitor they do not. More quantitative characterization should be done to validate the capacitor model. If it were possible to measure instantaneous flow through the scaffold, this would be ideal. Since there are obvious difficulties measuring flow in nL/ms, other methods may be more practical. The displacement of the capacitor membrane could be measured across time using an optical system. This displacement could be converted to a volume and flow could be calculated from a change in volume.

7.1.2 Capacitor Optimization

The capacitor is used to filter fluid pulses before they pass through the scaffold. The larger the capacitor is, the better it will perform. Unfortunately, a larger capacitor also requires more fluid underneath the scaffold. Since this fluid is inaccessible, extra wash steps are required when exchanging all of the medium in the system. Smaller capacitors should be investigated and tested with cells. If performance is comparable, and inaccessible volume can be significantly reduced, smaller capacitors should be considered.

There are also other types of capacitors that could be employed. An effective capacitor only requires a fluidic resistance and a fluid volume that can expand with

increasing pressure. This volume could be created in many different ways. For example, something as simple as a large air bubble trapped in the system would serve as a capacitor. Capacitance can be achieved if the scaffold is allowed to move up and down. It can also be achieved by inserting a soft rubber or foam in the system. Basically, any deformable material between the scaffold and pump will serve as a capacitor.

7.2 Pneumatic System

7.2.1 System Model

Flow through the pump can be externally manipulated using the controller. In order to flow at 1 μL/channel/minute (assuming 861 channels), the pump frequency is set to 15 Hz. The frequency can be decreased significantly, or can be increased to 25 Hz corresponding to flows near 1.4 mL/minute. One of the limiting factors here is the time required to change from positive to negative pressure under the valves. The pneumatic lines must have time to fill and drain with air. It is possible that higher frequencies could be obtained if the pneumatics are optimized to minimize the volume in the system while maintaining a low fluidic resistance in the lines.

A model of the pneumatic system would help in determining the optimal connective tubing between the reactor and controller. The output of this model would be the estimated pressure under the valve for a given configuration, input pressure setting and time. Flow to and from the valves and total flow though the pneumatic regulators would also be found. These values would help with the proper selection of regulators.

7.2.2 Quick Connectors

The pneumatic lines are connected to three separate nozzles on the bioreactor. Each time the bioreactor is moved, for example to change medium, the lines are disconnected and reconnected upon returning. If these lines are accidentally reversed, flow through the bioreactor will also reverse. Also, when disconnecting these lines it is easy to jar the bioreactor causing spillage of medium. A quick disconnect for these lines could be used to solve both of these issues. The connecting piece would not allow the lines to be reversed, and disconnecting the lines would be easier.

7.2.3 House Vacuum

In order to run the bioreactor, the controller is connected to house pressure and vacuum. If a nearby vacuum port is used, the vacuum supplied to the bioreactor can drop severely. When this occurs, the bioreactor pumping system can temporarily stop pumping. There are several ways to combat this issue. First, the bioreactor could be modified so that the dependence on vacuum is minimized or eliminated. Also, the pneumatic manifold could be digitized and an alarm could sound if the vacuum drops below a certain value. In addition, a vacuum reservoir could be used that runs the bioreactor when the vacuum lines are being used. Lastly, a separate vacuum pump can be used.

7.2.4 Secondary Channels

Due to the nature of the pumping system, the secondary channels, Figure 2.31, create a leak in pneumatics between adjacent valves. Although this leak is not expected to be problematic, it should be investigated further. If it can be minimized without sacrificing bioreactor performance, those steps should be taken.

7.3 Controller

The current controller was designed for developmental purposes. Although it works for the current system, it may have too much functionality for the average user. For example, there are eight different buttons that can run eight different subroutines. The average user will need to flow fluid in forward and reverse, and could potentially need one more routine for seeding cells.

A more user-friendly controller should be designed. Ideally, the user will be able to set flow directly on the controller, and view that flow on an LCD. This would eliminate the need to reprogram the device when different scaffolds are used.

7.4 Retaining Rings

The retaining rings in the scaffold assembly are used to create a seal so that no fluid can bypass the scaffold. This seal is crucial to the performance of the bioreactor. The rings work by applying pressure to the sides of the reactor well, creating a holding force from friction between the two surfaces. Since the holding force is only secondarily applied, it is not deterministic. A new method should be employed for creating a deterministic seal in the reactor well. The amount of force needed to create a seal should be calculated or measured. Then a retaining system with a holding force that matches this force should be developed.

7.5 Seeding Cells

7.5.1 Cell Isolates

The seeding of freshly isolated hepatocytes can offer several advantages over seeding spheroids into the reactor. For one, the efficiency of cell usage is severely compromised when making spheroids. Also, it is very difficult to determine the number of cells in a spheroid population and thus there is uncertainty as to how many cells are being added to a reactor when seeding.

Unfortunately, there are some obstacles to making this feasible. When cell isolates are seeded into the reactor they seem to settle to the bottom of the channel rather than adhering to the channel walls. Scaffolds could be produced with an open-cell-foam-like filler in the channels. This filler could potentially provide micro scaffolding that the cells could attach to. The inclusion of various amounts of collagen in the cell suspension used for seeding could also improve this situation.

Different flow patterns in the reactor may help as well. Flow could be reversed sooner so that flow pushes the cells upward in the channels. Similarly, the reactor could be programmed to flow upwards at low rates soon after seeding. These rates would be small enough that cells would not be blown out of their channels.

7.5.2 Counting Spheroids

Seeding cells into the bioreactor requires that the user pipette a certain volume of cell suspension into the reactor well. Since it is impossible to know ahead of time how many cells are being dispensed, the user must check under a microscope to get a feel for how full the scaffold is, then pipette more cells if need be. This guess-and-check method is both time consuming and unreliable. This problem could be resolved if there was a method for estimating the number of spheroids in a given volume.

A quick method that should prove to be helpful in this process is to simply count the number of spheroids in a small sample of medium. This could be done during the three minute centrifuge that occurs just before seeding. During this time, the user could count the number of spheroids, enter that number into a spreadsheet, and read out the proper amount of medium to re-suspend the cells in. There are several reasons why this method will not be exact, but it is far more scientific than the current method.

7.6 Scaffold Materials

A basic requirement of the bioreactor is that the scaffold promotes good cell adhesion. To improve initial cell attachment, the scaffolds are coated with collagen. Collagen deposition can vary dramatically between different materials. For example, silicon surfaces only require 30 minutes for coating, whereas polycarbonate surfaces must coat for 2 hours, and the collagen should be allowed to dry for another 2 hours. Also, polycarbonate scaffolds cannot be autoclaved, and must soak in ethanol for 30 minutes before collagen coating. This can add 4 hours to an experiment. Silicon scaffolds also have disadvantages in that they are brittle and difficult to manufacture.

During the development of this reactor a new method for manufacturing scaffolds was developed. This method has made it possible to manufacture a scaffold using nearly any polymer. New scaffold materials should be tested for collagen absorption and cell adhesion. Some polymer scaffolds, like PEEK, may need to be plasma treated before usage [30].

7.7 Priming the Reactor

If this bioreactor is to become a product, there are different levels of work that can be asked of the user. The user could be responsible for the sterilization, assembly, use, disassembly and storage of the bioreactor, or they could buy a fully assembled,

sterile bioreactor, use it, and throw it away. The later of these two options will result in the sale of more bioreactors and it is easier on the user.

Currently, the bioreactor is not a disposable device that can be shipped fully assembled. There are several steps that have to be taken in order to reach this point. First, the device must be mass produced. Fortunately, the design of the bioreactor, in its simplest terms, is nothing but two plastic plates that sandwich a membrane. These plates could certainly be produced in bulk and a membrane could be bonded between them. Each reactor unit on the plate contains 10 items that must be inserted to complete the reactor assembly. It is also possible that each of these components could be produced in bulk.

The troubles lie in the assembly. The assembly of these 120 reactor components occurs after the device has been primed with fluid. Priming ensures that no bubbles are trapped in the pumping system, and that flow will pass thorough all points in the scaffold. A method for priming a fully assembled bioreactor should be developed.

Secondly, the scaffolds are coated with collagen to promote cell adhesion. This step requires that scaffolds are not inserted into the bioreactor until just before use. Ideally, a scaffold can be developed that either does not need to be coated, or can be coated well in advance. If neither of these options is possible, the scaffold should at least be easy to pop into an assembled system.

7.8 Oxygen Transport

The calculations regarding oxygen transport to the cells all assume that the medium is 100% saturated with oxygen prior to being sent through the scaffold. This may not be a valid assumption. If medium flows across the bottom of the surface

channel when it circulates through the reactor, there may be a concentration gradient from the surface of the reactor to where fluid is flowing through the loop.

Cells in the reactor should be tested so see if they are hypoxic. If they are, the surface channel could be made shallower, requiring that all medium travel close to the surface of the fluid in the reactor. Making this channel shallower does have a drawback, in that there is less flexibility in the total volume of fluid that can be used in the reactor.

8. SUMMARY AND CONCLUSIONS

This thesis focuses on the development of a high throughput bioreactor for culturing liver tissue. A system that mimics the format of a 24 well tissue culture plate was developed. This system integrates 12 separate reactor units, including the scaffold, pump and reservoir, on a single bioreactor plate. Scaffolds are readily interchangeable and several different types of scaffolds have been tested. The pumps are driven pneumatically and are all controlled externally by an electronic/pneumatic controller. Fluidic capacitors are utilized to minimize pulses of flow sent to the cells. The capacitors also help maintain consistent flows when pumping frequencies are tuned for different scaffolds. The operation of the micro-pumps has been modeled and tested. Cells have been successfully cultured in the bioreactor and the liver like functions of the tissue have been examined.

REFERENCES

1. Lu, F.C., *Biotransformation of Toxicants*, in *Basic Toxicology Fundementals, Target Organs and Risk Assessment*. 1996, Taylor and Francis: Washington, DC. p. 27-39.

2. DiMasi, J.A., R.W. Hansen, and H.G. Grabowski, *The price of innovation: new estimates of drug development costs.* J Heath Econ, 2003. **22**(2): p. 151-85.

3. DiMasi, J.A., *Risks in new drug development: approval success rates for investigational drugs.* Clin Pharmocol Ther, 2001. **69**(5): p. 297-307.

4. Lee, W.M., *Drug-induced hepatotoxicity.* N Engl J Med, 1995. **333**(17): p. 1118-27.

5. Lipper, RA, E Pluribus Product: How can we optimize selection of drug development candidates from many compounds at the drug discovery stage? Modern Drug Discovery, 1999. 2(1): p. 55-60.

6. Davila, J.C., et al., *Predictive value of in vitro model systems in toxicology.* Annu Rev Pharmacol Toxicol, 1998. **38**: p. 63-96.

7. Brandon, E..F., et al., *An update on in vitro test methods in human hepatic drug biotransformation research: pros and cons.* Toxicol Appl Pharmacol, 2003. **189**(3): p. 233-46.

8. LeCluyse, E.L., Bullock, P.L., Parkinson, A., and Hochman, J.H., *Cultured Rat Hepatocytes*, in *Models for Assessing Drug Absorption and Metabolism*, P.L.S. Ronald T.Bochardt, Gynn Wilson, Editor. 1996, Plenum Press: New York. p. 121-159.

9. Lecluyse, E.L., Peter L. Bullock, Andrew Parkinson, *Strategies for the restoration and maintenance of normal hepatic structures and function in long term cultures of rat hepatocytes.* Advanced Drug Delivery Reviews, 1996. **22**: p. 133-186.

10. Thohan, S. and G.M. Rosen, *Liver slice technology as an in vitro model for metabolic and toxicity studies.* Methods Mol Biol, 2002. **196**: p. 291-303.

11. Dilworth, C., et al., *The use of liver spheroids as an in vitro model for studying induction of the stress response as a marker of chemical toxicity.* Toxicol In Vitro, 2000. **14**(2): p. 169-76.

12. Cross, D.M. and M.K. Bayliss, *A commentary on the use of hepatocytes in drug metabolism studies during drug discovery and development.* Drug Metab Rev, 2000. **32**(2): p. 219-40.

13. Sivaraman, A, Leach, J.K., Townsend, S, Iida, T., Hogan, B.J., Stolz, D.B., Fry, R., Samson, L.D., Tannenbaum, S.R., Griffith, L.G., *A Microscale In Vitro Physiological*

Model of the Liver: Predictive Screens for Drug Metabolism and Enzyme Induction. Curr Drug Metab, 2005 Dec; **6**(6): p. 569-91.

14. Arias, I.M., J.L. Boyer, et al., *The Liver: Biology and Pathology.* 2001, New York: Lippincott.

15. Stamatoglou SC, Hughes RC., *Cell adhesion molecules in liver function and pattern formation.* FASEB J. 1994 Apr 1; **8**(6):420-7. Review.

16. Griffith L.G., Lopina S., *Microdistribution of substratum-bound ligands affects cell function: hepatocyte spreading on PEO-tethered galactose.* Biomaterials. 1998 Jun; **19**(11-12):979-86.

17. Guengerich, F.P. *Mammalian Cytochrome P450.* 1987, Boca Raton, Florida: CRC Press.

18. Waterman, E.R., and Johnson, E.F., *Cytochrome P450: Methods in Enzymology.* Vol. 206. 1991, New York: Academic Press.

19. Sivaraman, A., *A microfabricated 3D tissue engineered "Liver on a Chip": High information content assays for in vitro drug metabolism studies.* Ph.D. Thesis, Chemical Engineering. 2004 Massachusetts Institute of Technology.

20. Powers, M.J., Domansky, K., Kaazempur-Mofrad, M.R., Kalezi, A., Capitano, A., Upadhyaya, A., Kurzawski, P., Wack, K.E., Stolz, D.B., Kamm, R., Griffith, L.G., *A Microfabricated Array Bioreactor for Perfused 3D Liver Culture.* Biotechnol Bioeng. 2002 May 5; **78**(3): p. 257-69.

21. Powers, M.J., Janigan, D.M., Wack, K.E., Baker, C.S., Stolz, D.B., Griffith, L.G., *Functional Behavior of Primary Rat Liver Cells in a Three-Dimensional Perfused Microarray Bioreactor.* Tissue Eng. 2002. **8**(3): p. 499-513.

22. Domansky, K., Sivaraman, A., Griffith, L.G., *Micromachined bioreactor for in vitro cell self-assembly and 3D tissue formation*, in *Lab-on-Chips for Cellomics: Micro and Nanotechnologies for Life Science*, H. Anderson, and Van Den Berg, A., Editor. in press, Kluwer Academic Publishers.

23. Domansky, K., Inman, W., Serdy, J., Griffith, L.G., *Perfused Microreactors for Liver Tissue Engineering*, Proceedings of the 27th International Conference of the IEEE-EMBS, Shanghai, September 1 - 4, 2005.

24. Astle, T.W., *Microplate Standardization.* Molecules. 1996. **1**; p. 106-113.

25. Tilles AW, Baskaran H, Roy P, Yarmush ML, Toner M., *Effects of oxygenation and flow on the viability and function of rat hepatocytes cocultured in a microchannel flat-plate bioreactor.* Biotechnol Bioeng. 2001 Jun 5; **73**(5): p. 379-89.

26. Papadaki M, Eskin SG., *Effects of fluid shear stress on gene regulation of vascular cells*. Biotechnol Prog. 1997 May-Jun;13(3): p. 209-21.

27. Hoen PAC't, Bijsterboschbosch, M.K., Van Berkel, T.J.C., Vermeulen, N.P.E., Commandeur, J.N.M., *Midazolam Is a Phenobarbital-Like Cytochrome P450 Inducer in Rats*. The Journal of Pharmacology and Experimental Therapeutics. 2001. **299**(3). p. 921-927.

28. Powers, M.J., Griffith-Cima, L., *Motility Behavior of Hepatocytes on Extracellular Matrix Substrata During Aggregation*. Biotechnol Bioeng. 1996 October 15; **50**: p. 392-403.

29. Semler EJ, Ranucci CS, Moghe PV., *Mechanochemical manipulation of hepatocyte aggregation can selectively induce or repress liver-specific function*. Biotechnol Bioeng. 2000 Aug 20; **69**(4): p. 359-69.

30. Briem, D., Strametz, S., Schroder, K., Meenen, N.M., Lehmann, W., Linhart, W., Ohl, A., Rueger, J.M., *Response of primary fibroblasts and osteoblasts to plasma treated polyetheretherketone (PEEK) surfaces.* Journal of Materials Science: Materials in Medicine 2005. **16**: p. 671-677.

APPENDIX

A1 Dimensioned Drawings for the Bioreactor

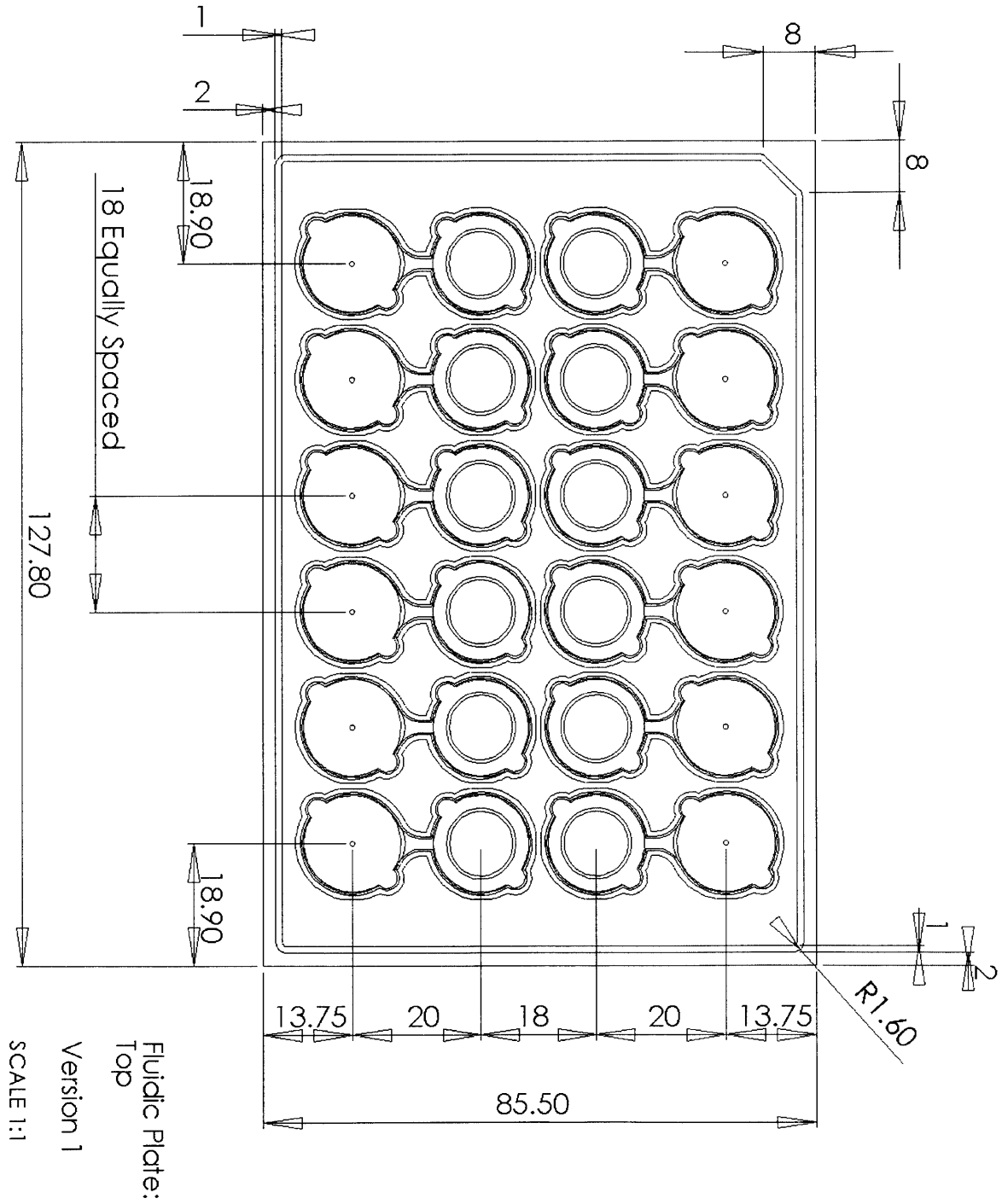

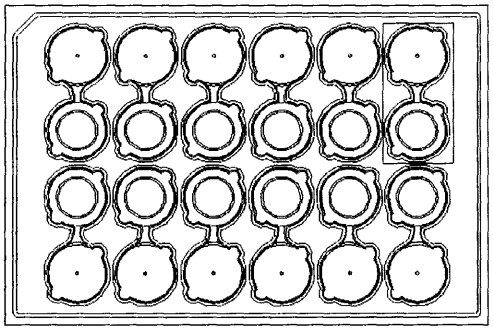

A

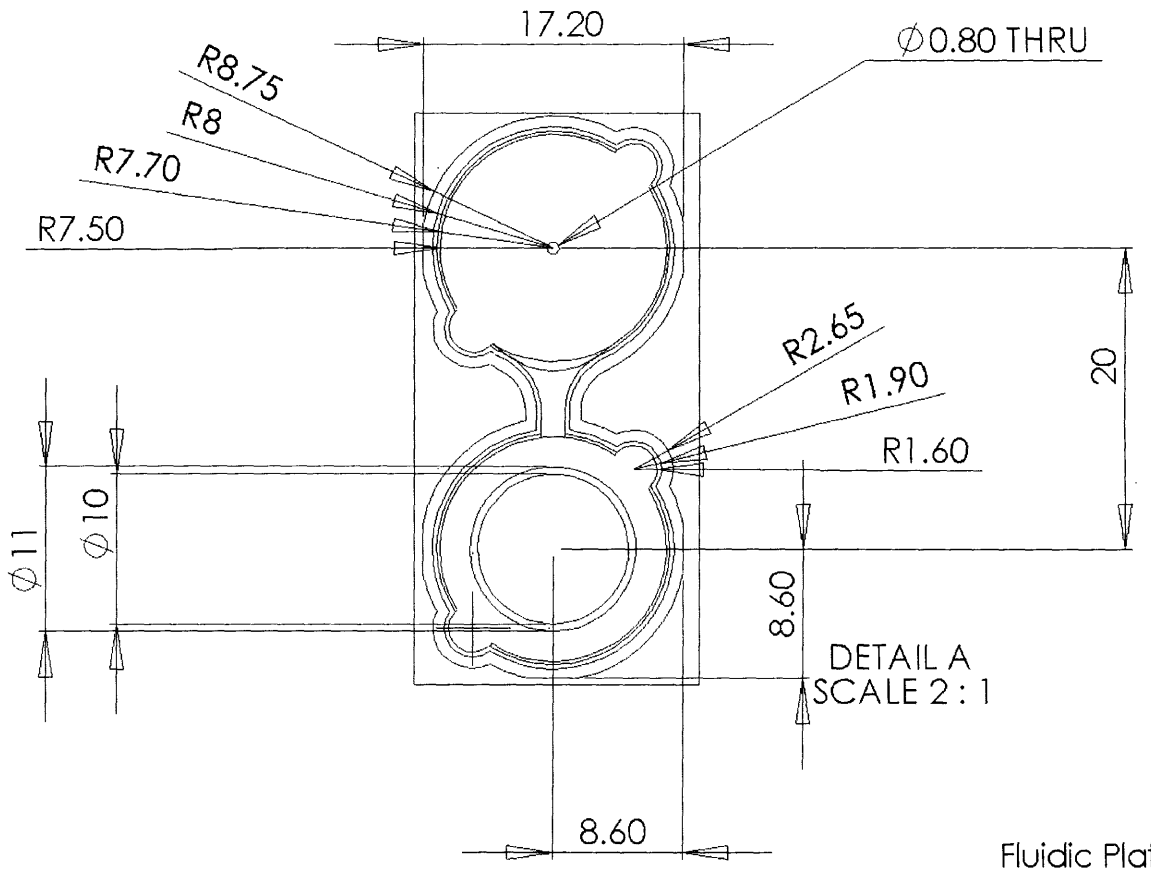

Fluidic Plate:
Reactor Unit

Version 1

SCALE 1:2

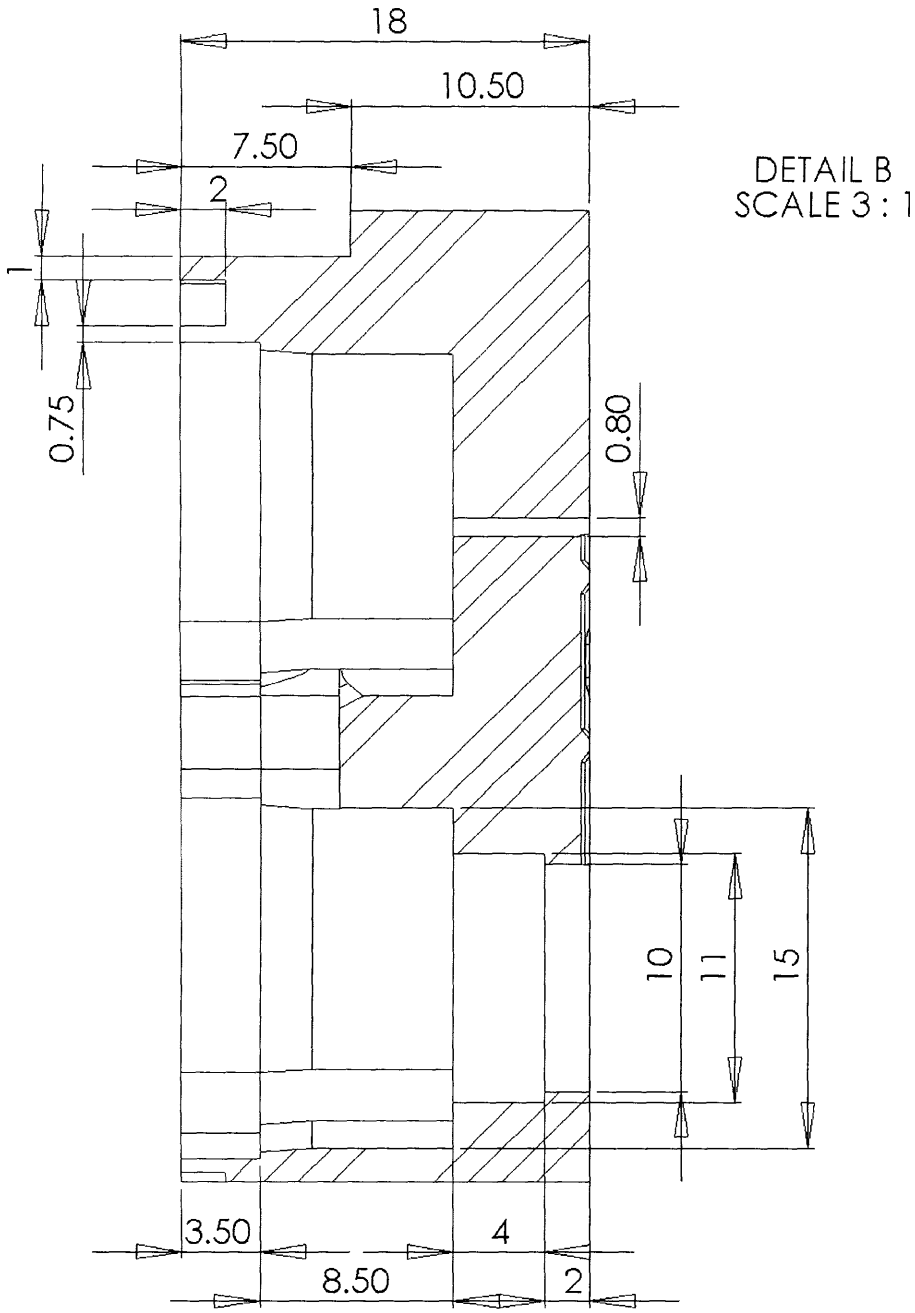

DETAIL B
SCALE 3 : 1

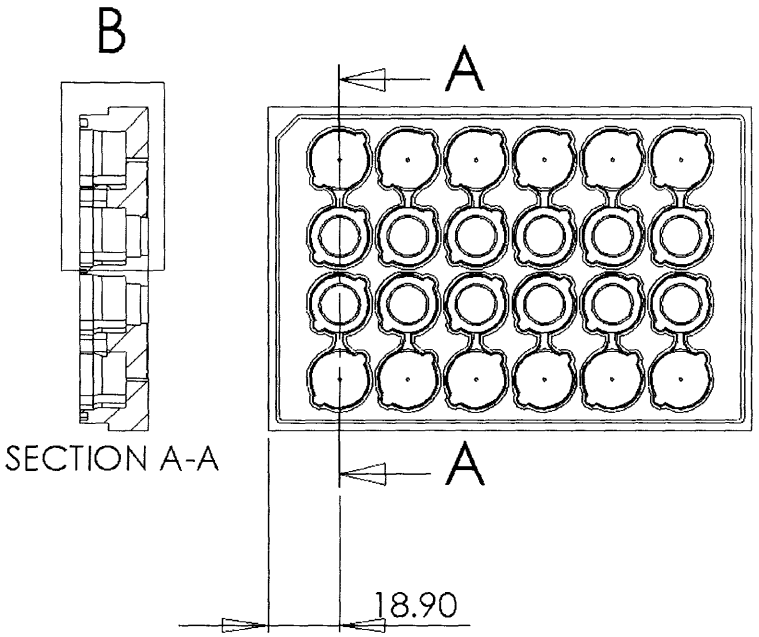

SECTION A-A

130

Fluidic Plate:
Cross-Section - Reactor Unit

Version 1

SCALE 1:2

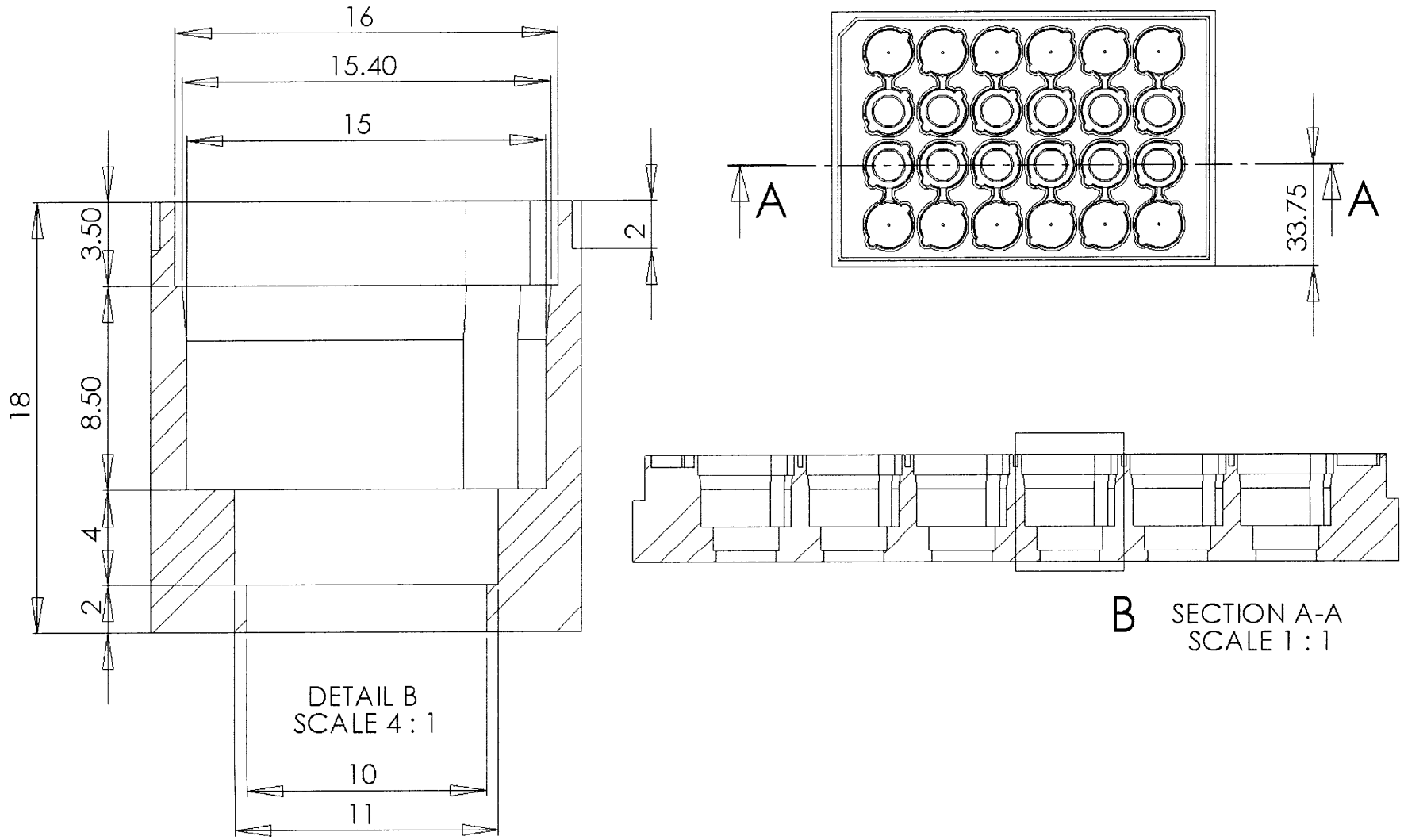

Fluidic Plate:
Cross-Section - Reactor

Version 1

SCALE 1:2

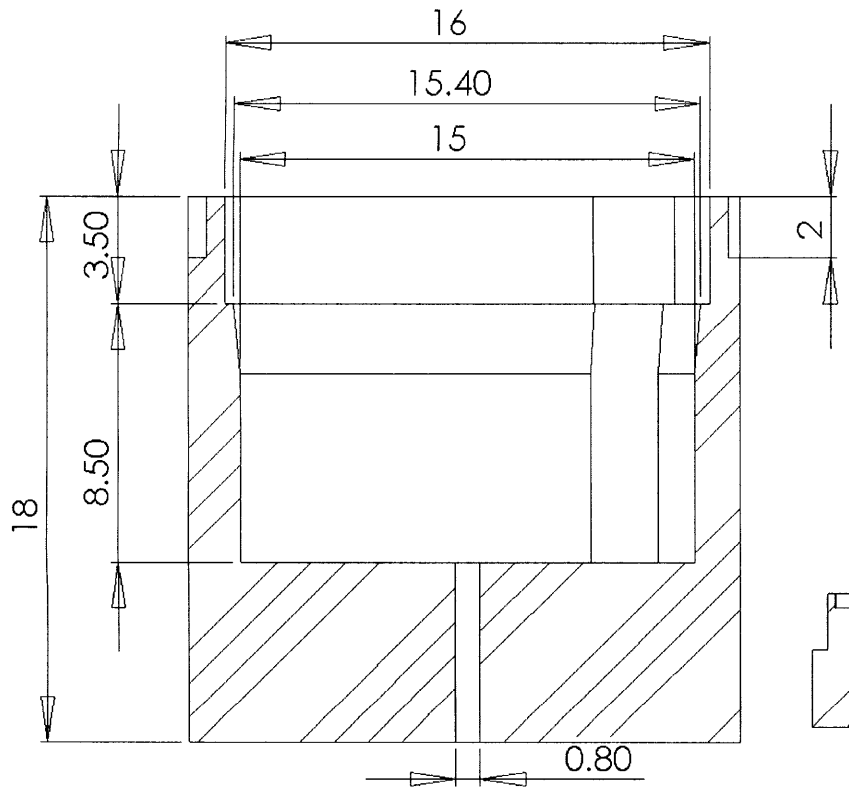

DETAIL B
SCALE 4 : 1

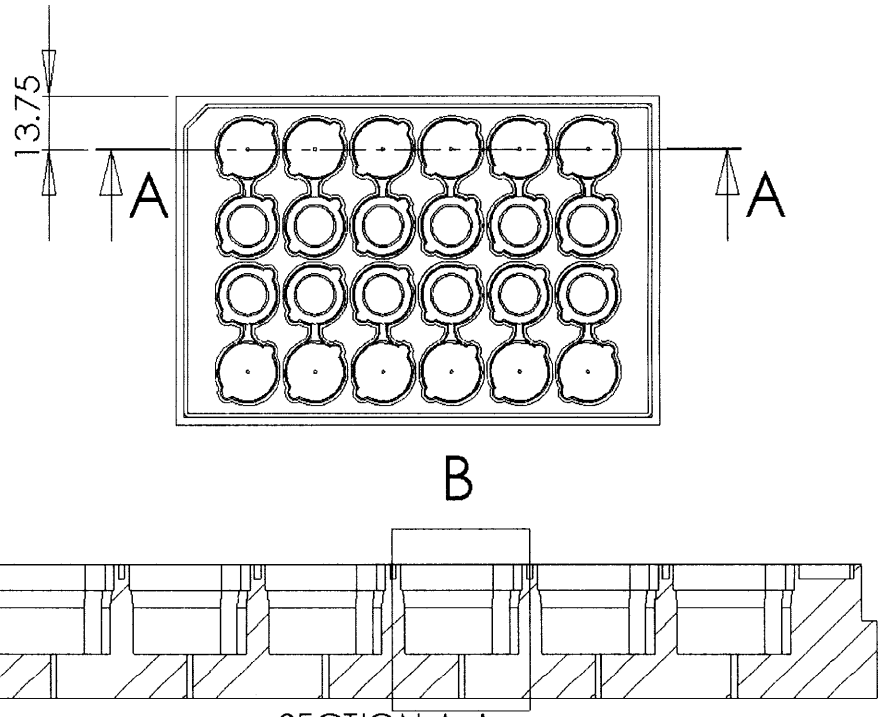

SECTION A-A
SCALE 1 : 1

Fluidic Plate:
Cross-Section: Reservoir

Version 1

SCALE 1:2

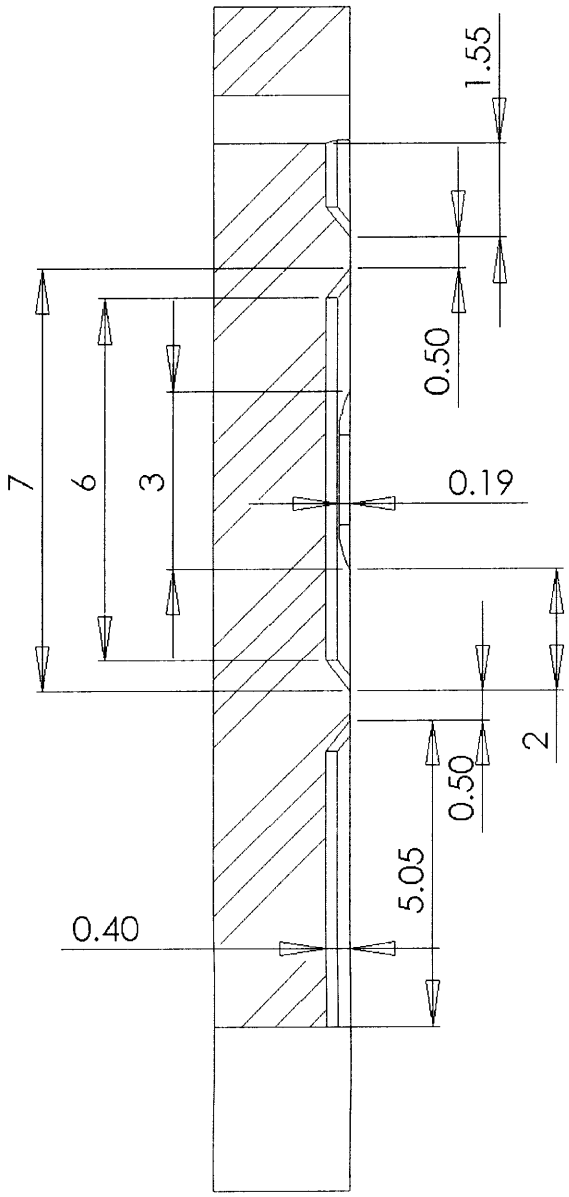

DETAIL C
SCALE 8 : 1

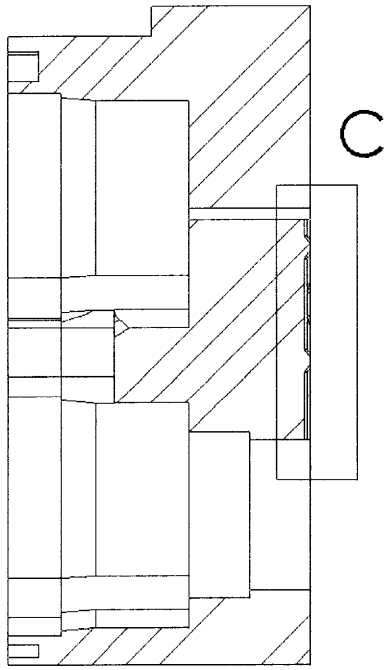

DETAIL B
SCALE 2 : 1

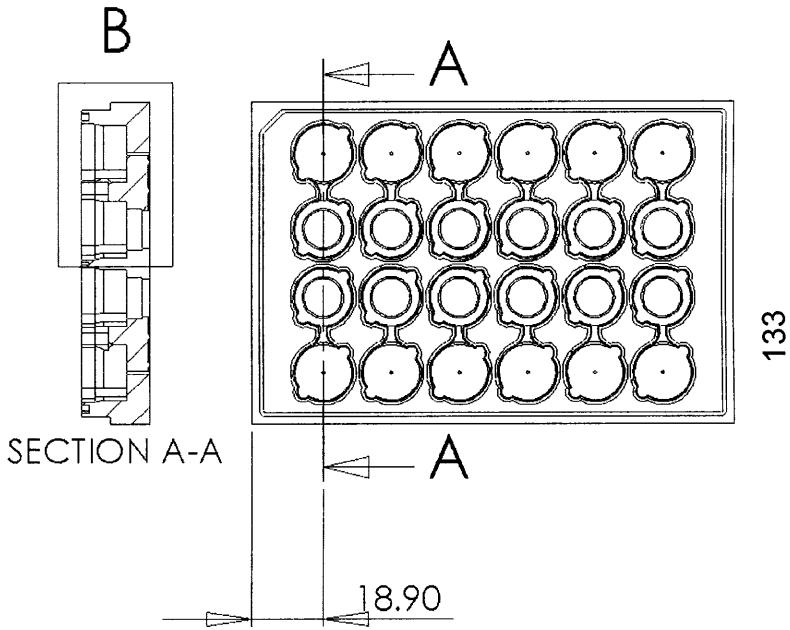

SECTION A-A

Fluidic Plate:
Cross-Section - Channel Zoom

Version 1

SCALE 1:2

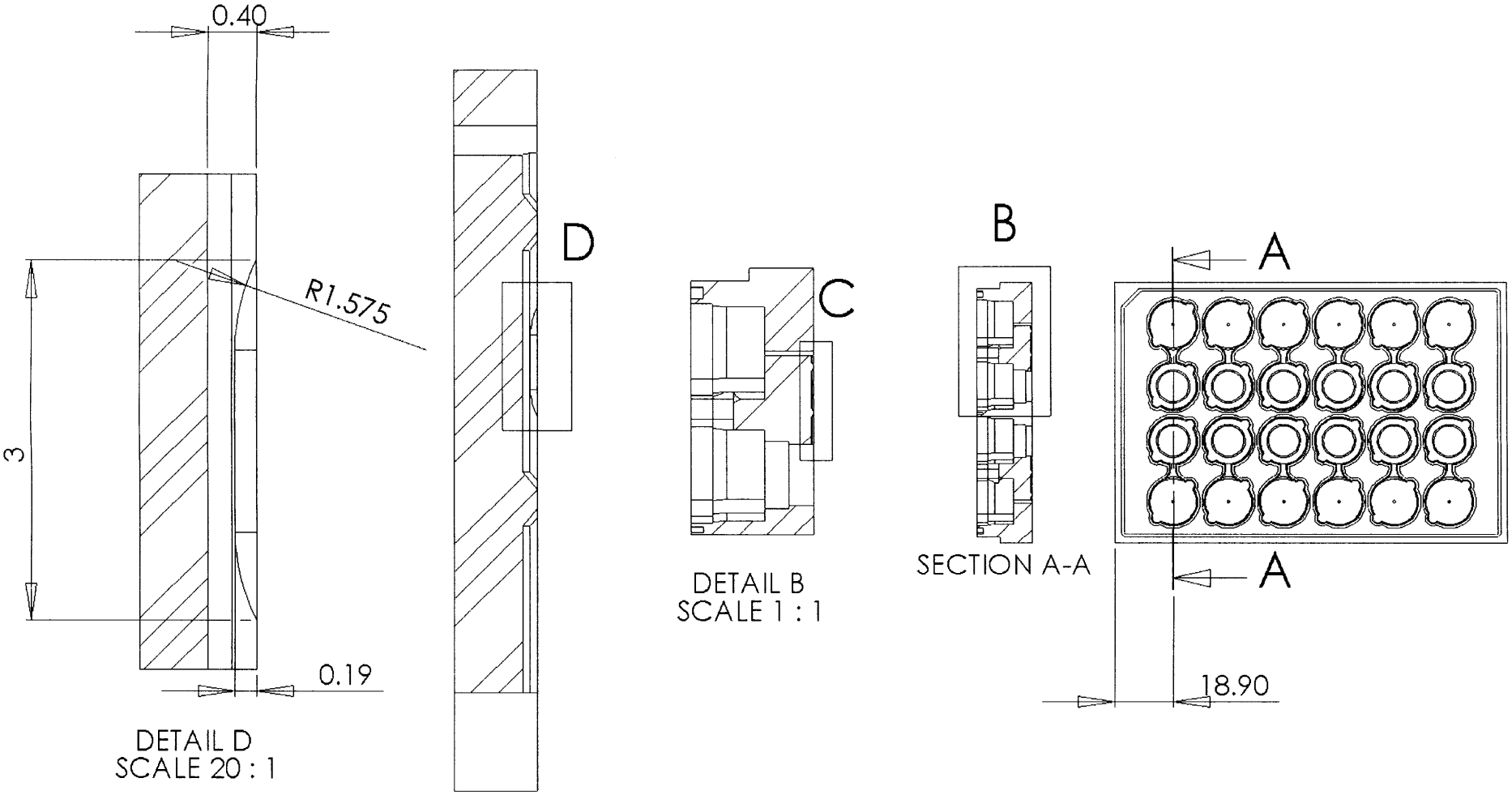

DETAIL D
SCALE 20 : 1

DETAIL C
SCALE 6 : 1

DETAIL B
SCALE 1 : 1

SECTION A-A

Fluidic Plate:
Cross-Section - Channel Zoom - 2

Version 1

SCALE 1:2

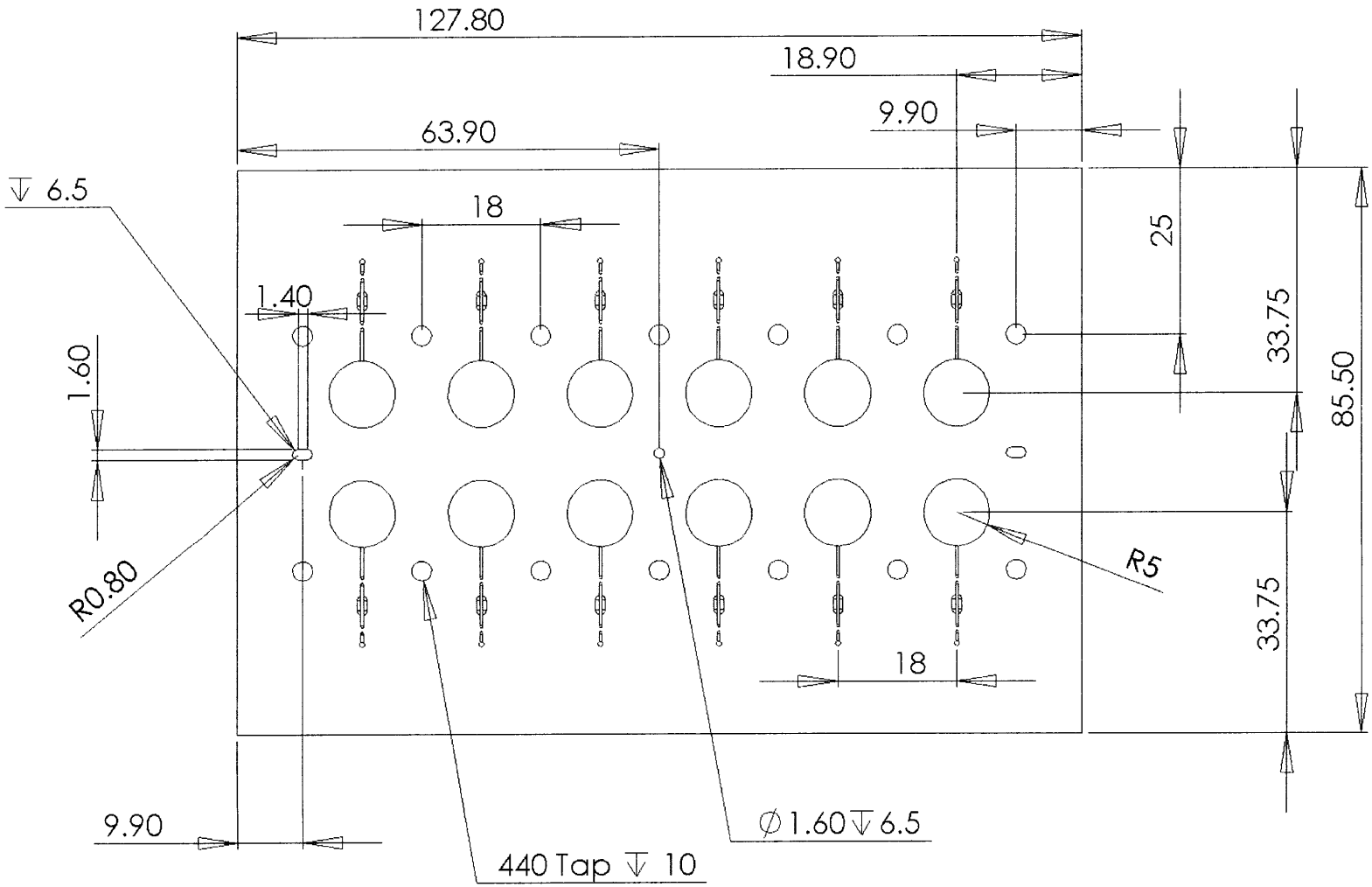

Fluidic Plate:
Bottom

Version 1

SCALE 1:1

A

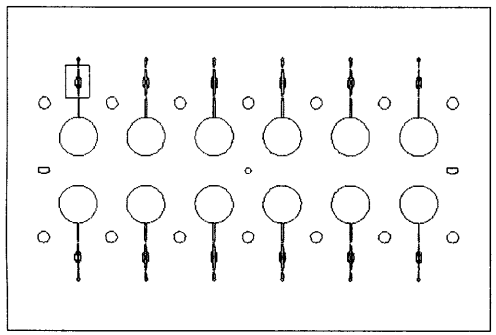

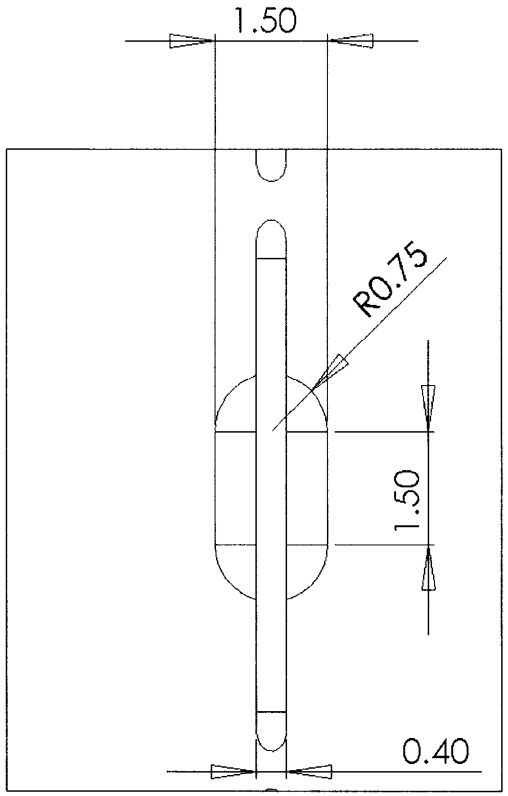

DETAIL A
SCALE 10 : 1

Fluidic Plate:
Bottom - Pumping Chamber

Version 1

SCALE 1:2

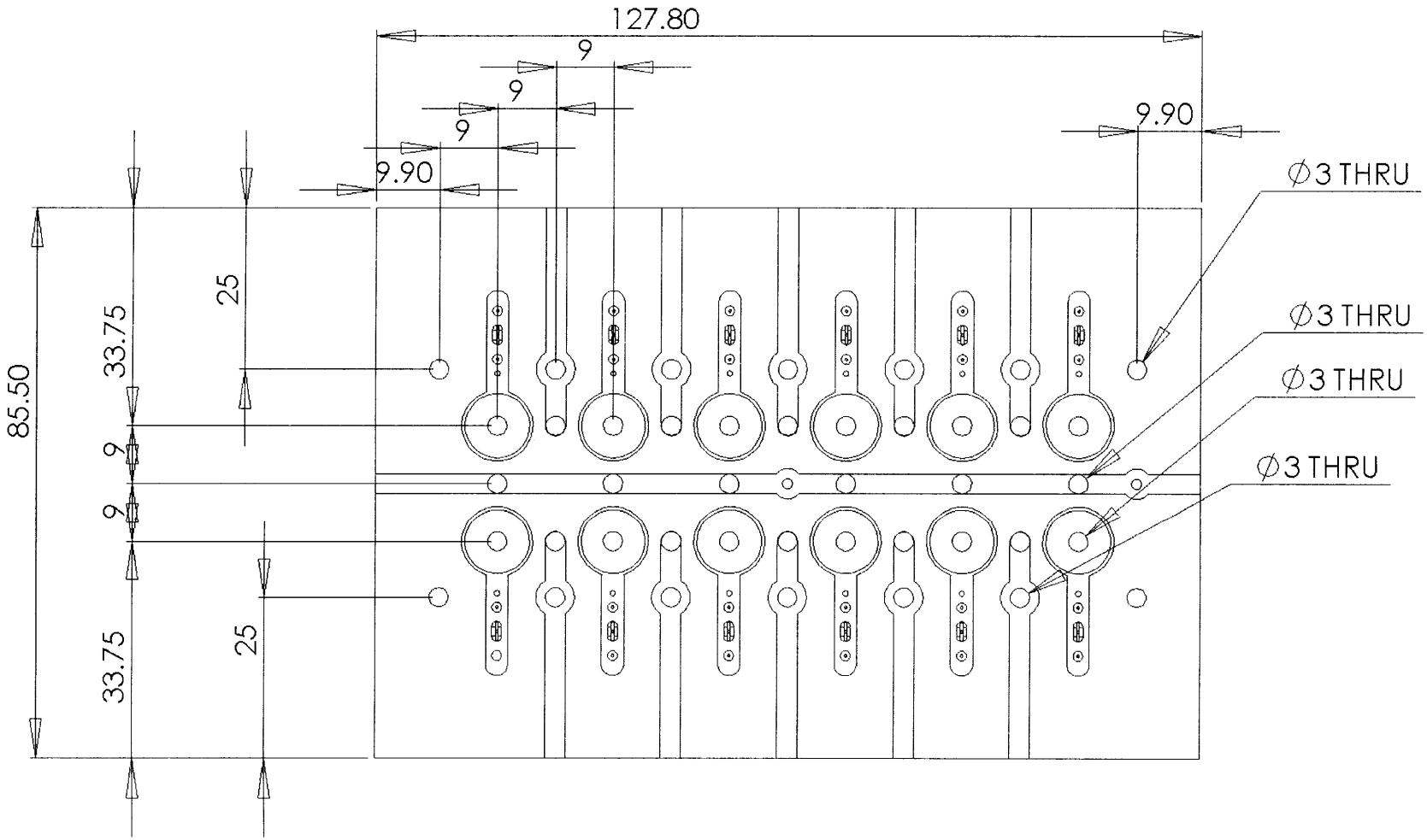

Pneumatic Plate:
Top - Holes

Version 1

SCALE 1:1

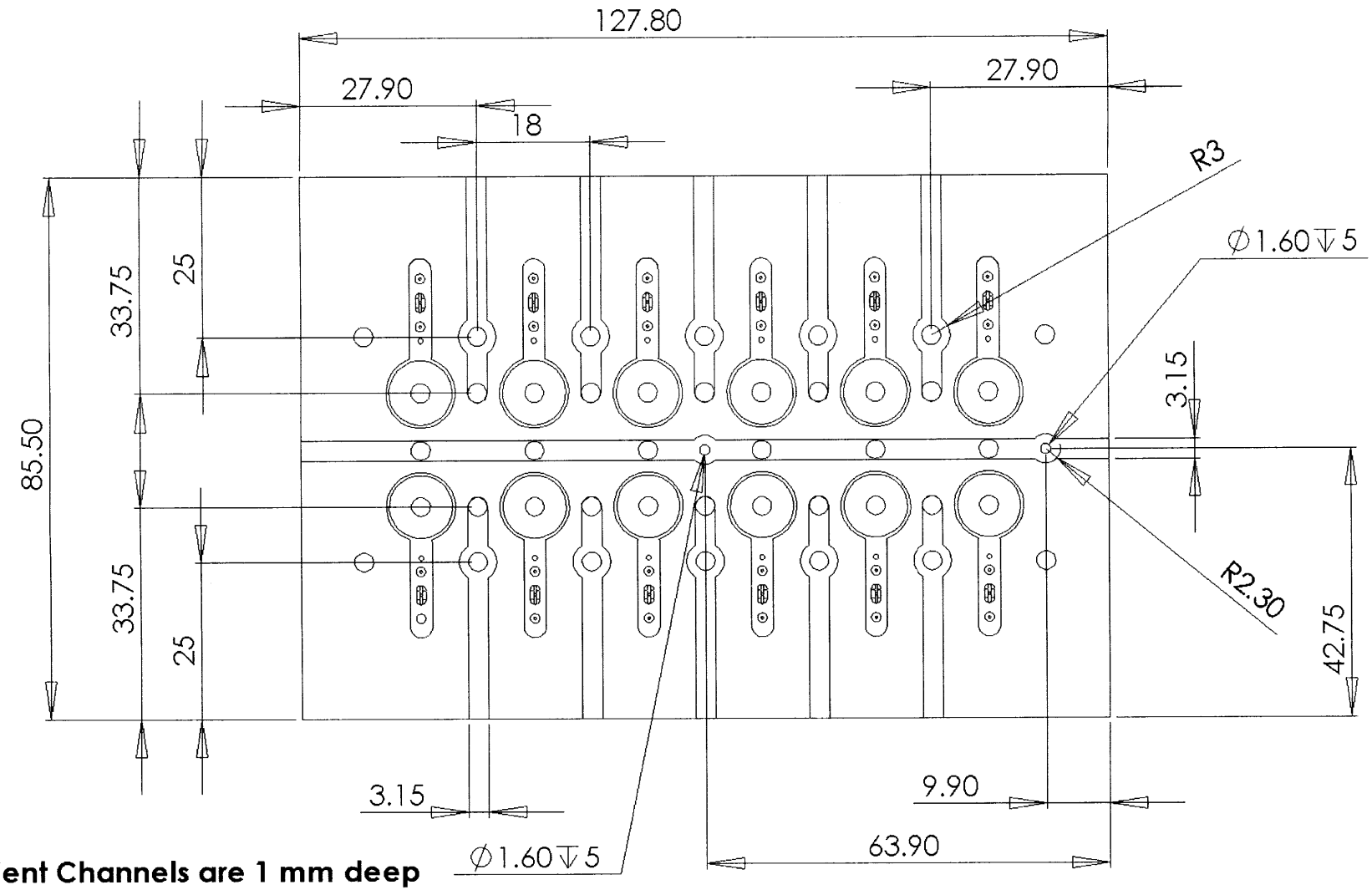

All Vent Channels are 1 mm deep

Pneumatic Plate:
Vent Channels

Version 1

SCALE 1:1

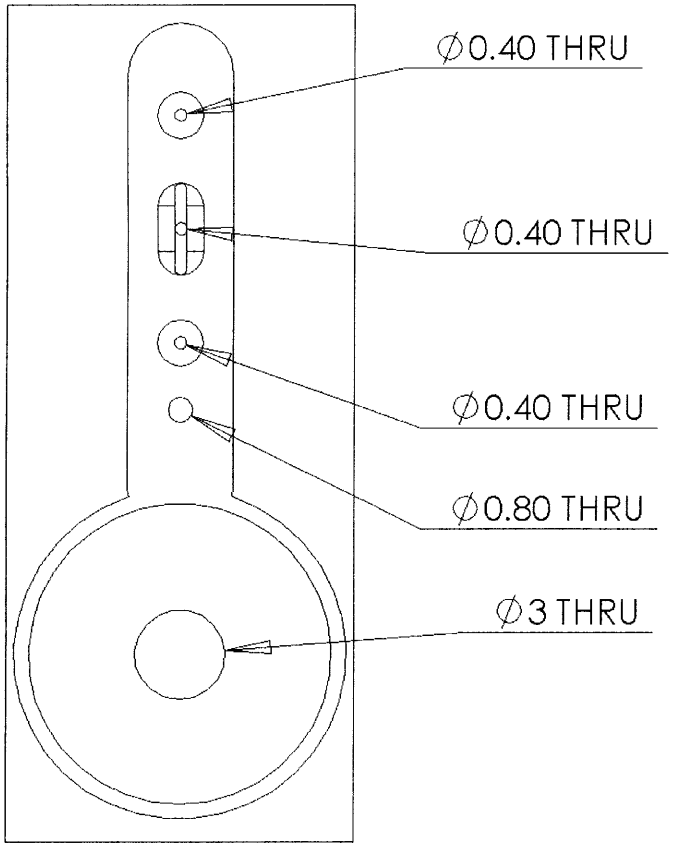

DETAIL A
SCALE 4 : 1

A

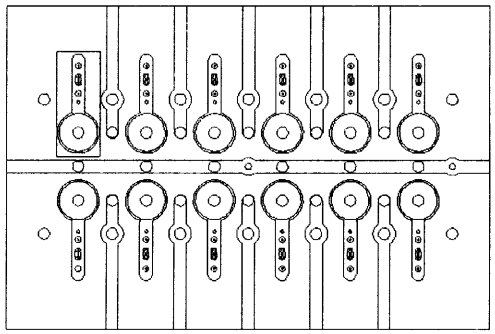

Pneumatic Plate
Pumping Island - Hole Locations

Version 1

SCALE 1:2

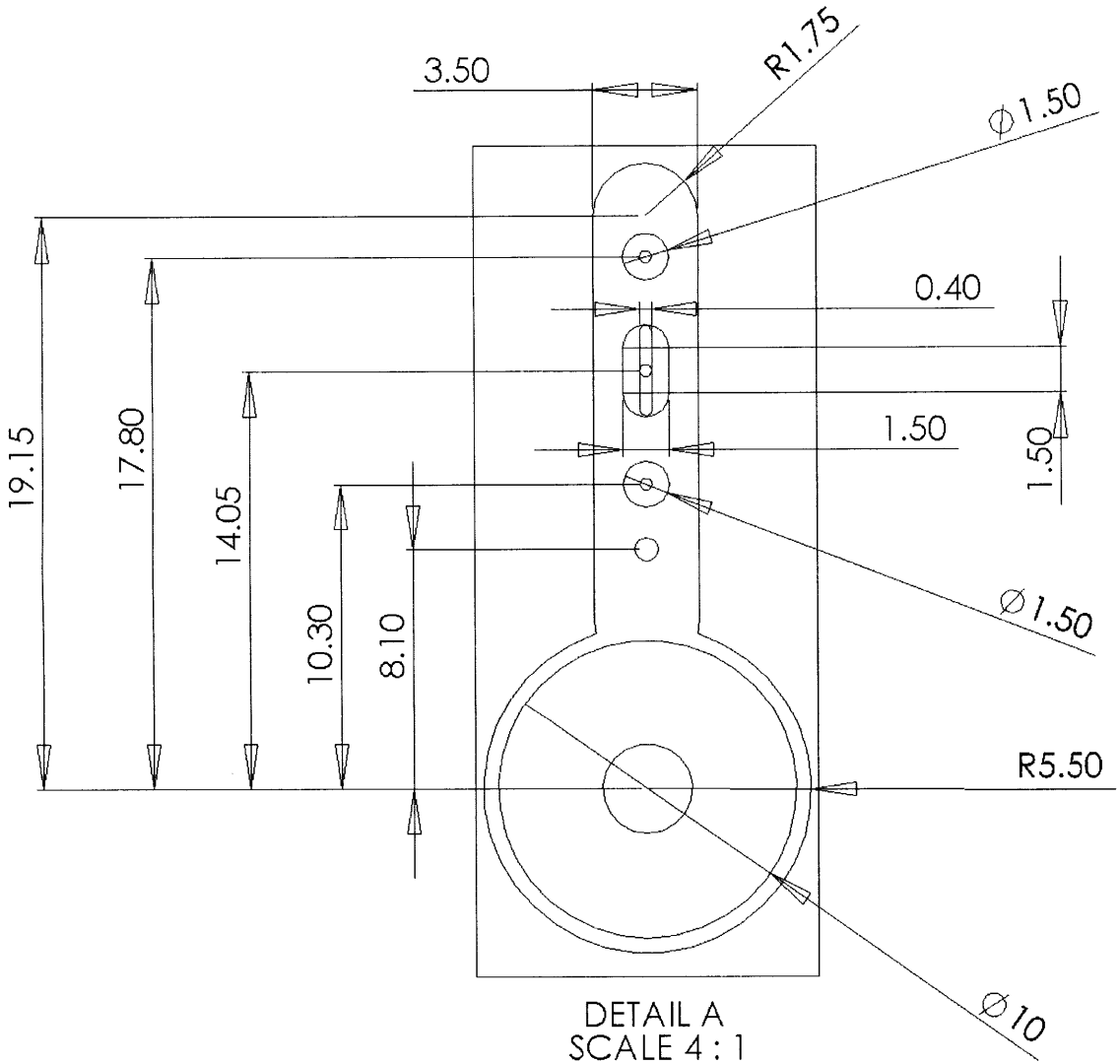

DETAIL A
SCALE 4 : 1

A

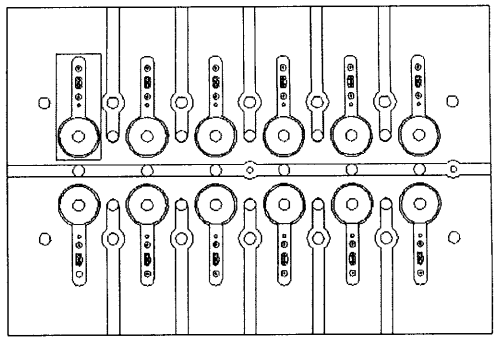

Pneumatic Plate
Pumping Island - Pump Positions

Version 1

SCALE 1:2

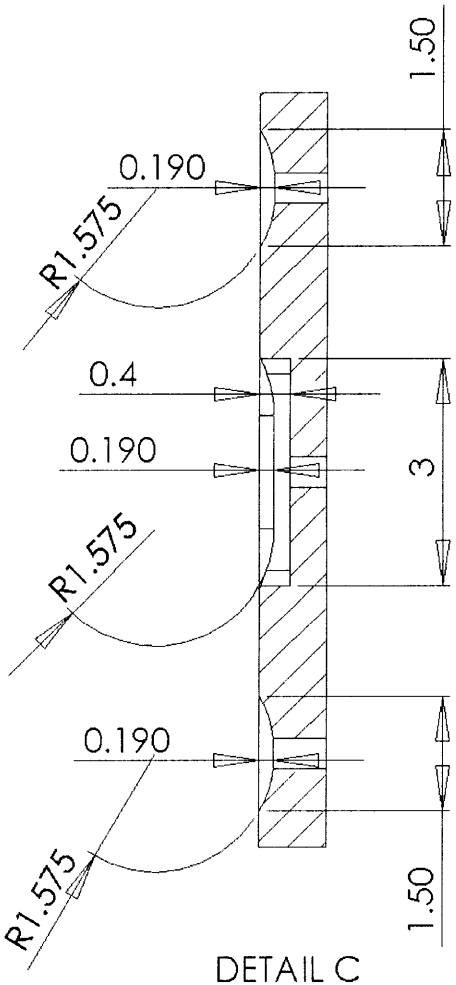

DETAIL C
SCALE 10 : 1

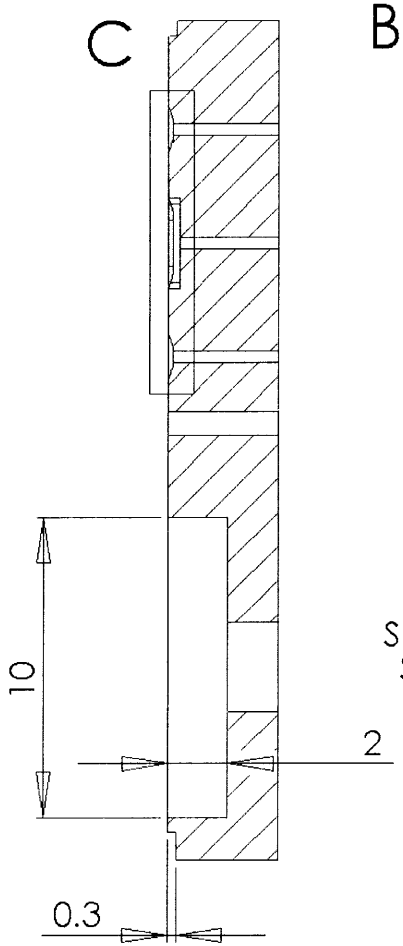

DETAIL B
SCALE 4 : 1

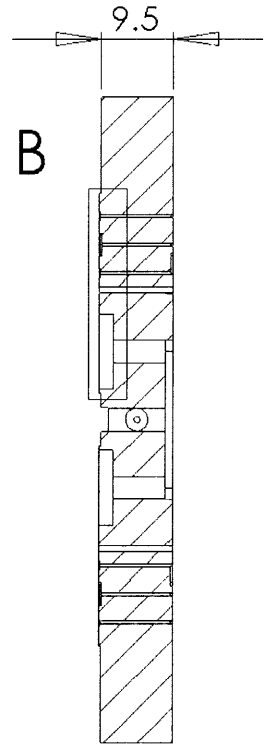

SECTION A-A
SCALE 2 : 1

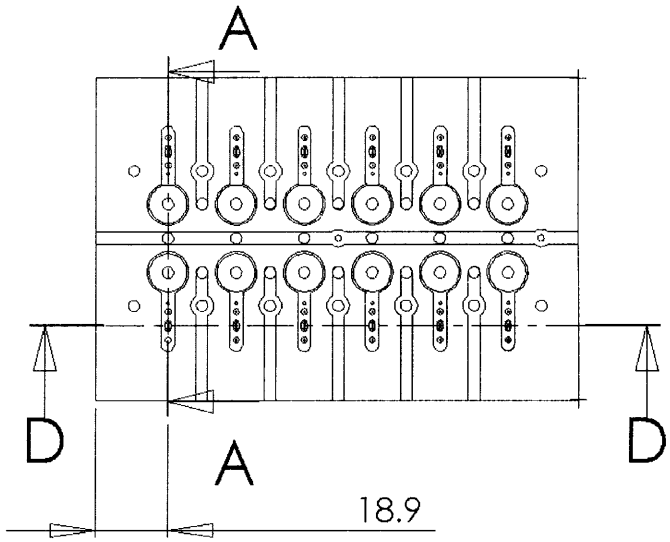

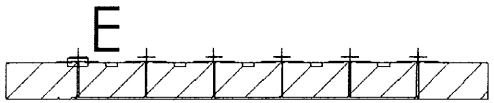

SECTION D-D

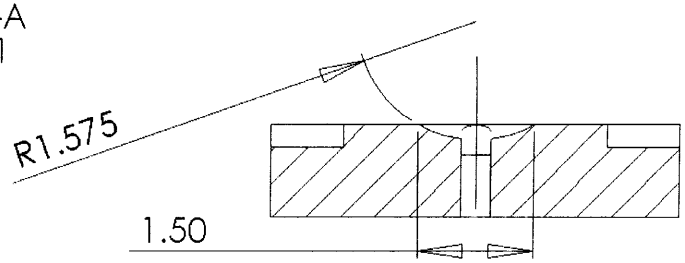

DETAIL E
SCALE 10 : 1

Pneumatic Plate:
Cross-Section - Zoom

Version 1

SCALE 1:2

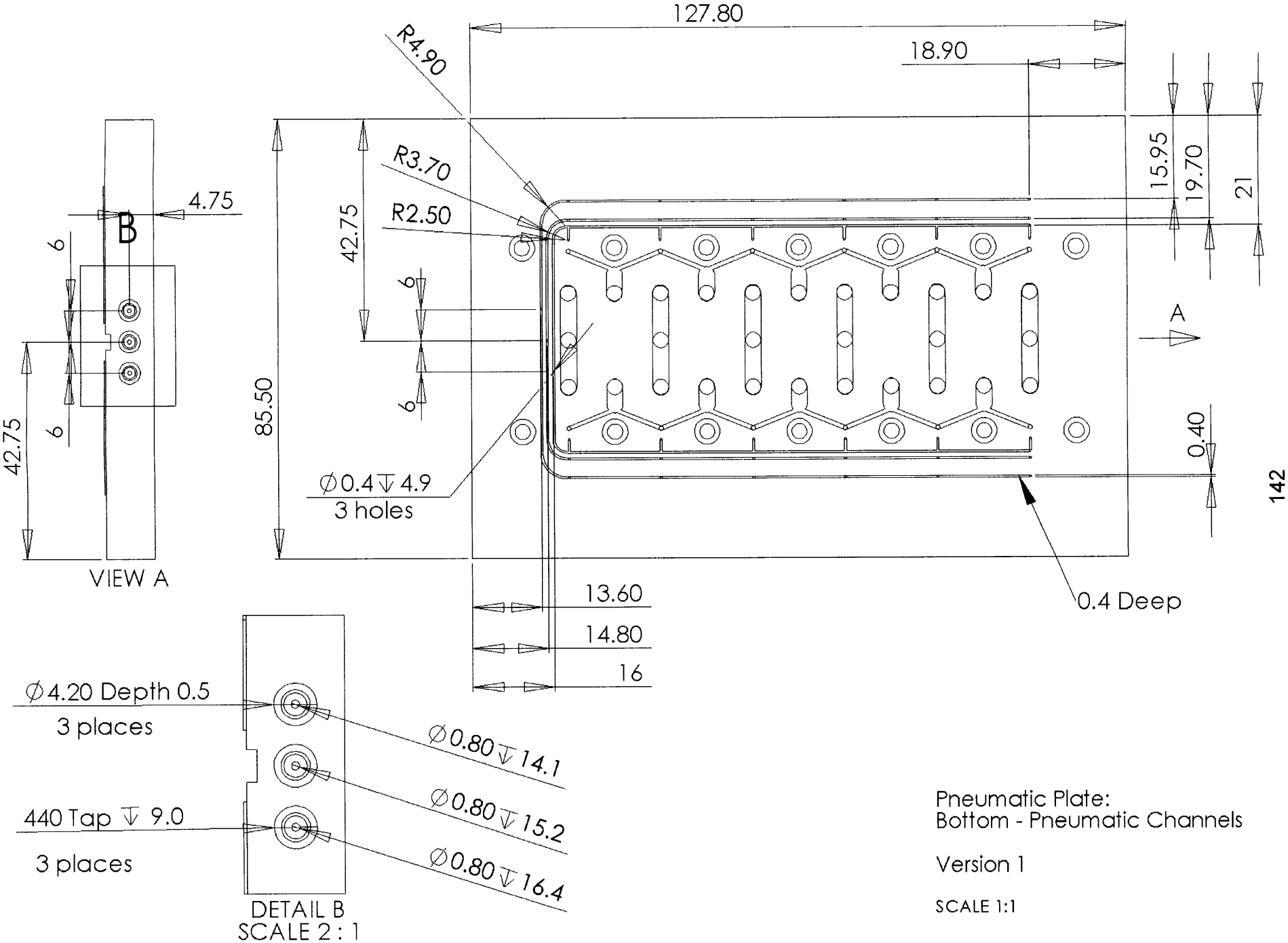

Pneumatic Plate:
Bottom - Pneumatic Channels

Version 1

SCALE 1:1

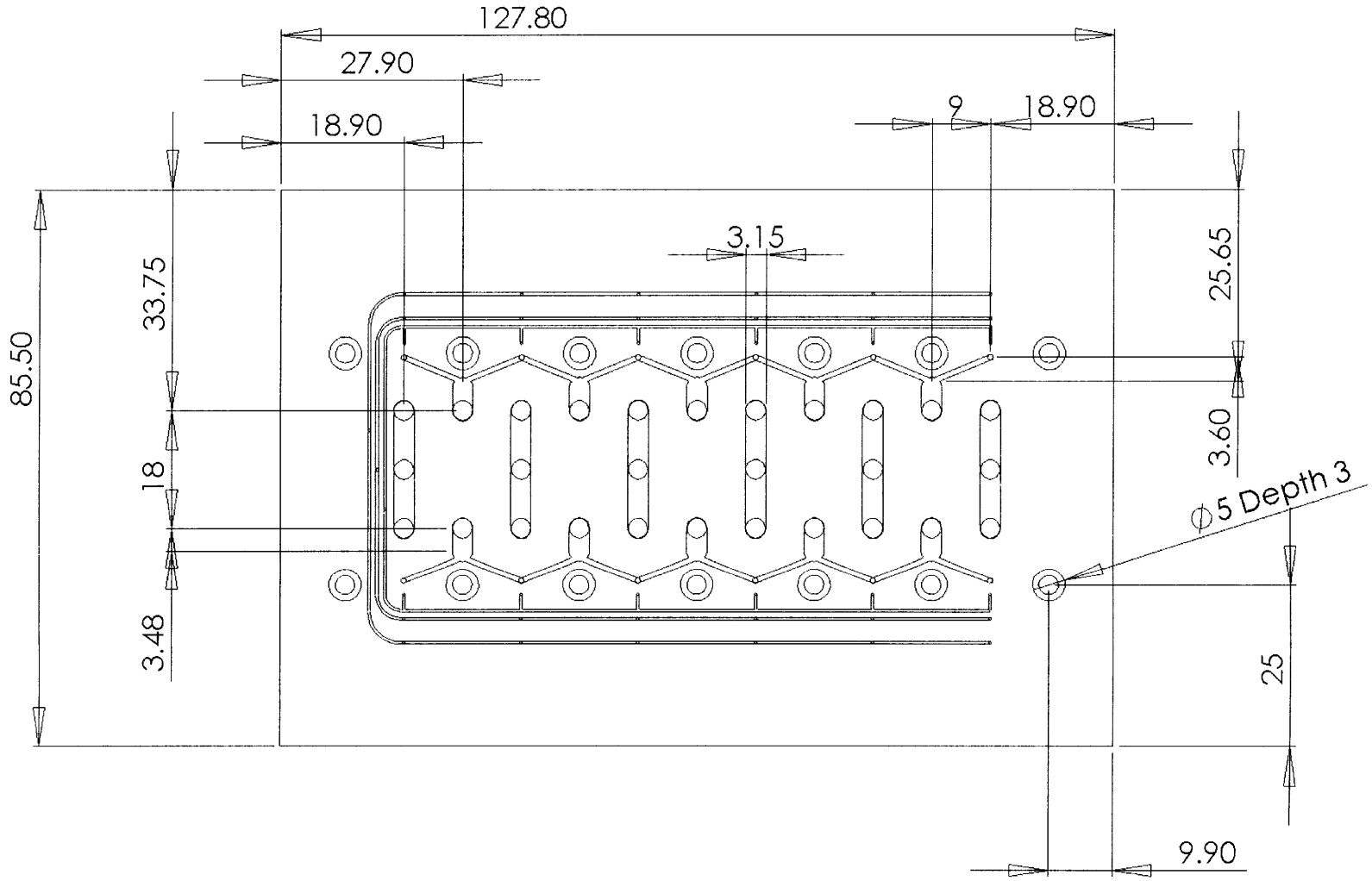

Pneumatic Plate:
Bottom - Vent Channels

Version 1

SCALE 1:1

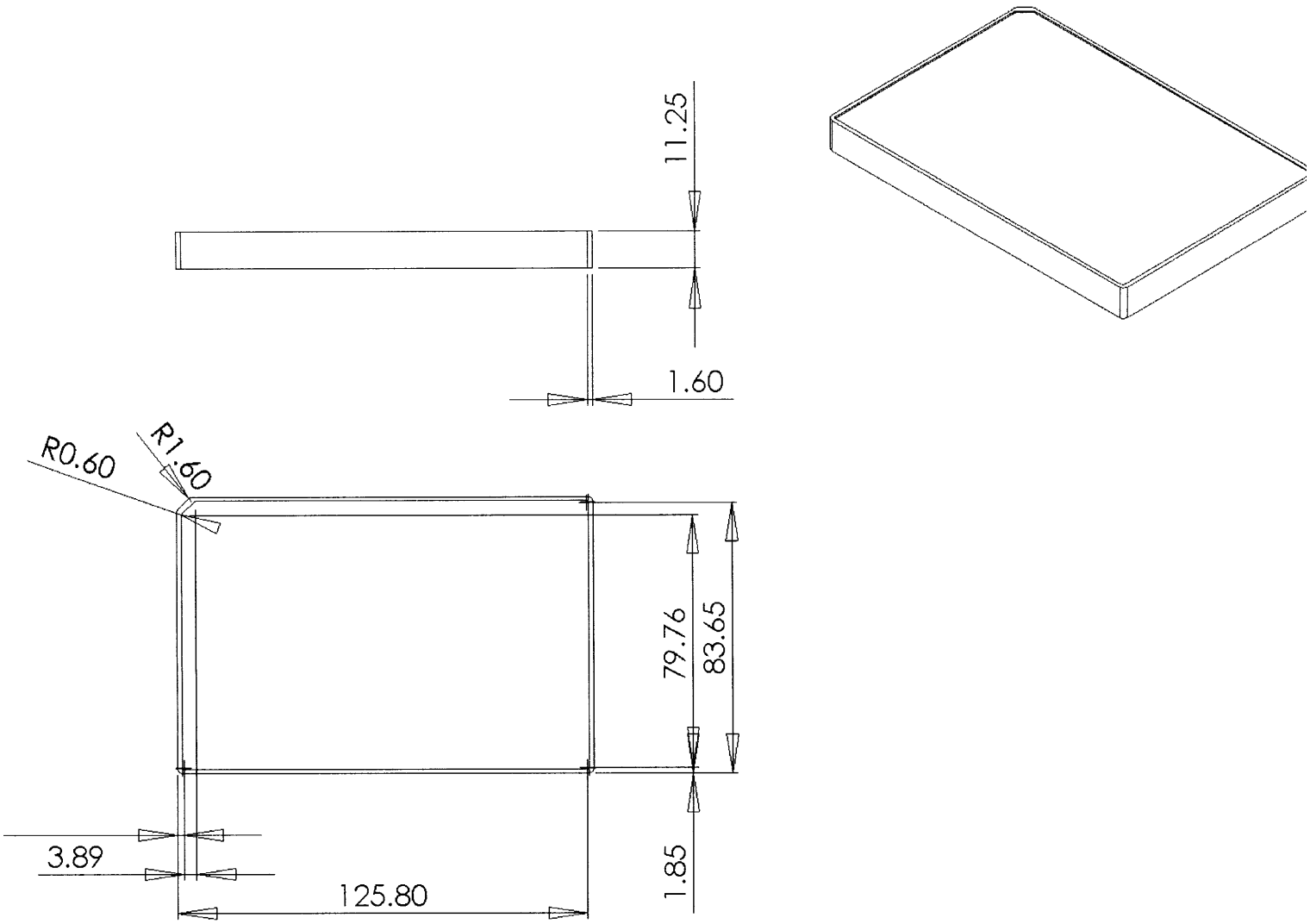

Lid

Version 1

SCALE 1:2

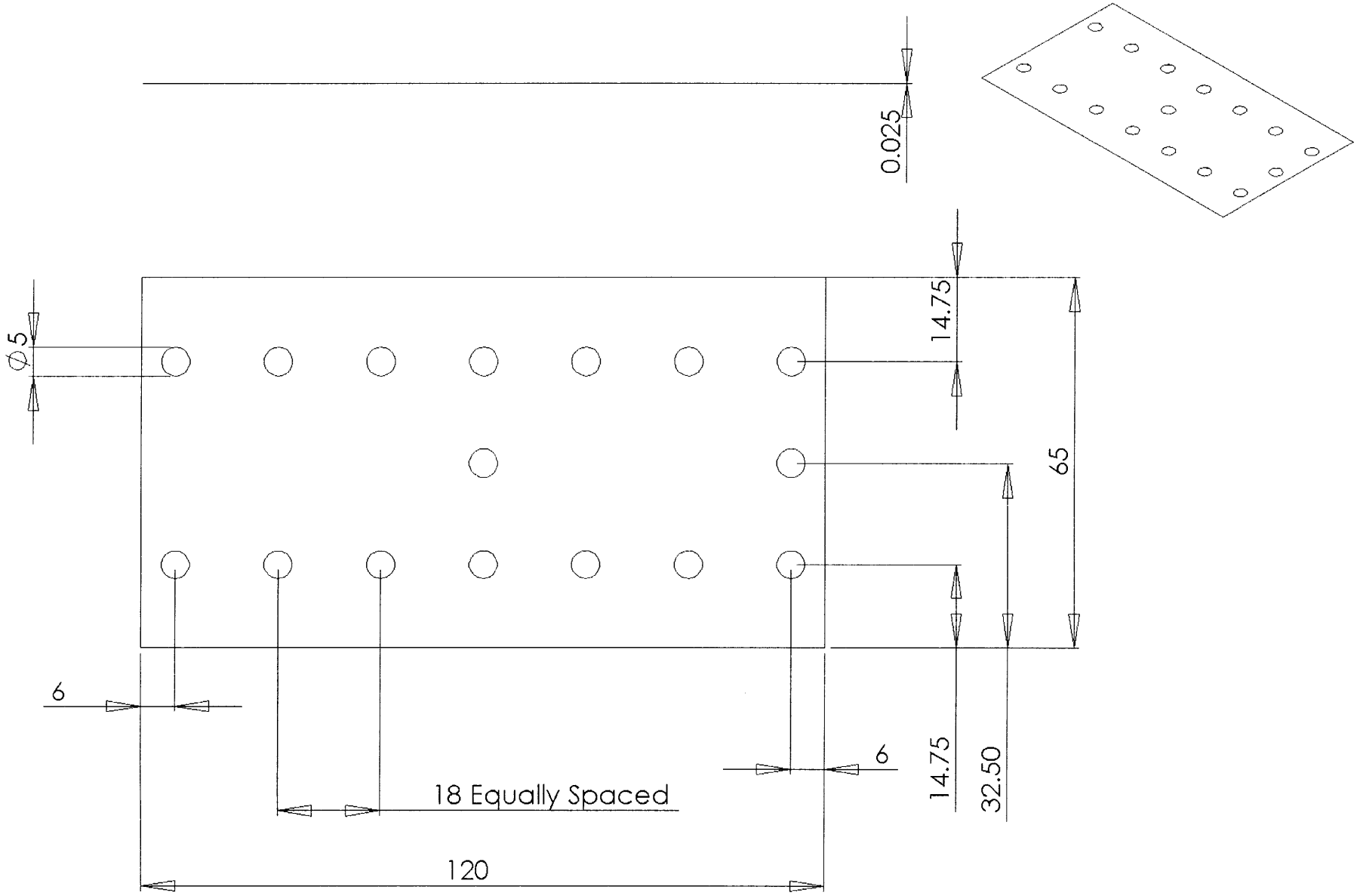

Membrane

Version 1

SCALE 1:1

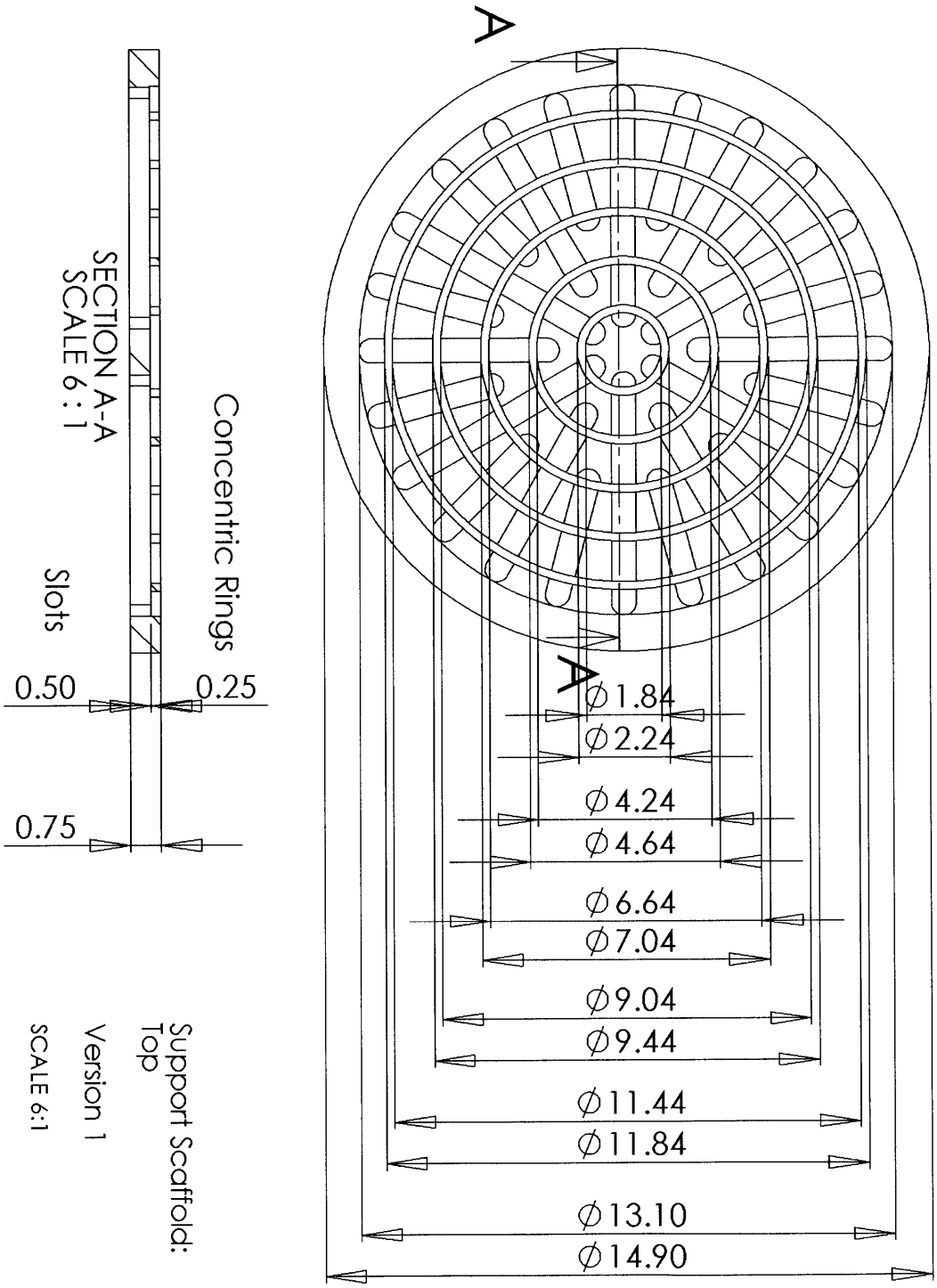
A
A
Ø1.84
Ø2.24
Ø4.24
Ø4.64
Ø6.64
Ø7.04
Ø9.04
Ø9.44
Ø11.44
Ø11.84
Ø13.10
Ø14.90
SECTION A-A
SCALE 6 : 1
Concentric Rings
Slots
0.50
0.25
0.75
Support Scaffold:
Top
Version 1
SCALE 6:1

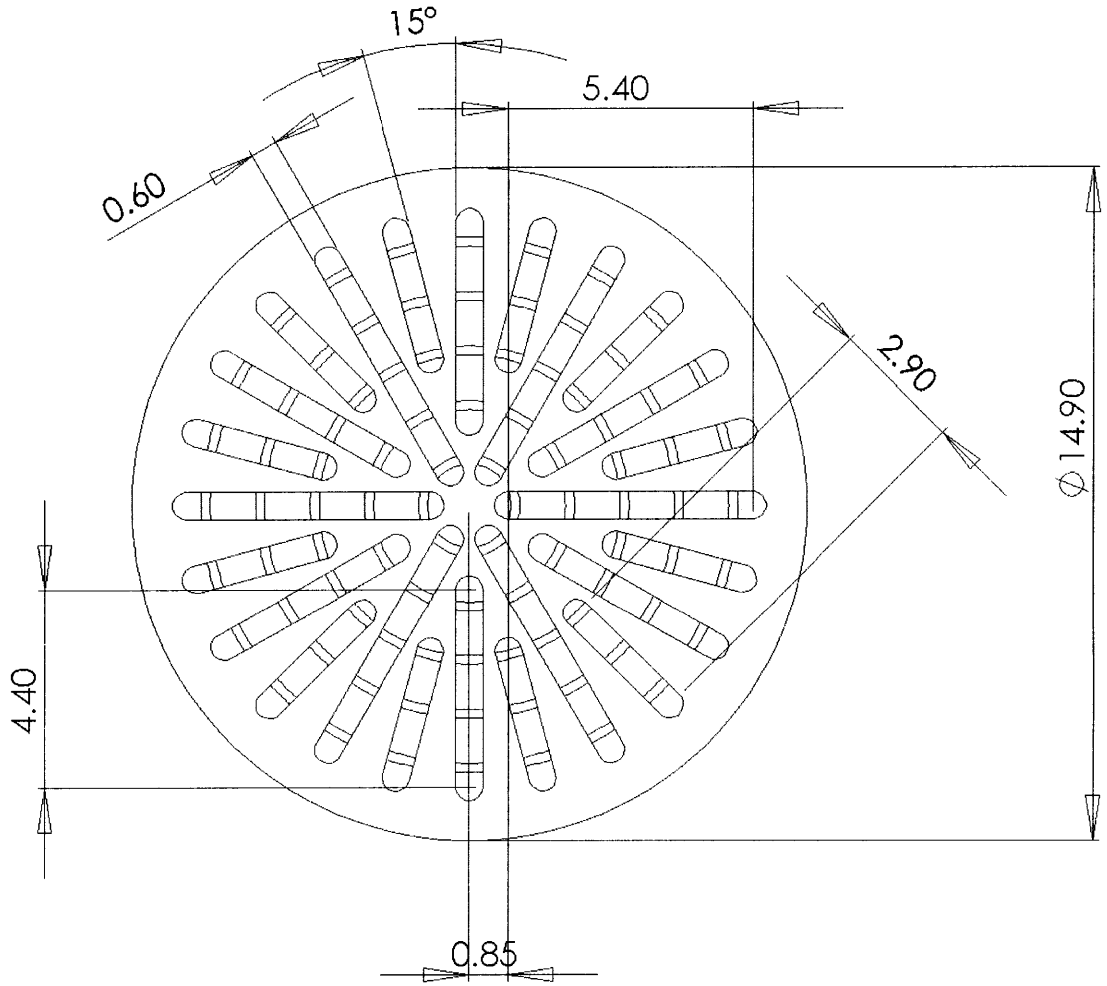

Support Scaffold:
Bottom

Version 1

SCALE 6:1

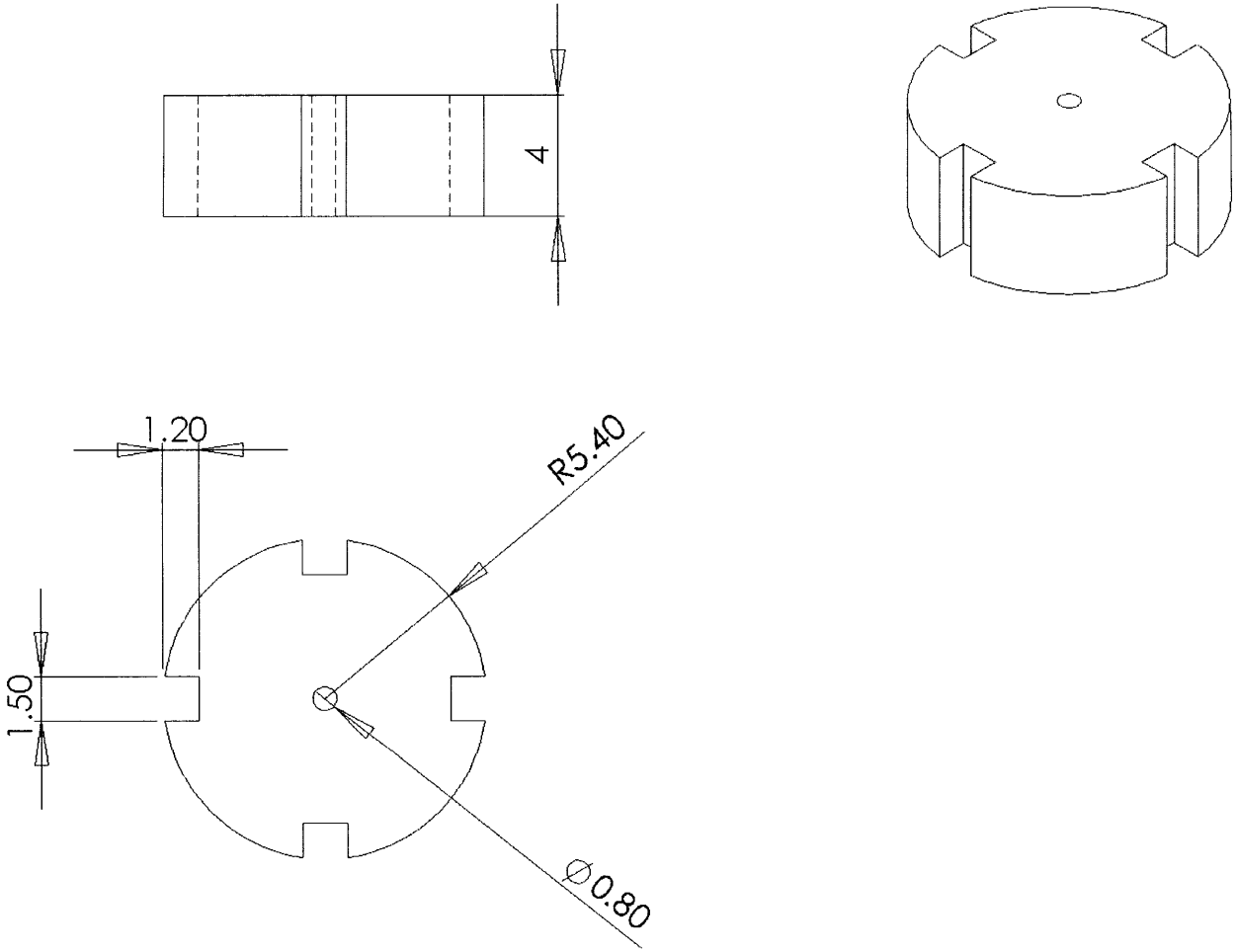

Insert

Version 1

SCALE 4:1

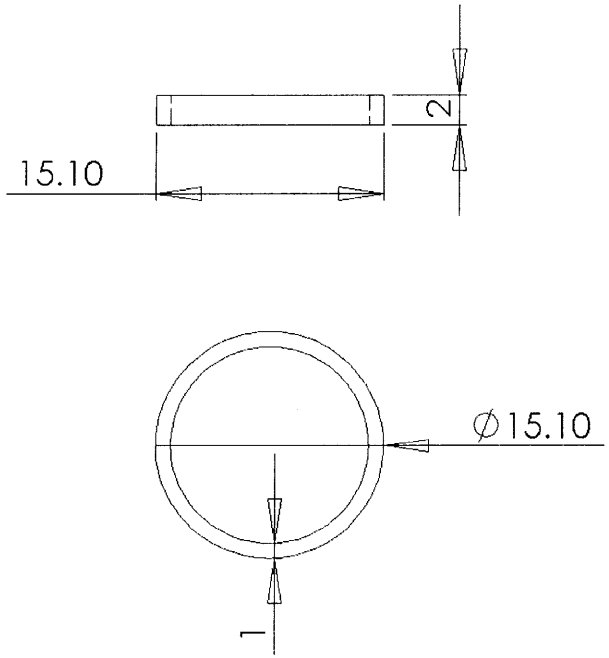

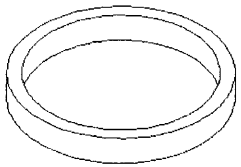

Retaining Ring

Version 1

SCALE 2:1

A2 Calculations for Pressure Across a Membrane

$E = 0.3749$ N/mm

$w = 1.5$ mm

$l = 3$ mm

$r = 1.575$ mm

Calculating Strain

$$\varepsilon = \frac{l_f - l_i}{l_i} = \frac{2r}{w} \cdot \sin^{-1}\left(\frac{w}{2r}\right) - 1, \tag{4.9}$$

$$\varepsilon = \frac{l_f - 1.5}{1.5} = \frac{2 \cdot 1.575}{1.5} \cdot \sin^{-1}\left(\frac{1.5}{2 \cdot 1.575}\right) - 1 = 4.2\%$$

Calculating Pressure

$$P = \frac{2E}{w}\left(1 + \frac{\pi w^2}{4l^2 - 4wl + \pi wl}\right)\left(\sin^{-1}\left(\frac{w}{2r}\right) - \frac{w}{2r}\right), \tag{4.12}$$

$$P = \frac{2 \cdot 0.3749}{1.5}\left(1 + \frac{\pi \cdot 1.5^2}{4 \cdot 1.5^2 - 4 \cdot 1.5 \cdot 3 + \pi \cdot 1.5 \cdot 3}\right)\left(\sin^{-1}\left(\frac{1.5}{2 \cdot 1.575}\right) - \frac{1.5}{2 \cdot 1.575}\right)$$

$$P = 0.012 \text{ N/mm}^2 = 12 \text{ kPa}$$

A3 Bioreactor Program and make file

'bioreactor.c'

```
/* this program runs three solenoid valves in
sequence the output depends on an input from a
bank of buttons

0 = Suction
1 = Pressure

[Reservoir  P Chamber Reactor]
[0 0 1] = 0x40
[0 1 1] = 0x60
[1 1 0] = 0x30
[1 0 0] = 0x10
[0 0 0] = 0x00
[1 1 1] = 0x70

Switch Bank
0x7F    0xFE
0xBF    0xFD
0xDF    0xFB
0xEF    0xF7
*/

#include <inttypes.h>
#include <avr/io.h>

void initialization(void);
void check_input(void);
void forward(void);
void reverse(void);
void set_cycles(void);
void set_cycles_half(void);
void super_slow(void);
void manual(void);
void delay(uint8_t);
uint8_t INPUT;


// takes in a delay and pauses
void delay(uint8_t n){
    uint8_t a, b, c;
    for (a = 1; a<n; a++){
        if (PINA != 0xFF){
            INPUT = PINA;
            }
        for (b = 1; b<=50; b++)
            for (c = 1; c<50; c++);
    }}

void initialization(void){
    // set PORTB as output
    DDRB = 0xFF;
    // set PORTA as input
    DDRA = 0x00;
    // turns pull up resistors on
    PORTA = 0xFF;
    }

void check_input(void){
    if (PINA != 0xFF){
        INPUT = PINA;
        }
    if (INPUT == 0xFE){
        forward();
        }
    else if (INPUT == 0xFD){
        reverse();
        }
    else if (INPUT == 0xFB){
        set_cycles();
        }
    else if (INPUT == 0xF7){
        set_cycles_half();
        }
    else if (INPUT == 0x7F){
        super_slow();
        }
    else if (INPUT == 0xEF | INPUT == 0xDF |
    INPUT == 0xBF){
        PORTB = PORTB & 0xF0;
        manual();
        }
    }

void forward(void){

    PORTB =  0x61;      // valve output [0 1 1]
    delay(75);
    PORTB = 0x41;       // valve output [0 0 1]
    delay(75);
    PORTB =  0x11;      // valve output [1 0 0]
    delay(75);
    PORTB = 0x31;       // valve output [1 1 0]
    delay(75);
    }

void reverse(void){
    PORTB = 0x44;       // valve output [0 0 1]
    delay(75);
```

```
    PORTB = 0x64;       // valve output [0 1 1]
    delay(75);
    PORTB = 0x34;       // valve output [1 1 0]
    delay(75);
    PORTB = 0x14;       // valve output [1 0 0]
    delay(75);
    }

void set_cycles(void){
// Runs 1.75 mL forward (1750 cyc)
    uint8_t a, b;
    for (b = 1; b<8; b++){
    for (a = 1; a<251; a++){
        PORTB =  0x61;
        delay(75);
        PORTB = 0x41;
        delay(75);
        PORTB =  0x11;
        delay(75);
        PORTB = 0x31;
        delay(75);
    }}
    INPUT = 0xFF;
    PORTB = 0x70;
    }

void set_cycles_half(void){
// Runs 1/2 mL in reverse (500 cyc)
    uint8_t a, b;
    for (b = 1; b<3; b++){
    for (a = 1; a<251; a++){
        PORTB = 0x44;
        delay(75);
        PORTB = 0x64;
        delay(75);
        PORTB = 0x34;
        delay(75);
        PORTB = 0x14;
        delay(75);
    }}
    INPUT = 0xFF;
    PORTB = 0x70;
    }

void super_slow(void){
    PORTB = 0x44;
    delay(250);
    delay(250);
    delay(250);
    delay(250);
    PORTB = 0x64;
    delay(250);
    delay(250);
    delay(250);
    delay(250);
    PORTB = 0x34;
    delay(250);
    delay(250);
    delay(250);
    delay(250);
    PORTB = 0x14;
    delay(250);
    delay(250);
    delay(250);
    delay(250);
    }

void manual(void){
        uint8_t a;
        if (PINA == 0xBF){
            for (a = 1; a<100; a++)
            while(PINA == 0xBF){}
            for (a = 1; a<100; a++)
            PORTB = PORTB ^ 0x10;
            }
        else if (PINA == 0xDF){
            for (a = 1; a<100; a++)
            while(PINA == 0xDF){}
            for (a = 1; a<100; a++)
            PORTB = PORTB ^ 0x20;
            }
        else if (PINA == 0xEF){
            for (a = 1; a<100; a++)
            while(PINA == 0xEF){}
            for (a = 1; a<100; a++)
            PORTB = PORTB ^ 0x40;
    }}

int main (){
    initialization();
    while(1){
        check_input();
//      back_forth();
        }
    return(1);
    }
```

Makefile

```
# Example Makefile for bioreactor controls
# Copied from http://www.enteract.com/~rneswold/avr/x421.html
# with "clean" added

CC=avr-gcc
OBJCOPY=avr-objcopy

CFLAGS=-g -mmcu=attiny26 -DATtiny26

all: rom.hex

rom.hex : bioreactor.out
	$(OBJCOPY) -j .text -O ihex clock.out rom.hex

bioreactor.out : bioreactor.o
	$(CC) $(CFLAGS) -o clock.out -Wl,-Map,bioreactor.map bioreactor.o

bioreactor.o : bioreactor.c
	$(CC) $(CFLAGS) -Os -c bioreactor.c

clean:
	rm -f *.o *.out *.map *.hex

rd_fuses:
	uisp -dprog=stk500 -dpart=ATtiny26 --rd_fuses
program:
	avrdude -c stk500 -p ATtiny26 -e
	avrdude -c stk500 -p ATtiny26 -U  flash:w:rom.hex
#	uisp -dprog=stk500 -dpart=ATtiny26 --erase --upload --verify if=rom.hex
```

A4 Machining code for the bioreactor

A 0.02 mm thick shim was used to set the tool height above the surface of the part. This thickness is accounted for in the programming code. The zeros for X and Y coordinates were set at the upper left corner of the part. This corner is aligned flush with the left side of the vise.

Program	Label	Diameter	Note
Reactor Top - A.6.2		RE-ZERO & CHECK TRAM, Fly cut, Center: y=-43.25	
Tool 1	1/2" end mill	12.72	piece must be at least 128.3 x 86, 13 mm from vice
Flip over to top, face, make sure you have 8 mm clearance from vice			
Tool 2	3/8" end mill	9.54	
Tool 3	1/8" end mill	3.15	1900, 125%, 30 min
Tool 4	Tapered End Mill	0	
Tool 5	1.6 mm end mill	1.6	15 min
Tool 6	1/4" Countersink	6.37	
Reactor Bottom - A.6.3		Flip top over bottom, fly cut down to 18 mm thick	
Tool 1	1/32" Drill	0	
Tool 2	# 43 Drill	0	1500 rpm
Tool 3	# 53 Drill	0	& 0.064 Reemer
Tool 4	1.6 mm End Mill	1.6	1900 rpm
Tool 5	5.5 mm End Mill	0	cut the capacitor holes to the right diameter
Tool 6	1/8" Ball Mill	1.5	Set tool height from center pad (63.9, -42.75)
Tool 7	1/64" Ball Mill	0	
Pumping Top - A.6.4		Fly cut, need 1.5 mm clearance from vice	
Tool 1	1/32" Drill		
Tool 2	#53 Drill	0	& 0.063" Reemer
Tool 3	#32 Drill	0	
Tool 4	1/64" Drill	0	
Tool 5	1/8" End Mill	3.15	Set tool 6 too (1900 RPM)
Tool 6	1/8" End Mill	3.15	Cuts the sealing surface flat (2500 rpm 75%)
Tool 7	1/64" End Mill	0.4	
Tool 8	1/8" Ball Mill	1.5	
Tool 9	3/8" End Mill	9.54	tool height on 72.9, -33.75
Pumping Bottom - A.6.5		FLY CUT & RE-ZERO BEFORE STARTING	
Tool 1	1/64" Drill	0	slow to 50
Tool 2	1/64" Ball Mill	0	slow to 50 / 75 w/ acrylic
Tool 3	1.2 mm Ball Mill	0	slow cutcomp to75
Tool 4	1/8" Mill	3.15	speed up long slots, change repeat on circle
Pumping Side - Turn on Side, face cuts towards machine			
Tool 5	1/8" Mill	3.15	
Tool 6	#43 Drill	0	
Tool 7	1/32" Drill	0	
Ridges on Reactor - A.6.6			
Tool 1	1.6 mm End Mill	1.6	
Tool 2	1/32" End Mill	0.8	
Scaffold - A.6.7 & A.6.8			
Tool 1	# 80 drill		
Filter Support - A.6.9			
Tool 1	0.6 mm Mill	0.6	4000 RPM
Flip Piece Over			
Tool 2	0.6 mm Mill	0.6	4000 RPM

The Top of the Fluidic Plate

```
0000 EZTRAK    1 MODE|MM  |SAT JAN 29 18:08:09 2005
0010 || TOOLCHG T1
0020 RECT|EDGE OUT X1 Y-86 Z.08 Z12.1 Z12.1 X127.8 Y85.5 R0 P.2 P0 D12.72 F222 F222
0030 || TOOLCHG T2
0040 REPEAT 1 X0. Y-38 Z0.
0050 REPEAT 1 X0. Y-20 Z0.
0060 REPEAT 5 X18 Y0 Z0.
0070 CIRCLE IN X18.9 Y-13.75 Z.08 Z12.05 Z4.1 R7.45 P1.6 P0 D9.54 F300 F300
0080 END|REPEAT
0090 END|REPEAT
0100 END|REPEAT
0110 REPEAT 1 X0. Y-18 Z0.
0120 REPEAT 5 X18 Y0 Z0.
0130 CIRCLE IN X18.9 Y-33.75 Z.08 Z16.1 Z12 R5.5 P.1 P0 D9.54 F200 F200
0140 CIRCLE IN X18.9 Y-33.75 Z.08 Z19 Z16 R5 P.1 P0 D9.54 F200 F200
0150 END|REPEAT
0160 END|REPEAT
0170 COMP|ON LFT D9.54 X63.9 Y-83.5 Z.08 Z-7.52 P.01 F200
0180 BLEND|LN ABS X2 Y-83.5 Z-7.52 R1.6 CW F200
0190 BLEND|LN ABS X2 Y-8 Z-7.52 R1.6 CW F200
0200 BLEND|LN ABS X8 Y-2 Z-7.52 R1.6 CW F200
0210 BLEND|LN ABS X125.8 Y-2 Z-7.52 R1.6 CW F200
0220 BLEND|LN ABS X125.8 Y-83.5 Z-7.52 R1.6 CW F200
0230 LINE ABS X60 Y-83.5 Z-7.52 F200
0240 COMP|OFF Z.08
0250 || TOOLCHG T3
0260 REPEAT 1 X0 Y-38 Z0.
0270 REPEAT 1 X0 Y-20 Z0.
0280 REPEAT 5 X18 Y0 Z0.
0290 CIRCLE IN X24.2033 Y-8.4467 Z.08 Z3.6 Z15 R1.9 P.5 P0 D3.15 F150 F150
0300 CIRCLE IN X24.2033 Y-8.4467 Z.08 Z12.1 Z15 R1.6 P.1 P0 D3.15 F150 F150
0310 CIRCLE IN X13.5967 Y-19.0533 Z.08 Z3.6 Z15 R1.9 P.5 P0 D3.15 F150 F150
0320 CIRCLE IN X13.5967 Y-19.0533 Z.08 Z12.1 Z15 R1.6 P.1 P0 D3.15 F150 F150
0330 CIRCLE IN X18.9 Y-13.75 Z.08 Z3.6 Z12 R8 P.5 P0 D3.15 F150 F150
0340 CIRCLE PKT X18.9 Y-13.75 Z.08 Z12.1 Z15 R7.5 P0 P0 P2.5 D3.15 F300 F300
0350 END|REPEAT
0360 END|REPEAT
0370 END|REPEAT
0380 || TOOLCHG T4
0390 REPEAT 1 X0 Y-38 Z0.
0400 REPEAT 1 X0 Y-20 Z0.
0410 REPEAT 5 X18 Y0 Z0.
0420 CIRCLE IN X18.9 Y-13.75 Z.08 Z7.029 Z15 R6.6063 P0 P0 D0 F300 F300
0430 END|REPEAT
0440 END|REPEAT
0450 END|REPEAT
0460 || TOOLCHG T5
0470 REPEAT 5 X18 Y0. Z0.
0480 REPEAT 1 X0 Y0 Z-2.5
0490 COMP|ON LFT D1.6 X14.5789 Y-20.4826 Z.08 Z-1.02 P0 F300
0500 BLEND|LN ABS X17.8 Y-22.55 Z-1.02 R3.5757 CW F300
0510 LINE ABS X17.8 Y-28 Z-1.02 F300
0520 LINE ABS X20 Y-28 Z-1.02 F300
```

```
0530 BLEND|LN ABS X20 Y-22.55 Z-1.02 R3.5757 CW F300
0540 LINE ABS X23.2211 Y-20.4826 Z-1.02 F300
0550 COMP|OFF Z-1.02
0560 COMP|ON LFT D1.6 X14.7149 Y-19.9738 Z.08 Z-4.52 P0 F60
0570 BLEND|LN ABS X18.1 Y-22.25 Z-4.52 R4 CW F60
0580 LINE ABS X18.1 Y-29 Z-4.52 F60
0590 LINE ABS X19.7 Y-29 Z-4.52 F60
0600 BLEND|LN ABS X19.7 Y-22.25 Z-4.52 R4 CW F60
0610 LINE ABS X23.0851 Y-19.9738 Z-4.52 F60
0620 COMP|OFF Z2.58
0630 RAPID ABS X18.9 Y-42.75 Z2.58
0640 TRANSLATE MIRROR XY
0650 COMP|ON LFT D1.6 X14.5789 Y-20.4826 Z0 Z-1.02 P0 F300
0660 BLEND|LN ABS X17.8 Y-22.55 Z-1.02 R3.5757 CW F300
0670 LINE ABS X17.8 Y-28 Z-1.02 F300
0680 LINE ABS X20 Y-28 Z-1.02 F300
0690 BLEND|LN ABS X20 Y-22.55 Z-1.02 R3.5757 CW F300
0700 LINE ABS X23.2211 Y-20.4826 Z-1.02 F300
0710 COMP|OFF Z-1.02
0720 COMP|ON LFT D1.6 X14.7149 Y-19.9738 Z.08 Z-4.52 P0 F60
0730 BLEND|LN ABS X18.1 Y-22.25 Z-4.52 R4 CW F60
0740 LINE ABS X18.1 Y-29 Z-4.52 F60
0750 LINE ABS X19.7 Y-29 Z-4.52 F60
0760 BLEND|LN ABS X19.7 Y-22.25 Z-4.52 R4 CW F60
0770 LINE ABS X23.0851 Y-19.9738 Z-4.52 F60
0780 COMP|OFF Z2.58
0790 TRANSLATE MIRROR OFF
0800 END|REPEAT
0810 END|REPEAT
0820 || TOOLCHG T6
0830 REPEAT 5 X18 Y0. Z0.
0840 COMP|ON LFT D6.37 X14.7149 Y-19.9738 Z0.08 Z-10.66 P0 F150
0850 BLEND|LN ABS X18.9 Y-22.7879 Z-10.66 R4.9 CCW F150
0860 LINE ABS X23.0851 Y-19.9738 Z-10.66 F150
0870 COMP|OFF Z.08
0880 COMP|ON LFT D6.37 X23.0851 Y-65.5262 Z.08 Z-10.66 P0 F150
0890 BLEND|LN ABS X18.9 Y-62.7121 Z-10.66 R4.9 CCW F150
0900 LINE ABS X14.7149 Y-65.5262 Z-10.66 F150
0910 COMP|OFF Z.08
0920 END|REPEAT
0930 || END|PRGM
```

The Bottom of the Fluidic Plate

```
0000 EZTRAK    1 MODE|MM  |SAT JAN 29 18:08:09 2005
0010 || TOOLCHG T1
0020 REPEAT 1 X0 Y-58 Z0.
0040 REPEAT 5 X18 Y0. Z0.
0050 DR|PT ABS X18.9 Y-13.75 Z.08 Z7.1 Z.5 Z.8 F100
0070 END|REPEAT
0080 END|REPEAT
0090 || TOOLCHG T2
0100 REPEAT 1 X0 Y-35.5 Z0.
0110 REPEAT 6 X18 Y0. Z0.
```

```
0120 DR|PT ABS X9.9 Y-25 Z.08 Z10.1 Z1.1 Z2.5 F150
0130 END|REPEAT
0140 END|REPEAT
0150 || TOOLCHG T3
0160 DR|PT ABS X63.9 Y-42.75 Z.08 Z6.5 Z.9 Z1.6 F100
0170 || TOOLCHG T4
0180 REPEAT 1 X108 Y0. Z0.
0190 SLOT X9.2 Y-42.75 Z.08 Z6.5 Z2.2 P3 P1.6 P0 D1.6 F100
0200 END|REPEAT
0210 || TOOLCHG T5
0220 REPEAT 5 X18 Y0. Z0
0230 COMP|ON LFT D0 X18.9 Y-20 Z.08 Z-.07 P0 F200
0240 LINE ABS X18.9 Y-13.75 Z-.12 F200
0240 LINE ABS X18.9 Y-28.75 Z-.12 F200
0250 ARC|CNTRPT ABS CCW X18.9 Y-28.75 Z-.12 XC18.9 YC-33.75 F200
0260 LINE ABS X18.9 Y-20 Z-.12 F200
0270 COMP|OFF Z.08
0280 RAPID ABS X18.9 Y-42.75 Z.08
0290 TRANSLATE MIRROR XY
0300 COMP|ON LFT D0 X18.9 Y-20 Z.08 Z-.07 P0 F200
0310 LINE ABS X18.9 Y-13.75 Z-.12 F200
0320 LINE ABS X18.9 Y-28.75 Z-.12 F200
0330 ARC|CNTRPT ABS CCW X18.9 Y-28.75 Z-.12 XC18.9 YC-33.75 F200
0340 LINE ABS X18.9 Y-20 Z-.12 F200
0350 COMP|OFF Z.08
0350 TRANSLATE MIRROR OFF
0360 END|REPEAT
0370 CIRCLE IN X63.9 Y-42.75 Z.08 Z.2 Z1.6 R6 P0 P0 D5.5 F200 F200
0450 || TOOLCHG T6
0460 REPEAT 1 X0 Y-46.1 Z0
0470 REPEAT 5 X18 Y0 Z0.
0480 SLOT X18.9 Y-18.95 Z.23 Z.44 Z1 P3 P1.5 P270 D1.5 F100
0490 END|REPEAT
0500 END|REPEAT
0570 || TOOLCHG T7
0580 REPEAT 5 X18 Y0. Z0.
0590 REPEAT 1 X0. Y0. Z-.27
0600 COMP|ON LFT D0 X18.9 Y-13.75 Z.35 Z-.15 P0 F100
0610 LINE ABS X18.9 Y-15 Z-.15 F100
0620 LINE ABS X18.9 Y-15.2 Z-.15 F100
0630 LINE ABS X18.9 Y-15.63 Z.25 F100
0640 COMP|OFF Z.35
0650 COMP|ON LFT D0 X18.9 Y-16.27 Z.35 Z.25 P0 F100
0660 LINE ABS X18.9 Y-16.7 Z-.15 F100
0670 LINE ABS X18.9 Y-22.7 Z-.15 F100
0680 LINE ABS X18.9 Y-23.13 Z.25 F100
0690 COMP|OFF Z.35
0700 COMP|ON LFT D0 X18.9 Y-23.77 Z.35 Z.25 P0 F100
0710 LINE ABS X18.9 Y-24.2 Z-.15 F100
0720 LINE ABS X18.9 Y-25 Z-.15 F100
0730 LINE ABS X18.9 Y-29 Z-.15 F100
0740 COMP|OFF Z.5
0750 COMP|ON LFT D0 X18.9 Y-56.5 Z.35 Z-.15 P0 F100
0760 LINE ABS X18.9 Y-58 Z-.15 F100
0770 LINE ABS X18.9 Y-61.3 Z-.15 F100
0780 LINE ABS X18.9 Y-61.73 Z.25 F100
```

```
0790 COMP|OFF Z.35
0800 COMP|ON LFT D0 X18.9 Y-62.37 Z.35 Z.25 P0 F100
0810 LINE ABS X18.9 Y-62.8 Z-.15 F100
0820 LINE ABS X18.9 Y-68.8 Z-.15 F100
0830 LINE ABS X18.9 Y-69.23 Z.25 F100
0840 COMP|OFF Z.35
0850 COMP|ON LFT D0 X18.9 Y-69.87 Z.35 Z.25 P0 F100
0860 LINE ABS X18.9 Y-70.3 Z-.15 F100
0870 LINE ABS X18.9 Y-71 Z-.15 F100
0880 LINE ABS X18.9 Y-71.75 Z-.15 F100
0890 COMP|OFF Z.5
0900 END|REPEAT
0910 END|REPEAT
0920 || END|PRGM
```

The Top of the Pneumatic Plate

```
0000 EZTRAK    1 MODE|MM  |THU JAN 27 10:34:34 2005
0010 || TOOLCHG T1
0020 REPEAT 1 X0 Y-34.2 Z0.
0030 REPEAT 5 X18 Y0. Z0
0040 DR|PT ABS X18.9 Y-25.65 Z.08 Z11 Z.4 Z.4 F100
0050 END|REPEAT
0060 END|REPEAT
0070 || TOOLCHG T2
0080 REPEAT 1 X54 Y0 Z0.
0090 DR|PT ABS X63.9 Y-42.75 Z.08 Z6.5 Z.8 Z.8 F100
0100 END|REPEAT
0110 || TOOLCHG T3
0120 REPEAT 1 X0 Y-18 Z0.
0130 REPEAT 4 X18 Y0 Z0.
0140 DR|PT ABS X27.9 Y-33.75 Z.08 Z11 Z1.1 Z1.25 F100
0150 END|REPEAT
0160 END|REPEAT
0170 REPEAT 5 X18 Y0 Z0.
0180 REPEAT 2 X0. Y-9 Z0.
0190 DR|PT ABS X18.9 Y-33.75 Z.08 Z11 Z1.1 Z1.25 F100
0200 END|REPEAT
0210 END|REPEAT
0220 REPEAT 1 X0 Y-35.5 Z0.
0230 REPEAT 6 X18 Y0 Z0.
0240 DR|PT ABS X9.9 Y-25 Z.08 Z11 Z1.1 Z1.25 F100
0250 END|REPEAT
0260 END|REPEAT
0270 || TOOLCHG T4
0280 REPEAT 5 X18 Y0 Z0.
0290 DR|PT ABS X18.9 Y-15.95 Z.08 Z6.1 Z.3 Z.4 F100
0300 DR|PT ABS X18.9 Y-19.7 Z.08 Z6.1 Z.3 Z.4 F100
0310 DR|PT ABS X18.9 Y-23.45 Z.08 Z6.1 Z.3 Z.4 F100
0320 DR|PT ABS X18.9 Y-62.05 Z.08 Z6.1 Z.3 Z.4 F100
0330 DR|PT ABS X18.9 Y-65.8 Z.08 Z6.1 Z.3 Z.4 F100
0340 DR|PT ABS X18.9 Y-69.55 Z.08 Z6.1 Z.3 Z.4 F100
0350 END|REPEAT
0360 || TOOLCHG T5
```

```
0370 REPEAT 1 X54 Y0 Z0.
0380 CIRCLE IN X63.9 Y-42.75 Z.08 Z1.15 Z1.5 R2.3 P.2 P0 D3.15 F200 F200
0390 END|REPEAT
0400 REPEAT 1 X0 Y-35.5 Z0.
0410 REPEAT 4 X18 Y0 Z0.
0420 CIRCLE IN X27.9 Y-25 Z.08 Z1.15 Z1.5 R3 P.2 P0 D3.15 F200 F200
0430 END|REPEAT
0440 END|REPEAT
0450 SLOT X-.95 Y-42.75 Z.08 Z1.15 Z2 P132.85 P3.15 P0 D3.15 F300
0460 REPEAT 1 X0 Y-51.85 Z0.
0470 REPEAT 4 X18 Y0 Z0.
0480 SLOT X27.9 Y.1 Z.08 Z1.15 Z2 P37 P3.15 P270 D3.15 F300
0490 END|REPEAT
0500 END|REPEAT
0510 REPEAT 5 X18 Y0 Z0.
0520 COMP|ON LFT D3.15 X17.15 Y-20 Z.08 Z-.32 P0 F150
0530 LINE ABS X17.15 Y-14.6 Z-.32 F150
0540 ARC|CNTRPT ABS CW X20.65 Y-14.6 Z-.32 XC18.9 YC-14.6 F150
0550 LINE ABS X20.65 Y-28.5358 Z-.32 F150
0560 ARC|CNTRPT ABS CW X17.15 Y-28.5358 Z-.32 XC18.9 YC-33.75 F150
0570 LINE ABS X17.15 Y-18 Z-.32 F150
0580 COMP|OFF Z.08
0590 RAPID ABS X18.9 Y-42.75 Z.08
0600 TRANSLATE MIRROR XY
0610 COMP|ON LFT D3.15 X17.15 Y-20 Z.08 Z-.32 P0 F150
0620 LINE ABS X17.15 Y-14.6 Z-.32 F150
0630 ARC|CNTRPT ABS CW X20.65 Y-14.6 Z-.32 XC18.9 YC-14.6 F150
0640 LINE ABS X20.65 Y-28.5358 Z-.32 F150
0650 ARC|CNTRPT ABS CW X17.15 Y-28.5358 Z-.32 XC18.9 YC-33.75 F150
0660 LINE ABS X17.15 Y-18 Z-.32 F150
0670 COMP|OFF Z.08
0680 TRANSLATE MIRROR OFF
0690 END|REPEAT
0700 REPEAT 4 X18 Y0 Z0.
0710 RECT|CNTR IN X27.9 Y-42.75 Z.08 Z.4 Z3 X6 Y18 R0 P.1 P0 D3.15 F200 F200
0720 END|REPEAT
0730 || TOOLCHG T6
0740 REPEAT 5 X18 Y0. Z0
0750 COMP|ON LFT D3.15 X15.95 Y-24.7 Z.08 Z-.07 P0 F222
0760 LINE ABS X15.95 Y-27.402 Z-.07 F222
0770 ARC|CNTRPT ABS CCW X21.85 Y-27.402 Z-.07 XC18.9 YC-33.75 F222
0780 LINE ABS X21.85 Y-14.6 Z-.07 F222
0790 ARC|CNTRPT ABS CCW X15.95 Y-14.6 Z-.07 XC18.9 YC-14.6 F222
0800 LINE ABS X15.95 Y-25.3 Z-.07 F222
0810 COMP|OFF Z.08
0820 RAPID ABS X18.9 Y-42.75 Z.08
0830 TRANSLATE MIRROR XY
0840 COMP|ON LFT D3.15 X15.95 Y-24.7 Z.08 Z-.07 P0 F222
0850 LINE ABS X15.95 Y-27.402 Z-.07 F222
0860 ARC|CNTRPT ABS CCW X21.85 Y-27.402 Z-.07 XC18.9 YC-33.75 F222
0870 LINE ABS X21.85 Y-14.6 Z-.07 F222
0880 ARC|CNTRPT ABS CCW X15.95 Y-14.6 Z-.07 XC18.9 YC-14.6 F222
0890 LINE ABS X15.95 Y-25.3 Z-.07 F222
0900 COMP|OFF Z.08
0910 TRANSLATE MIRROR OFF
0920 END|REPEAT
```

```
0930 CIRCLE IN X54.9 Y-33.75 Z.08 Z.15 Z2 R4.9 P0 P2 D3.15 F222 F222
0940 || TOOLCHG T7
0950 REPEAT 1 X0 Y-46.1 Z0.
0960 REPEAT 5 X18 Y0 Z0.
0970 SLOT X18.9 Y-18.4 Z.08 Z.5 Z1 P3 P.4 P270 D.4 F100
0980 END|REPEAT
0990 END|REPEAT
1000 || TOOLCHG T8
1010 REPEAT 1 X0 Y-46.1 Z0.
1020 REPEAT 5 X18 Y0 Z0.
1030 SLOT X18.9 Y-18.95 Z.08 Z.29 Z1 P3 P1.5 P270 D1.5 F100
1040 END|REPEAT
1050 END|REPEAT
1060 REPEAT 1 X0 Y-46.1 Z0.
1070 REPEAT 5 X18 Y0 Z0.
1080 REPEAT 1 X0 Y-7.5 Z0.
1090 DR|PT ABS X18.9 Y-15.95 Z.08 Z.29 Z1 Z1 F100
1100 END|REPEAT
1110 END|REPEAT
1120 END|REPEAT
1130 || TOOLCHG T9
1140 REPEAT 1 X0 Y-74.9 Z0.
1150 RECT|CNTR IN X63.9 Y-5.3 Z.08 Z.35 Z2 X137.34 Y13 R0 P.5 P0 D9.54 F300 F300
1160 END|REPEAT
1170 REPEAT 1 X117.4 Y0 Z0.
1180 RECT|CNTR IN X5.2 Y-42.75 Z.08 Z.35 Z2 X11.4 Y75.65 R0 P0 P0 D9.54 F300 F300
1190 END|REPEAT
1200 REPEAT 1 X0 Y-45.5 Z0.
1210 REPEAT 6 X18 Y0 Z0.
1220 RECT|CNTR IN X9.9 Y-20 Z.08 Z.35 Z2 X11 Y23 R0 P.5 P0 D9.54 F300 F300
1230 END|REPEAT
1240 END|REPEAT
1250 REPEAT 6 X18 Y0 Z0.
1260 CIRCLE IN X9.9 Y-42.75 Z.08 Z.35 Z2 R7 P.1 P0 D9.54 F300 F300
1270 END|REPEAT
1280 REPEAT 1 X0 Y-18 Z0.
1290 REPEAT 5 X18 Y0 Z0.
1300 CIRCLE IN X18.9 Y-33.75 Z.08 Z2.1 Z3 R5 P.05 P0 D9.54 F75 F75
1310 END|REPEAT
1320 END|REPEAT
1330 || END|PRGM
```

The Bottom of the Pneumatic Plate

One Pneumatic Input

```
0000 EZTRAK    1 MODE|MM  |THU JAN 27 10:34:34 2005
0010 || TOOLCHG T1
0020 REPEAT 5 X18 Y0 Z0.
0030 DR|PT ABS X18.9 Y-15.95 Z.08 Z5.5 Z.2 Z.4 F100
0040 DR|PT ABS X18.9 Y-19.7 Z.08 Z5.5 Z.2 Z.4 F100
0050 DR|PT ABS X18.9 Y-23.45 Z.08 Z5.5 Z.2 Z.4 F100
0060 DR|PT ABS X18.9 Y-62.05 Z.08 Z5.5 Z.2 Z.4 F100
```

```
0070 DR|PT ABS X18.9 Y-65.8 Z.08 Z5.5 Z.2 Z.4 F100
0080 DR|PT ABS X18.9 Y-69.55 Z.08 Z5.5 Z.2 Z.4 F100
0090 END|REPEAT
0100 DR|PT ABS X13.6 Y-36.75 Z.08 Z5.5 Z.2 Z.4 F150
0110 DR|PT ABS X14.8 Y-42.75 Z.08 Z5.5 Z.2 Z.4 F150
0120 DR|PT ABS X16 Y-48.75 Z.08 Z5.5 Z.2 Z.4 F150
0130 || TOOLCHG T2
0140 COMP|ON LFT D0 X108.9 Y-15.95 Z.08 Z-.42 P0 F125
0150 BLEND|LN ABS X13.6 Y-15.95 Z-.42 R4.9 CCW F125
0160 BLEND|LN ABS X13.6 Y-69.55 Z-.42 R4.9 CCW F125
0170 LINE ABS X108.9 Y-69.55 Z-.42 F125
0180 COMP|OFF Z.08
0190 COMP|ON LFT D0 X108.9 Y-19.7 Z.08 Z-.42 P0 F125
0200 BLEND|LN ABS X14.8 Y-19.7 Z-.42 R3.7 CCW F125
0210 BLEND|LN ABS X14.8 Y-65.8 Z-.42 R3.7 CCW F125
0220 LINE ABS X108.9 Y-65.8 Z-.42 F125
0230 COMP|OFF Z.08
0240 COMP|ON LFT D0 X108.9 Y-21 Z.08 Z-.42 P0 F125
0250 BLEND|LN ABS X16 Y-21 Z-.42 R2.5 CCW F125
0260 BLEND|LN ABS X16 Y-64.5 Z-.42 R2.5 CCW F125
0270 LINE ABS X108.9 Y-64.5 Z-.42 F125
0280 COMP|OFF Z.08
0290 REPEAT 1 X0 Y-41.05 Z0.
0300 REPEAT 5 X18 Y0 Z0.
0310 SLOT X18.9 Y-21 Z.08 Z.5 Z1 P2.45 P0 P270 D0 F200
0320 END|REPEAT
0330 END|REPEAT
0340 || TOOLCHG T3
0350 COMP|ON LFT D0 X18.9 Y-25.65 Z.08 Z-1.02 P0 F150
0360 LINE ABS X27.9 Y-29.3 Z-1.02 F150
0370 LINE ABS X36.9 Y-25.65 Z-1.02 F150
0380 LINE ABS X45.9 Y-29.3 Z-1.02 F150
0390 LINE ABS X54.9 Y-25.65 Z-1.02 F150
0400 LINE ABS X63.9 Y-29.3 Z-1.02 F150
0410 LINE ABS X72.9 Y-25.65 Z-1.02 F150
0420 LINE ABS X81.9 Y-29.3 Z-1.02 F150
0430 LINE ABS X90.9 Y-25.65 Z-1.02 F150
0440 LINE ABS X99.9 Y-29.3 Z-1.02 F150
0450 LINE ABS X108.9 Y-25.65 Z-1.02 F150
0460 COMP|OFF Z.08
0470 RAPID ABS X63.9 Y-42.75 Z.08
0480 TRANSLATE MIRROR XY
0490 COMP|ON LFT D0 X18.9 Y-25.65 Z.08 Z-1.02 P0 F150
0500 LINE ABS X27.9 Y-29.3 Z-1.02 F150
0510 LINE ABS X36.9 Y-25.65 Z-1.02 F150
0520 LINE ABS X45.9 Y-29.3 Z-1.02 F150
0530 LINE ABS X54.9 Y-25.65 Z-1.02 F150
0540 LINE ABS X63.9 Y-29.3 Z-1.02 F150
0550 LINE ABS X72.9 Y-25.65 Z-1.02 F150
0560 LINE ABS X81.9 Y-29.3 Z-1.02 F150
0570 LINE ABS X90.9 Y-25.65 Z-1.02 F150
0580 LINE ABS X99.9 Y-29.3 Z-1.02 F150
0590 LINE ABS X108.9 Y-25.65 Z-1.02 F150
0600 COMP|OFF Z.08
0610 TRANSLATE MIRROR OFF
0620 || TOOLCHG T4
```

```
0640 REPEAT 1 X0 Y-35.5 Z0.
0650 REPEAT 6 X18 Y0 Z0.
0650 CIRCLE IN X9.9 Y-25 Z.08 Z3.1 Z4 R2.5 P.4 P0 D3.15 F125 F125
0660 END|REPEAT
0670 END|REPEAT
0680 REPEAT 1 X0 Y-21.475 Z0.
0690 REPEAT 4 X18 Y0 Z0.
0700 SLOT X27.9 Y-30.275 Z.08 Z1.1 Z1.5 P6.625 P3.15 P270 D3.15 F150
0710 END|REPEAT
0720 END|REPEAT
0730 REPEAT 5 X18 Y0 Z0.
0740 SLOT X18.9 Y-33.75 Z.08 Z1.1 Z2 P21.15 P3.15 P270 D3.15 F150
0750 END|REPEAT
0760 || TOOLCHG T5
0770 REPEAT 2 X6 Y0 Z0.
0780 CIRCLE IN X36.75 Y-5 Z.08 Z.85 Z2 R2.1 P.25 P0 D3.15 F40 F10.
0790 END|REPEAT
0800 || TOOLCHG T6
0810 REPEAT 2 X6 Y0 Z0.
0820 DR|PT ABS X36.75 Y-5 Z.08 Z9.1 Z.5 Z1 F100
0830 END|REPEAT
0840 || TOOLCHG T7
0850 DR|PT ABS X36.75 Y-5 Z.08 Z14.1 Z8 Z.4 F100
0860 DR|PT ABS X42.75 Y-5 Z.08 Z15.3 Z8 Z.4 F100
0870 DR|PT ABS X48.75 Y-5 Z.08 Z16.5 Z8 Z.4 F100
0880 || END|PRGM
```

Two Pneumatic Inputs

```
0000 EZTRAK    1 MODE|MM  |THU JAN 27 10:34:34 2005
0010 || TOOLCHG T1
0020 REPEAT 5 X18 Y0 Z0.
0030 DR|PT ABS X18.9 Y-15.95 Z.08 Z5.5 Z.2 Z.4 F100
0040 DR|PT ABS X18.9 Y-19.7 Z.08 Z5.5 Z.2 Z.4 F100
0050 DR|PT ABS X18.9 Y-23.45 Z.08 Z5.5 Z.2 Z.4 F100
0060 DR|PT ABS X18.9 Y-62.05 Z.08 Z5.5 Z.2 Z.4 F100
0070 DR|PT ABS X18.9 Y-65.8 Z.08 Z5.5 Z.2 Z.4 F100
0080 DR|PT ABS X18.9 Y-69.55 Z.08 Z5.5 Z.2 Z.4 F100
0090 END|REPEAT
0100 REPEAT 1 X0. Y-60 Z0.
0110 REPEAT 2 X0. Y-6 Z0.
0120 DR|PT ABS X14.8 Y-6.75 Z.08 Z5.5 Z.2 Z.4 F150
0130 END|REPEAT
0140 END|REPEAT
0150 || TOOLCHG T2
0160 COMP|ON LFT D0 X108.9 Y-15.95 Z.08 Z-.42 P0 F125
0170 LINE ABS X90 Y-15.95 Z-.42 F125
0180 LINE ABS X80 Y-15.95 Z-.42 F125
0190 LINE ABS X18.5 Y-15.95 Z-.42 F125
0200 LINE ABS X14.8 Y-6.75 Z-.42 F125
0210 COMP|OFF Z.08
0220 COMP|ON LFT D0 X108.9 Y-19.7 Z.08 Z-.42 P0 F125
0230 LINE ABS X90 Y-19.7 Z-.42 F125
0240 LINE ABS X80 Y-19.7 Z-.42 F125
0250 LINE ABS X18.5 Y-19.7 Z-.42 F125
0260 LINE ABS X14.8 Y-12.75 Z-.42 F125
```

```
0270 COMP|OFF Z.08
0280 COMP|ON LFT D0 X108.9 Y-21 Z.08 Z-.42 P0 F125
0290 LINE ABS X90 Y-21 Z-.42 F125
0300 LINE ABS X80 Y-21 Z-.42 F125
0310 LINE ABS X18.5 Y-21 Z-.42 F125
0320 LINE ABS X14.8 Y-18.75 Z-.42 F125
0330 COMP|OFF Z.08
0340 RAPID ABS X63.9 Y-42.75 Z.08
0350 TRANSLATE MIRROR Y
0360 COMP|ON LFT D0 X108.9 Y-15.95 Z.08 Z-.42 P0 F125
0370 LINE ABS X90 Y-15.95 Z-.42 F125
0380 LINE ABS X80 Y-15.95 Z-.42 F125
0390 LINE ABS X18.5 Y-15.95 Z-.42 F125
0400 LINE ABS X14.8 Y-6.75 Z-.42 F125
0410 COMP|OFF Z.08
0420 COMP|ON LFT D0 X108.9 Y-19.7 Z.08 Z-.42 P0 F125
0430 LINE ABS X90 Y-19.7 Z-.42 F125
0440 LINE ABS X80 Y-19.7 Z-.42 F125
0450 LINE ABS X18.5 Y-19.7 Z-.42 F125
0460 LINE ABS X14.8 Y-12.75 Z-.42 F125
0470 COMP|OFF Z.08
0480 COMP|ON LFT D0 X108.9 Y-21 Z.08 Z-.42 P0 F125
0490 LINE ABS X90 Y-21 Z-.42 F125
0500 LINE ABS X80 Y-21 Z-.42 F125
0510 LINE ABS X18.5 Y-21 Z-.42 F125
0520 LINE ABS X14.8 Y-18.75 Z-.42 F125
0530 COMP|OFF Z.08
0540 TRANSLATE MIRROR OFF
0550 REPEAT 1 X0 Y-41.05 Z0.
0560 REPEAT 5 X18 Y0 Z0.
0570 SLOT X18.9 Y-21 Z.08 Z.5 Z1 P2.45 P0 P270 D0 F200
0580 END|REPEAT
0590 END|REPEAT
0600 || TOOLCHG T3
0610 COMP|ON LFT D0 X18.9 Y-25.65 Z.08 Z-1.02 P0 F150
0620 LINE ABS X27.9 Y-29.3 Z-1.02 F150
0630 LINE ABS X36.9 Y-25.65 Z-1.02 F150
0640 LINE ABS X45.9 Y-29.3 Z-1.02 F150
0650 LINE ABS X54.9 Y-25.65 Z-1.02 F150
0660 LINE ABS X63.9 Y-29.3 Z-1.02 F150
0670 LINE ABS X72.9 Y-25.65 Z-1.02 F150
0680 LINE ABS X81.9 Y-29.3 Z-1.02 F150
0690 LINE ABS X90.9 Y-25.65 Z-1.02 F150
0700 LINE ABS X99.9 Y-29.3 Z-1.02 F150
0710 LINE ABS X108.9 Y-25.65 Z-1.02 F150
0720 COMP|OFF Z.08
0730 RAPID ABS X63.9 Y-42.75 Z.08
0740 TRANSLATE MIRROR XY
0750 COMP|ON LFT D0 X18.9 Y-25.65 Z.08 Z-1.02 P0 F150
0760 LINE ABS X27.9 Y-29.3 Z-1.02 F150
0770 LINE ABS X36.9 Y-25.65 Z-1.02 F150
0780 LINE ABS X45.9 Y-29.3 Z-1.02 F150
0790 LINE ABS X54.9 Y-25.65 Z-1.02 F150
0800 LINE ABS X63.9 Y-29.3 Z-1.02 F150
0810 LINE ABS X72.9 Y-25.65 Z-1.02 F150
0820 LINE ABS X81.9 Y-29.3 Z-1.02 F150
```

```
0830 LINE ABS X90.9 Y-25.65 Z-1.02 F150
0840 LINE ABS X99.9 Y-29.3 Z-1.02 F150
0850 LINE ABS X108.9 Y-25.65 Z-1.02 F150
0860 COMP|OFF Z.08
0870 TRANSLATE MIRROR OFF
0880 || TOOLCHG T4
0900 REPEAT 1 X0 Y-35.5 Z0.
0910 REPEAT 6 X18 Y0 Z0.
0910 CIRCLE IN X9.9 Y-25 Z.08 Z3.1 Z4 R2.5 P.4 P0 D3.15 F125 F125
0920 END|REPEAT
0930 END|REPEAT
0940 REPEAT 1 X0 Y-21.475 Z0.
0950 REPEAT 4 X18 Y0 Z0.
0960 SLOT X27.9 Y-30.275 Z.08 Z1.1 Z1.5 P6.625 P3.15 P270 D3.15 F150
0970 END|REPEAT
0980 END|REPEAT
0990 REPEAT 5 X18 Y0 Z0.
1000 SLOT X18.9 Y-33.75 Z.08 Z1.1 Z2 P21.15 P3.15 P270 D3.15 F150
1010 END|REPEAT
1020 || TOOLCHG T5
1030 REPEAT 1 X60 Y0 Z0.
1030 REPEAT 2 X6 Y0 Z0.
1040 CIRCLE IN X6.75 Y-5 Z.08 Z.85 Z2 R2.1 P.25 P0 D3.15 F40 F10.
1050 END|REPEAT
1050 END|REPEAT
1060 || TOOLCHG T6
1070 REPEAT 1 X60 Y0 Z0.
1070 REPEAT 2 X6 Y0 Z0.
1080 DR|PT ABS X6.75 Y-5 Z.08 Z9.1 Z.5 Z1 F100
1090 END|REPEAT
1100 END|REPEAT
1100 || TOOLCHG T7
1110 REPEAT 1 X60 Y0 Z0.
1120 REPEAT 2 X6 Y0 Z0.
1120 DR|PT ABS X6.75 Y-5 Z.08 Z15.3 Z8 Z.4 F100
1130 END|REPEAT
1140 END|REPEAT
1140 || END|PRGM
```

A Scaffold with a Circular Arrangement of Channels

```
0000 EZTRAK    1 MODE|MM  |WED FEB 09 16:48:24 2005
0010 || TOOLCHG T1
0020 DR|PT ABS X12.5 Y-15 Z.08 Z1 Z.7 Z.3 F555
0030 DR|BC R.443 XC12.5 YC-15 Z.08 Z1 Z.7 Z.3 A0. P6 F555
0040 DR|BC R.886 XC12.5 YC-15 Z.08 Z1 Z.7 Z.3 A0. P12 F555
0050 DR|BC R1.329 XC12.5 YC-15 Z.08 Z1 Z.7 Z.3 A0. P18 F555
0060 DR|BC R1.772 XC12.5 YC-15 Z.08 Z1 Z.7 Z.3 A0. P24 F555
0070 DR|BC R2.215 XC12.5 YC-15 Z.08 Z1 Z.7 Z.3 A0. P30 F555
0080 DR|BC R2.658 XC12.5 YC-15 Z.08 Z1 Z.7 Z.3 A0. P36 F555
0090 DR|BC R3.101 XC12.5 YC-15 Z.08 Z1 Z.7 Z.3 A0. P42 F555
0100 DR|BC R3.544 XC12.5 YC-15 Z.08 Z1 Z.7 Z.3 A0. P48 F555
0110 DR|BC R3.987 XC12.5 YC-15 Z.08 Z1 Z.7 Z.3 A0. P54 F555
0120 DR|BC R4.43 XC12.5 YC-15 Z.08 Z1 Z.7 Z.3 A0. P60 F555
0130 DR|BC R4.873 XC12.5 YC-15 Z.08 Z1 Z.7 Z.3 A0. P66 F555
```

```
0140 DR|BC R5.316 XC12.5 YC-15 Z.08 Z1 Z.7 Z.3 A0. P72 F555
0150 DR|BC R5.759 XC12.5 YC-15 Z.08 Z1 Z.7 Z.3 A0. P78 F555
0160 DR|BC R6.202 XC12.5 YC-15 Z.08 Z1 Z.7 Z.3 A0. P84 F555
0170 || END|PRGM
```

A Scaffold with an offset Linear Arrangement of Channels

```
0000 EZTRAK    1 MODE|MM  |THU DEC 22 13:23:21 2005
0010 || TOOLCHG T1
0020 DR|ROW ABS X11.8355 Y-13.082 Z.08 Z1 Z.7 Z.3 X1.329 Y0 P4 F222
0030 DR|ROW ABS X11.171 Y-13.4656 Z.08 Z1 Z.7 Z.3 X2.658 Y0 P7 F222
0040 DR|ROW ABS X10.9459 Y-13.8492 Z.08 Z1 Z.7 Z.3 X3.1046 Y0 P8 F222
0050 DR|ROW ABS X10.728 Y-14.2328 Z.08 Z1 Z.7 Z.3 X3.544 Y0 P9 F222
0060 DR|ROW ABS X10.5065 Y-14.6164 Z.08 Z1 Z.7 Z.3 X3.987 Y0 P10 F222
0070 DR|ROW ABS X10.728 Y-15 Z.08 Z1 Z.7 Z.3 X3.544 Y0 P9 F222
0080 DR|ROW ABS X10.5065 Y-15.3836 Z.08 Z1 Z.7 Z.3 X3.987 Y0 P10 F222
0090 DR|ROW ABS X10.728 Y-15.7672 Z.08 Z1 Z.7 Z.3 X3.544 Y0 P9 F222
0100 DR|ROW ABS X10.9459 Y-16.1508 Z.08 Z1 Z.7 Z.3 X3.1046 Y0 P8 F222
0110 DR|ROW ABS X11.171 Y-16.5344 Z.08 Z1 Z.7 Z.3 X2.658 Y0 P7 F222
0120 DR|ROW ABS X11.8355 Y-16.918 Z.08 Z1 Z.7 Z.3 X1.329 Y0 P4 F222
0130 || END|PRGM
```

The Filter Support

```
0000 EZTRAK    1 MODE|MM  |THU JAN 27 10:34:34 2005
0010 || TOOLCHG T1
0020 SLOT X6.275 Y0 Z.08 Z.7 Z2 P6 P.6 P180 D.6 F100
0030 SLOT X6.0612 Y1.6241 Z.08 Z.7 Z2 P3.5 P.6 P195 D.6 F100
0040 SLOT X5.4343 Y3.1375 Z.08 Z.7 Z2 P5 P.6 P210 D.6 F100
0050 SLOT X4.4371 Y4.4371 Z.08 Z.7 Z2 P3.5 P.6 P225 D.6 F100
0060 SLOT X3.1375 Y5.4343 Z.08 Z.7 Z2 P6 P.6 P240 D.6 F100
0070 SLOT X1.6241 Y6.0612 Z.08 Z.7 Z2 P3.5 P.6 P255 D.6 F100
0080 SLOT X0 Y6.2750 Z.08 Z.7 Z2 P5 P.6 P270 D.6 F100
0090 SLOT X-1.6241 Y6.0612 Z.08 Z.7 Z2 P3.5 P.6 P285 D.6 F100
0100 SLOT X-3.1375 Y5.4343 Z.08 Z.7 Z2 P6 P.6 P300 D.6 F100
0110 SLOT X-4.4371 Y4.4371 Z.08 Z.7 Z2 P3.5 P.6 P315 D.6 F100
0120 SLOT X-5.4343 Y3.1375 Z.08 Z.7 Z2 P5 P.6 P330 D.6 F100
0130 SLOT X-6.0612 Y1.6241 Z.08 Z.7 Z2 P3.5 P.6 P345 D.6 F100
0140 SLOT X-6.275 Y0 Z.08 Z.7 Z2 P6 P.6 P0 D.6 F100
0150 SLOT X-6.0612 Y-1.6241 Z.08 Z.7 Z2 P3.5 P.6 P15 D.6 F100
0160 SLOT X-5.4343 Y-3.1375 Z.08 Z.7 Z2 P5 P.6 P30 D.6 F100
0170 SLOT X-4.4371 Y-4.4371 Z.08 Z.7 Z2 P3.5 P.6 P45 D.6 F100
0180 SLOT X-3.1375 Y-5.4343 Z.08 Z.7 Z2 P6 P.6 P60 D.6 F100
0190 SLOT X-1.6241 Y-6.0612 Z.08 Z.7 Z2 P3.5 P.6 P75 D.6 F100
0200 SLOT X0 Y-6.275 Z.08 Z.7 Z2 P5 P.6 P90 D.6 F100
0210 SLOT X1.6241 Y-6.0612 Z.08 Z.7 Z2 P3.5 P.6 P105 D.6 F100
0220 SLOT X3.1375 Y-5.4343 Z.08 Z.7 Z2 P6 P.6 P120 D.6 F100
0230 SLOT X4.4371 Y-4.4371 Z.08 Z.7 Z2 P3.5 P.6 P135 D.6 F100
0240 SLOT X5.4343 Y-3.1375 Z.08 Z.7 Z2 P5 P.6 P150 D.6 F100
0250 SLOT X6.0612 Y-1.6241 Z.08 Z.7 Z2 P3.5 P.6 P165 D.6 F100
0260 || TOOLCHG T2
```

```
0270 CIRCLE IN X0 Y0 Z.08 Z.4 Z1 R6.55 P.05 P0 D.6 F70 F70
0280 CIRCLE OUT X0 Y0 Z.08 Z.4 Z1 R5.875 P.05 P0 D.6 F110 F110
0290 CIRCLE IN X0 Y0 Z.08 Z.4 Z1 R5.725 P.2 P0 D.6 F70 F70
0300 CIRCLE OUT X0 Y0 Z.08 Z.4 Z1 R4.675 P.2 P0 D.6 F110 F110
0310 CIRCLE IN X0 Y0 Z.08 Z.4 Z1 R4.525 P.2 P0 D.6 F70 F70
0320 CIRCLE OUT X0 Y0 Z.08 Z.4 Z1 R3.475 P.2 P0 D.6 F110 F110
0330 CIRCLE IN X0 Y0 Z.08 Z.4 Z1 R3.325 P.2 P0 D.6 F70 F70
0340 CIRCLE OUT X0 Y0 Z.08 Z.4 Z1 R2.275 P.2 P0 D.6 F110 F110
0350 CIRCLE IN X0 Y0 Z.08 Z.4 Z1 R2.125 P.2 P0 D.6 F70 F70
0360 CIRCLE OUT X0 Y0 Z.08 Z.4 Z1 R1.075 P.2 P0 D.6 F110 F110
0370 CIRCLE IN X0 Y0 Z.08 Z.4 Z1 R.4 P.1 P0 D.6 F70 F70
0380 CIRCLE IN X0 Y0 Z.08 Z.4 Z1 R.925 P.2 P0 D.6 F110 F110
0390 || END|PRGM
```

A5 Tool Paths for Tapered Cuts

Since the bioreactor fluidic channels are made using a ball shaped end mill, determining the path of the tool is not trivial. The desired path is shown in Figure A1 and depends on both the slope of the channel and the size of the tool. This path must be defined with respect to the tip of the center of the tool.

The tops of the reactor wells are cut at a 5° taper. This feature was created using a modified tapered end mill, Figure A2. The end mill must only cut the desired edge without modifying the ridge above it. Again, the tool position is defined relative to the tip.

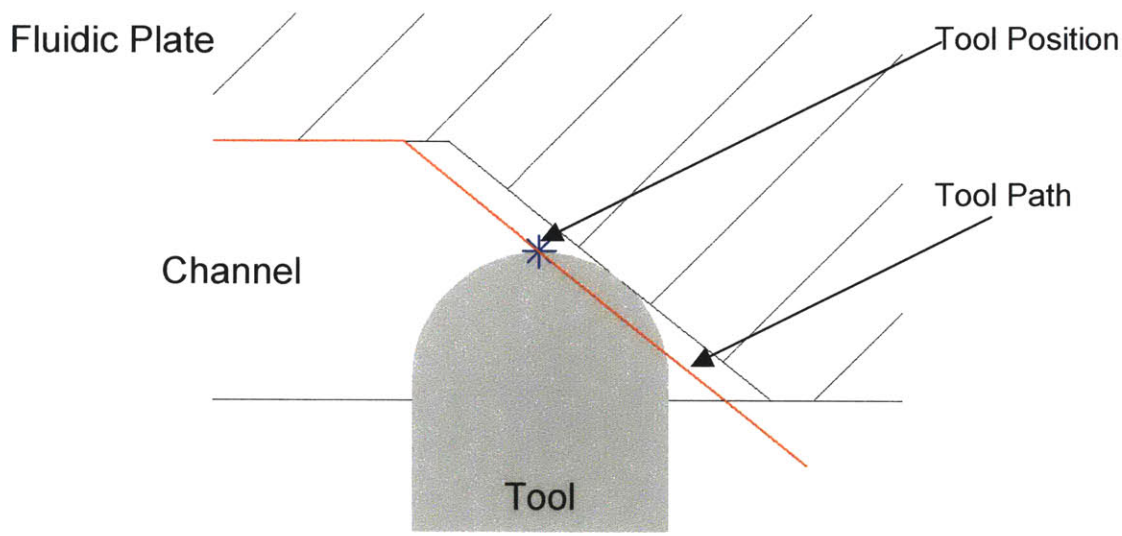

Figure A1: The programmed path of the tool used to cut the fluidic channels

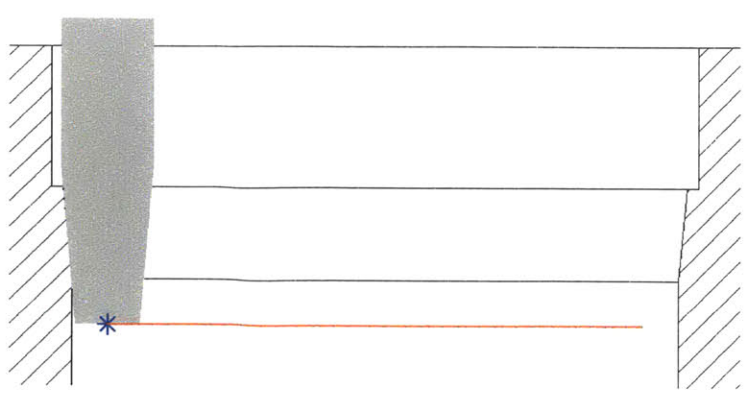

Figure A2: The path of the tool used taper the top of reactor and reservoir wells

There is also a taper at the ledge created by the surface channel. This taper is machined at 60° using a different tool. In this case, the tip of the tool has been removed. This cut initially follows the same tangent to the reservoir well used by the surface channel, then cuts ~ 0.5 mm into the ledge. Here, cutter compensation was used so the position of the tool was defined from a different point, Figure A3.

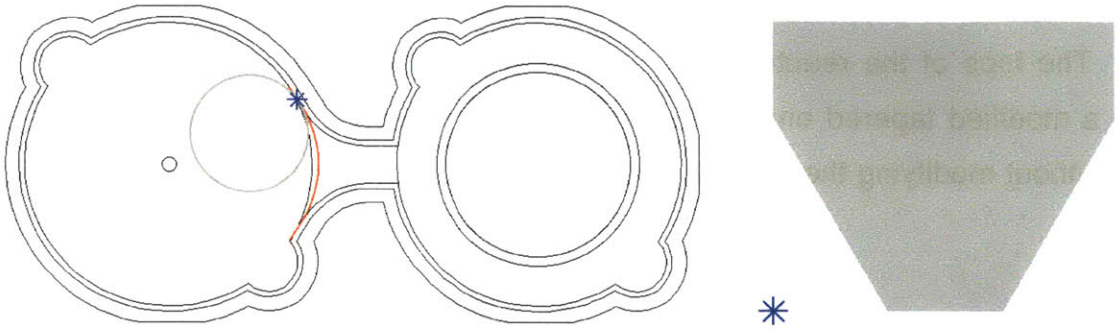

Figure A3: The path of the tool used to taper the ledge created by the surface channel

A6 Scaffold Hole Placement

Spacing between circles 0.1 mm
Hole Diameter 0.343 mm

Ring num	ring diameter (out to out)	Holes in ring	Holes in scaffold	Bore Circle Radius (mm)	Angle Between holes	Distance Between Holes
1	0.343	1	1	0	360	0
2	1.229	6	7	0.443	60	0.1
3	2.115	12	19	0.886	30	0.116
4	3.001	18	37	1.329	20	0.119
5	3.887	24	61	1.772	15	0.120
6	4.773	30	91	2.215	12	0.120
7	5.659	36	127	2.658	10	0.120
8	6.545	42	169	3.101	8.57	0.120
9	7.431	48	217	3.544	7.5	0.121
10	8.317	54	271	3.987	6.67	0.121
11	9.203	60	331	4.43	6	0.121
12	10.089	66	397	4.873	5.45	0.121
13	10.975	72	469	5.316	5	0.121
14	11.861	78	547	5.759	4.62	0.121
15	12.747	84	631	6.202	4.29	0.121

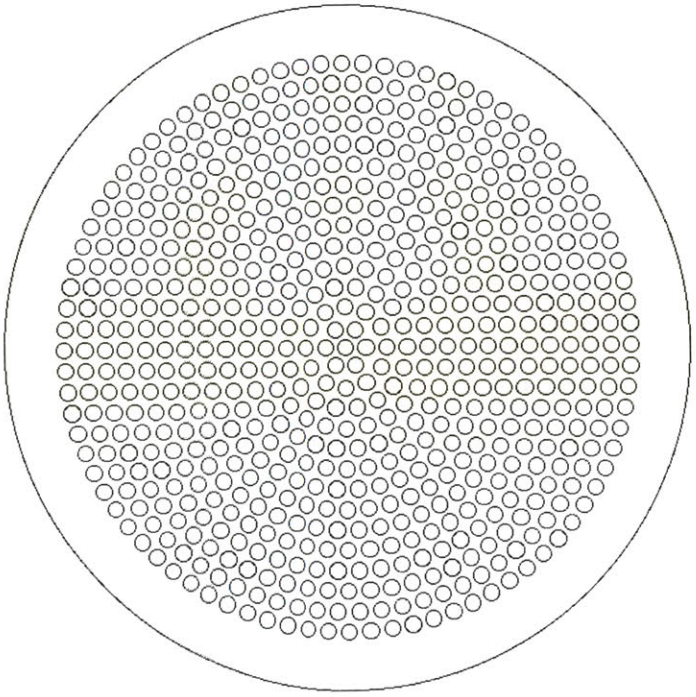

Figure A4: Hole placement for a drilled scaffold

A7 Mask for Etching Silicon Scaffolds

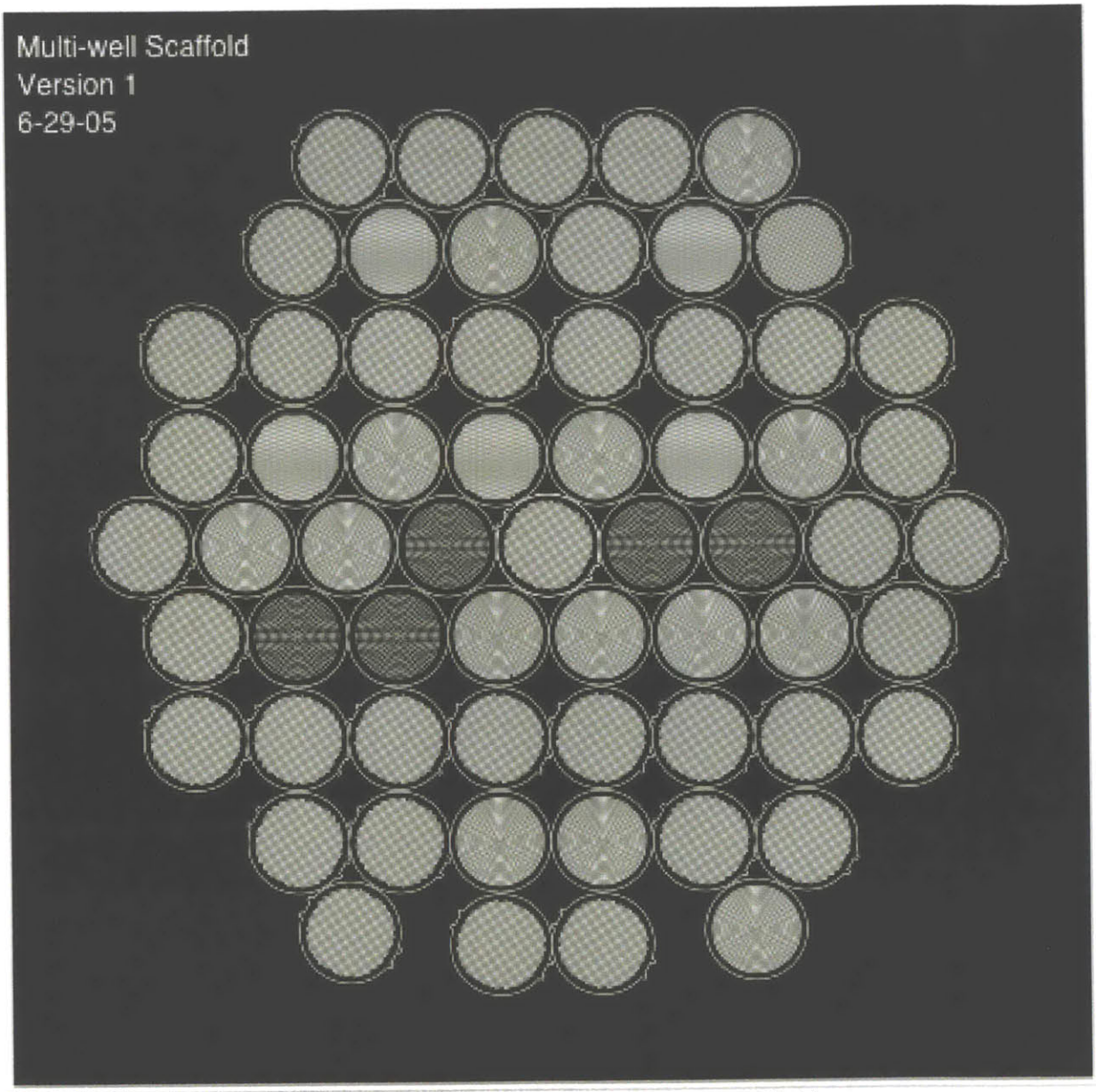

Figure A5: Mask for etching silicon scaffolds

A8 Sample Capacitance Calculation

1. A radius of curvature in the membrane is used to find a pressure and volume

w = 10 mm

r = 23.4 mm

$$V = \frac{\pi}{24}\left[16r^3 - \left(8r^2 + w^2\right)\sqrt{4r^2 - w^2}\right], \tag{4.2}$$

$$P = \frac{4E}{w}\left(\sin^{-1}\left(\frac{w}{2r}\right) - \frac{w}{2r}\right), \tag{4.8}$$

V = 21.33 μL
P = 0.250 kPa

2. A second radius (r + dr) is used to find another pressure and volume

r = 23.6 mm,

now

V = 21.11 μL
P = 0.242 kPa

3. Capacitance is found by dividing ΔV / ΔP

$$C = \frac{V_2 - V_1}{P_2 - P_1} = \frac{21.11 - 21.33}{0.242 - 0.250} = 29{,}239 \,\mu\mathrm{L}/\mathrm{N/mm^2} = 29.24 \frac{\mathrm{mL}}{\mathrm{N/mm^2}}$$

A9 Dynamic Capacitor Model for a Round Capacitor

```
function [t,V_in,Q_in,Q_out]=cap_flow(d,chan,Q,V_pump,n)
%this program models flow through the scaffold
%inputs: capacitor diameter - 13, number of channels - 861, flow rate - 1 uL/chan/min,
%inputs: pumping chamber volume - 0.93 uL
%inputs: effective area of filter (1 for channels, 2 for entire filter, 0.1 for filled channels)
%outputs: flow through scaffold, flow from pump, time vector
%outputs: volume through the scaffold, volume from the pump
%pump breaks down at frequencies above 35 Hz

E=.3749;                          %membrane E/thickness (N/mm)

%determining hydraulic resistance
if n==1
   m='Assumes fluidic resistance from empty channels'
elseif n==2
   m='Assumes fluidic resistance from the entire filter'
elseif n==.1
   m='Assumes fluidic resistance from full channels'
else
   m='Unknown Fluidic Resistance'
end
hp_filt=73.5;                     %filter hydraulic permeability (mL/s)/(N/sq mm)/cm^2
area_chan=pi*(.34/2)^2*10^-2;     %channel area (cm^2)
area_t=area_chan*chan*n;          %effective filter area (cm^2) (ASSUMES EMPTY CHANNELS)
resist=10^-3/(area_t*hp_filt);    %fluidic resistance (N/sq mm)/(μL/s)

%pumping parameters
del_t=.01;                        %time to pump one stroke (s)
t_cycle=V_pump*60/(Q*chan);       %pump cycle time (s), governed by desired flow, typ=.0612
Q_p=V_pump/del_t;                 %flow into capacitor (when flow occurs) (μL/s)
V_valve=.16;                      %volume of the valves (μL)
Q_v=V_valve/del_t;                %flow into and from valves

%finds starting point for quasi steady state
p_0=Q*chan/60*resist*10^6;        %finds the initial pressure required to flow at average rate
                                  %multiplying by 10^6 improves the accuracy of the calculation
r_0=d/10*(2*E/p_0)^(1/2.5);       %estimates r from p
opt=optimset('Display','off');
r_0=real(fsolve(@(r) find_rp(r,p_0,E,d), r_0, opt));                    % finds r from p & estimated r
V_0=pi/24*(16*r_0^3-(8*r_0^2+d^2)*(4*r_0^2-d^2)^(1/2))-V_pump*.5;       %finds initial capacitor volume

%sets up the time vector for the model
dt=del_t/10;                      %time increments in output(sec)
total_time=300*dt;                %total time (sec)
a=0;
for i=1:(total_time/dt)
   t(i)=a;
   a=a+dt;
end

%creates flow pattern to the capacitor from the pump, Q_in (μL/sec)
if (V_pump>4*V_valve)
   %neglects the volume of valves
   for i=1:length(t)
      if (t(i) <= t_cycle)
```

```
        if (t(i) <= del_t)
            Q_in(i)=Q_p;
        else
            Q_in(i)=0;
        end
        a=i-1;
    else
        Q_in(i)=Q_in(i-a);
    end
  end
else
  %includes the valve volume
  for i=1:length(t)
    if (t(i) <= t_cycle)
        if (t(i) <= del_t)
            Q_in(i)=Q_p;
        elseif (t(i) <= t_cycle/4)
            Q_in(i)=0;
        elseif (t(i) <= t_cycle/4+del_t)
            Q_in(i)=Q_v;
        elseif (t(i) <= 3*t_cycle/4)
            Q_in(i)=0;
        elseif (t(i) <= 3*t_cycle/4+del_t)
            Q_in(i)=-1*Q_v;
        else
            Q_in(i)=0;
        end
        a=i-1;
    else
        Q_in(i)=Q_in(i-a);
    end
  end
end

%finds the flow pattern from the capacitor through the cells, Q_out (µL/sec)
V(1)=V_0;
r(1)=r_0;
for i=1:length(t)
    r(i+1)=fsolve(@(r) find_rv(r,V(i),d), r(i), opt);
    p(i)=4*E/d*(asin(d/(2*r(i)))-d/(2*r(i)));
    Q_out(i)=p(i)/resist;
    V(i+1)=Q_in(i)*dt-Q_out(i)*dt+V(i);
    h(i)=r(i+1)-((r(i+1))^2-(d/2)^2)^(1/2);  % finds the deflection of the capacitor
end

Q_in=Q_in*60/chan;                  %converts to µL/chan/min
Q_out=Q_out*60/chan;                %converts to µL/chan/min
t=t*1000;                           %converts the time to ms
%t=t/60;                            %converts to time in minutes

V_in(1)=0;
V_out(1)=0;
for i=2:length(t)
    V_in(i)=Q_in(i)*dt/60+V_in(i-1);
    V_out(i)=Q_out(i)*dt/60+V_out(i-1);
end

freqency=round((1/t_cycle)*10)/10    %prints the pump frequency
```

```
time_per_delay=.202;                    %time (ms) per controller delay
controller_delay=round(t_cycle*10^3/(4*time_per_delay))      %calculates the delay for the controller
maximum_deflection=max(h)               %finds the maximum deflection of the capacitor
maximum_flowrate=max(Q_out)             %prints the maximum flow rate (µL/channel/min)

subplot(2,1,1), plot(t,Q_out,t,Q_in), xlabel('time (ms)'), ylabel('flow rate (uL/channel/min)'), axis tight
subplot(2,1,2), plot(t,V_out,t,V_in), xlabel('time (ms)'), ylabel('volume pumped (uL/channel)'), axis tight
```

```
function F = find_rp(r,P,E,d)
%takes in a radius, a pressure, membrane thickness, valve diameter
%should return zero
%multiplying by 10^6 improves the accuracy of the calculation

F=4*10^6*E/d*(asin(d/(2*r))-d/(2*r))-P;
```

```
function F = find_rv(r,V,d)
%takes in values for radius, volume, valve diameter
%should return zero

F=pi/24*(16*r^3-(8*r^2+d^2)*(4*r^2-d^2)^(1/2))-V;
```

A10 Dynamic Capacitor Model for an Oblong Capacitor

```
function [height,Q_out,Q_in,t,V_out,V_in]=obl_cap_flow(w,l,chan,Q,V_pump,n)
%this program models flow through the scaffold for an oblong capacitor
%inputs: capacitor width, capacitor length (larger of 2), number of channels
%inputs: flow rate (uL/chan/min), pumping chamber volume (uL)
%inputs: effective area of filter (1 for channels, 2 for entire filter, 0.1 for filled channels)
%outputs: flow through scaffold, flow from pump, time vector
%outputs: volume through the scaffold, volume from the pump
%pump breaks down at frequencies above 35 Hz

E=.3749;                          %membrane E/thickness (N/mm)

%determining hydraulic resistance
if n==1
   m='Assumes fluidic resistance from empty channels'
elseif n==2
   m='Assumes fluidic resistance from the entire filter'
elseif n==.1
   m='Assumes fluidic resistance from full channels'
else
   m='Unknown Fluidic Resistance'
end
hp_filt=73.5;                     %filter hydraulic permeability (mL/s)/(N/sq mm)/cm^2
area_chan=pi*(.34/2)^2*10^-2;     %channel area (cm^2)
area_t=area_chan*chan*n;          %effective filter area (cm^2) (ASSUMES EMPTY CHANNELS)
resist=10^-3/(area_t*hp_filt);    %fluidic resistance (N/sq mm)/(µL/s)

%pumping parameters
del_t=.01;                        %time to pump one stroke (s)
t_cycle=V_pump*60/(Q*chan);       %pump cycle time (s), governed by desired flow, typ=.0612
Q_p=V_pump/del_t;                 %flow into capacitor (when flow occurs) (µL/s)
V_valve=.16;                      %volume of the valves (µL)
Q_v=V_valve/del_t;                %flow into and from valves

%finds starting point for steady state
p_0=Q*chan/60*resist*10^6;        %finds the initial pressure required to flow at average rate
                                  %multiplying by 10^6 improves the accuracy of the calculation
r_0=w/10*(w*E/w*(1+(pi*w^2)/(4*l^2-4*w*l+pi*w*l))/p_0)^(1/2.5);        %estimates r from p
opt=optimset('Display','iter');
r_0=real(fsolve(@(r) find_r_p(r,p_0,E,w,l), r_0, opt));                %finds r from p
%finds V_0
V_0=pi/3*(2*r_0^3-(2*r_0^2+(w/2)^2)*(r_0^2-(w/2)^2)^(1/2))+(l-w)*(r_0^2*asin(w/(2*r_0))-(w/2)*(r_0^2-
(w/2)^2)^(1/2))-V_pump;

%sets up the time vector for the model
dt=del_t/10;                      %time increments in output(sec)
total_time=300*dt;                %total time (sec)
a=0;
for i=1:(total_time/dt+1)
   t(i)=a;
   a=a+dt;
end

%creates flow pattern to the capacitor from the pump, Q_in (µL/sec)
if (V_pump>4*V_valve)
   %neglects the volume of valves
```

```
  for i=1:length(t)
     if (t(i) <= t_cycle)
        if (t(i) <= del_t)
           Q_in(i)=Q_p;
        else
           Q_in(i)=0;
        end
        a=i-1;
     else
        Q_in(i)=Q_in(i-a);
     end
  end
else
  %includes the valve volume
  for i=1:length(t)
     if (t(i) <= t_cycle)
        if (t(i) <= del_t)
           Q_in(i)=Q_p;
        elseif (t(i) <= t_cycle/4)
           Q_in(i)=0;
        elseif (t(i) <= t_cycle/4+del_t)
           Q_in(i)=Q_v;
        elseif (t(i) <= 3*t_cycle/4)
           Q_in(i)=0;
        elseif (t(i) <= 3*t_cycle/4+del_t)
           Q_in(i)=-1*Q_v;
        else
           Q_in(i)=0;
        end
        a=i-1;
     else
        Q_in(i)=Q_in(i-a);
     end
  end
end

%finds the flow pattern from the capacitor through the cells, Q_out (µL/sec)
opt=optimset('Display','off');
V_0=V_0-V_pump;
V(1)=V_0;
r(1)=fsolve(@(r) find_r_v(r,V_0,w,l), r_0, opt);
for i=1:length(t)
   r(i+1)=fsolve(@(r) find_r_v(r,V(i),w,l), r(i), opt);
   p(i)=2*E/w*(1+(pi*w^2)/(4*l^2-4*w*l+pi*w*l))*(asin(w/(2*r(i)))-w/(2*r(i)));
   Q_out(i)=p(i)/resist;
   V(i+1)=Q_in(i)*dt-Q_out(i)*dt+V(i);
   height(i)=r(i+1)-((r(i+1))^2-(w/2)^2)^(1/2);
end

Q_in=Q_in*60/chan;                    %converts to µL/chan/min
Q_out=Q_out*60/chan;                  %converts to µL/chan/min
%t=t*1000;                            %converts the time to ms
t=t/60;                               %converts to time in minutes

V_in(1)=0;
V_out(1)=0;
for i=2:length(t)
   V_in(i)=Q_in(i)*dt/60+V_in(i-1);
```

```
  V_out(i)=Q_out(i)*dt/60+V_out(i-1);
end


maximum_flowrate=max(Q_out)        %prints the maximum flow rate (µL/channel/min)
freqency=round(1/t_cycle)          %prints the pump frequency
time_per_delay=.204;               %time (ms) per controller delay
controller_delay=round(t_cycle*10^3/(4*time_per_delay))        %calculates the delay for the controller
new_V_0=mean(V)

subplot(2,1,1), plot(t,Q_out,t,Q_in), xlabel('time (min)'), ylabel('flow rate (uL/channel/min)'), axis tight
subplot(2,1,2), plot(t,V_out,t,V_in), xlabel('time (min)'), ylabel('volume pumped (uL/channel)'), axis tight




function F = find_r_p(r,P,E,w,l)
%takes in a radius, a pressure, membrane thickness, valve width and length
%should return zero
%multiplying by 10^6 improves the accuracy of the calculation

F=2*10^6*E/w*(1+(pi*w^2)/(4*l^2-4*w*l+pi*w*l))*(asin(w/(2*r))-w/(2*r))-P;




function F = find_r_v(r,V,w,l)
%takes in values for radius, volume, valve width and length
%should return zero

F=pi/3*(2*r^3-(2*r^2+(w/2)^2)*(r^2-(w/2)^2)^(1/2))+(l-w)*(r^2*asin(w/(2*r))-(w/2)*(r^2-(w/2)^2)^(1/2))-V;
```

A11 Assembling the Reactor

1. Place membrane on pneumatic plate such that all of the screw holes line up with holes in the membrane

2. Place the fluidic plate onto the pneumatic plate using the alignment pins as guides

3. Flip over the reactor and insert all 14 screws

4. Tighten screws in the order shown in Figure A6

5. Connect pneumatic lines to controller without crossing any lines, Figure A7

6. Place fluid in reservoirs and start pumps in forward direction

7. Set pneumatic pressures to ±35 kPa on the pneumatic manifold

8. Check to make sure each of the pumps are flowing

9. Fill reactor units with fluid taking care that fluid primes across the surface channel

10. Insert all scaffold assembly components individually, taking care that no bubbles are trapped underneath scaffold

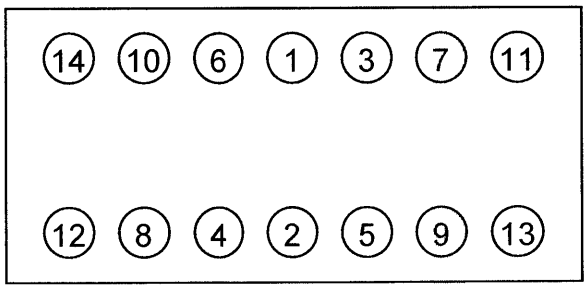

Figure A6: Order for tightening screws

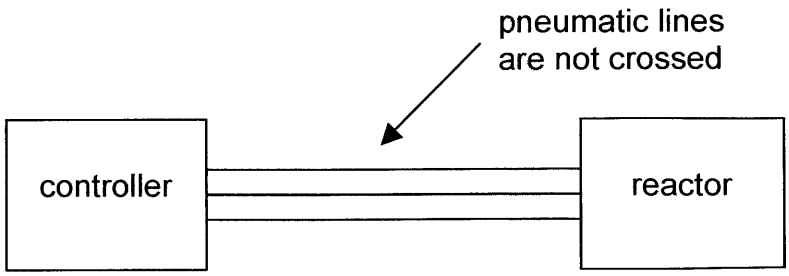

Figure A7: Connecting pneumatic lines

2198-35